ROBERTS, KEITH

THE MARGINAL ROCKS OF THE RUSTENBURG

LAYERED SUITE OF THE BUSHVELD COMPLEX

NORTHWEST OF PRETORIA

PhD   UP   1992

The marginal rocks of the Rustenburg Layered Suite

of the Bushveld Complex northwest of Pretoria

by

Keith Roberts

Submitted in partial fulfilment of the requirements

for the degree of

DOCTOR OF PHILOSOPHY

in the Faculty of Natural Sciences

University of Pretoria

Pretoria

April 1992

The marginal rocks of the Rustenburg Layered Suite
of the Bushveld Complex northwest of Pretoria

by

Keith Roberts

Supervisor: Prof. G. von Gruenewaldt.

Department: Geology.

Degree: Doctor of Philosophy.

ABSTRACT

Geological mapping has re-defined the floor of the Bushveld Complex in an area northwest of Pretoria. Although broadly conformable elsewhere in the area, in the central region the contact of the Rustenburg Layered Suite transgresses the floor, and rises in an easterly direction. Thus the base of the Complex is formed by the lower critical zone (Ruighoek Pyroxenite) in the west and by the lowermost portion of the main zone (Pyramid Gabbro-Norite) in the east. The overall cumulate succession, although broadly comparable with that found in the eastern lobe of the Complex, differs in that the lower group chromitites are absent, the Merensky Reef is much thicker (± 12 m), and cumulus plagioclase occurs below the middle group chromitites.

Throughout the study area the Rustenburg Layered Suite is separated from the underlying floor and other marginal rocks by a zone of contaminated quartz gabbronorite. This is a contaminated variant of a microgabbronorite that forms a chilled margin against portions of the floor. This chilled margin is however only well developed at stratigraphic levels above the lower critical zone.

In the west, the Rustenburg Layered Suite is separated from the underlying Magaliesberg Quartzite by only 100 m of quartz gabbronorite. In the east, the total thickness of floor and marginal rocks above the Magaliesberg Quartzite exceeds 700 m. Here the main zone is underlain by quartz gabbronorite, chilled microgabbronorite (including screens of metaquartzite) and metamorphosed quartzofeldspathic sediments. Beneath this, 300 m of predominantly noritic cumulates, sheathed by meta quartz – dolerites, form a thick sill overlying the Magaliesberg Quartzite.

The Magaliesberg Quartzite and underlying Silverton Shale are intruded by several suites of sills, broadly comprising metadolerites and related meta quartz – dolerites, micropyroxenites, as well as pyroxenites and norites. The sparse metadolerites and their much more abundant, contaminated equivalents, the meta quartz – dolerites, predate formation of the Bushveld Complex, as does the related thick sill above the Magaliesberg Quartzite.

The micropyroxenites are similar to rocks described from elsewhere in the Bushveld Complex, being characterised by a variety of quench features including spinifex-like and cone diabase textures. These rocks have high initial ratios of $^{87}Sr/^{86}Sr$ (0.7024 – 0.7063 at 2.05 Ga) and are unusual for basic rocks in having Rb/Sr ratios of 0.2 and high weight per cent contents of SiO_2 (55.5), K_2O (0.9), LREE, and MgO (13.3). Geochemically, in many respects, they resemble boninites.

The geochemistry and mineralogy of the micropyroxenites indicate that they are representative of the parental magma to the lower portion of the Rustenburg Layered Suite. Furthermore, geochemical data indicate that this magma was primarily generated by extensive (±35 per cent) partial melting of a mantle source. However, whether this source was highly enriched in K_2O and LREE or whether, as has recently been proposed, these components were derived from a metasomatised zone close to the source cannot be elucidated from the current data. The high Ni content (i.e. ±300 ppm) of these rocks precludes the possibility of olivine fractionation as an explanation for their high SiO_2 content.

Die randgesteentes van die Rustenburg Gelaagde Suite
van die Bosveldkompleks noordwes van Pretoria

deur

Keith Roberts

Promotor: Prof. G. von Gruenewaldt.
Departement: Geologie.
Graad: Doktor in Filosofie.

SAMEVATTING

Geologiese kartefring het die vloer van die Bosveldkompleks in 'n gebied noordwes van Pretoria herdefinieer. Hoewel oor die algemeen konkordant elders in die gebied, sny die kontak van die Rustenburg Gelaagde Suite in die sentrale gedeelte transgressief oor die vloer, sodat die laer kritiese sone (Ruighoek Pirokseniet) die basis van die Kompleks in die weste vorm en die onderste gedeelte van die hoofsone (Piramied Gabbronoriet) die basis in die ooste. Die kumulaatopeenvolging is, oor die algemeen, vergelykbaar met dié van die oostelike Kompleks, maar dit verskil in dat die laer groep chromitietlae afwesig is, die Merenskyrif is heelwat dikker (± 12 m) en kumulus plagioklaas verskyn onderkant die middelste groep van chromitietlae.

Dwarsdeur die studiegebied is die Rustenburg Gelaagde Suite geskei van die onderliggende vloer en ander randgesteentes deur 'n sone van gekontamineerde kwarts gabbronoriet. Hierdie is 'n gekontamineerde variant van 'n mikrogabbronoriet wat 'n kilrand teen porsies van die vloer vorm. Hierdie kilrand is slegs goed ontwikkeld op stratigrafiese vlakke bo die laer kritiese sone.

In die weste word die Rustenburg Gelaagde Suite van die onderliggende Magaliesberg Kwartsiet geskei deur 'n 100 m dik kwartsgabbronoriet. In die ooste oorskrei die totale dikte van die vloer en die randgesteentes bo die Magaliesberg Kwartsiet egter 700 m. Hier word die hoofsone onderlê deur kwarts gabbronoriet, gekilde mikrogabbronoriet (insluitende xenoliete van metakwartsiet) en gemetamorfoseerde kwarts-feldspaat gesteente van sedimentêre oorsprong. Hierbenede vorm 300 m van hoofsaaklik noritiese kumulate, omhul deur meta-kwartsdoleriete, 'n dik plaat wat die Magaliesberg Kwartsiet oorlê.

Die Magaliesberg Kwartsiet en onderliggende Silverton Skalie is ingedring deur verskeie suites van plate, oor die algemene bestaande uit metadoleriete en verwante meta-kwartsdoleriete, mikropirokseniete, asook pirokseniete en noriete. Die verspreide metadoleriete en hulle gekontamineerde ekwivalente, die meta-kwartsdoleriete, gaan vorming van die Bosveldkompleks vooraf, net soos die verwante dik plaat bo die Magaliesberg Kwartsiet.

Die mikropirokseniete is soortgelyk aan die gesteentes beskryf van elders in die Bosveldkompleks, en word gekarakteriseer deur 'n verskeidenheid van blustekstuure, insluitende spinifex-agtige en kegeldiabaas teksture. Hierdie gesteentes het hoë inisiëleverhoudings van $^{87}Sr/^{86}Sr$ (0.7024 – 0.7063 teen 2.05 Ga) wat ongewoon is vir basiese gesteentes vanweë Rb/Sr verhoudings van 0.2 en hoë gewigpersentasie-inhoude van SiO_2 (55.5), K_2O (0.9), LRAE, en MgO (13.3). Hulle kom geochemies in verskeie opsigte ooreen met boniniete.

Die geochemie en mineralogie van die mikropirokseniete dui daarop dat hulle verteenwoordigend is van die bronmagma tot die laer gedeelte van die Rustenburg Gelaagde Suite. Voorts dui geochemiese data dat hierdie magma hoofsaaklik ontstaan het deur omvangryke (±35 per cent) gedeeltelike smelting van 'n mantel bron. Maar, of hierdie bron hoogs verryk was in K_2O en LRAE of, soos onlangs voorgestel, hierdie komponente ontleen is aan 'n gemetasomatiseerde sone naby die bron kan nie uit die huidige data verklaar word nie. Die hoë Ni inhoud (nl. ±300 dpm) van hierdie gesteentes sluit die moontlikheid van vroeë olivien-fraksionasie uit as 'n verklaring van hulle hoë SiO_2 inhoud.

TABLE OF CONTENTS

IV

LIST OF TABLES

TABLE

LIST OF FIGURES

FIGURE

FOLDER 1

1: 50 000 scale map entitled "The geology of the lower part of the Rustenburg Layered Suite and marginal rocks of the Bushveld Complex N.W. of Pretoria".

1. INTRODUCTION

1.1 SCOPE OF STUDY

This thesis presents the results of geological mapping and subsequent petrological/geochemical studies in an area northwest of Pretoria, roughly bounded by Rosslyn, Brits, Hartbeespoort Dam and Pretoria (Fig. 1.1; Folder 1). Initial aims of this field orientated project were to study laterial variation in the rocks of the Rustenburg Layered Suite (SACS, 1980) and also to reinvestigate the contact between these rocks and the floor.

However, early in the mapping it became apparent that the critical zone of the Rustenburg Layered Suite (SACS, 1980) does not extend as far east as was previously thought (Coertze 1974). The majority of the northeastern part of the area is in fact underlain either by pre-Bushveld rocks or by rocks associated with the margins of the Bushveld Complex, (Fig. 1.1; Folder 1) and not by critical zone rocks. Thus the emphasis of the project was shifted and attention was centred largely on the marginal rocks, their interrelationships, and possible genetic associations with the Rustenburg Layered Suite. Work on the latter was predominantly restricted to the documentation of a vertical lithological and mineralogical profile.

Although much of the area was investigated in detail, the usefulness of larger scale maps is precluded by the paucity of outcrop and mapping at the 1:50 000 scale was considered appropriate for the ±350 sq km area (Fig. 1.1, Folder 1).

In addition to geological mapping, approximately 3 200 m of borehole core from the area south of Brits were logged and sampled. Approximately 240 samples of the marginal rocks and sills were also collected for whole-rock and trace element analysis. In addition, twelve of these rocks were selected for REE and Sr^{87}/Sr^{86} analysis. Approximately 250 microprobe analyses were also undertaken.

1.2 PREVIOUS WORK

Since outcrop is rather poor and inconspicuous in the region, previous investigations of the Complex and its margins in the area have been restricted to rather generalised reconnaissance surveys and compilations (Kynaston, 1904;

Fig. 1.1. Geological map of the area northwest of Pretoria.

28°00

GA-RANKUWA

ROSSLYN

BRITS

25°40

Hornsnek

Silkaatsnek

Hartbeespoort
Dam

LEGEND

SYMBOLS

Fault —f—
Road
River

GEOLOGICAL
BOUNDARIES

Observed
Inferred
Conjectured

0 1 2 3 4 5
Km

FLOOR ROCKS

Quartzofelspathic rocks,
locally granophyric or
spotted, with mafic clots

Magaliesberg Quartzite
with pelitic and calc-
silicate hornfels (\ \)

Silverton Shale,
(largely hornfelsed)

SILLS IN THE FLOOR

n — Norites, often cumulate
textured

p — Pyroxenite cumulates

cd — Micropyroxenites and
micronorites (Spinifex-like
and Cone Diabase textured)

md — Meta quartz-dolerites
(contaminated)

m — Metadolerites

Noritic cumulates with
rare anorthosite layers
(altered in part) } LAYERED
SILL

Meta quartz-dolerites
(contaminated)

BUSHVELD COMPLEX AND YOUNGER ROCKS

Post-Bushveld syenite
and gabbro dykes (locally
composite)

Hortonolite dunite and
pyroxenite pegmatoids

Cpx ± plag ± opx cumulates
Main Mottled anorthosite (■—■) } MAIN
ZONE

Opx ± plag ± chromite cumulates
Inferred position of Merensky
Reef (—M—) } UPPER

Opx ± plag ± chromite cumulates } LOWER } CRITICAL
ZONE

Quartz gabbronorite
(contaminated) } MARGINAL
PHASES

Microgabbronorite

1907); Kynaston et al. (1929); Nel (1940); Coertze (1970, 1974). Hall and du Toit (1923) however, give a detailed account of a traverse across the Complex margins, exposed in the then newly excavated irrigation canals north of the Hartbeespoort damwall.

Because of this generalised approach of previous workers it was considered necessary to adopt a detailed mapping approach so as to provide a firm foundation for later petrological study. The efficacy of such an approach was stressed by Sharpe (1980, p. 21), who pointed out that many authors have chosen inappropriate samples for research work (e.g. for use in melting experiments) in the absence of detailed mapping. Furthermore, the tendency in the past has been to concentrate on the Rustenberg Layered Suite, and to group the marginal rocks together as a unit, thus obscuring many of the lithological differences between the constituents of the marginal 'zone'. The mapping of the author has subsequently revealed that there are more complex geological relationships within the marginal unit than were hitherto supposed, although Nel (1940) also described a more complicated contact region than was recognised by later investigators. His 'zone of diabases' and 'zone of quartzite xenoliths' has been re-mapped and re-interpreted by the author as a ± 300 m thick, pre-Bushveld, layered sill, overlain by metaquartzite. The recognition that this sill forms part of the floor of the Bushveld Complex and not part of the marginal zone (SACS = Kolobeng Norite) is important. The conclusion to be drawn from this is that the floor of the Complex rises obliquely eastwards such that successive zones overlap each other and abut against successively higher components of the floor (Fig. 1.1; Folder 1). This is in contrast with previous concepts in which the Layered Suite was considered essentially concordant with the floor (Coertze 1974).

Beneath the Complex several distinct suites of sills are also recognised, largely in agreement with the findings of Cawthorn et al. (1981) and Davies (1982) to the west of the present area and Sharpe (1981) in the eastern lobe of the Bushveld.

1.3   RELIEF AND DRAINAGE

The area is divided into two regions by the E-W trending Magaliesberg. The crest of this prominent quartzite cuesta, with an average elevation of 1 600 m, is interrupted in only a few places by small 'Neks' associated with faults or possibly master joints. A much larger displacement, along major faults bounding

the Brits Graben[1] at Hartbeespoort and Kommandonek, shift the crest line of the northerly dipping quartzite some 1 000 m to the south. North of these steep dip slopes the area possesses a gentle northerly incline, being interrupted only by the two parallel ridges of quartzite south of Ga-rankuwa (Fig. 1.1, Folder 1), and isolated quartzite 'koppies'. Low, whale-back shaped mounds also occur as a result of the isolated, smaller quartzite xenoliths shown on the geological map (Fig. 1.1, Folder 1). Below the scarp face of the Magaliesberg, steep, talus covered slopes occur, comprising quartzite blocks with occasional outcrops of doleritic rocks and hornfelses. These slopes give way southward to a shallow southerly slope devoid of outcrop (with the exception of a few sills) presumably underlain by hornfelses or possibly shales.

The only major water course in the area, the Crocodile River has exploited the line of weakness at Hartbeespoort, giving rise to a short, narrow, incised river valley. Across this narrow valley a dam wall was constructed in the early 1920's giving rise to the only substantial body of standing water in the area, i.e. Hartbeespoort Dam. Rivers elsewhere in the area are small and intermittent.

---

[1] The rift structure south of Brits (Fig. 1.1.; folder 1) is hereafter referred to as the Brits Graben.

2.   FIELD RELATIONSHIPS

Only macroscopic field relations are dealt with here, more detailed relationships are discussed in the individual chapters dealing with specific rock units. Throughout this chapter relationships are discussed with reference to the geological map (Fig. 1.1; Folder 1) and the nomenclature follows SACS terminology (SACS, 1980) as closely as possible.

The Bushveld Complex is emplaced into the Transvaal Sequence, the latter comprising a 12-km-thick succession of clastic and chemical sedimentary rocks within which volcanic formations form an important component (Hunter and Hamilton, 1978; Tankard et al. 1982). This sequence is represented in the present area by the Magaliesberg Quartzite and the underlying Silverton Shale. The discontinuous outcrops of metaquartzite overlying the Middelwater Layered Sill (see below for nomenclature) and the smaller, irregularly shaped occurrences of metaquartzite are considered to be xenolithic bodies, derived from the underlying Magaliesberg Quartzite (Fig. 1.1, Folder 1). Although there are some thin (< 2m) layers of calc silicate and pelitic hornfels intercalated with impure quartzite within these bodies, there is no evidence of any substantial intervening shale sequence above the Magaliesberg Quartzite, whereas in the eastern Transvaal. Button (1976) describes some 1 000 m of Vermont Shale separating the Magaliesberg and overlying Lakenvalei Quartzites. Use of the term Rayton Formation (or Lakenvalei Quartzite — Cawthorn, 1981) for these metaquartzites, is therefore not considered justified in the light of the present field data. As such, these discontinuous outcrops of quartzite simply appear to represent large, xenolithic bodies rafted from the main Magaliesberg outcrop. This is further substantiated by the observation, on published Geological Survey maps, that the Magaliesberg Quartzite thins remarkably in the precise region where the quartzites are found above it. Furthermore, the 'train' of inclusions at the western end of the Middelwater Layered Sill becomes difficult to explain if an intervening shale horizon is postulated.

Within and below the Magaliesberg Quartzite, several suites of sills are found. However, due presumably to geometric constraints imposed by the sedimentary layers, no intersecting relationships were observed and relative ages are not determinable.

Conformably overlying the Magaliesberg Quartzite in the eastern part of the area, is the 300 m thick, cumulate textured, Middelwater Layered Sill. This sill is well exposed on the farms Vissershoek 435JQ, Wildebeesthoek 310JR and Middelwater 436JQ, (Folder 1) and its name is derived from the latter farm, where it is best exposed. The sill is sheathed by metadoleritic rocks, within which two large xenoliths of quartzite occur. Within the layered portion of the sill, xenoliths are rare, with the exception of a few small (less than 1m long)) sub-rounded but elongated, partially digested quartzite inclusions. A larger inclusion of quartzofeldspathic rocks, lying between the marginal and layered rocks, occurs just east of the Hornsnek to Ga-rankuwa road. One other smaller but similar occurrence was also noted west of this. These rocks are similar to the overlying quartzofeldspathic lithologies.

Sandwiched conformably between the top of the Middelwater Layered Sill and overlying quartzite is a more extensive group of quartzofeldspathic rocks which exhibit a variety of textures (chapter 5.2.3). These appear to grade downwards into meta-dolerites but field evidence is inconclusive. Similarly the upper contact of the quartzofeldspathic rocks is not exposed, although just west of the Church in the suburb 'The Orchards', outcrops of granophyric-textured quartzofeldspathic rocks occur within several metres of metaquartzite. The contact therefore appears to be quite sharp. The occurrence of these rocks as xenoliths in the Middelwater Layered Sill and their textural and compositional variability suggests that they are metasediments (See chapter 7.5).

In the western part of the area, layered cumulates of the Rustenburg Layered Suite crop out. Although the overall strike of the layering suggests a conformable relationship with the floor, the few measured dip values for the Layered Suite outside of the Brits Graben (i.e. 12, 14 and 20 degrees) are generally lower than the dip for the Magaliesberg Quartzite (18, 20, 24 and 28 degrees). Unless the dip of the quartzite decreases northwards therefore, this discrepancy indicates that a similar type of overlap situation, such as that exposed (in profile) against the floor to the east, exists below the present erosion level. That is, the contact of the Layered Suite and floor is not conformable. From geometrical considerations this in turn implies the existence further northwards, at greater depths, of lower critical zone or even lower zone rocks.

Along the contact zone of the Rustenburg Layered Suite and the floor, two distinct lithologies occur. A fine-grained gabbronorite (chapter 5.1.1) and a coarse-grained, quartz bearing gabbronorite (chapter 5.1.2). Although occurring as sparse xenoliths at stratigraphically lower levels, i.e. within the quartz-gabbronorite just east of the Brits Graben, the fine-grained variety only appears in abundance at a stratigraphic level coinciding approximately with the level at which abundant cumulus plagioclase first appears in rocks of the Rustenburg Layered Suite. The quartz-gabbronorite effectively forms the contact zone adjacent to the Rustenburg Layered Suite throughout the entire area.

South of Brits, poorly exposed, small, pegmatitic bodies occur. These are similar to the discordant hortonolite dunite pipes described from many parts of the Bushveld Complex, e.g. Wagner and Mellor (1925), Wagner (1929), Coertze (1974), Viljoen and Scoon (1985). However, as emphasised by the last authors, Wagner initially recognised two types of occurrence, i.e. platiniferous and non-platiniferous. In the former, magnesian dunite is associated with the hortonolite dunite whereas in the latter, non-platiniferous occurrence, pegmatitic wehrlite and clinopyroxenite are common associates. In the area under investigation Coertze (1974) has already given an account of the larger pipe adjacent to the Brits-Silkaatsnek road, in which a large proportion of diallagite (clinopyroxenite) occurs. This rock type is also characteristic of the other smaller occurrence which is not shown on previous maps. Because of their probable non-economic potential and previous description of the larger pipe, these rock types were not investigated in detail.

Dykes of syenite and gabbro (sometimes composite) obliquely cut the Rustenburg Layered Suite in the western part of the area. On previously published maps they have a general trend towards the alkaline Pilanesberg Complex, further northwest. Cousins and Feringa (1964) noted that similar dykes are associated with considerable displacement of ichromitite layers . However consideration of the outcrop shape of the dyke, just west of the larger dunite pipe (Fig. 1.1; Folder 1) suggests that in some cases at least, this is a passive, rather than an active association, in that such dykes are probably intruded along pre-existing fault planes.

3.   THE FLOOR ROCKS

3.1   THE SILVERTON SHALE

This formation of the Pretoria Group is very poorly exposed, being represented by a few sparse, rubbly, outcrops or more commonly, loose blocks of hornfels on the scarp slope of the Magaliesberg. The only large exposure of the Silverton Shale is in the deeply weathered road cutting at Hornsnek. Nevertheless, despite the poor quality of the exposure, flaser bedding and other relict sedimentary structures are still clearly visible. A few 'kernels' of spheroidally weathered material at this locality proved to be hornfels, possibly of local origin due to sill intrusion, otherwise the rest is apparently deeply weathered shale.

Further west, in the Silkaatsnek region, outcrops of the Silverton Shale are much fresher and consist entirely of hornfels, although retention of sedimentary layering in these rocks, is widespread. This layering is due to slight alternations in grain size and/or composition and even signs of graded bedding are observed.

In hand specimen these dark grey to black hornfelses are finely banded, fine grained to aphanitic rocks, which precludes any recognition of groundmass mineralogy. However, abundant porhpyroblastic cordierite, particularly in the coarser grained, felsic, layers leads to a pronounced, pin-prick like, pitting of the weathered surface. At two other localities (Silkaatsnek and just north of the Hartbeespoort Dam) tiny (less than 1 mm diameter) pink andalusite porphyroblasts were noted. Thin section petrography is given in chapter 3.3.

3.2   THE MAGALIESBERG QUARTZITE

This massive, predominantly orthoquartzitic formation is very uniform throughout the area. Thin intercalations of impure quartzites and beds of pelitic and calcsilicate hornfels do however occur, particularly in the upper part of the sequence. The northerly outcrops, south of Ga-Rankuwa, are predominantly orthoquartzite, although below these 'ridge formers' impure quartzite and several thin (< 2m) layers of hornfels are also found.

Sedimentary structures, including ripple marks, trough cross bedding and mudcracks are common in this formation and are well described elsewhere, e.g. Hiemstra and van Biljon (1959), Button (1976). In places these structures are virtually obliterated by the development of a coarse grained (5-8 mm) granular, recrystallisation texture (Fig. 3.1). This texture, first described by Mellor (1903, quoted in Hall and du Toit, 1923) is restricted to the very pure quartzite layers and is particularly well developed in the northerly outcrops near De Wildt, the smaller xenolithic bodies and the main outcrop in the western part of the area. Elsewhere, the original sedimentary structures are unaffected, grain size is much finer (.5 - 1 mm) and a 'sugary' granular texture is observed. In some outcrops near the base of the northerly bodies, a peculiar spotted texture is developed consisting of some 5 to 10 per cent biotitic mottles (3 - 5 mm across) distributed evenly throughout the granular groundmass.

The pelitic hornfelses in the upper part of the formation comprise two types: banded and massive. The banded variety is identical to that of the Silverton Shale whereas the massive variety is coarser grained with abundant biotite visible on the fresh, black, fracture surfaces (despite the coarser grain size, the term hornfels is retained for these contact metamorphosed rocks). Relict sedimentary features are also absent in the massive hornfels although whether this lack of structure is original, or due to an increased degree of metamorphism (due perhaps to the proximity of basic sills) could not be established in the field, owing to poor exposure.

Outcrops of hornfels are predominantly of the massive type in the eastern part of the area (i.e. east of Silkaatsnek) while banded hornfels predominate in the west. Outcrops of banded hornfels, intercalated with banded calc silicates, are well exposed just east of the Hartbeespoort fault. Both rock types also occur as numerous xenoliths within the quartz-gabbronorite just north of this region. Whether the geographical distribution of (pelitic) hornfels type is an artefact of exposure, related to differing degrees of metamorphism, or an original stratigraphic feature, is not clear.

The calc silicates are typically serpentinised and banding appears to be due to a combination of grain size variation, compositional differences and degree of serpentinisation. In places fresh, granular, bright green clinopyroxene is observed in these rocks.

Fig. 3.1. Coarse recrystallisation texture in Magaliesberg Quartzite, south of Ga-Rankuwa.

3.3. PETROGRAPHY

3.3.1   Introductory note

Since the banded hornfelses from the upper portions of the Magaliesberg Quartzite are indistinguishable from those of the Silverton Shale, both are described together as banded hornfels in this chapter. In addition, since these hornfelses are variable in grain size, mineral content and to some extent relict structure, by virtue of their sedimentary parentage, their petrography is outlined in a general fashion, except where specific features are considered important.

3.3.2   Pelitic hornfelses

The pelitic hornfelses comprise two distinct types, corresponding to the field divisions outlined above. The fine-grained, banded variety invariably exhibits a typical granular hornfelsic texture (i.e. polygonal granoblastic — Spry, 1967) which is particularly well developed in the coarser, felsic laminae (Fig. 3.2). In contrast, the coarser grained, massive hornfels is dominated by an extensive variety of micrographic textures (Fig. 3.3). In terms of mineral constituents, however both rock types are characterised by abundant quartz and biotite with lesser amounts of feldspar, hypersthene and or cordierite. Variation in mineral proportions and or grain size, typically .2-.5 mm in the massive hornfelses and .05 mm (finer laminae) to .1 mm (coarser, felsic laminae) in the banded hornfels leads to their distinctive differences.

Quartz is scarce in the finer layers of the banded rocks, where it retains its sedimentary outline and occurs as small, isolated, subangular to subrounded grains. In the coarser laminae, recrystallisation is more evident because of the mutual interference of quartz-quartz and quartz-plagioclase grains. Even so, expected 120 degree triple junctions between the felsic grains are not common as they appear to be modified by the occurrence of minute scales of biotite along grain boundaries.

In the coarser grained, massive hornfels quartz normally occurs as part of the micrographic intergrowths (Fig. 3.3) or more rarely as larger, irregularly shaped grains.
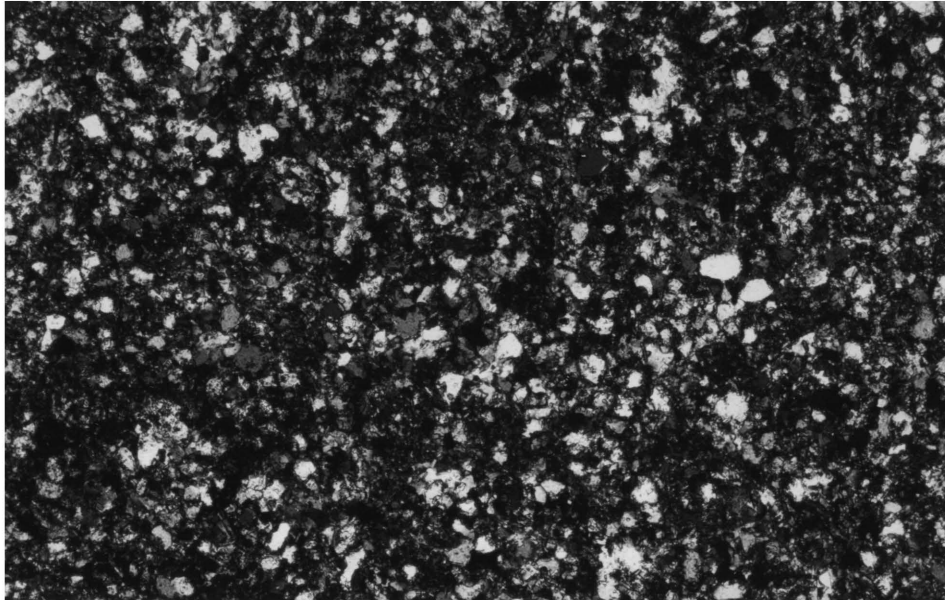
O.5 MM

Fig. 3.2. Polygonal granoblastic texture in banded hornfels. Abundant, minute, biotite scales occur between the felsic grains. Crossed polars.
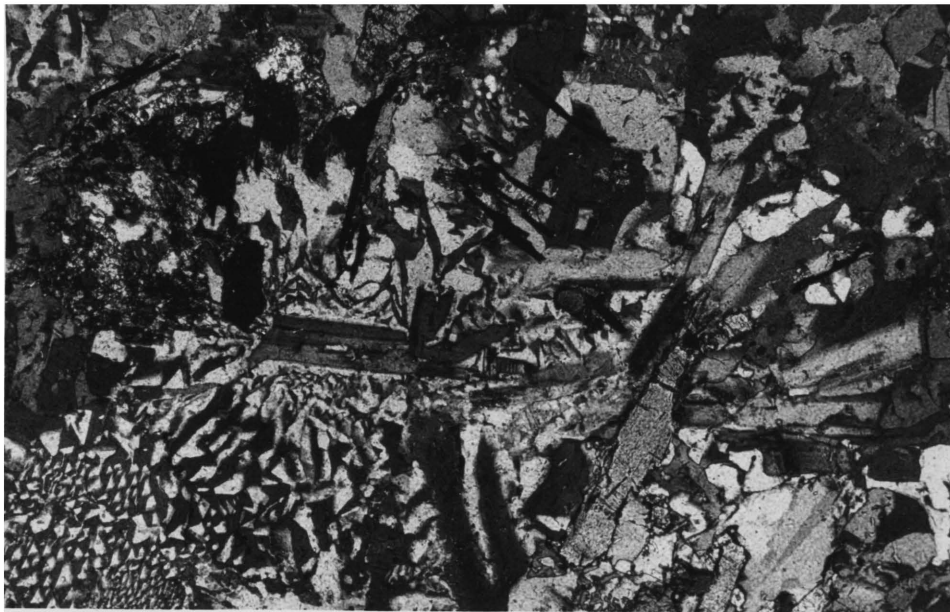
O.5 MM

Fig. 3.3. Micrographic texture in the coarser grained hornfels. Note graphite needles, top centre. Crossed polars.

<u>Biotite</u> is the sole or major groundmass mineral in the finer grained layers of the banded hornfels. Here it occurs as small red brown to pale brown pleochroic, scaly crystals exhibiting a decussate texture (Harker, 1932). In some sections however, biotite shows a relict preferred optical and dimensional orientation, parallel to the original bedding. In the coarser grained layers the modal proportion of biotite is much lower and its habit is similar to that in the massive hornfels.

In the massive hornfels similarly coloured biotite occurs as small aggregates and flakes, often showing pleochroic haloes around included zircons. These aggregates and flakes are randomly distributed in the thin sections, between the micrographic intergrowths.

Biotite may also occur as irregular grains marginal to and replacing hypersthene and is widespread as inclusions in cordierite.

<u>Plagioclase</u> is absent in the finer grained laminae of the banded hornfels while in the coarse grained laminae it occurs as sparse, polysynthetically twinned crystals, intergrown granoblastically with quartz. Limited optical examination suggests core compositions in the $An_{30} - An_{40}$ range, although normal zoning is present. In the massive hornfels, plagioclase is much more abundant. It typically occurs as rod-like to tabular crystals, often with a 'partially digested' appearance in which the irregular crystal outlines grade into micrographic intergrowths with quartz. A vague radial or fan-like arrangement of plagioclase is also observed in some thin sections. Optically determined core compositions are similar to those of plagioclase in the banded hornfels.

<u>Cordierite</u> is abundant and along with biotite, forms the bulk of the finer grained layers of the banded hornfels. Here it exhibits a nodular texture (Spry, 1967), occurring as spongy, low relief porphyroblasts, densely packed with minute biotite flakes (Fig. 3.4.). In the coarser grained laminae this texture may also prevail but in other examples cordierite resembles that in the massive hornfels. In this case it occurs as discrete rounded crystals lacking inclusions and showing complex (sectorial) twinning (Fig. 3.5). Pinitic retrogression was noted in two samples.
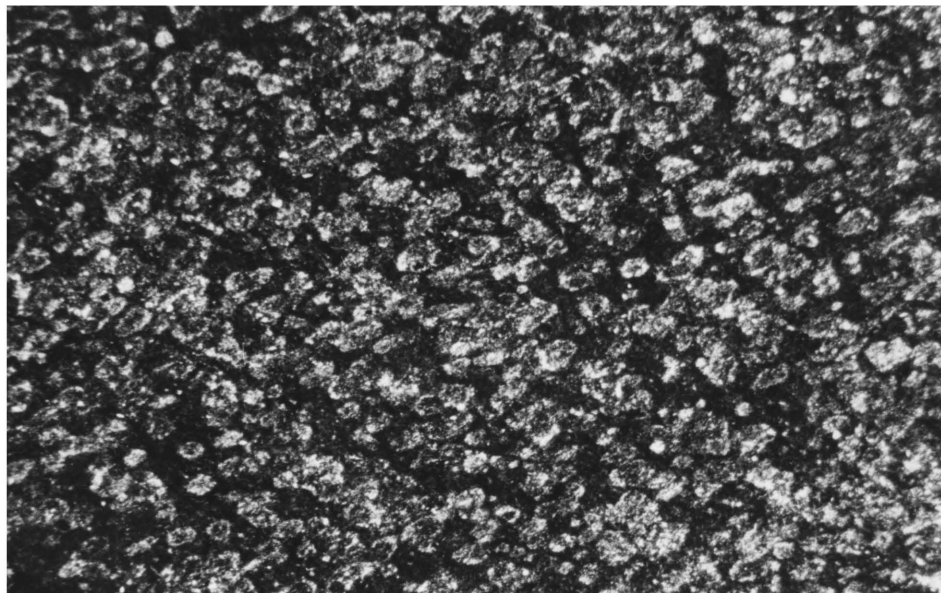
1 MM

Fig. 3.4. Nodular cordierite in the finer grained laminae of the banded
hornfels. The groundmass consists almost exclusively of biotite. Crossed
polars.
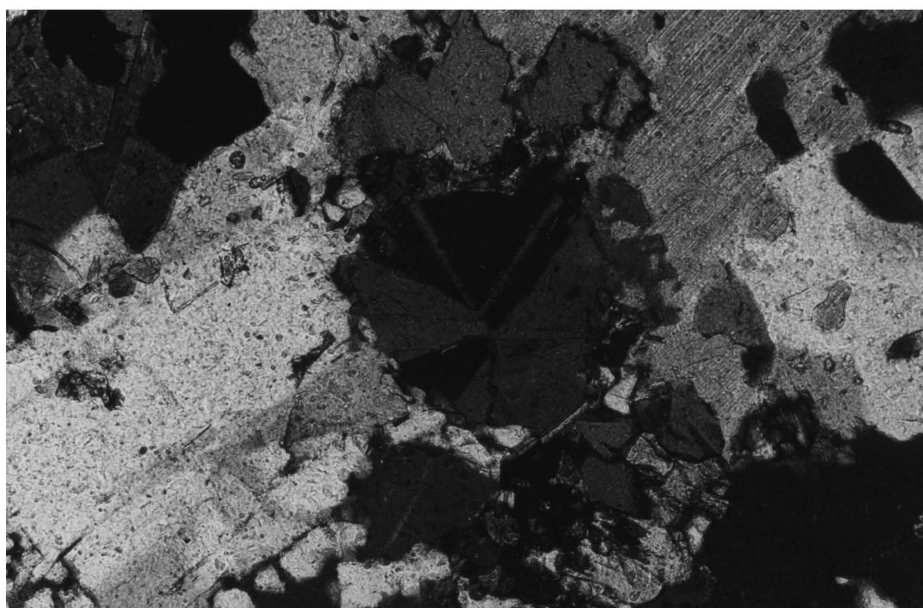
0.20 MM

Fig. 3.5. Cordierite porphyroblast (centre) exhibiting complex sectorial
twinning. Crossed polars.

Hypersthene characteristically occurs in hornfelses from the western part of the area, although it was noted at two localities in the central part of the area. In most types of hornfels the mineral typically occurs as ragged, anhedral to subhedral grains, partially retrogressed to biotite. In some banded varieties it may occur as diffuse patches, which still however maintain optical continuity throughout. In some of the massive hornfelses and also in the banded hornfelses occurring as xenoliths within the quartz gabbronorite, hypersthene occurs as subhedral stubby prisms. In this case the mineral is distinctly pleochroic from pale grey-green to pale pink.

Andalusite occurs as small granular porphyroblasts in two specimens of banded hornfels in the western part of the area (chapter 3.1). The grains are irregular to rounded in shape, while a rim of biotite is also characteristic (Fig. 3.6).

Microcline posseses a similar habit and mode of occurrence to plagioclase but is generally much less abundant, having been observed in only a few thin sections of banded hornfels.

Actinolite occurs as colourless to very pale green pleochroic grains with a high birefringence. It replaces biotite and hypersthene in places.

Graphite is fairly ubiquitous, occurring in two modes. In the massive, micrographic textured hornfels, distinct needles of graphite occur, (Fig. 3.3) while in the banded hornfels fine, dusty granules lying along the bedding are tentatively identified as graphite.

Magnetite is widespread but rarely occurs in any abundance. Rounded, irregular to skeletal grains are typical.

Pyrite occurs as sparse euhedral to anhedral crystals often lying in the bedding plane, as defined by the coarser felsic layers, in the banded hornfels.

3.3.3 Calc Silicates

Of the nine thin sections of calc silicate examined, four are totally serpentinised, with little sign of relict textures (Fig. 3.7) while the other five consist of virtually monomineralic, polygonal granoblastic aggregates of
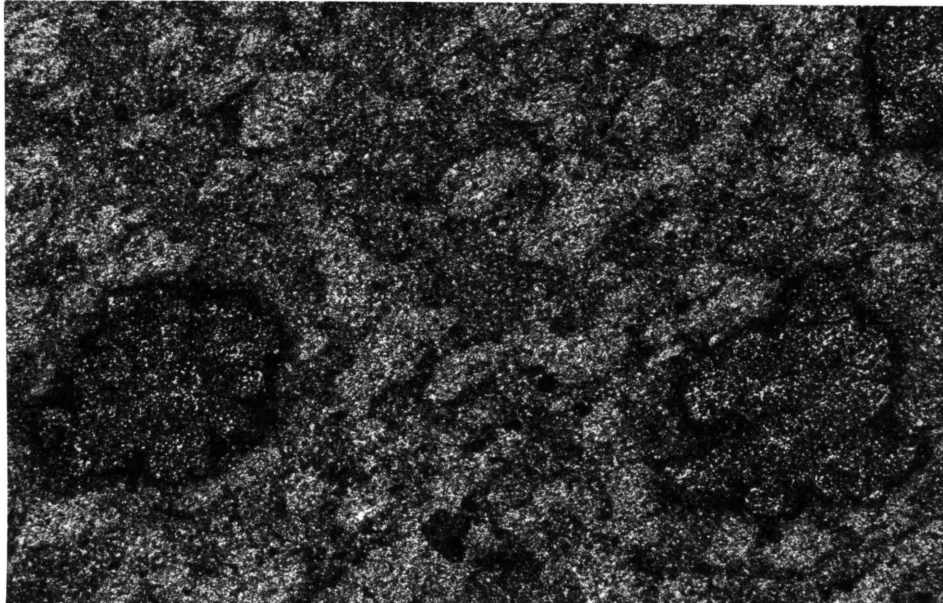
0.5 MM

Fig. 3.6. Andalusite porphyroblasts in the finer grained laminae of the banded hornfels. Paler grey mottles in the groundmass comprise spongy cordierite porphyroblasts. Both sets of porphyroblasts have partially excluded biotite during growth, leaving dark rims around the respective crystals. In places, incomplete exclusion from the andalusite has resulted in the incipient development of chiastolitic texture. Crossed polars.

clinopyroxene (Fig. 3.8). Grain size variation in these five sections defines the macroscopic layering seen in hand specimen. Serpentinised samples consist of a network of antigorite within which occasional relict clinopyroxenes may occur. These clinopyroxenes may in turn be enclosed by actinolite in an uncharacteristic poikiloblastic habit.

The clinopyroxene in the fresher samples is only locally affected by serpentinisation, usually in zones parallel to the megascopic layering (Fig. 3.8). Elsewhere the mineral exhibits extinction angles similar to diopside but without going to full extinction. Instead an anomalous 'Berlin Blue' colour is produced at 'extinction', typical of the calcium-alumina rich clinopyroxene, fassaite (L.J. Hulbert, pers. comm.). In addition, qualitative spectra obtained on an SEM-EDS system from 10 spot analyses, all indicated relatively high alumina contents relative to diopside, further supporting this identification. Fassaite bearing calc silicates have also been described from the eastern lobe of the Bushveld Complex (Willemse and Bensch, 1964).
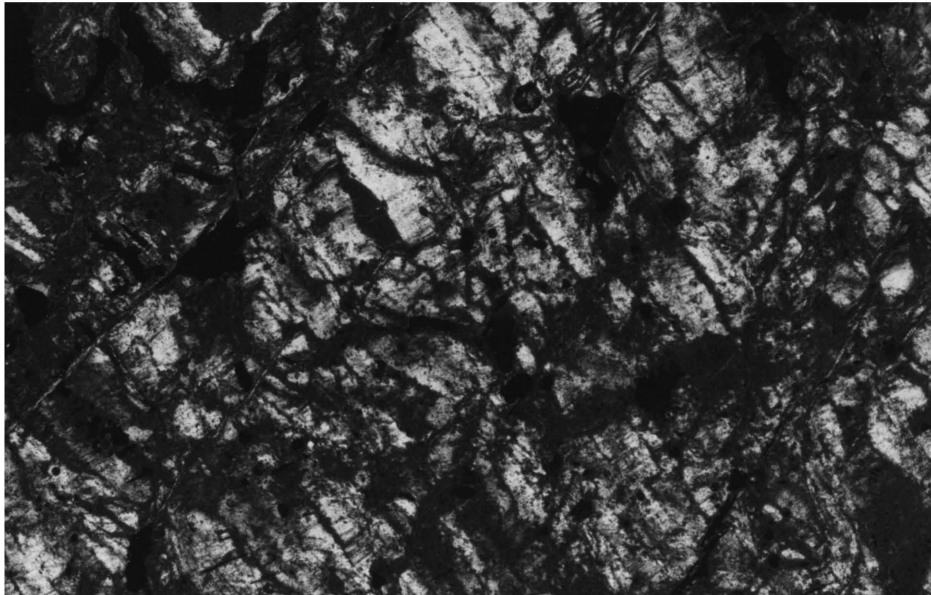
0.5 MM

Fig. 3.7. Serpentinised calc silicate from within the quartz gabbronorite. Crossed polars.
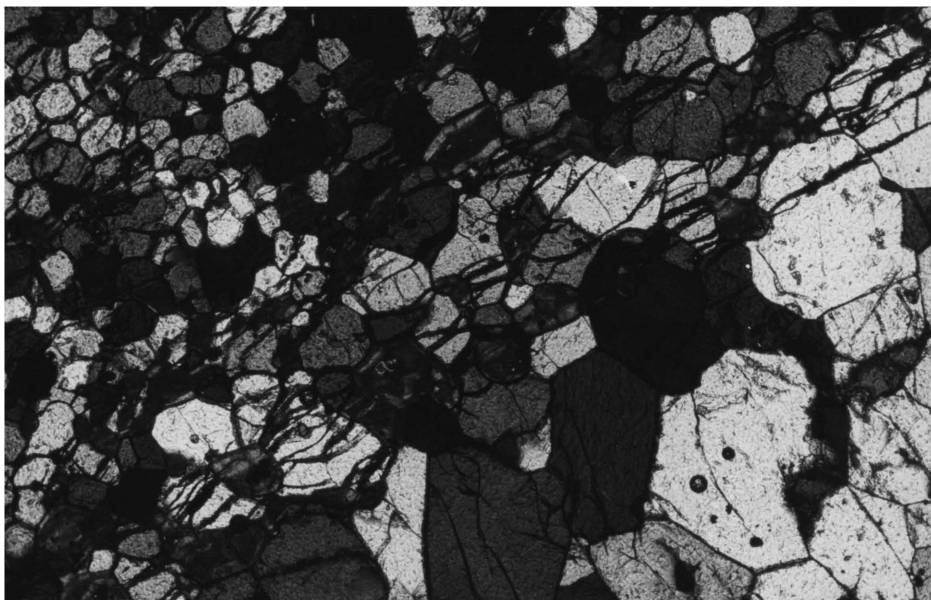
0.5 MM

Fig. 3.8. Polygonal granoblastic aggregates of clinopyroxene in calc silicate. Note grain size variation which defines macroscopic layering and partial serpentinisation (bottom right) which enhances this feature. Crossed polars.

4.   THE RUSTENBURG LAYERED SUITE

4.1   GENERAL INTRODUCTION

The Rustenburg Suite has been previously subdivided by various authors into a series of zones and sub-zones, e.g. Hall (1932), Schwellnus et al. 1962, Wager and Brown (1968), Willemse (1969) and Coertze (1974), (Fig. 4.1). Because of the varied criteria applied by different authors in the demarcation of the subdivisions, the nomenclature has become confused and correlations are not always possible. Consequently a more recent attempt to standardise nomenclature was published by the South African Committee for Stratigraphy (SACS, 1980). In this classification the zonal nomenclature was abandoned and formal names were given to rock units according to the scheme proposed by Sohl (1977, Fig. 4.1, Fig. 4.2).

Subdivisions within this scheme (Fig. 4.2) were based largely on the first appearance of specific 'cumulus minerals' as for example defined by Wager et al., (1960).

However, since this nomenclature has also not, to date, been generally adopted[1], both the formal and the informal zonal divisions previously in use are retained here. This is because the broad informal zonal divisions are essentially based on the same criteria as that of the formal divisions and are therefore easily correlatable. Thus, the (informal) pyroxenite or lower, and anorthosite or upper, subzones of the critical zone, may be correlated with the Ruighoek Pyroxenite and Mathlagame Norite-Anorthosite respectively. Similarly the lower part of the main zone exposed in the study area, is correlatable with the Pyramid Gabbro-Norite of the formal nomenclature.

A generalised stratigraphic column is shown in Figure 4.3. This column was compiled largely with the aid of 3 200 m of borehole core drilled in the area south of Brits. African Selection Trust Exploration (Pty) Ltd (A.S.T.E.) generously allowed the author to sample this material and to have access to

---

[1] See for example Economic Geology volume 80, (1985), as well as the more recent debate by Kruger (1990), Mitchell and Scoon (1991) and the reply by Kruger (1991).

Subdivision and nomenclature of various authors						
Hall (1932)	Lombaard (1941)	Schwellnus et al. (1962)	Wager and Brown (1967)	Willemse (1969)	Cameron (1970, 1971)	Coertze (1974)
Upper Zone	Upper Zone	Ferrogabbro	Upper Zone	Upper Zone	Upper Zone	Ferrogabbro Unit
..	Main Zone					
Main Zone				Main Zone	Main Norite Zone	Gabbro Unit
(uncertain — not clearly defined)		Leoloberg Gabbro	Main Zone			
Critical Zone	Critical Zone	Paschaskraal Norite with intrusive sheets of pegmatitic feldspathic pyroxenite and porphyrite Winnaarshoek Pyroxenite	Critical Series	Critical Zone	Critical Zone	Porphyritic Pyroxenite Unit
						Norite Unit
						Anorthosite Unit
Tranisition Zone	Basal Zone	Chromiferous Pyroxenite with intrusive sheet of peridotite	INTEGRATION STAGE / Basal Series	Basal Zone	Transition Zone	PYROXENITE UNIT / Harzburgite Unit
						Harzburgite Unit
					Lower Zone	
Basal or Chill Zone	Norite-Diabase Zone	Hendriksplaats Norite	Marginal Zone	Chill Zone (Maruleng norite)		Basal Norite Unit

Fig. 4.1. Previous classifications of the Rustenburg Layered Suite of the Bushveld Complex. Reproduced from SACS, (1980, p 234).

The more important lithological units in the western part		Approx. thickness (m)	
Subdivision by SACS	Lithology	E Bushveld	W Bushveld
Bierkraal Magnetite Gabbro	Magnetite gabbro with layers of magnetitite and anorthosite	1 000 / 750 / 250	1 700
Pyramid Gabbro-Norite	Gabbro and norite with interlayered anorthosite	800 / 1 500 / 1 200	2 700 to 4 400
Mathlagame Norite-Anorthosite	Alternating layers of leuconorite, anorthosite, pyroxenite and chromitite	1 000	450
Ruighoek Pyroxenite	Feldspathic pyroxenite with chromitite layers	500	480
Tweelaagte Bronzitite	Pyroxenite	300	50
Groenfontein Harzburgite	Alternating layers of harzburgite and pyroxenite	500	400
Makgope Bronzitite	Monomineralic pyroxenite	400	140
Eerlyk Bronzitite	Feldspathic pyroxenite with discontinuous harzburgite and norite layers near base	400	380
Kolobeng Norite	Norite and quartz norite	up to 100	up to 240

Fig. 4.2. Subdivisions of the western Bushveld Complex. Reproduced from SACS (1980, p235).
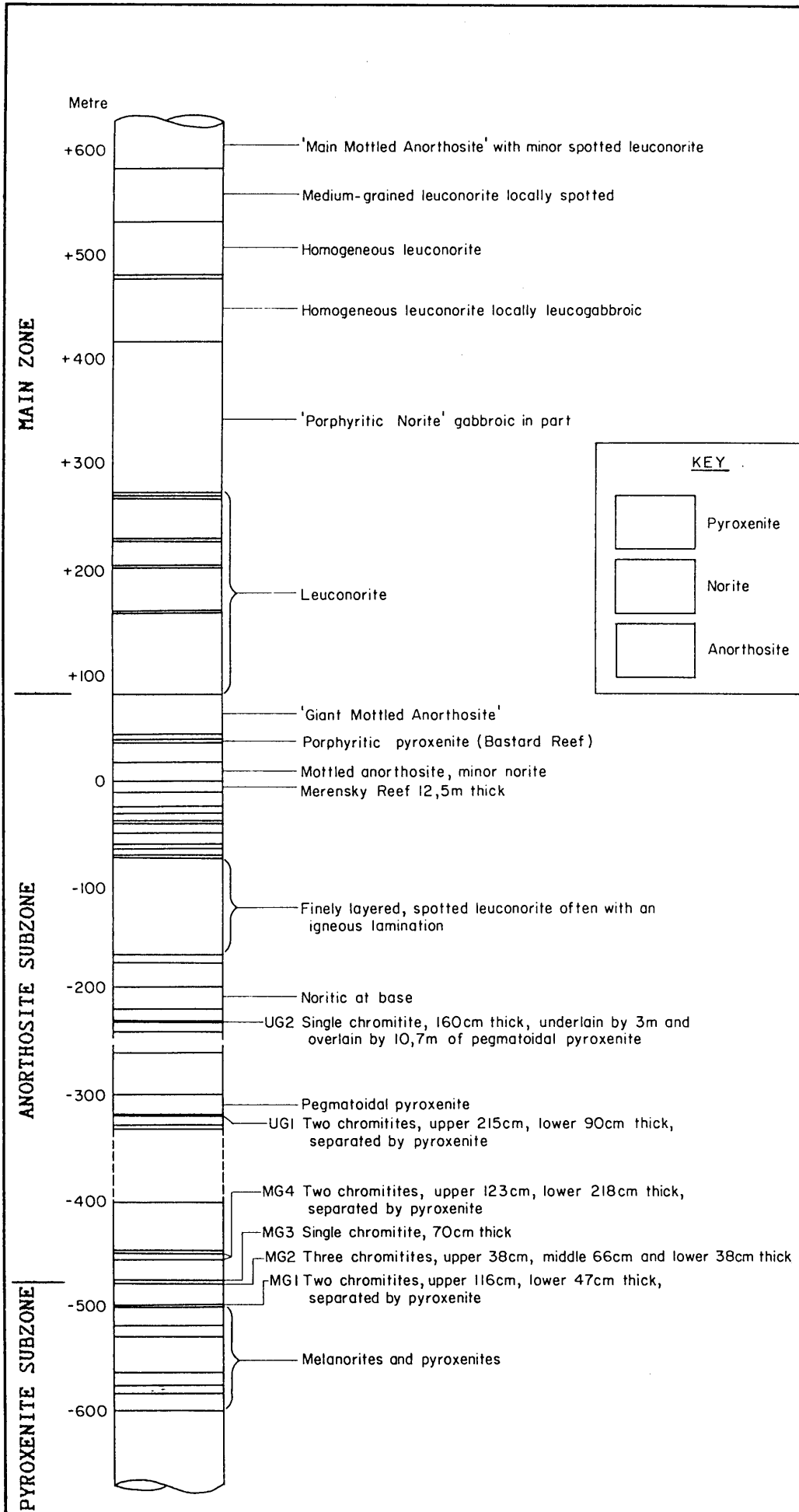
Fig. 4.3. General Stratigraphy of the Rustenburg Layered Suite south of Brits, as compiled from borehole data.

borehole logs, maps, etc. A borehole location map is also shown in Figure 4.4. Actual sample numbers used in the text and in Appendix 4 refer to approximate depths for any given sample, e.g. K13-200 refers to a sample from borehole K13 at an approximate depth of 200 m.

The stratigraphic section shown in Figure 4.3 is considered to represent the maximum development of the Rustenburg Layered Suite in the area, since the succession clearly thins eastward and wedges out against the floor (Fig. 1.1; Folder 1). Nomenclature follows Streckeisen (1976) as regards rock compositions but qualifying terminology peculiar to layered intrusions e.g. spotted anorthosite, mottled anorthosite, etc. is used in the sense of Willemse (1969). Thicknesses in Figure 4.3 are however only approximate, since the boreholes did not penetrate the entire sequence. Gaps in the succession were estimated from dip measurements on the core or strike-parallel extrapolation from the data of Cousins and Feringa (1964) in the Marikana area further west. According to Cousins and Feringa the succession thickens eastward from Marikana and this has been taken into account in the estimations. No correction for differences in dip between boreholes was applied, as the low dip angles (10-15) and uncertainties in extrapolation render this superfluous.

Since no samples of the major chromitite layers or Merensky Reef could be obtained, information on these units was taken from A.S.T.E. borehole logs. The uppermost part of the section was constructed from outcrops exposed in the Crocodile River south of Brits.

4.2   THE RUIGHOEK PYROXENITE AND MATHLAGAME NORITE-ANORTHOSITE (THE LOWER AND UPPER CRITICAL ZONE)

4.2.1   Subdivisions of the critical zone

Layered rocks of the critical zone are divided into lower and upper divisions on the basis of the first appearance of cumulus plagioclase in the sequence, which typically occurs above the lower two chromitites of the Middle Group Layers (Cameron, 1963, 1969, SACS, 1980). Thus, by definition the lower subdivision, the Ruighoek Pyroxenite (the pyroxenite subzone), comprises rock types with either orthopyroxene or chromite or both as cumulus minerals,

---

[1]Chromitite layers in the text are numbered according to the notation of Cousins and Feringa (1964))
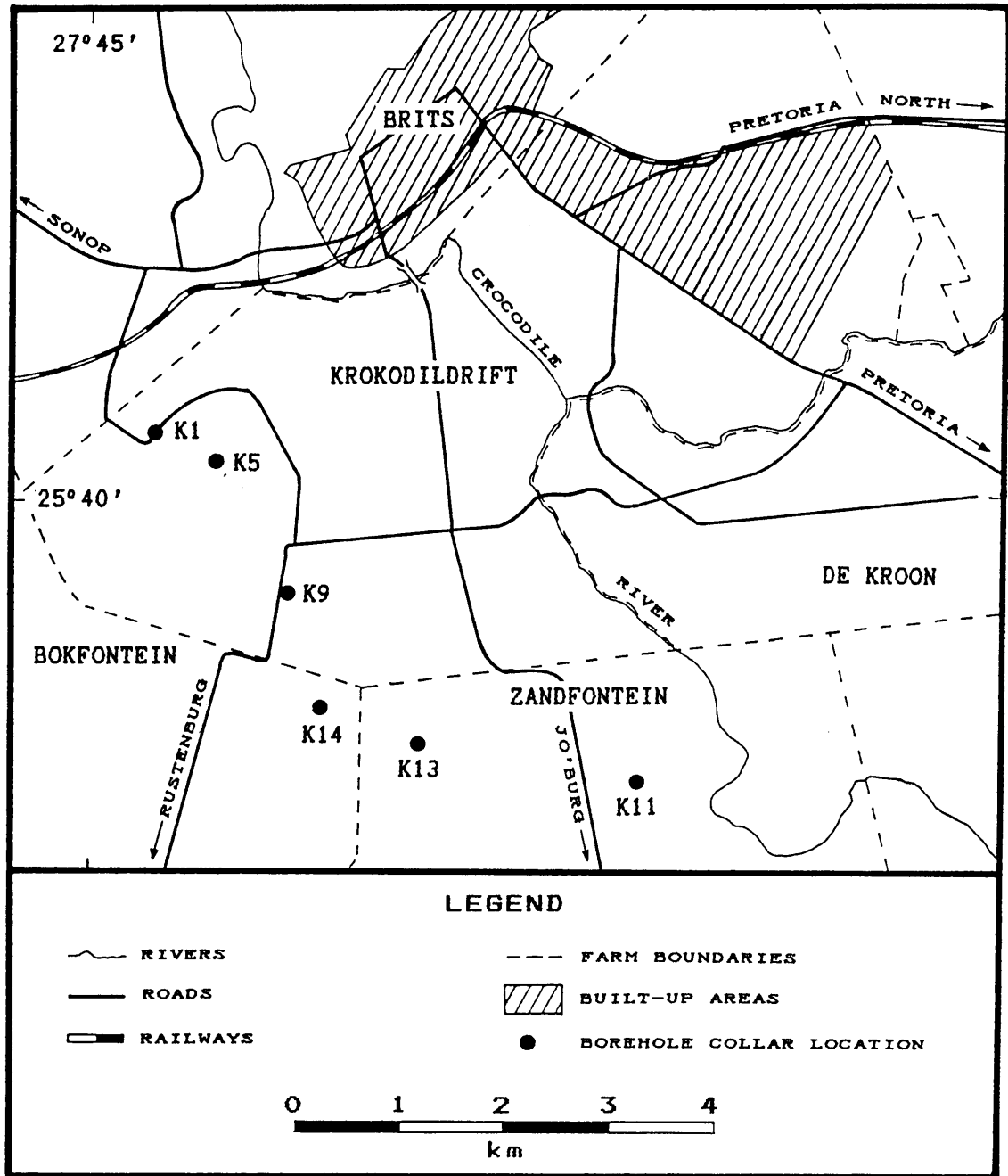
Fig. 4.4. Sketch map of borehole collar locations (after A.S.T.E. (PTY) Ltd.). All holes are vertical.

while the upper subdivision the Mathlagame Norite-Anorthosite (anorthosite subzone) comprises rocks in which orthopyroxene, chromite or plagioclase (or any combination of these three) are cumulus phases. Cumulus clinopyroxene may also be present in some of the rocks near the top of the anorthosite subzone.

Note however (chapter 6) that there is evidence from the present study of cumulus plagioclase occurring beneath the MG2[1], i.e within the Ruighoek Pyroxenite (pyroxenite subzone). This feature was also noted by Hatton and Von Gruenewaldt (1985) in the Rustenburg-Marikana area. The top of this subzone was therefore taken as the top of the MG 2, in order to conform with the general subdivisions used elsewhere in the Bushveld Complex.

4.2.1.1   The Ruighoek Pyroxenite (pyroxenite subzone)

The pyroxenite subzone occupies a wedge-shaped portion of the area east of the Hartbeespoort Fault. It also occurs as downfaulted rectangular blocks in the Brits Graben and extends west of the Kommandonek fault. Outcrops of this subzone are extremely sparse and are restricted to the more resistant, massive feldspathic pyroxenites. The succession can only be determined with any degree of accuracy from borehole information but unfortunately none of the boreholes entered the marginal rocks, so exact thicknesses are unknown. As shown in Figure 4.3, only about 120 m of the succession below the MG 2 is known in any detail. Apart from the presence of cumulus plagioclase another notable feature of this succession is the absence of the LG 6 (Lower Group) chromitite layer. The economically important LG 6 layer normally occurs within a 100m interval below the MG 1 (Middle Group) chromitite (Cameron, 1964; Hatton and von Gruenewaldt, 1987), however no chromitite layers were encountered in the ASTE boreholes down to a depth in excess of 100 m below the MG 1. Some recent drilling has intersected a few thin chromitite layers below the MG 1 (G. von Gruenewaldt, pers. comm.) but the massive development of the LG 6 and other lower group chromitites is clearly absent in the study area.

The MG 1 chromitite, which overlies the lower 100 m of the feldspathic pyroxenite-melanorite succession, is in fact divided into two separate units. The lower chromitite is approximately 50 cm thick while the upper attains a thickness of just over 1 metre, being separated from the lower unit by a metre thick layer of pyroxenite. Approximately 18 metres of homogeneous feldspathic pyroxenite separates the upper MG 1 chromitite from the three thin layers

(0.38 m, 0.66 m and 0.38 m thick, respectively) comprising the MG 2 chromitite unit. Above the uppermost MG 2 chromitite is a 5-6 metre thick mottled anorthosite unit which elsewhere contains the first occurrence of cumulus plagioclase in the sequence and thus forms the base of the succeeding anorthosite subzone. This junction is also elsewhere marked by discordant features (van Rensburg, 1962; Cameron, 1963, Cameron and Desborough, 1969; Sharpe, 1980) but unfortunately the borehole core intersecting this junction was unavailable for the present investigation.

4.2.1.2   Mathlagame Norite-Anorthosite (the anorthosite subzone)

The majority of the layered rocks exposed in the study area belong to the anorthosite subzone, occupying a broad belt of flat-lying country in the west of the region (Fig. 1.1; Folder 1). Outcrop, in contrast to the underlying subzone, is moderately abundant but no distinctive marker horizons are exposed. Layering throughout the succession is extremely well developed and this, along with the abundant development of leucocratic rocks, most notably spotted and mottled anorthosites and leuconorites, is very characteristic. The thickness of this subzone is estimated at 550 m.

The MG 3 and MG 4 chromitite layers which occur 6 m and 25-30 m respectively above the top of MG 2 (i.e. the base of the subzone) are separated by a series of alternating pyroxenitic and melanoritic rocks. The MG 3 comprises a single 70 cm thick chromitite while the MG 4, like the lower middle group layers, is split into two separate units by a 3-4 m thick pyroxenite selvage. The lower unit of the MG 4 is just over 2 m thick, while the upper unit is 1.2 m thick.

An estimated 100-125 m of predominantly noritic rocks occur between the MG 4 and UG 1 chromitite layers. The latter is however underlain by 8 m of feldspathic pyroxenite with at least 5 m of mottled anorthosite below that. An unusual feature of the UG 1 unit - which elsewhere is a most distinctive series of thin chromitites within anorthosite (Wager and Brown, 1968) - is the occurrence of a pyroxenitic, locally pegmatitic unit, approximately 20 m thick, which overlies the upper chromitite layer.

The UG 1 unit is further unusual in that its two chromitites (± 50 cm lower, ± 2 m - upper) are separated by 2 m of pyroxenite. However, it is possible that

the pegmatitic pyroxenite overlying the UG 1 is merely a local phenomenon encountered in the borehole, as Cousins and Feringa (1964) for example, note that elsewhere, in the vicinity of faults, discordant bodies of pegmatitic pyroxenite occur in association with chromitite layers. However, the paper by Coertze (1970) contains a photograph of the UG 1 unit, west of the present area, in which the silicate cumulates, although more typically leucocratic than in the present case, look distinctly pegmatitic.

An estimated 100 m of predominantly noritic rocks overlie the UG 1, of which ± 25 m is unknown from the boreholes. A 1.4 m thick chromitite layer, the UG 2, caps this succession which is overlain by 8 - 9 m of pegmatitic pyroxenite. This again is unusual in that normally the footwall and not the hanging wall of the UG 2 is pegmatitic. However three boreholes intersected the UG 2 layer and all had pegmatoid above the chromitite. On the other hand pegmatoid development above the UG 2 is rare and localised in the Crocodile River Mine (G. von Gruenewaldt pers. comm.) so perhaps these boreholes again intersected fault zones. A thick (20 m) unit of mottled anorthosite succeeds the pegmatoidal unit and for most of the 180 - 200 m of succession between the UG 2 and Merensky Reef, mottled and spotted anorthosite alternate with leuconoritic and noritic variants. Finely developed modal layering is particularly prominent in the noritic rocks which form a portion of the section.

The Merensky Reef is unusually thick (±12 m) in the study area consisting largely of sulphide bearing porphyritic pyroxenite which is locally pegmatoidal. Another feature of the Merensky Reef is the absence of the thin chromitite layers, which elsewhere normally occur at the base and top of the pegmatoidal reef below the Merensky pyroxenite, (Cousins, 1969; Kruger and Marsh, 1985).

Approximately 15 m of leuconorite and mottled anorthosite succeed the Merensky Reef, with some 20 m of noritic rocks above this. Overlying these norites is a 1.8 - 2 m thick layer of porphyritic pyroxenite, resembling that of the Merensky reef. This, so called 'Bastard Reef' is succeeded by several metres of leuconorite and this in turn by a 30 - 35 m thick, very prominent mottled anorthosite, with large poikilitic pyroxenes. This 'giant' mottled anorthosite forms the uppermost layer of the 'Bastard cyclic unit', the highest unit in which cumulus chromite is found. By correlation with a similar

---

unit in the eastern bushveld (SACS, 1980) the top of this anorthosite is taken as the top of the critical zone.

Finally, it may be noted that although cumulus clinopyroxene is generally found in the upper part of the anorthosite subzone (SACS 1980), none was observed in any of the samples examined (chapter 6). In fact, in this study clinopyroxene was found to be restricted to rocks some 150 – 200 m above the top of the critical zone, although intercumulus clinopyroxene is widespread in this interval. This may, however, be an artefact of the borehole sampling since Ferguson and Wright (1970) describe cumulus clinopyroxene from below the Merensky Reef in the De Kroon area, south of Brits.

4.3 PYRAMID GABBRO-NORITE (THE LOWER PART OF THE MAIN ZONE)

For 200 metres above the mottled anorthosite overlying the 'Bastard Reef' the succession consists predominantly of spotted leuconoritic, and leucogabbroic rocks with locally developed mottled anorthosites. This sequence is punctuated at fairly regular intervals by several thin (< 5 m) layers of feldspathic pyroxenite.

The 150 m thick 'porphyritic norite' unit with a thin norite unit at the base overlies the topmost pyroxenite. The so-called 'porphyritic norite' is a distinctive unit containing prominent grains of orthopyroxene up to 8 mm in diameter (chapter 6). These grains themselves, which comprise 15 – 25% of the rock, enclose numerous small plagioclase laths.

Modal analysis (chapter 6) shows in fact that parts of the 'porphyritic norite' are gabbroic, due to the presence of cumulus clinopyroxene. This is the lowest level at which cumulus clinopyroxene was noted in the present study. The 'porphyritic norite' is succeeded by approximately 200 m of leuconorites and leucogabbros containing thin layers of mottled anorthosite. The lower 100 m of this succession is finer grained than the overlying 100 m.

The prominent 70 m thick 'Main Mottled Anorthosite' which crops out along the Brits-Rosslyn road lies 200 m above the 'porphyritic' norite and some 550 m above the base of the main zone. This unit represents the top of the section studied in this investigation.

5.   THE MARGINAL ROCKS

5.1   GABBRONORITIC CONTACT LITHOLOGIES

5.1.1   The Microgabbronorite (MGN)

In the eastern part of the area, at stratigraphic levels above the top of the pyroxenite subzone, a rather fine grained rock of gabbronoritic composition crops out, sandwiched between the quartz-gabbronorite and floor rocks.(Fig. 1.1, Folder 1). Scarce outcrops are however found at lower stratigraphic levels, e.g. within the coarse-grained quartz gabbronorite just east of the Hartbeespoort fault.

Despite the occasional presence of metaquartzite xenoliths, evidence of wholescale assimilation is absent, and the microgabbronorite, although varying slightly in grainsize from outcrop to outcrop is fairly uniform over the whole area. Only in a few localities are sparse, anhedral, poikilitic hornblendes seen, possibly indicating small amounts of contamination. At the same localities no other assimilation features are evident, even though at one the contact with metaquartzite can be placed within centimetres (Fig. 5.1). At two other localities, small (< 1 m), sub-angular blocks of a very fine-grained basaltic phase occur in the gabbronorite. These small inclusions show a close-spaced, reticulate, pattern of jointing and veining (Fig. 5.2) similar to that described by Sharpe (1980) for his 'N' chill.

In outcrop the microgabbronorite is fairly distinctive due to its fine grain size, although its mineralogy is generally not discernible in hand specimen. Overall, the fine grain size throughout the unit and apparent lack of interaction with the floor rocks, suggests that the microgabbronorite represents a chilled igneous phase. Furthermore, in some outcrops a 5 mm diameter rosette-like texture is developed, presumably as a result of rapid cooling (See for example, Lofgren (1980)). Moreover, in thin section radiate chill textures are widespread, the rock typically comprising plagioclase feldspar, in excess of equal amounts of ortho- and clinopyroxene, together with lesser amounts of granular magnetite (chapter 6.2.1.1).

Fig. 5.1. Metaquartzite xenolith within the microgabbronorite. The knobbly surface of the latter (right foreground) is due to the occurrence of poikilitic hornblendes.

(Loc. 109)

Fig. 5.2. Reticulate jointing in very fine-grained microgabbronorite.
Approximate width of outcrop face illustrated is 70cm.

(Loc. 160)

5.1.2   The Quartz Gabbronorite

As shown in Figure 1.1 and Folder 1, this rock type effectively forms the contact zone between the Rustenburg Layered Suite and the floor. Contacts are moderately well exposed in places and in all cases are gradational upwards into the overlying subzones of the Complex. This occurs through a gradual decrease in xenolith content and contamination textures, accompanied by a sympathetic increase in the development of cumulate textures. The lower contact of this coarser grained gabbronorite with the underlying chilled microgabbronorite is not exposed. However at two adjacent localities (160 and 161) on the farm Schietfontein 437 JQ, 3.5 km southwest of De Wildt, rather rounded blocks of the microgabbronorite are included in the quartz gabbronorite (Fig. 5.3). There is no obvious chilling of one against the other, but there does appear to be a reaction along the boundary because a thin pyroxenite rind (approx. 1 cm thick) is developed in the finer grained phase (Fig. 5.4).

These observations, together with the several isolated occurrences of the chilled microgabbronorite within the outcrop width of the quartz gabbronorite argues strongly for the later injection of the coarse grained phase. The contact of the quartz gabbronorite with the floor appears concordant in the Hartbeespoort Dam and Brits Graben area, except for some quartzitic and hornfelsic rafts. Further east however the contact rises transgressively, crosscutting the western end of the Middelwater Layered Sill before again becoming roughly concordant with the underlying microgabbronorite and metaquartzite south of Ga-Rankuwa (Fig. 1.1, Folder 1). Although exposure is poor in the crucial central area, this crosscutting relationship is confirmed by two localities (194 and 195) 5 km southwest of De Wildt.

In the area just east of the Brits Graben, the appearance of the quartz gabbronorite differs from that seen further to the northeast where it overlies the microgabbronorite and metaquartzite south of Ga-Rankuwa. In the former area, exposure is relatively good, and the rock type, although obviously contaminated, is fairly homogeneous over a wide area. Pelitic hornfels and calc silicate are often abundant inclusions in the quartz gabbronorite in this region. Further northeast, the gabbronorite becomes somewhat heterogeneous, containing distinct xenocrystic or xenolithic patches of quartz and quartzite together with hornblende, biotite and often magnetite, set in a variable grain sized groundmass (Fig. 5.5, 5.6). Hornfels inclusions are lacking.
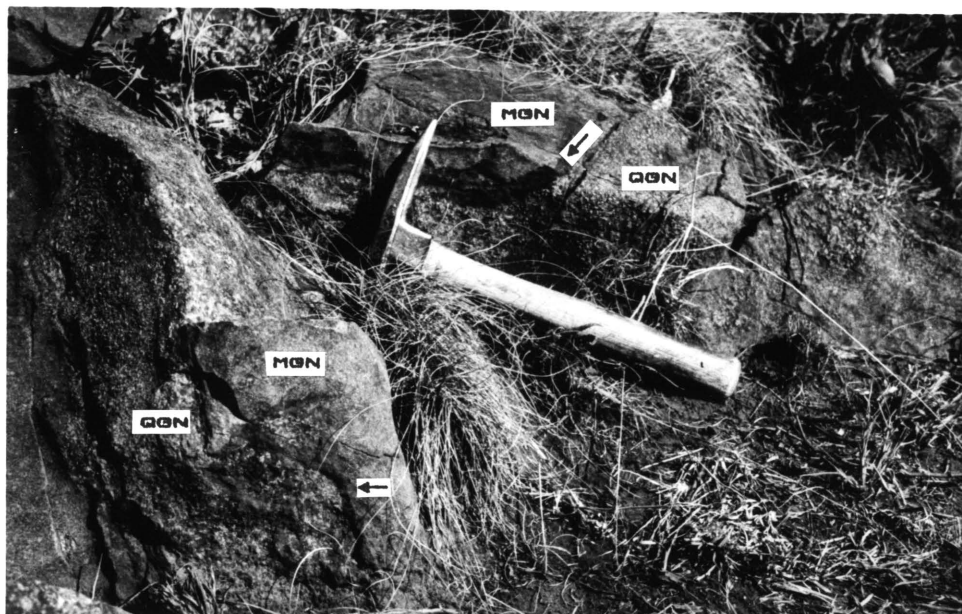
Fig. 5.3. Xenoliths of microgabbronorite in the quartz gabbronorite. Contacts between the two are arrowed.
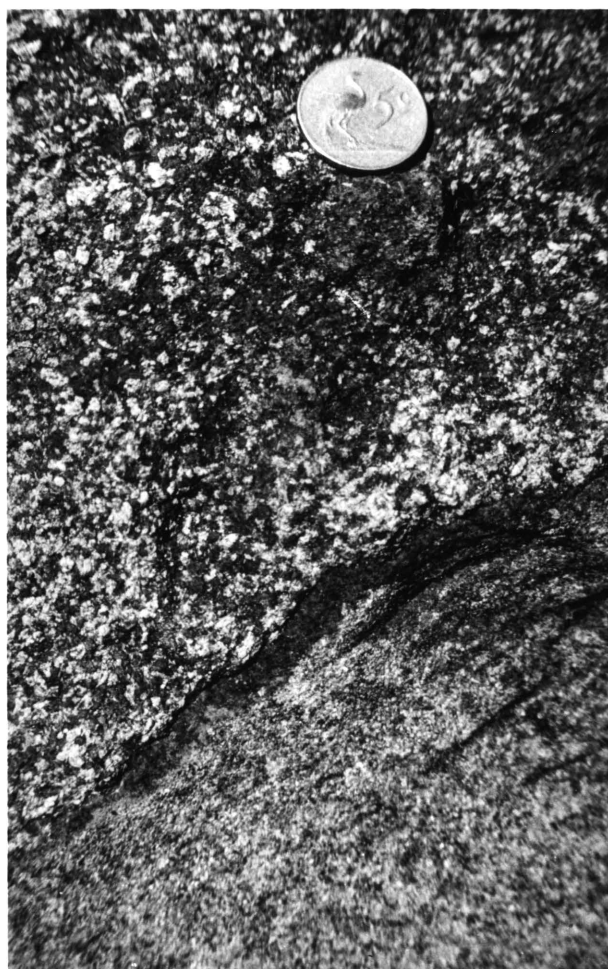
Fig. 5.4. Close-up of the contact between coarse grained quartz gabbronorite and the microgabbronorite. Note the thin pyroxenitic rind developed in the microgabbronorite.

(Loc. 161)

Fig. 5.5. Quartz xenocrysts in boulder of heterogeneous quartz gabbronorite
lying adjacent to the Ga-Rankuwa-Hornsnek road. Coin is 3cm in width.

Fig. 5.6. Close-up of quartz xenocrysts at the same locality as Fig.5.5.
Note the very coarse biotite flakes associated with the xenocrysts and the
presence of hornblende (arrowed).

(Loc. 13)

In outcrop, the rocks east of the graben are somewhat finer grained and less obviously xenocryst bearing, often showing a rather blue-green coloration on fresh surface. In part they resemble some of the marginal rocks of the Middelwater Layered Sill, but are fresher in appearance and characteristically exhibit the growth of coarse biotite flakes, 4-6 mm across, testifying to their contaminated nature. The latter mineral may locally comprise over 10 per cent of the rock, in which case there is often an inhomogeneous, patchy appearance to the outcrop. In cases where abundant xenoliths are found, there appears to be a gradation in grain size linked to the amount of contamination. Thus a variety of finer grained, less obviously contaminated lithologies, are intimately associated with the coarser grained, contaminated material. Some of these finer grained rock types are only slightly coarser than the chilled microgabbronorite. This spectrum of variation, between the microgabbronorite and the coarse grained quartz gabbronorite, is considered significant in view of the proposed model for the origin of the quartz gabbronorite, (chapter 7.7.3).

Hulbert (1983, p.33) also described a zone similar to the quartz gabbronorite, lying adjacent to the critical zone in the Potgietersrus area. Although its origin was not modelled, its field relationships indicate that it had a similar origin to that of the quartz gabbronorite (chapter 7.7.3). In contrast, the 'Hendriksplaats norite' of Willemse (1959), renamed the 'laminated marginal zone' by Sharpe (1981), also appears from published descriptions to be similar to the quartz gabbronorite. However, any correlation of the two units is precluded by their difference in origin (see chapter 7.7.3).

5.2   SILLS IN THE FLOOR

5.2.1   The Middelwater Layered Sill and associated quartzofeldspathic rocks

5.2.1.1   The Marginal Facies

The marginal facies of the Middelwater Layered Sill comprise amphibole bearing lithologies, considered to be metadolerites by the present author and previously grouped under the term diabase (e.g. Nel, 1940, Willemse, 1959). These appear to sheath the cumulate sequence from the country rocks, but outcrop is poor and contacts between the two are not exposed. Boulders and

pebbles in the soil suggest that the contact is gradational and no examples of any other likely 'chill' faces to the sill has been found. In addition, at two localities southwest of Rosslyn, these amphibolitic rocks take on a speckled appearance and grade downwards into relatively unaltered layered rocks. Possibly some of these amphibolitic rocks are metamorphosed cumulates.

Contacts between the marginal facies and country rocks are also unexposed, but appear to be broadly conformable, except for the large xenolith of granophyric material noted above and the larger inclusions of metaquartzite just north of the Magaliesberg dip slopes, (Fig. 1.1, Folder 1).

In outcrop, the marginal rocks lack obvious xenolithic material and are apparently homogeneous, with a blue-green colouration on fresh surface. However, on closer inspection, abundant quartz knots are clearly visible at some localities (Fig. 5.7) suggesting contamination. Relict sub-ophitic textures also appear at some localities, but this may be fortuitous and related to the growth habit of the amphibole. The latter in association with variable amounts of biotite, comprises 40-60 per cent of the rock, with the remainder comprising altered feldspar and granular quartz.

5.2.1.2   The Cumulate Sequence

Layered cumulate rocks underlie a series of low, bush covered mounds, clearly visible on air photographs, in the east central part of the area. Exposure on the farms Vissershoek 435JQ, Middelwater 436JQ and Wildebeesthoek 310JR is relatively good and allows for a reasonable study through the sequence.

The Middelwater Layered Sill is considered to be a singular body, since there are no signs of internal chilling or major intrusive contacts, although the observations outlined below suggests that the whole intrusion may not necessarily have been emplaced simultaneously. Possibly some of the internal structures observed result from vigorous discontinuous magma inputs, while tectonic instability and convection/density currents (Wager and Brown, 1968; Irvine, 1980) may also have been important causal mechanisms.

As already mentioned, both upper and lower margins appear gradational into the presumed, metadoleritic, chill facies and xenoliths are rare. Only at one

Fig. 5.7. Rough - weathering surface of a meta quartz-dolerite sill. Much of the rough texture is due to small quartz knots which stand out as positive features.

(Loc. 21)

locality are a few small (< 1 m), rounded to sub-angular, quartzitic inclusions observed, while elsewhere a larger fragment of amphibolitic rocks occurs within the sill, along with some smaller blocks of a granophyric textured rock. Here again, contacts are hidden. It is possible however, that the amphibolitic 'inclusion' is a more thoroughly metamorphosed version of the mafic rocks, since low-grade metamorphism is widespread within this cumulate sequence.

Rock types that form the main mass of the sill are predominantly norites, within which orthopyroxene is always cumulus, while plagioclase may be either cumulus or intercumulus. Thin streaks and irregular blebs of anorthositic and pyroxenitic material are common (Figs. 5.8, 5.9). Indeed, throughout much of the sill, a rather streaky, discontinuous layering is developed, with the occurrence of thin (< 5 cm) lenticular lamellae, of both mafic and felsic material set in a more 'normal' groundmass. Development of igneous lamination is also widespread. Rarely, thin (20 cm thick), often contorted, anorthositic layers and rootless folds are developed (Fig. 5.10), but these layers are laterally discontinuous.

5.2.1.3 Quartzofeldspathic Rocks

Sparse outcrops of quartzofeldspathic rocks are found overlying the Middelwater Layered Sill. Textures within these rocks range from granophyric through to equigranular, while a peculiar stellate recrystallisation texture is also found in some varieties.

This heterogeneous group of rocks is conformable with the overlying metasediments and underlying meta-igneous rocks. Nowhere are contacts seen, but in some localities there seems to be a gradation between the marginal meta quartz-dolerites and the granophyric varieties. Moreover, there is little evidence of cross cutting relationships, except for an inclusion of the granophyre in the marginal rocks of the Middelwater Layered Sill, just east of the Hornsnek Ga-Rankuwa road. Here again contacts are not exposed, but the granophyre appears to grade upwards into the metabasic rocks which are themselves overlain by granophyric material.
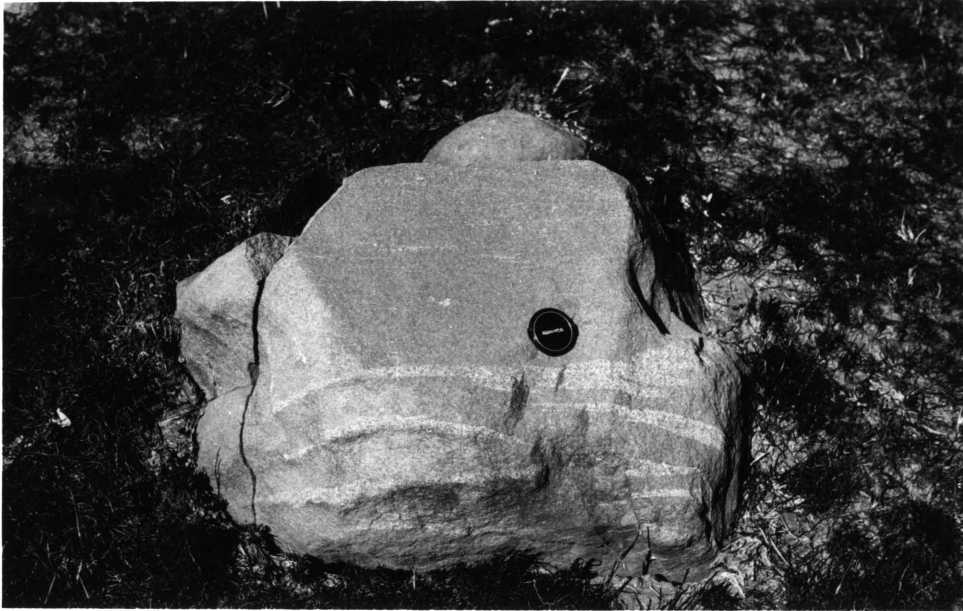
Fig. 5.8. Streaky, discontinous lamellae of anorthositic material in
noritic cumulates of the Middelwater Layered Sill.(Loc. 133)

Fig. 5.9. Irregular blebs and ghosted schlieren of pyroxenitic material in
noritic cumulates of the Middelwater Layered Sill.

(Loc. 128)

Fig. 5.10. Contorted anorthositic layers (slump structures ?) in noritic
cumulates of the Middelwater Layered Sill.

(Loc. 126)

5.2.2   Sills intruding the Magaliesberg Quartzite and Silverton Shale

5.2.2.1   General

Several distinctive suites of igneous rocks occur as concordant sheets within the floor sediments. These sills are difficult to trace laterally with any confidence because of discontinuous outcrop and the sills indicated on the map (Folder 1) and in Figure 1.1 are based on the author's interpretation of available outcrop data. In addition, contacts between the country rocks and sills are rarely discernible, so that thicknesses cannot be estimated with confidence. Few sills however appear to exceed 20 m in thickness. The sill types in the present area may be grouped into the following divisions, which are essentially those recognised by Cawthorn et al. (1981), namely:-

i.   Metadolerites (Diabases)

ii.   Quench textured Micropyroxenites

iii. Pyroxenites and Norites

The former two divisions are volumetrically the most important.

5.2.2.2.   Metadolerites (MD) including meta quartz-dolerites (MQD).

The metadolerites may be divided into two distinct types, on the basis of field appearance. The one type, corresponding to Cawthorn et al.'s (1981) metadolerite division, are rather scarce rock types in this area, being represented by a few isolated outcrops in the Silverton Shale, where contacts are unexposed. In outcrop, such rocks are usually greenish in colour and exhibit quite a variation in grain size between individual sills. Thus in some, a rather medium to fine grained size predominates and their mineralogy is hard to determine. In others, relict sub-ophitic textures may be seen comprising altered plagioclase in a matrix of amphibolitised pyroxene. At one locality one of these sills exhibits the growth of abundant, randomly orientated, amphibole blades, identical to those shown in Figure 3c of Cawthorn et al. (1981).

The other lithology, considered to be contaminated and mapped as meta quartz-dolerite, comprises approximately 50 per cent of the sills in the present area. These rocks are rather coarse grained and many show readily visible evidence of contamination. In part they resemble the coarse grained,

marginal quartz gabbronorite (chapter 5.1.2) but are not as fresh in appearance. Grain size may reach 2-3 mm. showing little sign of decreasing towards the sill margins. Contacts. however. are generally not exposed. Even where they can be placed with confidence. such junctions are deeply weathered. as for example in the Hornsnek roadcutting. Contamination is usually evidenced by the appearance of small. evenly distributed. quartz knots and xenocrysts. which may comprise 15 per cent of the rock. In most respects they resemble the marginal rocks of the Middelwater Layered Sill. taking on a blue-green coloration due to alteration of plagioclase and amphibolitisation of primary pyroxene. This observation suggests that the Middelwater Layered Sill is merely a thicker version of the metadolerite/meta quartz-dolerite suite of sills.

5.2.2.3 Quench textured Micropyroxenites (QTM)

The term micropyroxenite (Sharpe. 1981. Cawthorn et al. 1981) is retained for these rocks. although none of them are true pyroxenites with 90% or more pyroxene content. (Streckeisen 1976). Micromelanorite would be a better descriptive. although more cumbersome. term for these rocks.

Micropyroxenitic rocks comprise about 30 per cent of the sills in the present area. Such sills rarely exceed 10 metres in thickness and crop out. over most of the area. on both the scarp and dip slopes of the Magaliesberg. Textural types vary but these micropyroxenites include rock types described elsewhere as cone diabases (Sharpe. 1978) and in places spinifex-like textures (Nesbitt. 1971. Pyke et al. 1973. Arndt et al. 1977) are developed. The cone diabase texture consists primarily of conical cells with a polygonal cross section (20-30 cm wide). defined by radially orientated orthopyroxene and plagioclase sheaves (Fig. 5.11). On the other hand the spinifex-like texture consists of sub parallel sheaf-like intergrowths of orthopyroxene and plagioclase (Fig. 5.12).

Such textures are generally considered to be the result of rapid cooling or quenching (Lofgren et al. 1974; Walker et al. 1976; Sharpe 1978; Lofgren 1980). This is consistent with the observation that grain size remains fairly uniform throughout the sills and chilling therefore does not seem to be restricted solely to the margins. In several sills however, the development of cone diabase texture is only observed at the lower margins of the sill. giving way upwards to a rather randomly orientated quench texture. There appears to be no

Fig. 5.11. Cone-diabase texture in one of the micropyroxenite sills found just south of Hornsnek road cutting. Coin (arrowed) is 1cm in diameter. (Loc. DI-7)

Fig. 5.12. Spinifex-like texture in loose block of micropyroxenite from the same general locality as Fig. 5.11.

sharp junction between the two. The upper margins of these sills are however largely obscured by talus, and this restriction may therefore only be apparent, there being in fact a bimodal distribution. In this case the development of the cone diabase texture is possibly due to a greater degree of cooling at the margins of the sill and in effect therefore there is a 'chilled margin' to these sills.

5.2.2.4 Pyroxenites and Norites

Rock types of broadly pyroxenitic and noritic composition form the remainder of the sills in the present area. Apart from some of the pyroxenites discussed in chapter 7.4 however, their affinities are uncertain.

Mottled weathering, cumulate textured feldspathic pyroxenites and melanorites form quite a thick sill (± 30 m) east of Silkaatsnek, while a transgressive pyroxenite body just north of Hartbeespoort Dam (behind Kosmos village) is olivine and chromite bearing; similar olivine—bearing rocks also form a poorly exposed sill west of Kommandonek. Contacts with the surrounding sediments are however obscured. Elsewhere, the sparse noritic sills are not well exposed. Most are clearly contaminated and some show evidence of cumulate texture.

The affinities of the norites are uncertain. They are possibly local hybrid variants of the microgabbronorite or possibly offshoots of the Rustenburg Layered Suite. The latter origin for the genesis of the feldspathic pyroxenites/melanorites is suggested by their close resemblance to rocks of the pyroxenite subzone. The olivine—bearing pyroxenites are also considered to be offshoots of the Rustenburg Layered Suite although they do not resemble any of the cumulates exposed in the study area (cf. chapter 7.4). Their probable mode of formation (chapter 7.4) implies however, that olivine bearing cumulates occur beneath the present exposure level of the Rustenburg Layered Suite.

6.   MINERALOGY AND PETROGRAPHY

6.1   THE RUSTENBURG LAYERED SUITE

6.1.1   Introduction

Investigation of the Layered Suite was undertaken not only to document the sequence and compare it with that found elsewhere but also to try and correlate any changes, such as compositional variation in the cumulus phases, with possible influxes of fresh magma(s) as exemplified by the marginal rocks.

At the outset however it must be noted that detailed mineralogical work on the Layered Suite was considered unwarranted for three reasons. Firstly, either because outcrop data is lacking or unreliable due to the absence of exposed marker horizons; secondly because approximately 30 per cent of the available borehole core showed some evidence of alteration which made detailed sampling impossible and finally, because not all the core was available – the chromitite layers in particular, being absent.

In view of this, a generalised approach to sampling was adopted with samples of borehole core were taken at approximately 25 m intervals, and microprobe analyses of cumulus minerals being spaced at 50 m intervals. Chromite, since it is largely absent in many of the ± 60 thin sections examined and also because the 'reef' horizons were not obtainable, was not investigated. Mineral analyses of cumulus mineral phases were undertaken at the Geological Survey of South Africa, using the Jeol JXA 50 microprobe facility. On average three spot analyses per mineral per thin section were determined for the orthopyroxenes, using a slightly de-focussed beam (10 microns). This was necessary because of the very fine exsolution lamellae of the type described by Wager and Brown (1968; Fig 215) and shown in Figure 6.5.

In addition, where chromite was present in the thin section, care was taken to ensure that the selected orthopyroxene grains were as far away as possible, or at least not in contact with any chromite in the section. This precaution was taken because of possible sub-solidus re-equilibration effects of the type noted by Cameron (1975). Partial analysis of the Fe–Mg component of the orthopyroxene revealed little evidence of extensive zoning. Compositional

variation through the sequence is shown in Figure 6.1 and orthopyroxene analyses are given in Appendix 4.

On average four plagioclase grains were analysed as many are clearly zoned. However, analyses were determined closest to the centre of individual crystals on the assumption that, according to classical cumulate theory, these should represent the composition of the mineral 'at the point of settling'. Obviously however, the plane of sectioning may have an influence on the final analysis. Again compositional ranges of plagioclase cores are shown in Figure 6.1 and analyses are given in Appendix 4.

The Merensky Reef was taken as the datum for the present section of the Layered Suite because the borehole logs do not always clearly distinguish other stratigraphic boundaries.

6.1.2   Compositional variation in cumulus orthopyroxene and plagioclase

6.1.2.1   Orthopyroxene

A sample of feldspathic pyroxenite (K-261A), from just above the quartz gabbronorite east of the Hartbeespoort fault, presumably represents the lowest part of the stratigraphic section in the study area. However, the relationship of this sample to the borehole section is not very clear and hence mineral compositions are not shown in Figure 6.1. Nevertheless cumulus orthopyroxenes in this sample have Mg numbers (Mg*'s)[1] unexpectedly lower than those at the base of the borehole section, i.e. 0.74-0.76 as opposed to 0.80 - 0.82. This pyroxenite sample is however the only sample containing any significant content of quartz and biotite, and thus it appears to have been influenced either by proximity to the floor sediments, or by the contamination evident in the underlying quartz gabbronorite.

If this feature is an original crystallisation feature, then in more quantitative terms this anomalous situation can be explained by reference to the work of Longhi et al. (1978). These authors have shown that an increase in silica content has a marked effect on Fe-Mg exchange equilibria such that $Kd_{Fe-Mg}^{opx-liq}$ increases sympathetically with SiO_2 content. Consequently any

---

[1]Where Mg* = Mg^{2+}/(Mg^{2+} + Fe^{2+}) (Atomic)
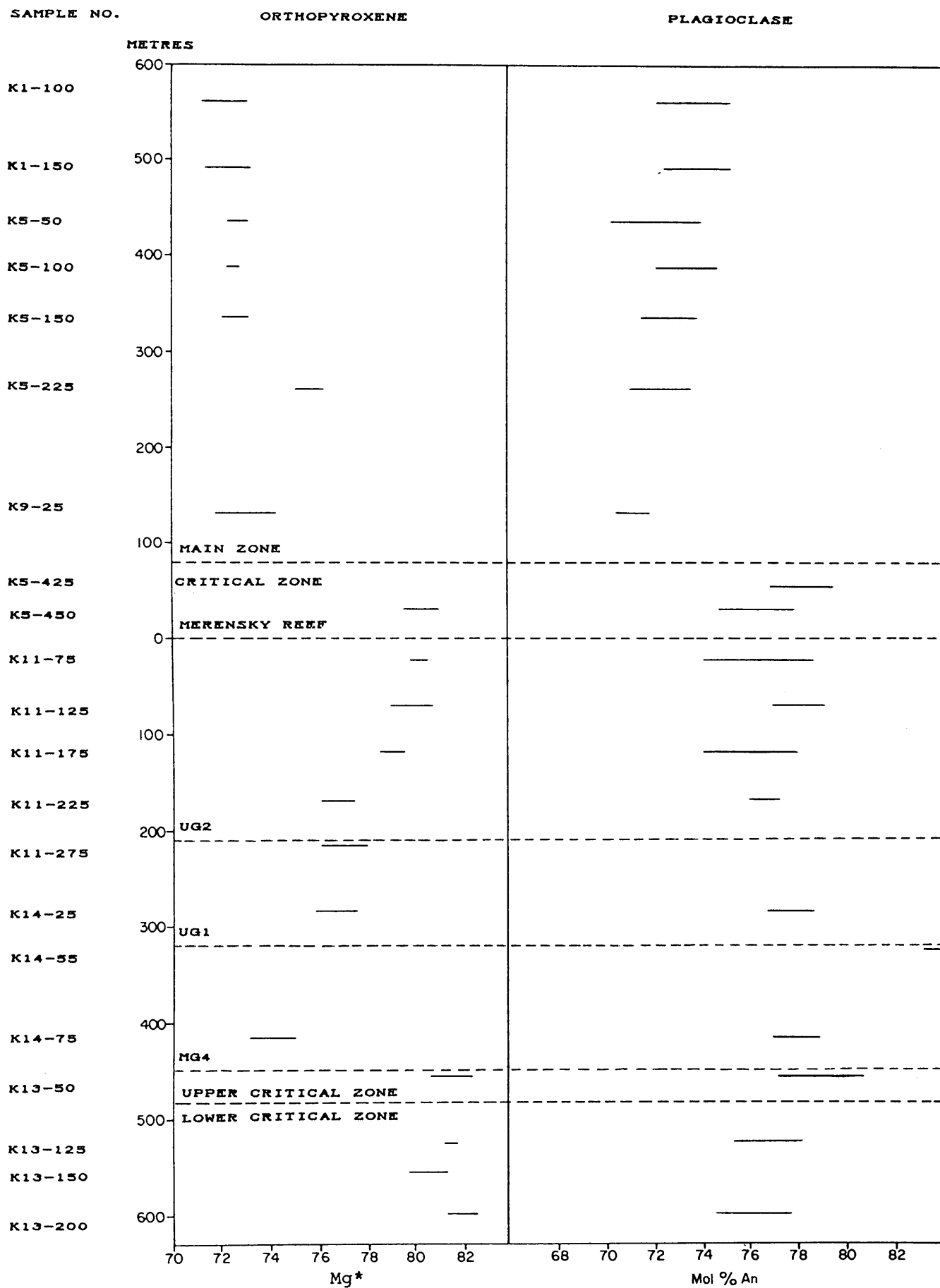
Fig. 6.1. Compositional ranges for cumulus minerals in the borehole
section south of Brits.

increase in SiO_2 content related to contamination by floor sediments would cause a decrease in the Mg^* of crystallising orthopyroxenes. Thus it is quite possible that the orthopyroxenes with the lower Mg^* actually crystallised from a magma with a higher Mg^* than that from which the overlying, more magnesian, cumulates were derived. Alternatively, if in fact the pyroxene has been affected by the contamination evident in the quartz gabbronorite, then this process is more likely to be one of re-equilibration rather than primary crystallisation. This is because intrusion of the quartz gabbronorite is thought to post-date the formation of the lower critical zone[1] and any contamination from below must have affected the overlying cumulates and not the overlying magma. In this event the decrease in Mg^* may well be the combined result of re-equilibration with infiltrating QGN liquid, which is both more siliceous and at the same time, less magnesian, than the cumulates.

For the lowermost 150 m of the succession shown in Figure 6.1, i.e. below the MG 4, the Mg^* of orthopyroxene is fairly constant at 0.80 - 0.82. Fifty metres above the MG 4 there is a sharp drop in Mg^* to 0.75 and then a gradual increase in values up to 0.80 above the level of the Merensky Reef. Although this contrasts with the eastern Bushveld where the compositional trends in the upper critical zone are not as pronounced (e.g. Cameron, 1982), the compositions at the base and top are nevertheless similar to those found in the eastern Bushveld (Cameron, ibid.). However work by Kruger and Marsh (1985) revealed that over intervals as small as 10m, Mg^*'s can vary by as much as 0.10., while more recent work by Eales et al. (1988; 1990) in the northwestern portion of the Complex has shown that even over intervals of less than 5 metres there may be significant changes in Mg^* of 0.05 or more. Eales et al. (ibid.) also illustrate that these variations define a number of cyclic units with

---

[1]For example, the quartz gabbronorite (QGN) also has a gradational contact with the upper critical zone (Chapter 5.1.2), which suggests that the cumulates of this (younger) subzone had already formed by the time the QGN was intruded. Furthermore the quartz gabbronorite is considered to have crystallised from a hybrid magma derived only after extended intrusion of the microgabbronorite. Because the microgabbronorite does not appear to have been intruded in substantial amounts prior to formation of the lower critical zone (chapter 7.8.4), then it is also unlikely that the QGN magma had been produced by the time of formation of the lower critical zone.

thicknesses of ± 20 metres. Clearly therefore much more detailed work is needed to define precise trends in the Layered Suite.

Because of lack of borehole core, the only Mg^* obtained for orthopyroxenes from the lower 150 m of the main zone, is a value of 0.73 from a sample some 100 m above the base of the zone (Fig. 6.1). This value is considerably lower than the Mg^*'s for the upper critical zone. Interestingly enough, Von Gruenewaldt (1973, p. 220) also noted a sharp drop in Mg^* across this zonal junction, recording an Mg^* for orthopyroxene of 0.66 in a sample 93 m above the Merensky Reef. While it must be borne in mind that this 'trend' could be an artefact of sample availability, Eales et al (1986) working in the northwestern portion of the Complex also noted a sharp drop in whole rock Mg^* across the critical zone – main zone junction. This feature is echoed by the orthopyroxene data of Mitchell (1990) from the same area. Mitchell (ibid.) also recorded Mg^* values of ± 0.65 to 0.67, at approximately the same level as that of von Gruenewaldt, and values of 0.72 to 0.74 for orthopyroxene at the same level as the present study, (i.e. ±100m above the base of the main zone).

The composition of the orthopyroxenes in the remaining 400 m of the section studied, remains fairly constant at approximately Mg^* 0.73, although there is some oscillation about this value (Fig. 6.1). Mitchell (ibid., Fig. 5) records similar overall Mg^* values for this interval, although in detail there is more variation (± 0.71 – 0.75).

6.1.2.2   Plagioclase

As noted above (chapter 4) this mineral occurs as a cumulus phase some 150 m below the MG 1, where compositions are similar to those in the overlying subzone, i.e. An_{75-78} (Fig. 6.1). Above the pyroxenite subzone, An values oscillate somewhat up to the level of the UG 2, although the An values for plagioclase associated with the UG 1 are higher (i.e An_{83-84}) than those found in the eastern Bushveld i.e. An_{75} (Cameron, 1982) and An_{77-79} (Gain 1985). In view of the unusual pegmatoidal nature of the UG 1 however, it seems likely that the increase in both An content and grain size is probably related to an increase in P_{H2O}. Such an increase, perhaps associated with local faulting and the consequent passage of filter pressed pore fluids richer in H_2O, would lead to depression of the plagioclase solidus and a decrease in viscosity, with consequent increase in the An content and size of crystallising plagioclase.

Above the UG 2 there is a slight but steady increase in An values, similar to that noted by Ferguson and Wright (1970). At the base of the main zone the sharp drop in Mg^* of orthopyroxene (chapter 6.1.2.1) is mirrored by an equally sharp decrease in the An content of plagioclase. Thus the An_{77-80} values at the top of the critical zone are reduced to An_{70-72} at the base of the main zone. Although this is similar to the drop in An values recorded by Von Gruenewaldt (ibid., p. 220) for a sample 93 m above the Merensky Reef, as noted above it must be borne in mind that more data are needed before this 'trend' can be confirmed. Nevertheless the more extensive whole rock - feldspar data of Eales et al. (1986) indicate a similar drop in An content across the critical zone-main zone boundary. Mitchell (1990, Fig. 6) also recorded a drop in An content from An_{70-75} at the top of the critical zone down to An_{65-70} at the base of the main zone, although these values are considerably lower than those of the present study.

For the remaining 400 m of the section studied, An values show a slight overall upward increase in An content from An_{71-72} up to An_{72-74} (Fig. 6.1). Mitchell's (ibid.) data from the northwestern part of the Complex are fairly constant over the lower portion of this interval (although with typical values of An_{65-70}) but an overall upward increase is also apparent, particularly in the upper 200 m, where values may reach An_{72}. On the other hand this contrasts with the data of Eales et al. (ibid) which shows a slight decrease from ± An_{73} down to An_{70} for this part of the Layered Suite.

6.1.3   Modal Analyses

Wherever possible, modal analyses were undertaken on only the more 'average' noritic/gabbroic rock types, avoiding the more extreme cumulate concentrations typified by pyroxenites and anorthosites. This was the approach followed by Von Gruenewaldt (1971) and modal analyses were undertaken for similar reasons as the above-mentioned author, namely,:-

1.   To assess whether any broad trends in rock composition are discernible.

2.   To determine whether any relationship exists between modal abundance, texture and/or composition of individual minerals.

3. To see if any of the above features could be correlated with possible influxes of fresh magma as exemplified by the compositions of the marginal rocks.

Modal analyses were determined using a Swift electronic point counter and standard 40 mm x 25 mm thin sections. E-W translations of the stage, equal to approximately one tenth of the average grain size of individual samples, were used, as suggested by Hutchison (1974, Chapter 3). The latter author also suggests that 1 000 - 2 000 points be counted in order to obtain a statistically valid analysis. Consequently between 1 500 and 2 000 points were counted for each analysis shown in Figure. 6.2. Grain sizes are reflected in Figure. 6.2 by the use of the I.C. number of Chayes (1956). This is simply the number of mineral Identity Changes in a 40 mm traverse of the thin section.

6.1.3.1   Modal variations

Orthopyroxene shows a fairly steady overall decrease upwards through the sequence. Thus it comprises between 40 to 60 per cent of the rocks in the pyroxenitic subzone, 20 to 40 per cent of the rocks in the overlying anorthosite subzone and decreases to less than 30 per cent in the rocks of the main zone (Fig. 6.2).

Plagioclase in contrast, presents an almost perfectly complementary relationship to the orthopyroxene trend, exhibiting a general but gradual increase in modal abundance upwards (Fig. 6.2). Note however that once clinopyroxene becomes a cumulus phase then the behaviour of plagioclase is decoupled from that of orthopyroxene and it subsequently exhibits a complementary relationship with clinopyroxene.

The general upward increase in modal plagioclase and concomitant decrease in orthopyroxene would initially seem compatible with early fractional crystallisation of orthopyroxene followed by the appearance of plagioclase and then clinopyroxene on the liquidus as crystallisation proceeded. However such a simple fractional crystallisation model, involving cotectic crystallisation, should lead to essentially constant orthopyroxene:plagioclase ratios, and some mechanism of crystal sorting is therefore required. Possibly the concept of buoyant plagioclase (Campbell et al., 1978) is important here.
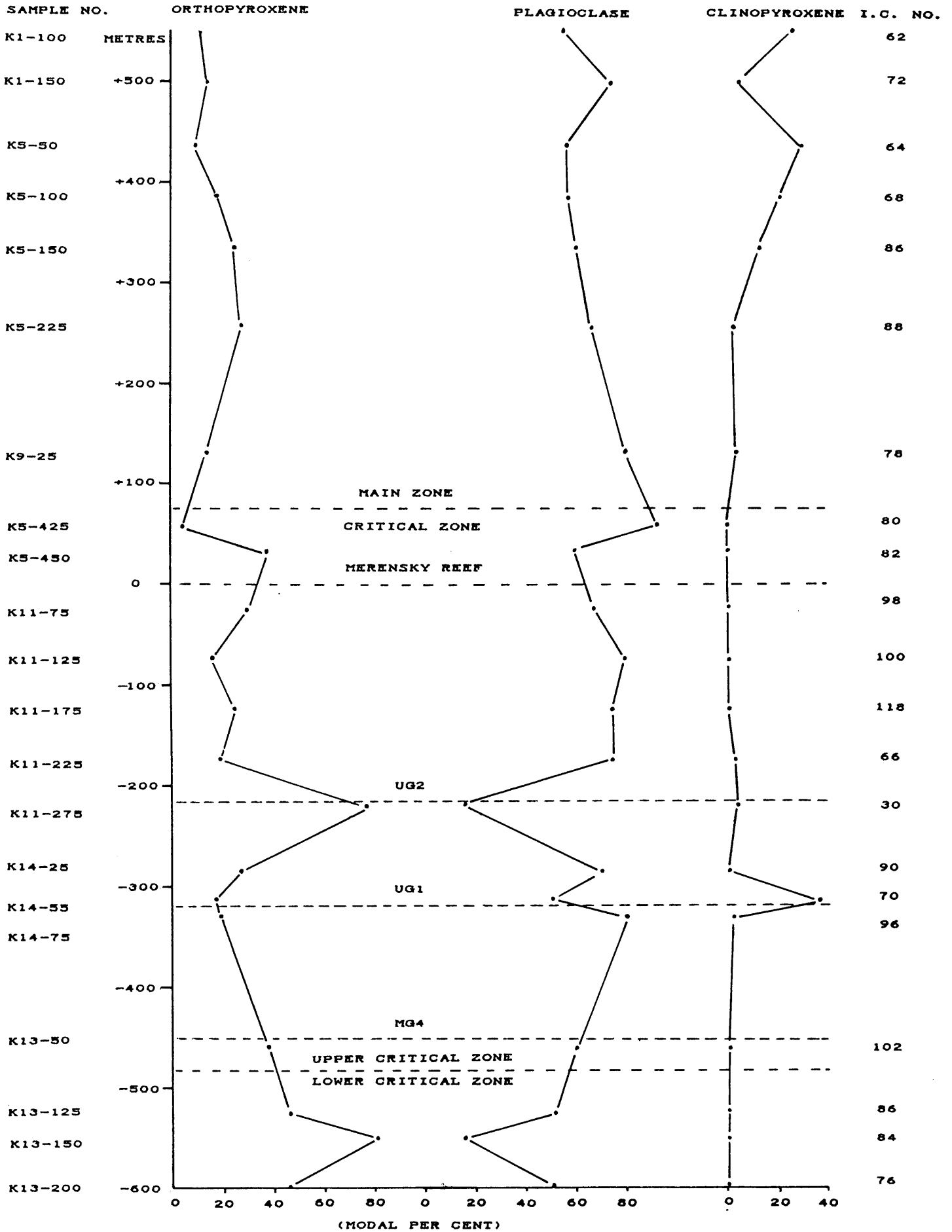
Fig. 6.2. Modal variation of constituent minerals in the borehole section

In addition, it is also possible that a new liquid, richer in potential plagioclase relative to the liquid in the chamber, was progressively introduced. In this regard it is perhaps significant that the chilled microgabbronorite (equivalent to the B2-type liquid of Sharpe (1981) which has plagioclase on the liquidus (Sharpe and Irvine, 1983)) first appears in abundance at the same stratigraphic level as the base of the anorthosite subzone (Chapters 2 and 5.1.1). Eales et al. (1986) have discussed how progressive mixing of such a liquid with residual liquid in the chamber could expand the primary phase volume of plagioclase in such a hybrid melt, leading to enhanced production of plagioclase relative to orthopyroxene. It must be borne in mind however that the modal analyses shown in Figure 6.2 ignore the great variety of anorthositic, pyroxenitic and indeed chromititic rock types that make up the sequence, particularly in the upper critical zone. As a result therefore the above possibilities are somewhat speculative.

Clinopyroxene is present as intercumulus, sometimes poikilitic material throughout the sequence, however, with the exception of sample K14-55, (which has a large amount of poikilitic clinopyroxene), it is only near the top of the section studied that it assumes any modal importance, (Fig. 6.2). This feature coincides with its entry as a cumulus phase some 340 m above the Merensky Reef, although as discussed above (chapter 4), this may be a sampling artefact. In places, cumulus clinopyroxene clearly crystallised earlier than orthopyroxene (K5-100) and by reducing the available magnesian component in the magma no doubt reduced the overall orthopyroxene content accordingly. Even where the order of crystallisation is not clear, there is an obvious inverse relationship between the modal abundance of orthopyroxene and clinopyroxene at this level (Fig. 6.2).

Accessory minerals, including quartz, biotite/phlogopite, chromite and other opaques, are present in only very minor amounts in the modally analysed rocks. With the exception of the outcrop sample discussed above (chapter 6.1.2.1), which contains nearly 6 modal per cent quartz and 2 per cent biotite, the accessory phases rarely exceed 0.5 per cent of the total volume of the rock and this is often due to the presence of cumulus chromite. This low modal content must reflect the almost total reduction of porosity by adcumulus growth (Wager et al., 1960), with little of the intercumulus liquid being trapped in the developing cumulate framework. This widespread adcumulus growth is not restricted solely to these 'average' rocks however as thin section examination of the more monomineralic feldspathic pyroxenites and anorthosites reveals very

low contents of non-cumulus accessory phases. For example, sample K11-275, a feldspathic pyroxenite from just below the UG 2 (Fig. 6.2) has about one modal per cent accessory minerals, mostly biotite/phlogopite with trace amounts of magnetite. Similarly a spotted anorthosite some 50 m higher carries only trace amounts of biotite/phlogopite. The only exception to this general rule is where intercumulus plagioclase forms large plates (Fig. 6.6) and appears to have pre-empted adcumulus growth by the growth of intercumulus material. Even so, there are only very sparse amounts of accessory phases present in such rocks.

6.1.4   Textures

In general mineral habits are closely allied to mode of occurrence. Thus, where minerals occur as cumulus phases, a subhedral form is common, except in extreme adcumulates, while intercumulus phases are typically anhedral. One exception to the latter rule is the large (± 10 mm) subhedral, green, poikilitic clinopyroxenes, common in the more pyroxenitic members of the critical zone. Furthermore, although igneous lamination is fairly common (Fig. 6.3) it is more characteristic of plagioclase-rich rocks, probably as a result of the greater aspect ratio of cumulus plagioclases, as compared with the pyroxene.

6.1.4.1   Orthopyroxene

Throughout much of the sequence, cumulus orthopyroxene forms stubby to prismatic, subhedral to euhedral crystals, up to 3 mm long and 0.5 – 1.5 mm across (Figs. 6.3, 6.6., 6.7). In the pyroxenite subzone alignment of prismatic orthopyroxenes produces an igneous lamination (Fig. 6.3) which is generally defined by plagioclase in overlying cumulates. Nearer the top of the succession in the 'porphyritic norite', orthopyroxene characteristically occurs in the form of large (up to 5 mm diameter) rounded, poikilitic crystals enclosing numerous small, prismatic plagioclases (Figs. 6.4, 6.5). Individual orthopyroxene crystals characteristically exhibit fine scale, regular exsolution lamellae of clinopyroxene parallel to {100} as shown in Figure 6.5.

Orthopyroxene may also occur more rarely as an intercumulus phase, in which case several distinct irregular grains are often seen to be in optical continuity in thin section, giving rise to 'spotted' and 'mottled' anorthosites

1 MM

Fig. 6.3. Orthopyroxene in melanorite of the pyroxenite subzone. Note alignment of prismatic subhedral crystals to produce an igneous lamination. Crossed polars.
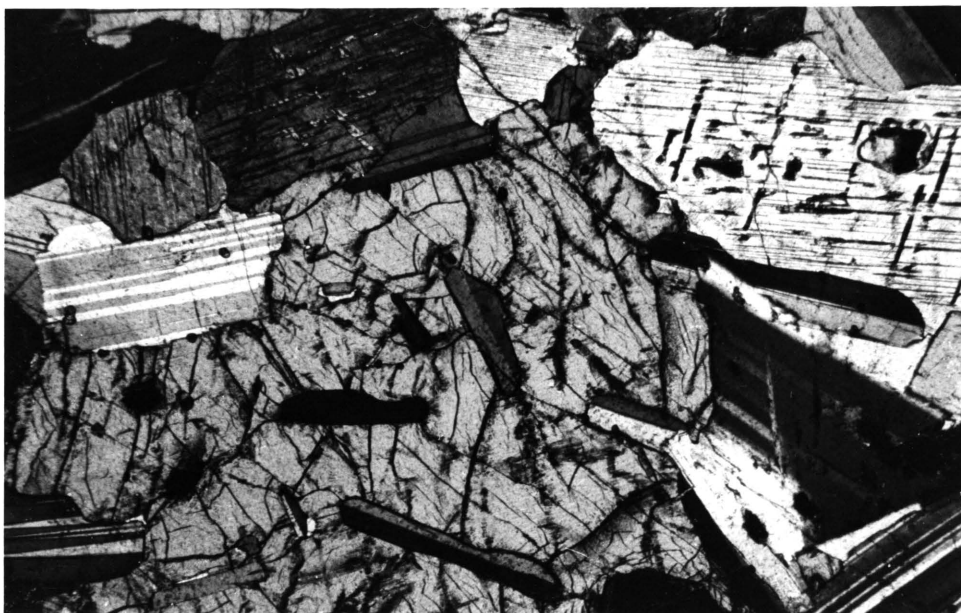
1 MM

Fig. 6.4. Gabbroic representative of the 'porphyritic norite'. Note clinopyroxene (top and top right) and the large poikilitic orthopyroxene enclosing numerous small prismatic plagioclases. Crossed polars.

Fig. 6.5. Portion of large poikilitic orthopyroxene in the 'porphyritic norite', showing fine-scale exsolution of clinopyroxene. Crossed polars.
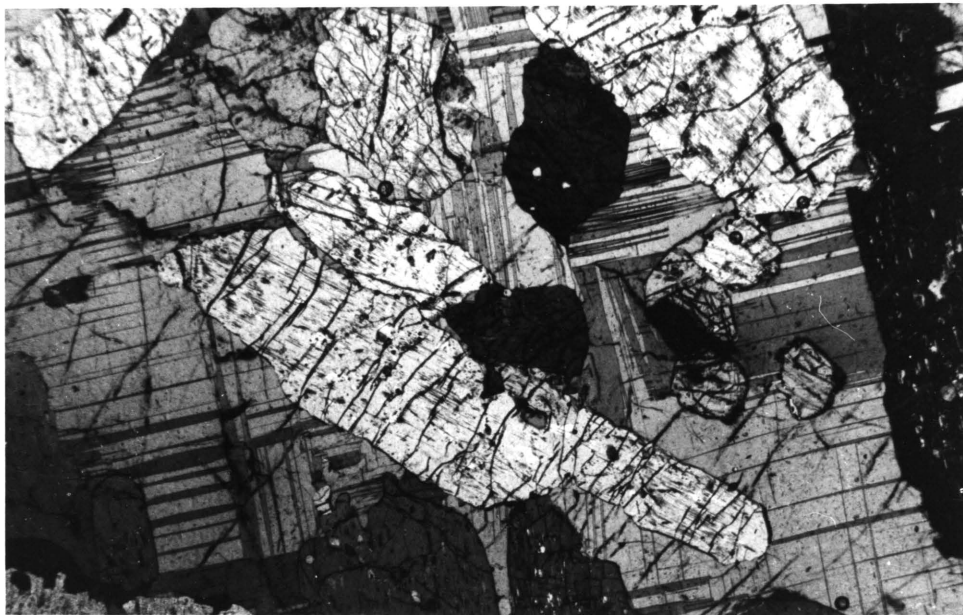
Fig. 6.6. Large plate of plagioclase poikilitically enclosing prismatic cumulus orthopyroxenes in melanorite from the pyroxenite subzone. Crossed polars.

in outcrop. These optically continuous patches may reach up to 20 - 25 mm in diameter and enclose numerous prismatic to rounded plagioclase grains.

6.1.4.2 Plagioclase

In the pyroxenite subzone plagioclase commonly occurs as large poikilitic plates up to 10 mm across (Fig. 6.6) or as small (< 1 mm wide) irregular interstitial patches. However, in two samples (K13-200 and K13-125), some 150 m and 40 m respectively below the MG 1 (Fig. 6.2), plagioclase also occurs as a cumulus phase. It is undoubtedly cumulus as it occurs as small, rounded crystals in the central portions of cumulus orthopyroxene (Fig. 6.7). This is in marked contrast to the eastern lobe of the Complex, where cumulus plagioclase is restricted to levels above the MG 2 chromitite, although Hatton and Von Gruenewaldt (1985) have previously argued for the existence of cumulus plagioclase below this level in the western Bushveld. While it is possible that the borehole passed through a fault zone below the middle group chromitites and intersected a higher part of the sequence, this is not thought to be the case in the present study. This is because the orthopyroxenes associated with the cumulus plagioclase have the highest Mg^*'s of all the orthopyroxenes analysed during the present study and this would suggest that the samples are not from higher in the sequence (Fig. 6.1).

Above the pyroxenite subzone, plagioclase commonly occurs as prismatic to tabular crystals 1 - 1.5 mm in length (Fig. 6.8) and often as much smaller prismatic to rounded grains included in orthopyroxene (Fig. 6.4). Alignment of plagioclase to form an igneous lamination is common (Fig. 6.8). About 200 m above the base of the main zone there is a general increase in grain size up to 4 mm. In the very leucocratic rocks plagioclase may possess a granular adcumulate texture and 120° triple junctions between grains are common (Fig. 6.9).

Throughout the sequence, zoning is common and includes normal, reversed and combined normal-reversed zoning of the type described by Wager and Brown (1968, p. 386). The latter type is by far the most common type of zoning although the above authors imply that it is restricted to the main zone. Ferguson and Wright (1970) nevertheless describe an example from the critical zone, south of Brits. This type of zoning is however not pronounced in many thin sections, often being obscured by polysynthetic twinning and it could

1 MM

Fig. 6.7. Melanorite sample K13-200, from approximately 150 m below the MG1. Note small, rounded cumulus crystals of plagioclase within cumulus orthopyroxene (centre left). Crossed polars.

1 MM

Fig. 6.8. Igneous lamination in leuconorite of the anorthosite subzone. Lamination is largely defined by sub-parallel alignment of prismatic to tabular, cumulus plagioclase crystals. Crossed polars.

easily be overlooked. Briefly, the observed zoning consists of an unzoned core region which is approximately one half to two thirds the overall dimension of the crystal, surrounded by a variable thickness of normally zoned material which in turn is mantled by a reverse zoned region (Fig. 6.10). The outer reverse-zoned portion is usually thin and may be discontinuous (Fig. 6.10). For the critical zone, partial microprobe analyses and optical determinations gave values for the three zones of approximately An_{74-76} for the core, reducing to An_{66-68} outwards with the outer reverse zoned portion increasing up to An_{76}. These values are similar for the main zone but core compositions are lower.

Wager and Brown were unable to fully account for the presence of this zoning and offered two possible explanations:–

1.   That pressures exerted in the locally confined pore spaces could increase the calcium content of crystallising plagioclase.

2.   Increase in P_{H2O} in the remaining pore fluid, as a result of crystallisation, would lower the liquidus/solidus of the system and thus cause the outer parts of the cumulus crystals to be made over to more calcic compositions.

Wager and Brown (ibid.) themselves discount the first explanation as it should also be operable in other layered intrusions, for which there is no evidence.

The second explanation initially appears to be reasonable but is at odds with petrographic evidence. This is because increase in P_{H2O}, as envisaged above, assumes that the system has become at least partially closed. Since many of the rock types studied are adcumulates, this is against the fundamental tenet of the adcumulus hypothesis whereby the system must remain open. This is required both to supply the requisite components to the areas of crystal growth and to remove the inappropriate components to the overlying magma. In fact, Irvine (1980b, p. 371) suggests that such a process may occur up to several hundred metres below the depositional interface, implying that the system remains open to a considerable depth below this boundary. Sparks et al., (1985) and Wadsworth (1985) similarly provide evidence for growth deep within the cumulate pile. Furthermore, as Cox et al. (1979) point out, removal of the intercumulus liquid is probably important in removing the latent heat of
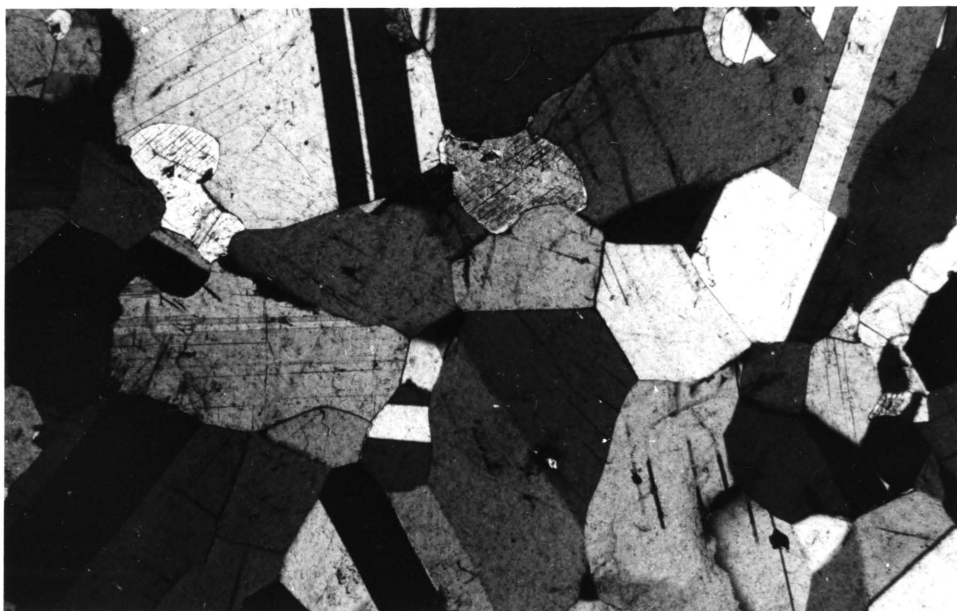
1 MM

Fig. 6.9. Anorthosite from the anorthosite subzone in which adcumulus
plagioclase exhibits mutual 120° triple junctions. Crossed polars.
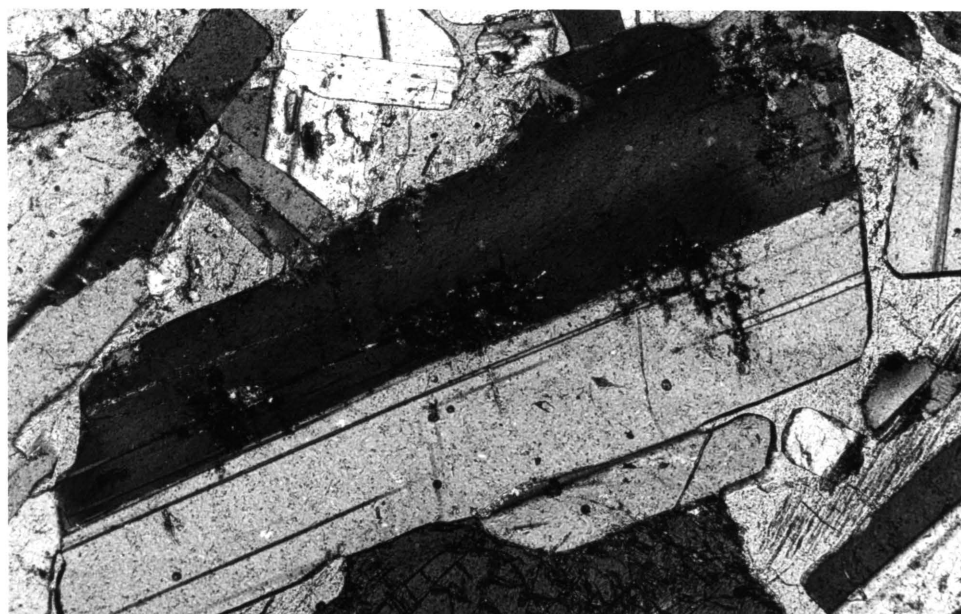
0.5 MM

Fig. 6.10. Normal-reversed zoning in plagioclase. Top twin of prominent
plagioclase crystal exhibits three distinct compositional zones. These
consist of a central core region (dark), surrounded by a lighter,
normal-zoned region which in turn is succeeded by a darker, discontinuous,
reverse-zoned region. Crossed polars.

crystallisation. If this did not occur, then presumably crystallisation would eventually cease until sufficient heat loss via conduction was achieved in order to allow crystallisation to proceed. However by this stage the continuing accumulation of overlying cumulates would presumably have become sufficient to prevent communication with the overlying magma, causing the eventual crystallisation of intercumulus liquid in situ.

Since textural evidence for the entrapment of pore liquids is generally lacking (Chapter 6.1.3.1) there would appear to be little evidence for closure of the magmatic plumbing system until solidification was at an advanced stage. Furthermore Reichardt (1989) found that rocks with the lowest amount of intercumulus material had in fact more fractionated (intercumulus) An compositions than those rocks with higher percentages of interstitial (i.e. trapped) phases. This is clearly the opposite of what would be expected with the Wager and Brown model, whereby the zoning is due to increasing P_{H2O} as the pore spaces become more confined.

Possibly a process such as infiltration metasomatism, as postulated by Irvine (1980b), may have operated, in which a gradual upward flow of intercumulus liquid occurs from lower levels. This upward flow in turn would occur in response to increased loading and compaction at the base of the cumulate pile as new cumulates were added at the top. A similar process of upwardly migrating interstitial liquid, driven by loading, was also proposed by Shirley (1986) who presented a rigorous quantitative analysis of cumulate compaction. In the present case it is envisaged that the core region of the feldspar represents the original 'settled' crystal and the normal zoned region represents the overgrowth due to initial crystallisation of pore liquid in situ. However, at some later stage as compaction increased, this pore liquid would be replaced by filter pressed liquids from lower in the sequence.

Since these liquids would presumably be in equilibrium with more 'calcic' plagioclase than their counterparts at higher levels, and perhaps even more H_2O rich, their passage through the overlying cumulates would lead to reversed zoning on the outer rims of the plagioclases. In fact, the reason the outer rim is in places discontinuous may be because only the reverse zoned portion of the crystal formed the wall of the channelway and consequently only this portion was made over to more calcic compositions. Note that the process of infiltration metasomatism differs from the process of compositional convection

(Tait et al., 1984) in that the pore fluids are not replaced by fresh undepleted magma from above but rather by depleted magma emanating from below.

One problem with the above explanation is the apparent lack of zoning in the orthopyroxenes. However, Reichardt (1989), through a detailed microprobe study of zoning in orthopyroxene from the critical zone, found that although the intra-grain Mg* remains fairly constant, there is often a marked variation in e.g. Al_2O_3, CaO, TiO_2 and Cr_2O_3 content towards the grain margin. He argues (p.60) that this is not due to disequilibrium during primary growth as the high atomic diffusivities and slow growth rate in large layered intrusions preclude such an explanation.

Furthermore, subsolidus re-equilibration between orthopyroxene and adjacent minerals can be ruled out, as the overall zoning pattern is similar regardless of whether the orthopyroxene is in contact with orthopyroxene, clinopyroxene, plagioclase or even K-feldspar. Reichardt (ibid.) argues therefore that the zoning must result from disequilibrium between orthopyroxene and interstitial liquid. In the absence of such a detailed microprobe study it is possible that such cryptic zoning is present in the orthopyroxenes of the present study. Note however that this does not necessarily require that all the interstitial fluid is "trapped", it seems equally possible for this feature to be caused by liquid migrating through the pore spaces. Such a process is still considered possible at porosities as low as 4 per cent (Mckenzie 1984; Tait et al. 1984). Presumably also, the longer the pore spaces remained open the more "fractionated" the An content of intercumulus plagioclase could become, as increasingly fractionated liquid passed through the cumulate pile. Actual trapping and crystallisation of pore liquid in situ would clearly limit the total "fractionation" possible (cf. Reichardt's observations (above) that the least fractionated (intercumulus) An compositions are found in rocks with the highest amounts of intercumulus material).

6.1.4.3   Clinopyroxene

Poikilitic clinopyroxene occurs as sparse, anhedral to subhedral postcumulus crystals throughout the critical zone. In thin section these poikilitic crystals appear either as irregular interstitial patches, in optical continuity with each other, or as large plates (up to 10 mm across) enclosing numerous cumulus crystals. Clinopyroxene may also occur as small blebs and

patches (0.1 mm across) associated with the margins of larger orthopyroxene grains. As noted above (Sect. 6.1.3.1) cumulus clinopyroxene first appears in samples from 200 m above the base of the main zone. In this case the mineral occurs as < 1 - 1.5mm long, prismatic, subhedral to anhedral crystals (Fig. 6.11), often showing simple twinning. Exsolution textures within clinopyroxene are ubiquitous and consist both of fine, closely spaced lamellae of orthopyroxene parallel to {100} and coarser, more irregular lamellae of orthopyroxene, roughly parallel to {001} (Fig. 6.11). In addition, within the finer lamellae numerous minute plates of clinopyroxene occur, lying more or less parallel to {001}, giving the orthopyroxene lamellae a banded appearance (Fig. 6.12).

6.2   THE MARGINAL ROCKS

6.2.1   Gabbronoritic contact lithologies

6.2.1.1   The microgabbronorite

Modally the MGN is somewhat variable but in general it contains between 50 and 60 per cent plagioclase with the remainder comprising pyroxene (30 modal per cent) together with accessory magnetite and minor quartz, biotite, ilmenite and sulphide. Clinopyroxene and orthopyroxene are present in approximately equal proportions, although either may predominate in individual thin sections. Magnetite, although very prominent in thin sections and in fact very characteristic of the MGN, rarely forms more than 5 modal per cent of the rock (Fig. 6.13.).

Grain size is also somewhat variable in the MGN ranging from fine to medium grained, while texturally the MGN is characterised by a series of granular to radiate textures, suggestive of rapid cooling (Carmichael et al., 1974; Lofgren, 1980; Figs. 6.14, 6.15 and 6.16). The granular texture is more usually found in the finer-grained rock types and can be reconciled with the observation that nucleation rates typically peak at temperatures below those at which crystal growth rates are at a maximum (Carmichael et al., 1974). Hence, with rapid cooling, a large number of nuclei form, from which crystal growth is relatively slow, resulting in a fine-grained rock. In the slightly coarser grained variants, plagioclase commonly appears to have nucleated on earlier formed pyroxene and thus become at least in part, radially arranged
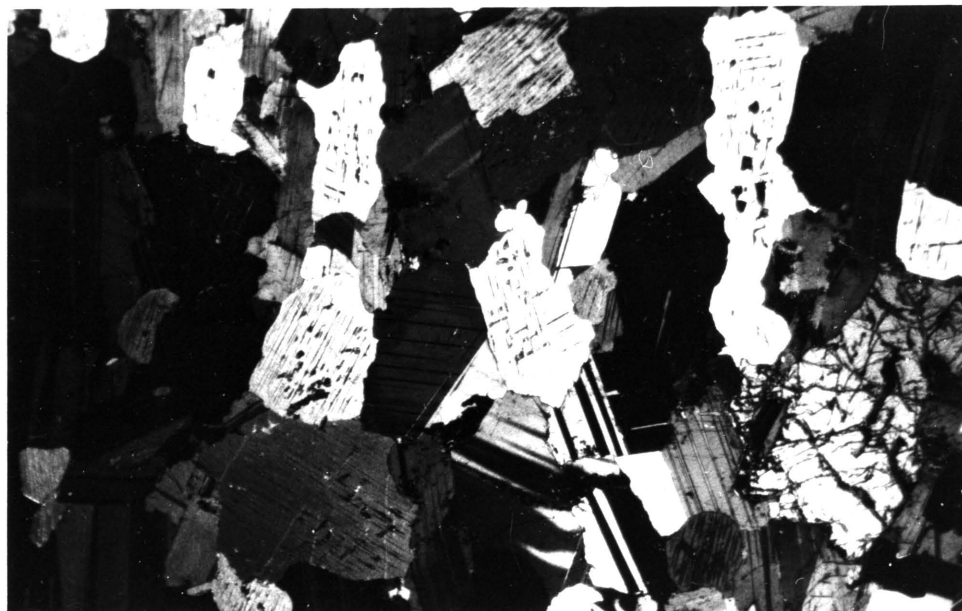
1 MM

Fig. 6.11. Cumulus clinopyroxene in main zone leucogabbro. Note prominent exsolution of orthopyroxene in both fine, closely spaced lamellae, parallel to {100} and in coarser lamellae approximately parallel to {001}. Crossed polars.
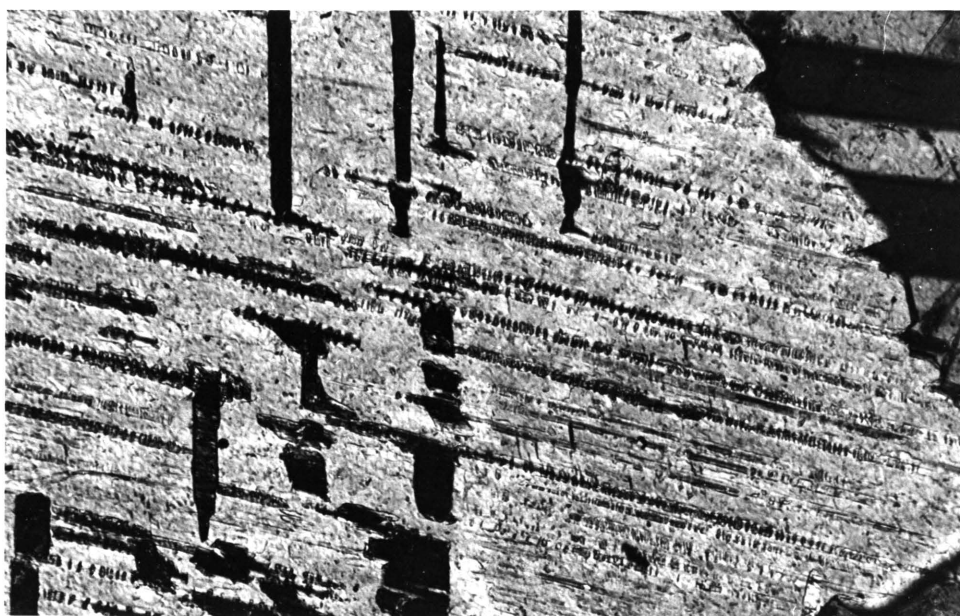
0.1 MM

Fig. 6.12. Detail of central crystal of Fig. 6.11, showing sub-horizontal lamellae of orthopyroxene (parallel to {100}) containing minute, transverse plates of clinopyroxene approximately parallel to {001}. Crossed polars.
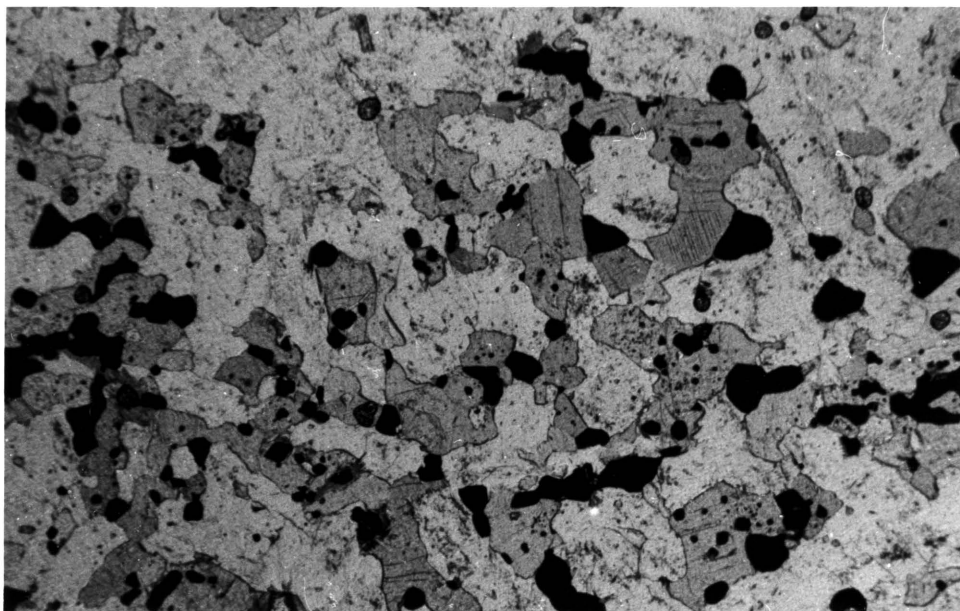
1 MM

Fig. 6.13. Abundant granular magnetite in the microgabbronorite.
Plane polarised light.
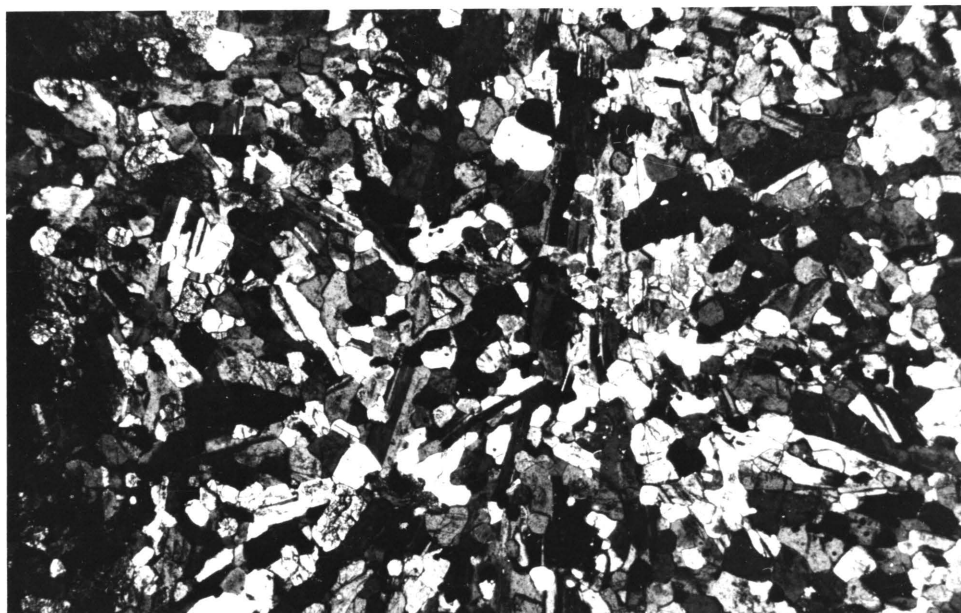
1 MM

Fig. 6.14. Granular to partially radiate texture in the finer grained
microgabbronorite. Crossed polars.
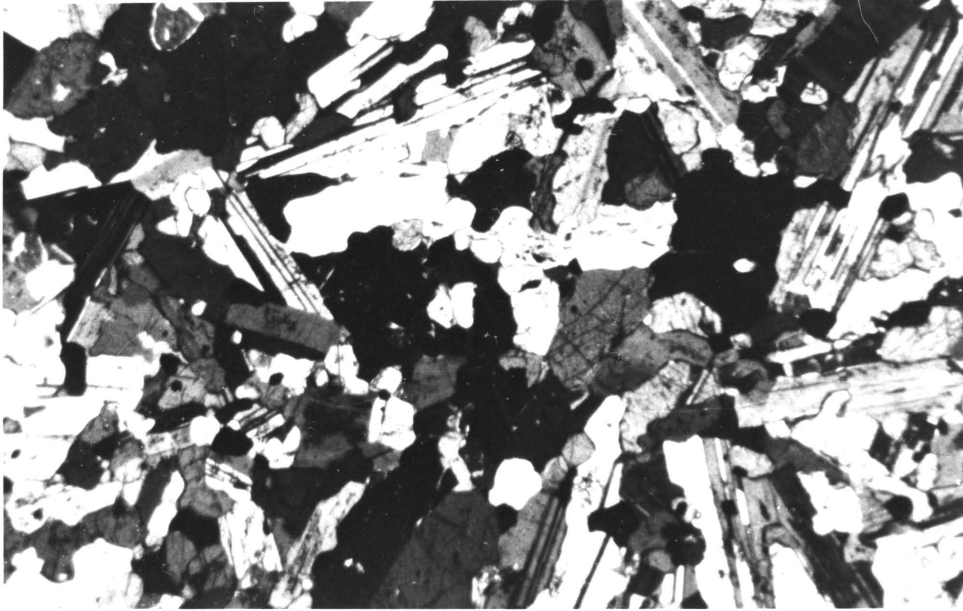
1 MM

Fig. 6.15. Radiate texture in the medium grained microgabbronorite.
Crossed polars.
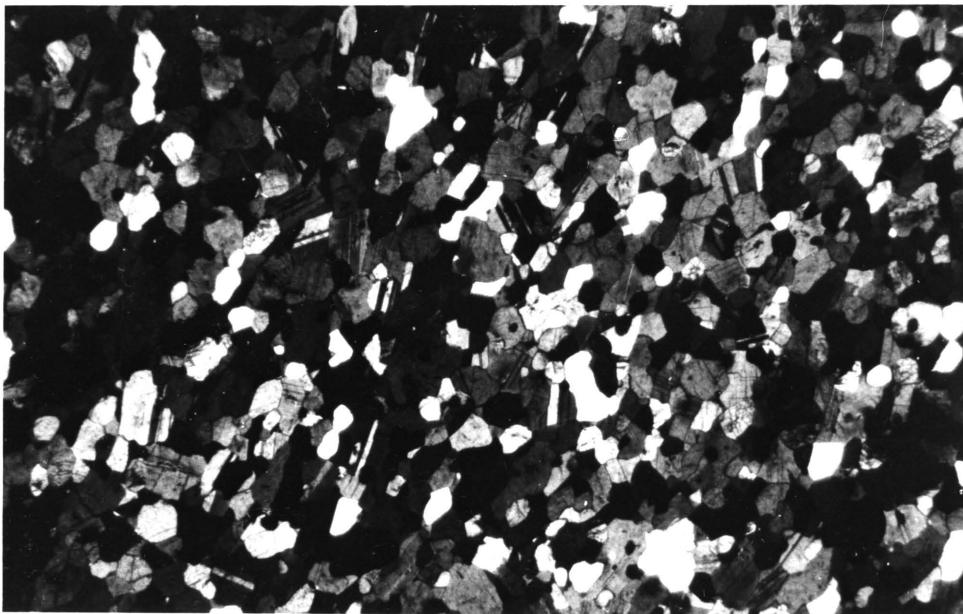
1 MM

Fig. 6.16. Granular texture in the finer grained microgabbronorite.
Crossed polars.

about pyroxene nuclei (Fig. 6.15). At high cooling rates Gibb (1974) suggested that plagioclase nucleation is suppressed and thus pre-existing pyroxene would presumably provide a convenient nucleation site, prior to random spontaneous crystallisation from the liquid. Similarly Walker et al. (1976) found that at high cooling rates plagioclase nucleation was significantly suppressed relative to other phases and the same argument applies. While there are some exceptions to the above (e.g. compare Figs. 6.13. and 6.14.) it is nevertheless considered that all the observed textures developed in response to rapid cooling, although the overall coarser grain size in most radiate textured rocks suggests that cooling rates were slightly lower than in the finer grained rocks.

The finer grained rock type typically consists of tabular to prismatic plagioclase, commonly 0.2 but occasionally up to 0.7 mm long, and granular pyroxene. The pyroxene being approximately 0.1 to 0.2 mm in diameter (Fig. 6.16). The ubiquitous granular magnetite (Fig. 6.13) is generally finer than the pyroxene. In places a rosette-like texture is developed. Here the plagioclase is long and thin, having dimensions up to 1 mm by 0.1 mm. These thin laths are arranged radially and there is some branching of individual crystals, again suggestive of rapid cooling (Lofgren, 1980). Pyroxene and magnetite habits resemble those in the other fine grained rocks.

The much more abundant, coarser grained MGN variety, typically possesses a partially radiate texture (Fig. 6.15), with normally zoned $(An_{65}-An_{55})$ prismatic plagioclase up to 1 mm in length, being partly arranged in a radial fashion about pyroxene nuclei. Both pyroxenes are anhedral often granular, ranging up to 0.5 mm in length or diameter. In several sections a poikilitic texture is observed and here either pyroxene may form anhedral grains up to 1 mm across, several of which are in optical continuity with each other. The poikilitic habit is however more common to orthopyroxene than it is to clinopyroxene. Anhedral magnetite grains in the coarser grained MGN are almost always associated with the margins of pyroxene even though they appear randomly distributed.

6.2.1.2   The quartz gabbronorite

As this rock type is essentially distinguished on its appearance in the field, there is, in thin section, a considerable variation in modal content, particularly with regard to quartz and biotite. Nevertheless the presence of

these two minerals in more than trace amounts and the overall coarser grain size serve to distinguish this rock type from the microgabbronorite, although there appears to be a gradation between them in places (chapter 5.1.2). Thus, in some cases partially radiate textures are seen, similar to those of the MGN, with only minor quartz and biotite (Fig. 6.17) while elsewhere quartz may exceed 20 modal per cent and coarse micrographic textures occur (Fig. 6.18).

The 'average' quartz gabbronorite lies somewhere between these two textural varieties, being characterised by abundant quartz (± 10 modal per cent) and similar amounts of biotite. Variable amounts of partially altered plagioclase (50-60 modal per cent) and pyroxene comprise the remainder along with minor magnetite and sulphides.

Plagioclase usually occurs as tabular to prismatic, subhedral crystals up to 1.5 mm in length. Alteration, particularly of the core region is common while strong normal zoning (An_{65}-An_{48}) is evident elsewhere. In some varieties the outer part of the crystal is intergrown with quartz in a fine micropegmatitic intergrowth.

Clinopyroxene possesses an irregular but elongate habit, with overall dimensions up to 1 mm by 3 mm. Modally it comprises approximately 50 per cent of the pyroxene content, although either pyroxene may predominate in individual varieties of the quartz gabbronorite. Clinopyroxene is frequently riddled with minute, opaque granules, while extensive exsolution of orthopyroxene and simple twinning is widespread.

Orthopyroxene typically occurs as rounded, subhedral crystals up to 0.5 mm in diameter, or, more rarely, as subhedral rod-shaped crystals 3 mm long by 0.5 mm across. In the rocks where clinopyroxene is riddled with opaque granules, the orthopyroxene appears to have recrystallised and now consists of a mosaic of smaller grains which pseudomorph a larger single individual. Coarse exsolution textures are rare in the smaller orthopyroxene crystals but the very fine exsolution lamellae of clinopyroxene, identical to those seen in the Rustenburg Layered Suite (Fig. 6.5), are common.

Quartz occurs as irregular 'pools', blebs, granular aggregates or occasionally as angular intersertal material or in micropegmatitic

1 MM

Fig. 6.17. Partially radiate texture in the quartz gabbronorite. Only minor amounts of quartz and biotite occur in this sample. Crossed polars.
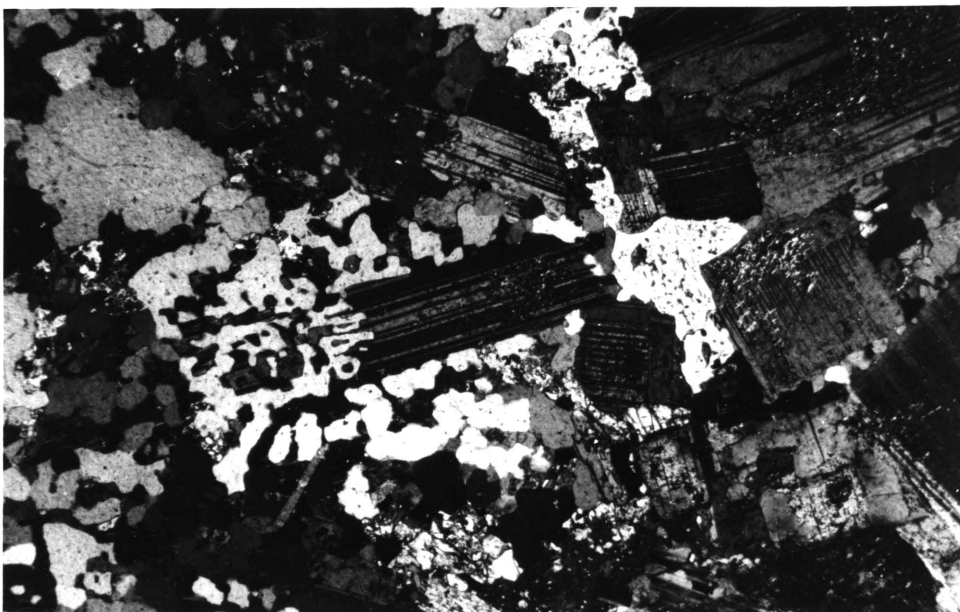
1 MM

Fig. 6.18. Coarse micrographic texture in heavily contaminated quartz gabbronorite. Crossed polars.

intergrowths. Some of the larger pools exceed 3 mm and contain rounded pyroxene and even a zircon in one instance (Fig. 6.19).

Biotite occurs as large, 1-3 mm wide flakes sometimes enclosing other mineral constituents poikilitically. Often several discrete flakes are in optical continuity over 10 mm or more and it is this characteristic of the quartz gabbronorite that is most obvious in hand specimen. Biotite is almost always associated with quartz and is often found partially replacing pyroxene.

Magnetite may form several per cent of some samples, usually occurring as irregular to skeletal grains associated with quartz and biotite. The isotropic dusty granules within clinopyroxene are tentatively identified as magnetite.

Hornblende occurs in several places forming pale green, pleochroic, irregular plates, with habits and dimensions similar to biotite.

6.2.2   Sills in the floor

6.2.2.1   The Middelwater Layered Sill and associated quartzofeldspathic rocks

6.2.2.1.1 The marginal facies

These meta quartz-dolerites show partial to almost complete alteration of primary mineralogy, and are characterised by the presence of varying amounts of quartz.

Plagioclase comprises 50 to 60 modal per cent of the rock and is invariably saussuritised to some extent. The original subhedral, 1 mm by 0.3 mm, blocky outlines of the mineral are retained however. In places plagioclase is partially enclosed in a sub-ophitic fashion by remnant pyroxene or its alteration products, commonly tremolite-actinolite (Fig. 6.20).

Pyroxene/Amphibole comprises 25 to 35 modal per cent of the rock. Although in places unaltered core regions of orthopyroxene remain (Fig. 6.21), pyroxene is usually completely replaced by felted masses and locally by long blades of amphibole. The latter is predominantly pale green to colourless tremolite - actinolite, although in places dark green to green pleochroic hornblende also occurs (Fig. 6.21).

1 MM

Fig. 6.19. Large quartz pool in the quartz gabbronorite containing a euhedral zircon (centre left). Although essentially a "basaltic rock" the presence of the zircon, along with the texture and overall abundance of quartz, suggests that the quartz gabbronorite is a contaminated rock type. Crossed polars.
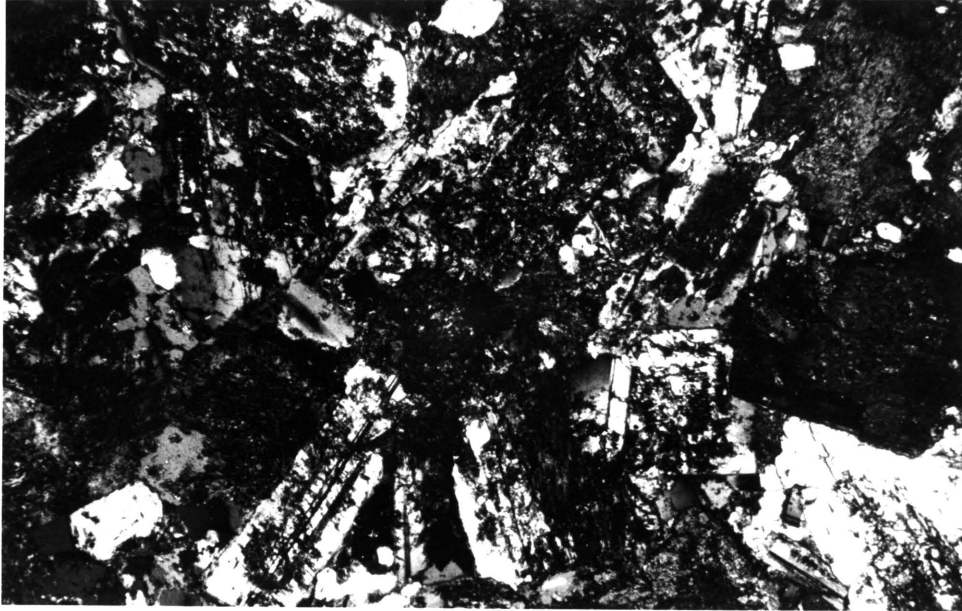
1 MM

Fig. 6.20. Relict sub-ophitic texture in meta quartz-dolerite of the Middelwater Layered Sill. Groundmass is predominantly tremolite-actinolite. Crossed polars.
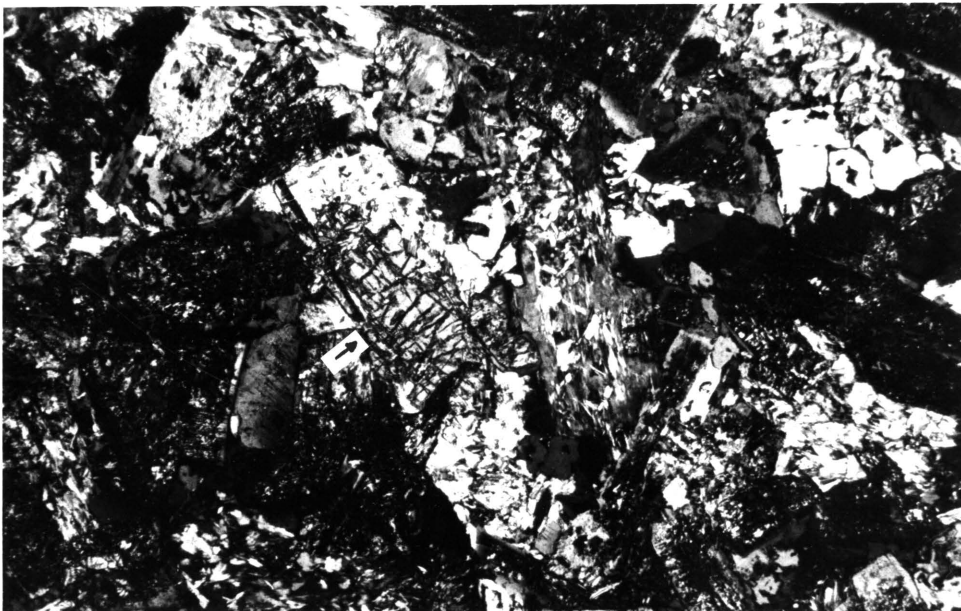
1 MM

Fig. 6.21. Relict orthopyroxene core (arrowed) in meta quartz-dolerite of the Middelwater Layered Sill. The adjacent "orthopyroxene" to the right is replaced by a felted mat of tremolite-actinolite. Crossed polars.

Quartz commonly occurs in two modes and may locally exceed 15 modal per cent of the rock. Micropegmatitic intergrowths with feldspar are common (Fig. 6.22) and these may be, at least in part, primary magmatic features. However the rather larger (0.5-1 mm, diameter), irregular to rounded blebs of quartz (Fig. 6.22), are interpreted as xenocrysts.

Quartz also occurs in some places as sub-rounded granular aggregates, up to 1.5 mm in diameter. These aggregates are also interpreted as xenocrysts and in fact the high modal content of quartz generally, is seen as convincing evidence of contamination in these rocks.

Biotite rarely exceeds 10 modal per cent and occurs as small pale brown to brown pleochroic flakes, 0.1 to 0.2 mm across, usually associated with amphibole, replacing pyroxene. It may also occur as similarly sized flakes intergrown with skeletal magnetite.

6.2.2.1.2 The cumulate sequence

The orthopyroxene - plagioclase adcumulates that make up the bulk of the Middelwater Layered Sill consist primarily of 40 to 60 modal per cent orthopyroxene, with the remainder plagioclase plus 5 to 10 modal per cent intercumulus clinopyroxene. Towards the top of the sequence, clinopyroxene occurs as a cumulus phase, where it may comprise 20 to 30 modal per cent of the rock. The rare plagioclase adcumulates (anorthosites) consist of 85 - 95 modal per cent plagioclase, with minor amounts of interstitial pyroxene. In thin section, 60 per cent of the samples studied exhibit slight to moderate alteration of pyroxene, while the accompanying plagioclase is invariably cloudy. In the remaining 40 per cent of the samples studied, the pyroxenes and feldspars are extensively altered (Fig. 6.23), as is the case with all the anorthositic rocks.

Orthopyroxene (Mg* 0.74-0.80) is always cumulus, except in the rare anorthosite layers, occurring either as rod-shaped (4 mm x 0.5 mm) crystals or stumpy subhedral prisms (1.5 mm x 0.75 mm) (Fig. 6.24). The orthopyroxenes, like those of the lower portion of the Rustenburg Layered Suite exhibit fine scale, parallel exsolution laminae of clinopyroxene (cf. Fig. 6.5.), while larger blebs of clinopyroxene also occur within the orthopyroxene host.

1 MM

Fig. 6.22. Micropegmatitic intergrowths in heavily contaminated meta quartz-dolerite of the Middelwater Layered Sill. Note also the large sub-rounded xenocrystic quartz grains (bottom right). Crossed polars.
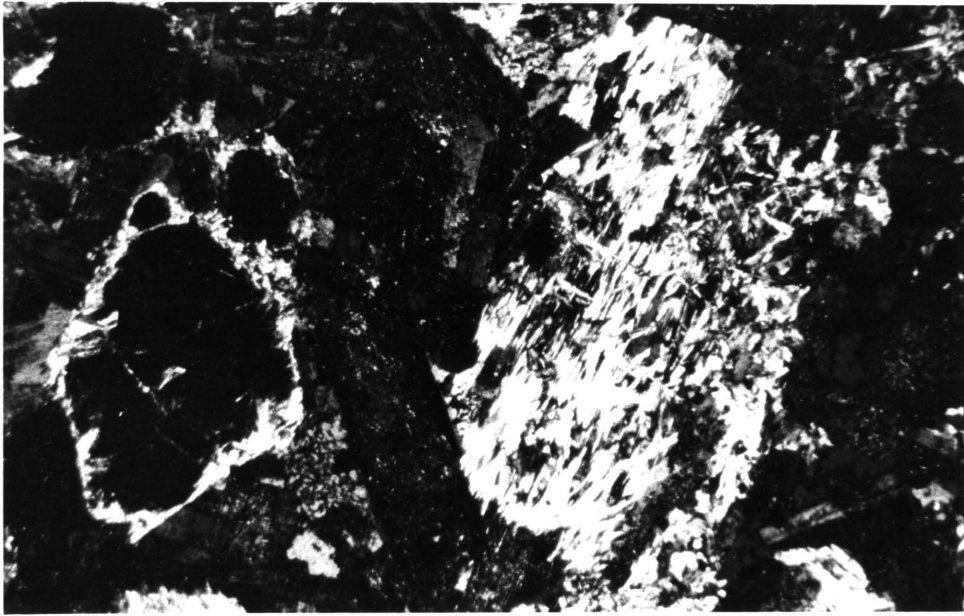
1 MM

Fig. 6.23. Extensively altered orthopyroxene and saussuritised plagioclase in noritic cumulates of the Middelwater Layered Sill. Relict orthopyroxene (left) occurs in places but the mineral is usually pseudomorphed by felted mats of tremolite-actinolite. Crossed polars.
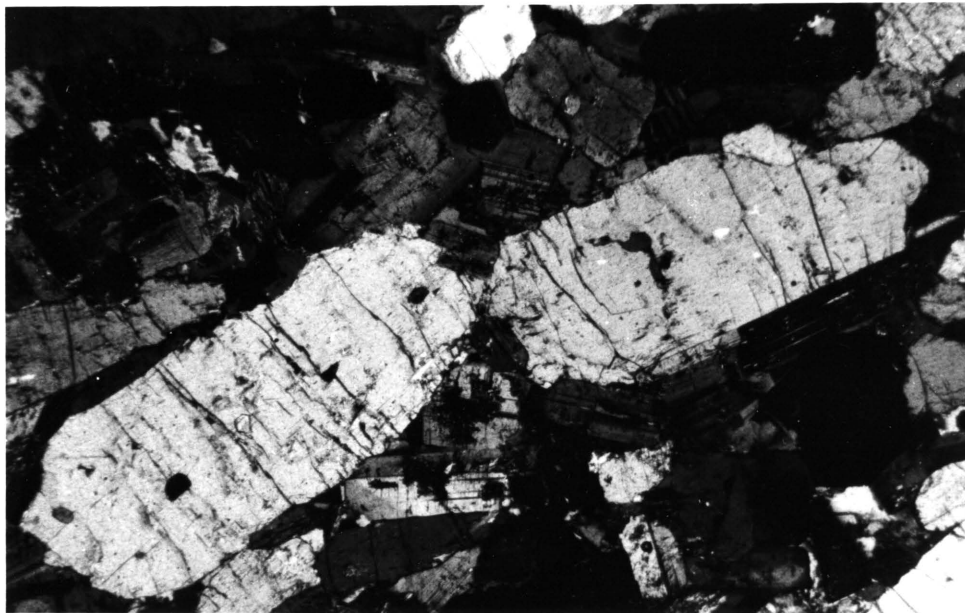
1 MM

Fig. 6.24. Stubby prisms of cumulus orthopyroxene in norite of the Middelwater Layered Sill. Crossed polars.

Plagioclase occurs as polysynthetically twinned, subhedral, cumulus crystals throughout most of the sequence, (Fig. 6.25). Although grain size varies, typical dimensions are 1.5 mm long by 0.5 mm in width, while sub-parallel alignment in places produces a weak igneous lamination (Fig. 6.25). One very characteristic feature of plagioclase from the Middelwater Layered Sill is its pronounced oscillatory zoning (Fig. 6.25), which clearly distinguishes these rocks from those of the Rustenburg Layered Suite further west. In places plagioclase is intercumulus, occurring as anhedral poikilitic plates enclosing orthopyroxene.

Another marked characteristic of plagioclase from the Middelwater Layered Sill is the ubiquitous dusty, or clouded appearance of the mineral (Fig. 6.26). Although the origin of this cloudiness is not clear, even at high magnifications, this is another feature which serves to separate the rocks of the Middelwater Layered Sill from those of the Rustenburg Layered Suite. This phenomenon also appears to be compositionally related in that the less calcic portions of the crystal are always more affected (Fig. 6.26). Clouding of plagioclase has received some attention in the literature and it is perhaps pertinent to briefly review its significance.

According to Macgregor (1931) clouded plagioclases are an undoubted indicator of thermal metamorphism. Poldervaart and Gilkey (1954) on the other hand, state that clouding of plagioclase is not necessarily the result of thermal metamorphism, although they concede that the requisite conditions to produce clouded plagioclases may frequently be realised during thermal metamorphism, especially in basic rocks. In view of this and the moderate to intense alteration of the pyroxenes (Fig. 6.23) it seems likely that the clouded plagioclases are indeed the result of thermal metamorphism. A conclusion also reached by Armbrustmacher and Banks (1974) for clouded plagioclase in metadolerites from Wyoming.

Clinopyroxene usually occurs either as large (6 mm by 3 mm) subhedral to anhedral poikilitic crystals or as small interstitial patches throughout most of the cumulate sequence (Fig. 6.27). However, near the top of the sequence the mineral occurs as subhedral to anhedral prismatic cumulus crystals up to 1.5 mm in length. The margins of these cumulus crystals are often altered to granular amphibole/magnetite intergrowths but there is no evidence of the exsolution

1 MM

Fig. 6.25. Cumulus plagioclase in norite of the Middelwater Layered Sill.
Note pronounced oscillatory zoning (arrowed) and weak alignment to produce
a crude igneous lamination. Crossed polars.
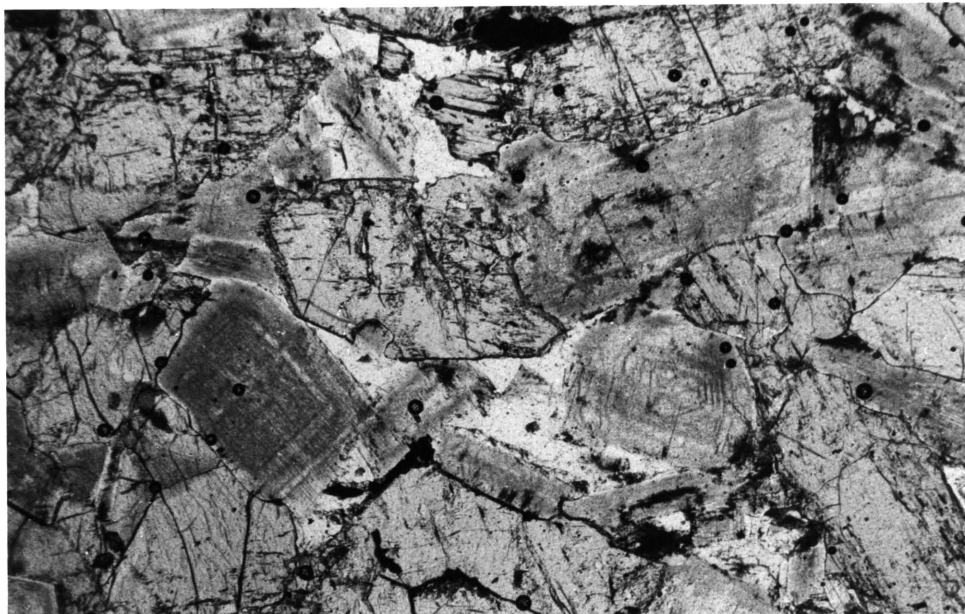
1 MM

Fig. 6.26. Characteristic clouded plagioclase in norite of the Middelwater
Layered Sill. Plane polarised light photomicrograph of the same field of
view as Fig. 6.25. Note that the oscillatory zoning is still clearly
visible, indicating that the degree of clouding is compositionally related.
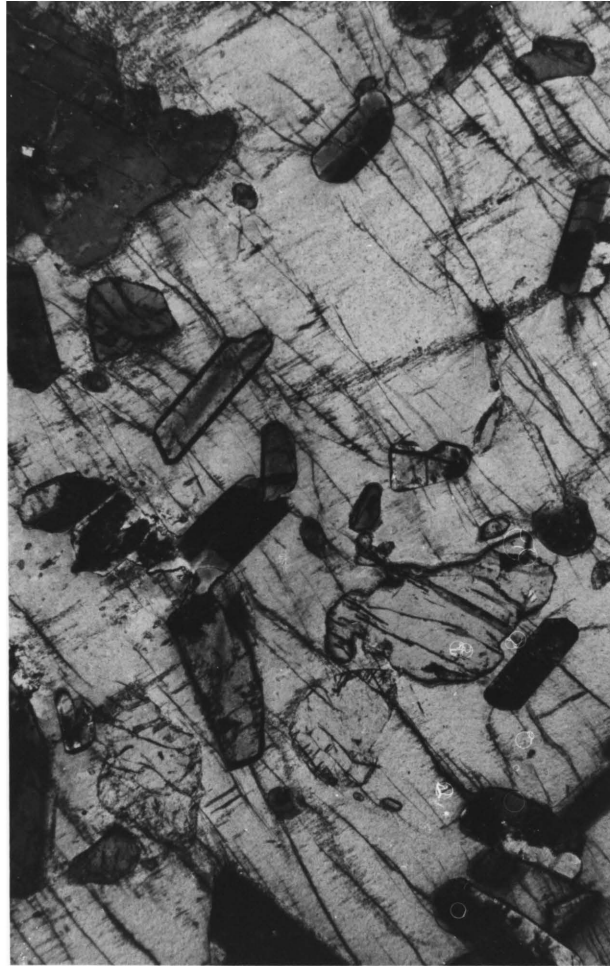
1 MM

Fig. 6.27. Large, slightly altered, poikilitic crystal of clinopyroxene in norite of the Middelwater Layered Sill. Note the lack of exsolution textures in the clinopyroxene. Crossed polars.

features seen in the clinopyroxenes of the Rustenburg Layered Suite (chapter 6.1.4.3).

Biotite locally comprises up to 2 modal per cent of the rock, occurring either as scattered anhedral flakes up to 0.5 mm in length or less often as smaller intercumulus scales.

Quartz occurs in some localities as angular intercumulus material but only in one place does it exceed one modal per cent of the rock. In this case quartz occurs as distinct 'pools' that make up some 10 modal per cent of the rock.

6.2.2.1.3 The quartzofeldspathic rocks

The petrography of this suite of rocks is somewhat varied, in keeping with the interpretation of them as a sequence of metamorphosed sediments. Thus only a generalised description is given here. Modally there appears to be little distinction between the two basic types i.e. the granophyric and granoblastic varieties (Figs. 6.28, 6.29), although some of the granophyric varieties have slightly higher feldspar contents. Thus both sets of rocks contain between 40 to 60 modal per cent quartz, 30 to 50 modal per cent feldspar and some 10 to 30 modal per cent mafics.

Although much of the feldspar is thoroughly saussuritised, the less altered crystals are clearly polysynthetically twinned plagioclase. Limited optical determinations indicate compositions of approximately An_{40}. In the granophyric rocks apart from the micrographic intergrowths, plagioclase also occurs as long prismatic crystals arranged in a radiating fashion. In the granoblastic rocks it occurs as smaller, anhedral to subhedral, prismatic or tabular crystals typically 0.3 mm in length.

The mafic minerals include green to dark green pleochroic hornblende and brown biotite. Either may predominate in individual rock types. In the granophyric rocks biotite often forms nested aggregates up to 1 mm across within which granular hornblende (0.1 – 0.2 mm across) and similarly sized irregular magnetite grains, occur.

In the granoblastic rocks individual biotite flakes up to 1 mm across and anhedral hornblende and magnetite are randomly distributed throughout the rock.
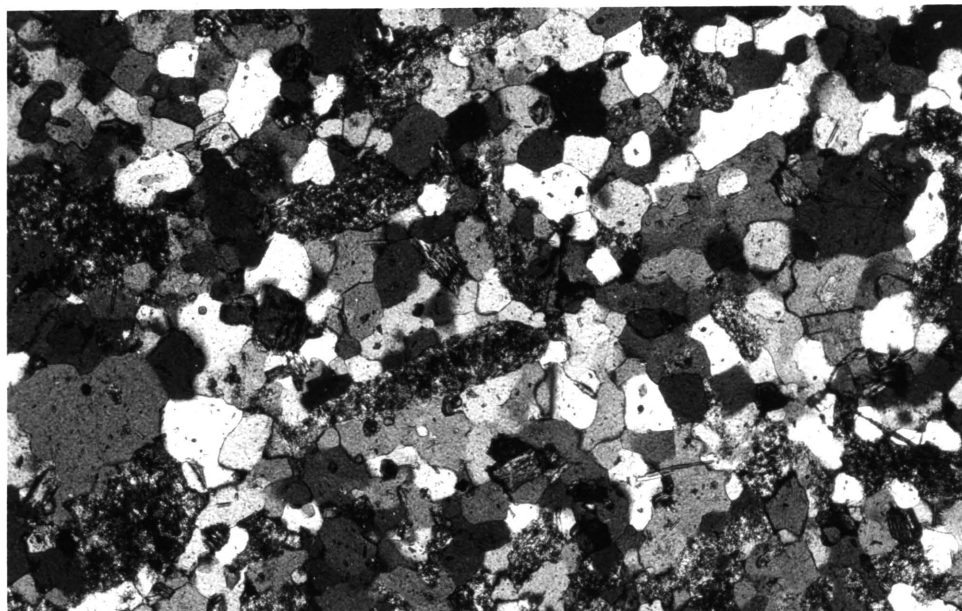
0.5 MM

Fig. 6.28. Granoblastic textured quartzofeldspathic rock. Feldspar is
typically saussuritised. Crossed polars.
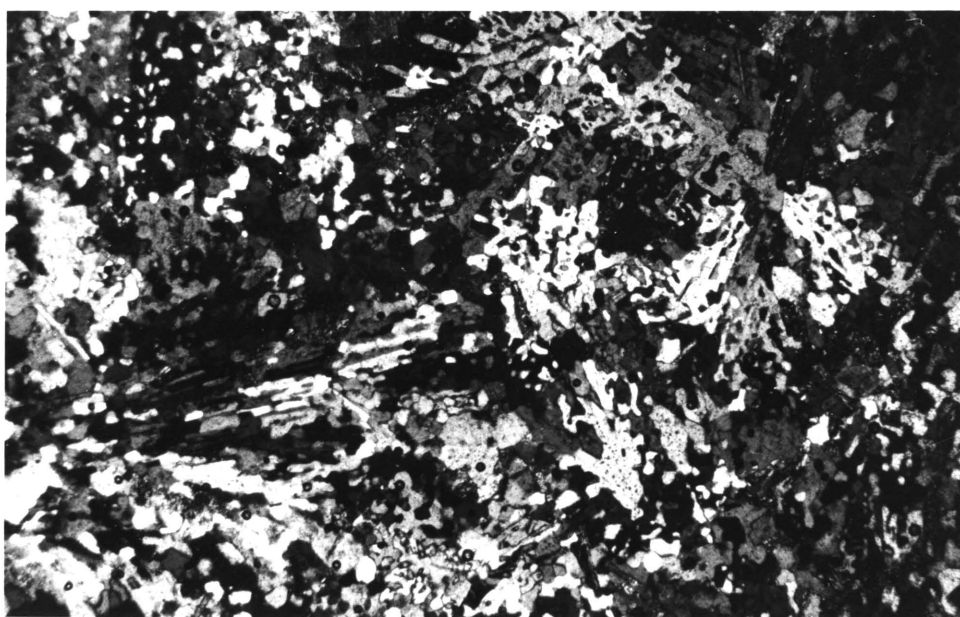
1 MM

Fig. 6.29. Granophyric textured quartzofeldspathic rock containing radiate,
fan-shaped plagioclase-quartz intergrowths. Crossed polars.

At one locality poikilitic hornblende occurs as sieve textured, sub-rounded, crystals, 1-2 mm across, containing numerous small round quartz grains.

6.2.2.2   Sills intruding the Magaliesberg Quartzite and Silverton Shale

6.2.2.2.1 The metadolerites

Of the seven thin sections of metadolerite examined, only two retain more than 10 modal per cent of their primary mineralogy. Even in these sections virtually none of the original mafic minerals are present while the feldspar, although still recognisable as such, is moderately altered. Relict chill textures are however still clearly visible (Fig. 6.30). Modally, plagioclase comprises approximately 40 per cent of the rock with the remainder largely tremolitic amphibole. The opaque minerals which comprise 1-2 modal per cent include randomly distributed aggregates of magnetite and minor pyrite. Rare interstitial patches of calcite are also present in the rocks at one locality.

In the remaining thin sections, ophitic to sub ophitic textures may still be recognised in places but generally little of the primary texture or mineralogy can be identified. These rocks consist for the most part of 50 to 60 modal per cent elongate, twinned blades of tremolite-actinolite, typically 1.5 mm long, set in a groundmass of saussuritised plagioclase. The latter mineral comprises the bulk of the remainder. The groundmass may also locally consist of fine radiating intergrowths of actinolite needles (< 0.1 mm long) and saussuritic alteration. Irregularly shaped serpentinitic and chloritic aggregates were also noted in two thin sections.

6.2.2.2.2 The meta quartz-dolerites

These rocks resemble the marginal rocks of the Middelwater Layered Sill in all respects, being rather variable both in modal composition, particularly with regard to quartz content and in degree of metamorphism.

Plagioclase is extensively to totally saussuritised in fifty per cent of the 30 thin sections examined, while in the remainder it is invariably altered to some degree. The mineral comprises 40 to 60 modal per cent of the rock typically occurring as short tabular crystals up to 1 mm in length. The outer

margins of many plagioclases are however intergrown micrographically with quartz (Fig. 6.31) so the mineral is rarely euhedral and often has a 'partially digested' appearance. Nevertheless, in places, euhedral core regions retain their original 'blocky' outlines surrounded by micrographic intergrowths. Pronounced normal zoning is widespread in plagioclase with optical measurements on combined carlsbad-albite twins indicating values of An_{40} decreasing to An_{20}.

Pyroxene/Amphibole comprises 30 to 40 modal per cent of the rock but only rarely is the original pyroxene recognisable. In this case pyroxene occurs as a relict core, surrounded by a felted mat of tremolite-actinolite, or more rarely by brown to green pleochroic hornblende. In two cases where both ortho- and clinopyroxene are still recognisable, clinopyroxene is slightly in excess of orthopyroxene.

Biotite comprises 5 to 10 modal per cent of the rock occurring either as small flakes < 0.1 mm long, intergrown with amphibole as replacement of pyroxene, or as larger flakes and aggregates up to 0.5 mm across commonly associated with skeletal magnetite in the groundmass.

Quartz makes up approximately 10 modal per cent of most rocks although in places up to 20 modal per cent occurs (Fig. 6.31). The mineral occurs predominantly as part of micrographic intergrowths with plagioclase or more rarely as discrete but irregularly shaped blebs up to 1 mm in diameter. The high modal percentage of micrographic material and the presence of discrete blebs which are interpreted as xenocrysts is considered to be evidence of contamination in these rocks.

6.2.2.2.3 The quench-textured micropyroxenites

These rocks are characterised by a variety of textures indicative of rapid cooling or quenching (Lofgren and Donaldson, 1975; Sharpe 1978; Lofgren 1980). Approximately 20 per cent of samples exhibit slight to moderate alteration of feldspar and pyroxene. Although there is a spectrum of textures, essentially two main types may be distinguished, by virtue of the grain size of their respective groundmasses. The one type is characterised by prominent orthopyroxene phenocrysts set in a devitrified or very fine grained matrix of acicular plagioclase, orthopyroxene and biotite (Figs. 6.32, 6.33). The acicular groundmass feldspar may be straight or curved and arranged in a

0.5 MM

Fig. 6.30. Sub-variolitic texture in one of the relatively fresh metadolerites. Partially altered, acicular feldspar is set in a groundmass of greenish tremolite-actinolite. Plane polarised light.
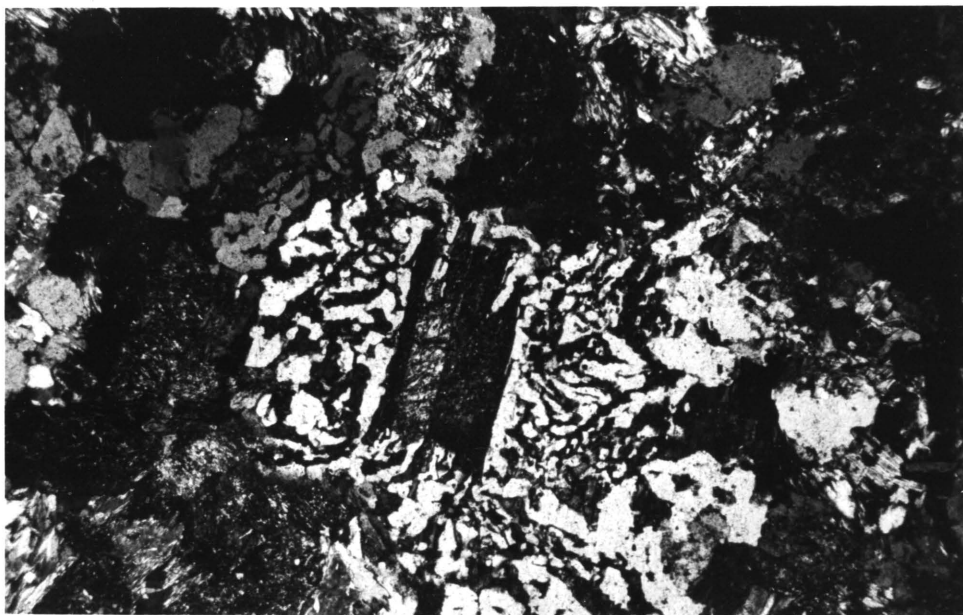
1 MM

Fig. 6.31. Micrographic intergrowths surrounding partially digested plagioclase in meta quartz-dolerite. Note the high modal percentage of quartz and the complete amphibolitisation of pyroxene. Crossed polars.
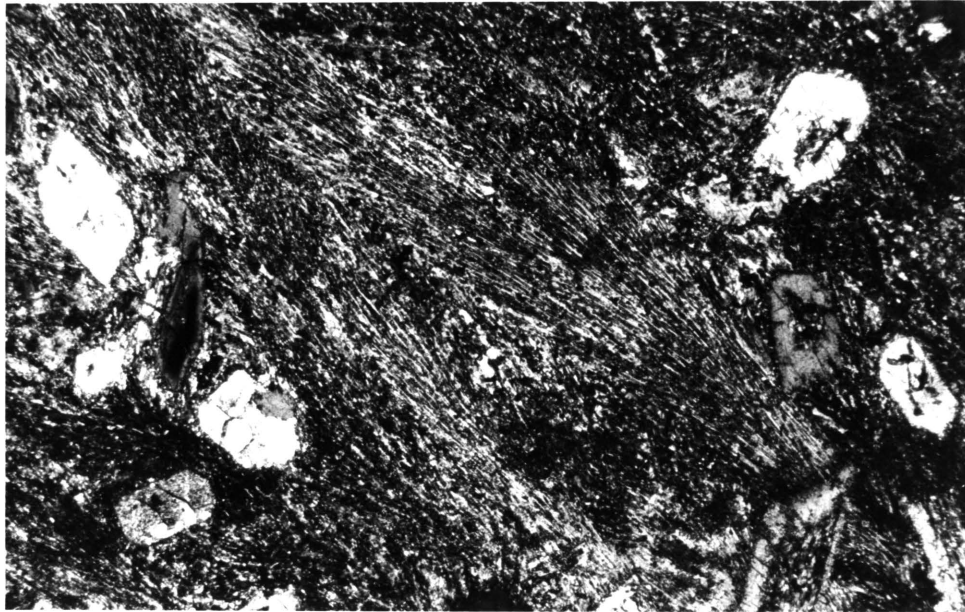
1 MM

Fig. 6.32. Sub parallel quench sheaves in very fine-grained QTM. The sheaves consist of acicular plagioclase enclosing minute granules of orthopyroxene and biotite. Crossed polars.
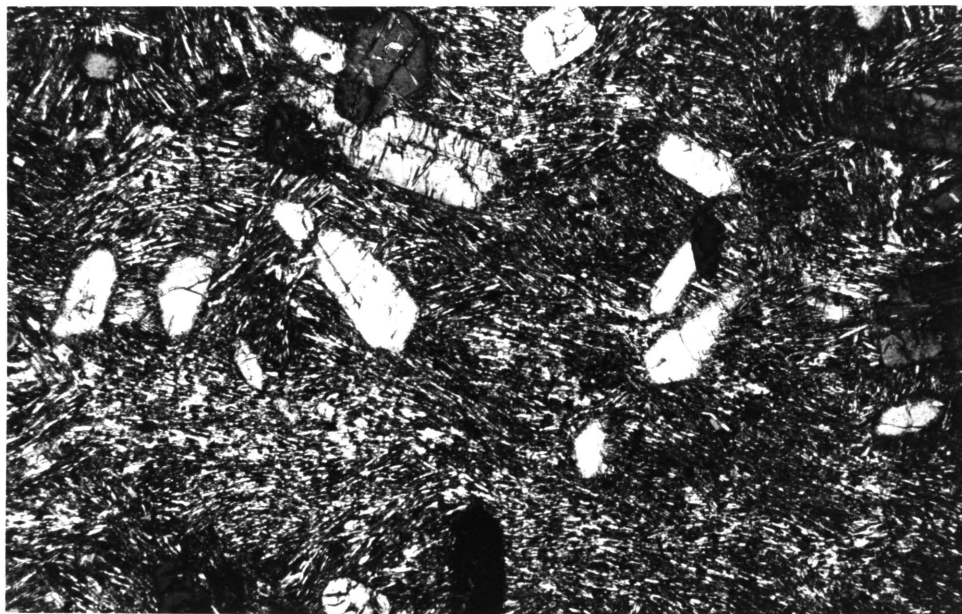
1 MM

Fig. 6.33. Pseudo-trachytoid texture in very fine-grained QTM. The texture is due to the mutual interference of small randomly orientated quench sheaves. Crossed polars.

fan-shaped or plumose fashion, forming small, random to sub-parallel quench sheaves (Fig. 6.32).

In places the matrix has an almost 'swirled' or trachytoid texture, although this appears to be due to mutual interference of sheaves during growth rather than the result of flow (Fig. 6.33). The very fine grained groundmass is restricted to the sills in which macroscopic 'cone diabase structures' are observed (chapter 5.2.2.3), regardless of whether the sample is taken from within the cone structures or not. In thin section the cone structures themselves are seen to be defined by the radial arrangement of sub-parallel plagioclase sheaves about a central focus, thus defining a quench cell. Angular differences between sheaves in adjacent cells define cone boundaries (Fig. 6.34). In the other textural variety, the groundmass is much coarser and plagioclase, retaining an acicular branching habit, may reach 1 mm in length (Fig. 6.35).

Some sills however, have textures intermediate between the two main types (Fig. 6.36) and thus it is considered that the variation in textural types is the result of individual cooling histories rather than intrinsic geochemical differences. Possibly the cone textured sills with the fine grained groundmass were intruded slightly earlier, pre-heating the country rocks into which the coarser grained sills were subsequently intruded. General petrography of these texturally variable rocks is as follows.

Orthopyroxene (Mg* 0.83 - 0.87) comprises 40 to 50 modal per cent of most rock types with approximately 10 to 20 modal per cent occurring as stubby to elongate, sometimes arcuate, skeletal prisms and hopper-shaped crystals (Fig. 6.37). These phenocrysts are often reverse zoned and may reach 5 mm in length but are typically 0.5-2 mm long. Some rare, extremely acicular crystals up to 20 mm long have also been observed. Dimensions vary greatly however, even within the same thin section, probably as a result of phenocryst orientation. In places interpenetration twins occur and a glomeroporphyritic texture may also be observed in some of the finer grained rocks.

The remaining 20 to 30 modal per cent of orthopyroxene occurs as much finer, granular to elongate crystals confined within the plagioclase sheaves of the groundmass. Grain sizes are typically 0.01 to 0.02 mm in the finer grained rocks and 0.1 to 0.2 mm in the coarser varieties.
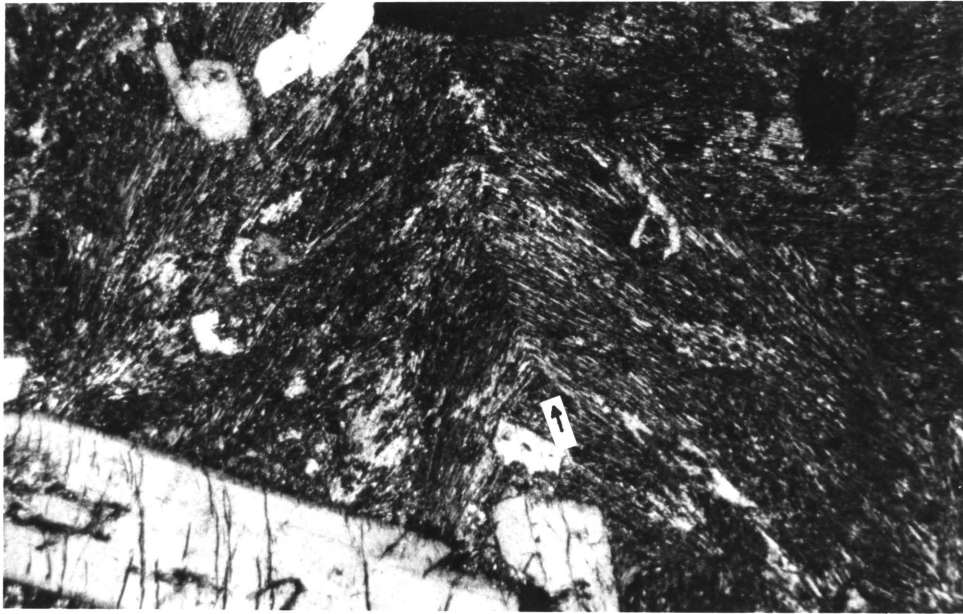
1 MM

Fig. 6.34. Junction between adjacent conical cells in cone diabase (arrowed). Sub parallel quench sheaves in the right hand cell lie more or less at right angles to those in the left hand cell. Crossed polars.

1 MM

Fig. 6.35. Comb-textured, acicular plagioclase in a coarser grained variant of the QTM. Crossed polars.

1 MM

Fig. 6.36. QTM with relatively large, curved, comb-textured plagioclase,
set in an extremely fine-grained, devitrified, glassy groundmass.
Crossed polars.
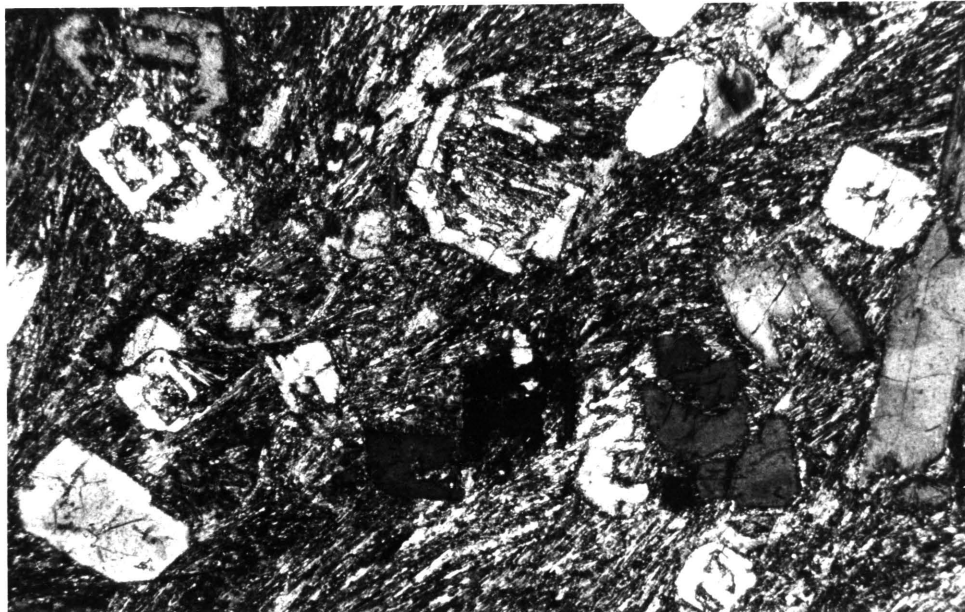
1 MM

Fig. 6.37. Skeletal prisms and hopper-shaped orthopyroxene phenocrysts in
fine-grained QTM. Crossed polars.

Plagioclase typically comprises 40 to 50 modal per cent of the rock and exhibits a variety of habits and textures. In general however, habits are acicular, with plagioclase forming sheaf-like radiating growths in the finer grained rock types (Figs. 6.32, 6.33) and a series of arcuate, branched, plumose or fan-shaped crystals and aggregates in the coarser grained varieties, (Figs. 6.35, 6.36). Some of the latter resemble textures developed in comb layering (Lofgren and Donaldson, ibid.; Donaldson, 1977). Plagioclase compositions are difficult to determine both because of grain size or shape and because of the presence of normal zoning and or cloudy alteration of crystal cores. Optically determined An values for plagioclase lie in the range $An_{60}-An_{75}$.

Biotite is a common accessory mineral in the groundmass of the finer grained rocks, consisting of minute anhedral grains and slightly elongate flakes, of similar dimensions and occurrence to the groundmass orthopyroxene. In places biotite may almost equal the latter in modal abundance, in which case it may consititute up to 15 modal per cent of the rock. In the coarser grained rocks biotite rarely exceeds 5 modal per cent, occurring as irregular interstitial flakes approximately 0.5 mm across, often in association with amphibole and or magnetite.

Amphibole is present in minor amounts in many places, usually as a uralitisation product. However, in the few places where alteration is more extensive, several modal per cent green to pale green pleochroic hornblende occurs, either as irregular grains associated with alteration of pyroxene phenocrysts or as much smaller, anhedral grains replacing pyroxene in the groundmass.

Micropegmatite occurs in minor amounts in two coarser grained variants, one of which exhibits an almost sub-ophitic texture whilst still containing arcuate and branched feldspar.

6.2.2.2.4 Pyroxenites

The rocks of the feldspathic pyroxenite-melanorite sill east of Silkaatsnek (Folder 1), strongly resemble cumulates from the pyroxenite sub-zone of the Rustenburg Layered Suite, even containing large intercumulus plates of plagioclase similar to those shown in Figure 6.6. This sill is considered to be a squeezed out mass of critical zone rocks.

The two olivine-bearing pyroxenites are however unique. in that these are the only olivine bearing cumulates exposed throughout the study area. Both occurrences are very similar petrographically and both contain a higher proportion of orthopyroxene than the sill east of Silkaatsnek. as well as cumulus chromite. Their origin is discussed in chapter 7.4 and their petrography is given below.

Orthopyroxene (Mg* 0.80 - 0.87) comprises 60 to 70 modal per cent of the rock. occurring as subhedral, stubby to elongate. cumulus prisms. typically 1 to 2 mm long by 0.5 mm wide (Fig. 6.38). In places there is also a sub-parallel alignment of the long axes of individual crystals. but igneous lamination is not generally pronounced (Fig. 6.38).

Plagioclase forms approximately 20 modal per cent of the rock either in the form of small intercumulus patches or as plates up to 2 mm across. enclosing smaller cumulus orthopyroxenes.

Olivine (Fo$_{79}$) comprises less than 5 modal per cent of the rock. occurring as small (0.2 - 0.4 mm diameter) rounded to subhedral. cumulus crystals (Fig. 6.39) which may be included in orthopyroxene. Olivine is not randomly distributed however. and in thin section it occurs only in certain discrete. olivine-rich areas of the thin section (Fig. 6.39).

Biotite forms 2 to 3 modal per cent of the rock. occurring as 0.5 mm to 1 mm long. intercumulus flakes.

Clinopyroxene comprises less than 2 modal per cent. consisting of rounded. irregular to ragged grains replacing orthopyroxene. It is rarely fresh and is commonly altered to amphibole. biotite and dusty opaques.

Chromite is prominent as tiny grains in thin section. although it forms less than one modal per cent of the rock. The mineral occurs as tiny, rounded to tetragonal shaped cumulus crystals. approximately 0.05 mm across (Fig. 6.40). Although widespread, chromite is almost always enclosed in cumulus orthopyroxene and olivine.

Micropegmatite forms less than 1 modal per cent of the rock, occurring as isolated intersertal patches, or marginal to intercumulus plagioclase.
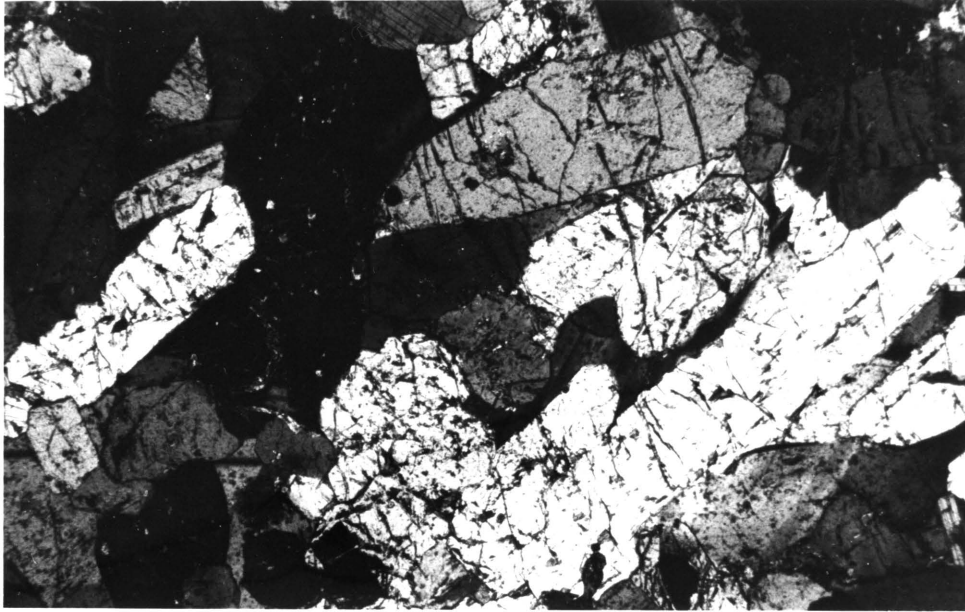
1 MM

Fig. 6.38. Stubby prisms of cumulus orthopyroxene and minor intercumulus plagioclase in olivine-bearing pyroxenite. There is some alignment of the orthopyroxene defining a weak igneous lamination. Crossed polars.
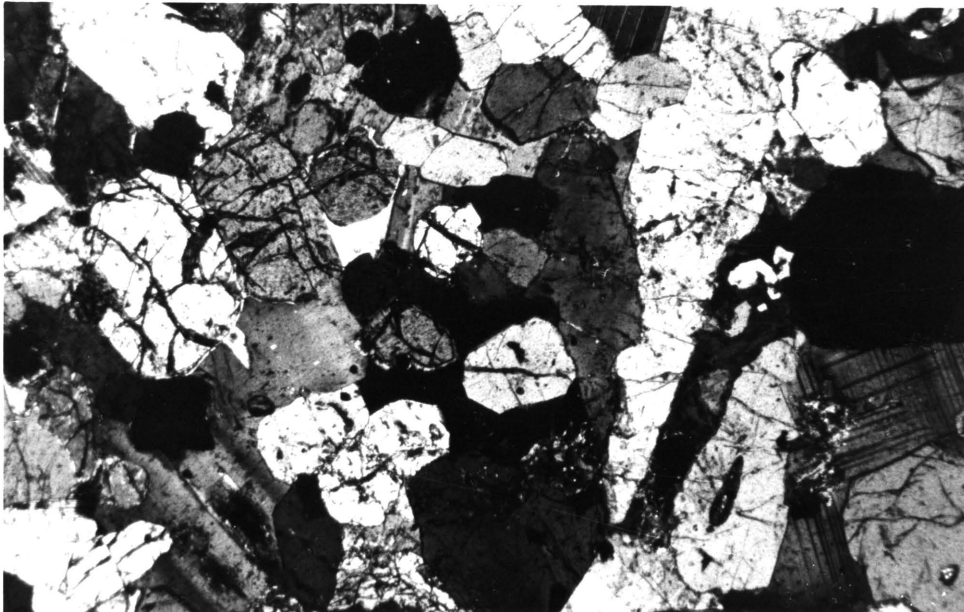
1 MM

Fig. 6.39. Rounded to subhedral olivine grains in olivine-bearing pyroxenite. Note the restriction of olivine to discrete areas of the rock (as shown by the top left quarter of the photomicrograph). Crossed polars.
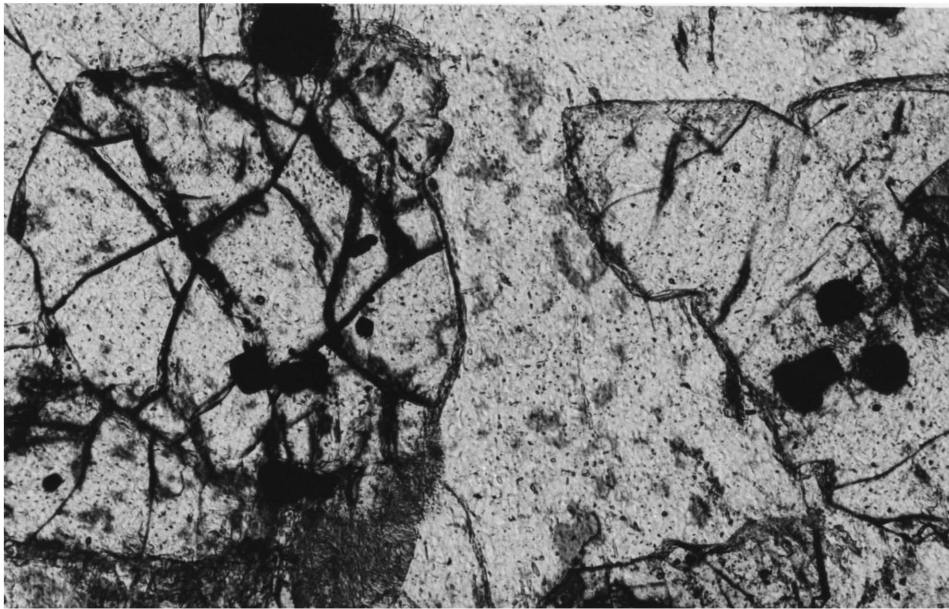
0.25 MM

Fig. 6.40. Tetragonal to rounded, cumulus chromite, enclosed in cumulus olivine (left) and cumulus orthopyroxene (right). Plane polarised light.

7.   GEOCHEMISTRY

7.1   INTRODUCTION

Whole rock major and trace element analyses on ±220 samples were undertaken. The initial aim of this was to characterise and correlate, or distinguish between, the various lithologies recognised in the field or petrographically. This is important since many of the rock types vary petrographically. Furthermore a better understanding of the petrogenesis of the various rock types, their interrelationships and their bearing on the formation of the Complex as a whole, has been gained from the geochemical investigation. Details of sample preparation, analytical techniques, precision and accuracy are given at the beginning of Appendix 1.

For various reasons it is inconvenient to retain the discrete separation called for in the earlier descriptive chapters on field relationships and petrography (i.e chapters 2, 5 and 6). In this chapter various rock groups are discussed in terms of natural groupings which will be validated by the ensuing discussion. Thus it is convenient to deal with the metadolerites, meta quartz-dolerites and the marginal rocks of the Middelwater Layered Sill together, since they form a natural grouping being older than the other igneous rocks in the area. Similarly, both the quench-textured pyroxenite and microgabbronorite are considered together, because being the most voluminous, fresh, uncontaminated rocks in the area they were considered to have possible parental relationships to the main Complex.

Throughout the text, the expression weight percent of major elements refers to the anhydrous normalised values, except in Section 7.2 where loss on ignition is necessarily included in the discussion.

7.2 THE METADOLERITES (MD), META QUARTZ-DOLERITES (MQD), AND MARGINAL ROCKS OF THE MIDDELWATER LAYERED SILL

As a first approach it is pertinent to establish whether the geochemistry of these rocks is original or whether it has been modified by alteration.

Combined water (H_2O+) has been used as a measure of the degree of alteration of basalts, (Hart et al. 1974). Although these authors only applied

this criterion to sea floor alteration, it should still prove a useful indicator of the degree of metamorphism of the rocks under discussion. This is because low grade metamorphism in these rocks is dominated by hydration reactions such as the conversion of pyroxene to amphibole. Although H_2O+ was not specifically determined but only loss on ignition (LOI), there is obviously some error in assuming that H_2O+ = LOI. However, in the absence of petrographic evidence for significant quantities of e.g. sulphides or calcite in these rocks, it is reasonable to assume that LOI is at least proportional to H_2O+.

To assess whether the geochemistry of these rocks has been significantly altered, a selection of the more important major and trace elements in the meta quartz-dolerites were plotted, using LOI as abscissa (Figs. 7.1 - 7.5).

It is apparent from Figures 7.1 to 7.3 that there is little change in major element content with increase in hydration i.e. metamorphism. For example in the SiO_2 vs. LOI plot for the meta quartz-dolerites (Fig. 7.1) the regression intercept at 0 per cent LOI on the X-axis is 55.69 SiO_2, while the calculated value at 2.5 per cent LOI is 55.03. Therefore, there is an approximate decrease of 0.7 wt per cent in SiO_2 (or 1.2 per cent relative) over the whole range of LOI values. No explanation for the very slight increase in SiO_2 in the metadolerites (± 2.0 per cent relative at 2.5 per cent LOI) is immediately apparent, although this may be an anomalous trend resulting from the small sample population (i.e. seven). Nevertheless this does not alter the fundamental tenet of the hypothesis i.e. that such small variations in major element content with increase in LOI, do not significar⁺ly influence the position of samples plotted on subsequent diagrams. Even Al_2O_3, CaO and K_2O, which are considered mobile under low grade conditions (Elliot, 1973; Pearce, 1975), show only a slight correlation with LOI; for example the decrease in Al_2O_3 is about 0.70 wt per cent at 2.5 wt per cent LOI. Although this represents an overall 4 per cent relative decrease in total Al_2O_3, this again has not significantly affected the position of samples plotted in subsequent figures (e.g. Fig. 7.35).

Plots of data points and calculation of regression lines for the metadolerites and Middelwater Layered Sill meta quartz-dolerites generally show similar results to those discussed above. That is, except for CaO in the metadolerites there is no significant increase or decrease in major element content with increase in LOI. For the sake of clarity however, only regression
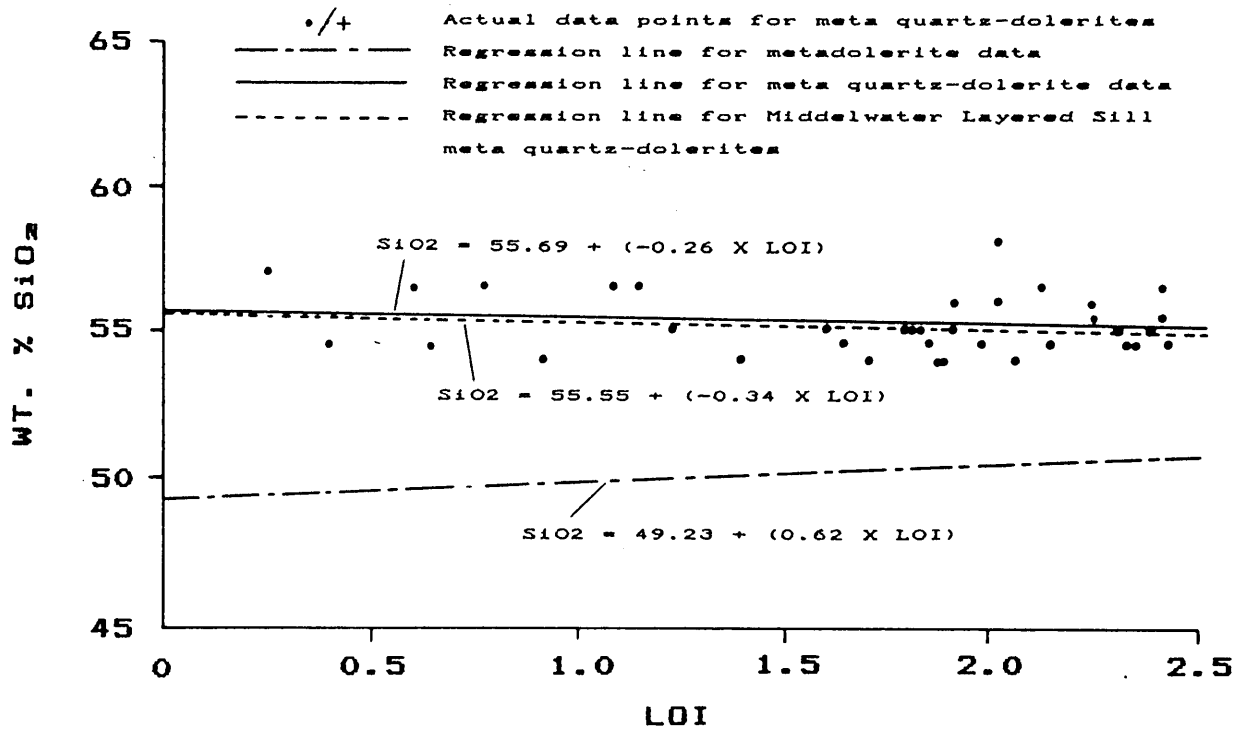
Fig. 7.1. Binary plot of SiO₂ vs. LOI.
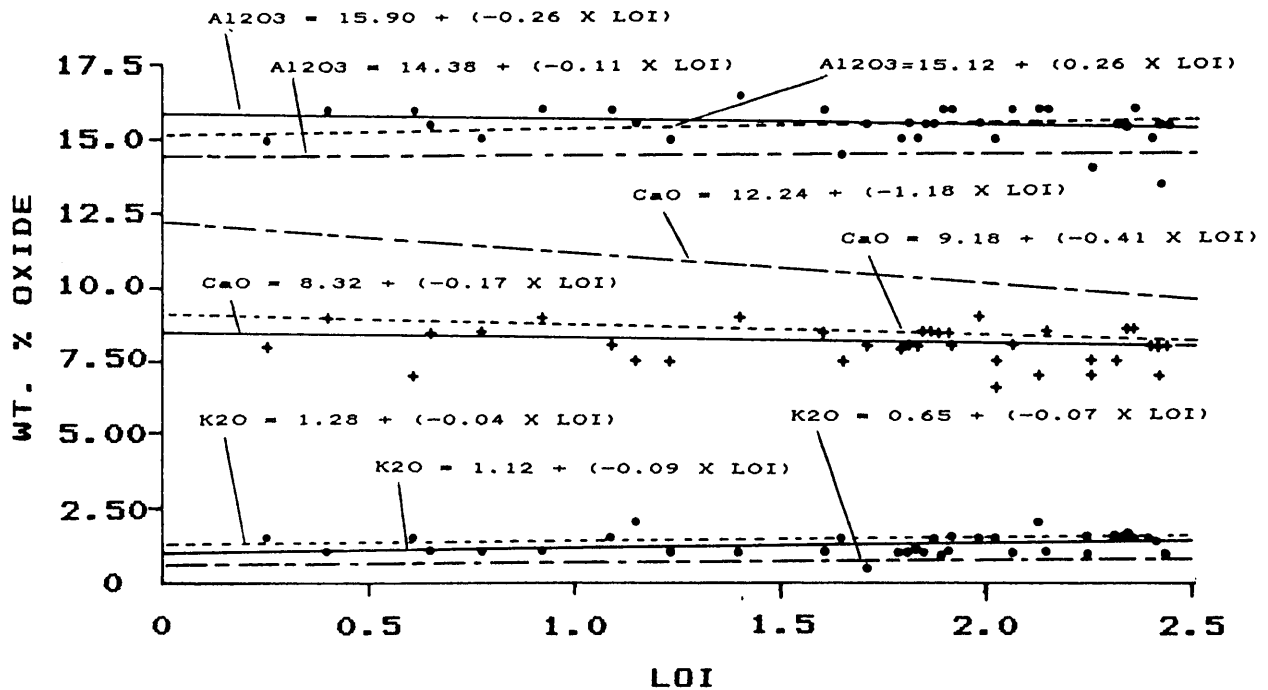
Fig. 7.2. Binary plot of Al₂O₃, CaO and K₂O vs. LOI.
Regression line symbols as for Fig. 7.1.
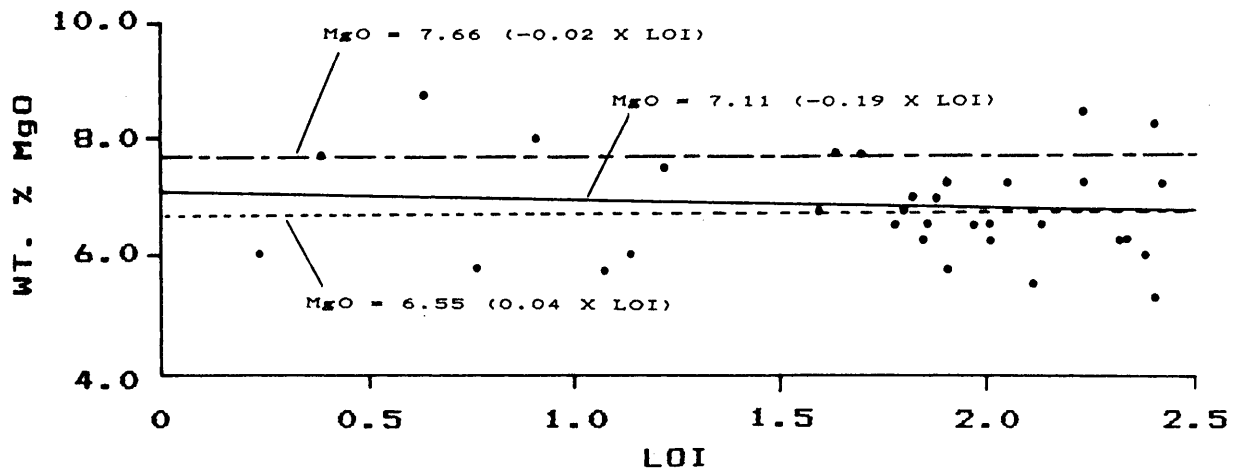
Fig. 7.3. Binary plot of MgO vs. LOI. Regression line symbols as for Fig. 7.1.
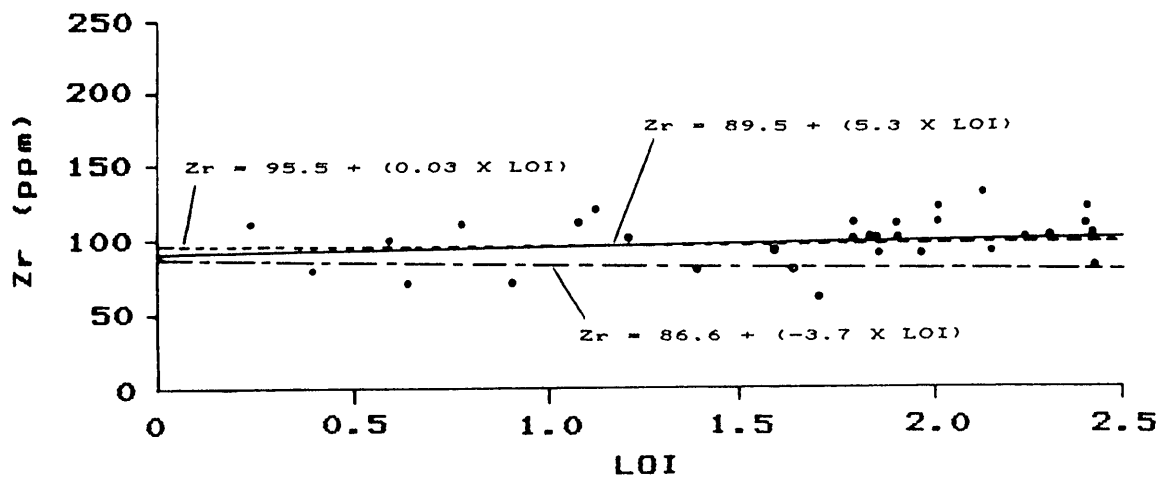
Fig. 7.4. Binary plot of Zr vs. LOI. Regression line symbols as for Fig. 7.1.
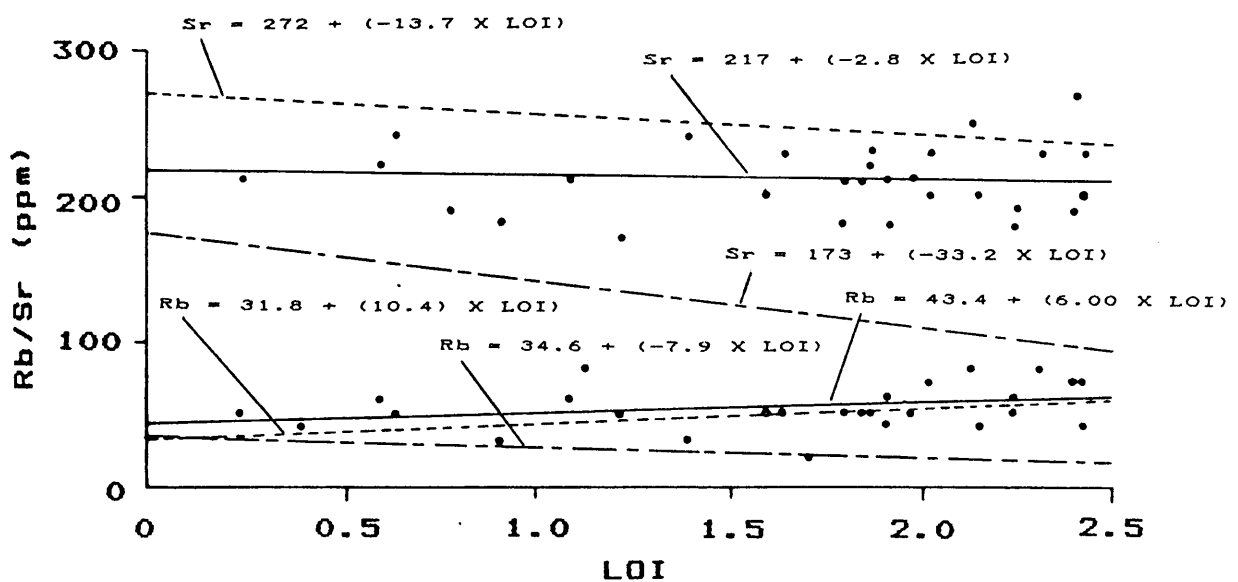
Fig. 7.5. Binary plot of Rb and Sr vs. LOI. Regression line symbols as for Fig. 7.1.

lines for this data are shown and these are superimposed on the meta quartz-dolerite data in Figures 7.1-7.3.

Plots and regression lines for the trace elements are similar in all three rock types for Zr (Fig. 7.4), although some slight positive correlation with LOI is apparent for both sets of meta quartz-dolerites, while this correlation is slightly negative for the metadolerites. With increase in metamorphism (LOI) Sr is largely unaffected in the meta quartz-dolerite sills, but like CaO, Sr shows a marked depletion with increase in LOI in the metadolerites, with a similar but less marked decrease in the marginal rocks of the Middelwater Layered Sill (Fig. 7.5). Rb exhibits similarly erratic behaviour increasing strongly in both sets of meta quartz-dolerites with increase in LOI, while the converse is true for the metadolerites[1].

As a result of the behaviour of trace elements, only Zr was considered appropriate for use in later diagrams (e.g. Fig. 7.36). In contrast however, it is clear that most of the major element data, with the possible exception of CaO, may be used with some degree of confidence.

Furthermore, since almost all elements have slightly negative correlations with LOI (possibly as a result of the "constant sum effect" - Chayes, 1964) recalculation to an anhydrous basis is likely to lessen the hydration effects even more. It is also apparent from Figures 7.1 - 7.5 that the geochemistry of the Middelwater Layered Sill meta quartz-dolerites and the other meta quartz-dolerite sills is virtually identical. This strongly supports the earlier suggestion (chapter 5.2.2.2) that the Middelwater Layered Sill is merely a thicker version of the meta quartz-dolerite sills. Chemically all of these quartz-dolerites (Appendices 1 and 2) are characterised by high weight per cent contents of SiO_2 and Rb, as compared with other continental basalts (Tables 7.1 and 7.2) i.e. 56 per cent (anhydrous normalised) and 45-50 ppm

---

[1]These strong increases or decreases are not immediately apparent from Figure 7.5 because of the scale on the vertical axis. However, consideration of the regression line equation for both sets of meta quartz-dolerites indicates a 35 to 80 per cent increase in Rb over the range of LOI values. Similarly a decrease of some 40 per cent is indicated for the metadolerites.

TABLE 7.1

Average major element composition of typical continental basalts and dolerites

	1	2	3	4	5	6	7
SiO_2	49.5	53.8	47.7	50.0	49.7	52.1	51.8
Al_2O_3	15.5	13.9	15.1	13.9	8.9	14.1	14.8
Fe_2O_3	3.8	2.6	6.4	8.7	2.0	3.7	3.9
FeO	7.8	9.2	5.5	5.3	10.5	8.4	7.3
MnO	0.2	0.2	0.2	0.2	0.2	0.2	0.2
MgO	6.2	4.1	8.2	4.4	15.3	5.5	7.1
CaO	10.2	7.9	7.6	5.4	.7.7	8.7	10.6
Na_2O	2.8	3.0	2.9	3.9	1.6	2.6	2.4
K_2O	0.6	1.5	0.8	1.6	1.6	1.7	0.7
TiO_2	1.6	2.0	1.5	2.7	2.7	2.6	1.1
P_2O_5	0.3	0.4	0.2	0.4	0.4	0.4	0.1
H_2O+			3.7	3.3	–	–	–
H_2O-	1.6	1.2	–	–	–	–	–
CO_2	–	–	0.2	0.3	–	–	–
TOTAL	100.1	99.8	100.0	100.1	100.6	100.0	100.0

	8	9	10	11	12	13	14
SiO_2	50.51	52.65	53.4	50.40	53.75	55.65	48.88
Al_2O_3	12.65	14.42	15.4	15.51	14.23	13.95	13.68
Fe_2O_3	3.12	2.76	0.8	0.99	2.23	3.24	–
FeO	11.23	10.02	8.4	7.83	7.61	7.38	13.43*
MnO	0.23	0.14	0.1	0.17	0.18	0.17	0.20
MgO	5.45	4.98	6.7	10.60	6.64	4.50	6.57
CaO	10.57	8.96	11.1	10.87	10.60	8.51	11.29
Na_2O	2.43	3.01	1.7	1.42	1.83	2.50	2.35
K_2O	0.61	1.08	1.0	0.37	0.81	1.45	0.26
TiO_2	2.85	1.70	0.6	0.44	0.70	1.03	2.57
P_2O_5	0.35	0.28	0.1	0.08	0.18	0.23	0.28
H_2O+	–	–	0.7	1.21	0.64	0.98	–
H_2O-	–	–	–	0.34	0.67	0.69	–
TOTAL	100.0	100.0	100.0	100.23	100.07	100.28	99.51

*Total iron as FeO

1,2 = Columbia River basalts
3,4 = Keweenawan basalts
5,6,7 = Karoo basalts
8,9 = Deccan basalts

10 = Tasmanian diabase
11,12,13 = Ferrar diabase
14 = Blosseville Coast basalt

(Data from Hughes, 1982; Table 10.7)

TABLE 7.2
Average concentration, in ppm, of selected trace elements in typical
continental basalts and dolerites

	1	2	3	4	5	6	7	8	9
Ni	44	19	763	170	73	249	85	53	79
Cr	79	38	875	280	317	352	142	59	148
Rb	11	33	–	–	–	12	30	50	2.5
Sr	241	280	1,200	706	190	100	126	138	287
Zr	160	200	285	196	85	53	83	157	151

1,2   = Columbia River basalts
3,4,5 = Karoo basalts
6,7,8 = Ferrar diabases
9   = Blosseville Coast basalt

(Data from Hughes, 1982; Table 10.8)

respectively. They are probably contaminated and do not therefore represent original magmatic compositions.

The metadolerites however, form a distinct group with several weight per cent less SiO_2 (51.5) and lower Rb contents (18 ppm) (Appendices 1 and 2) i.e. well within the range of typical continental basalts and dolerites (Tables 7.1 and 7.2). They lack visible evidence of contamination and are considered to represent pristine, although clearly not primary, magmatic compositions. They may be classified, on CIPW normative composition, as quartz tholeiites (Yoder and Tilley, 1962) with normative quartz contents averaging 3.6 per cent along with ±25 per cent essential hypersthene.

On discrimination diagrams for altered basalts (Winchester and Floyd, 1976), these rocks clearly fall into the tholeiite field (Fig. 7.6) and furthermore, on the Nb/Y vs. Zr/P_2O_5 x 10^4 diagram, (Fig. 7.7), there is a clear horizontal linear trend, typical of tholeiitic rocks (Winchester and Floyd, ibid). These plots are based on elements presumed to be 'immobile' during metamorphism and are preferable to the more widely used Ti-Zr-Y 'discrimination diagrams' of Pearce and Cann (1973), as shown by the work of Morrison (1978) and Holm (1982). These last two authors show that the Pearce and Cann plots are inapplicable to continental tholeiites. The metadolerites also fall well within the tholeiite field on the Na_2O + K_2O vs. SiO_2 diagram of Kuno (1966: Fig. 7.8). On the AFM diagram (Fig. 7.9) there is, as might be expected from such a small number of samples, little indication of a trend. Interestingly though, when the metadolerites are compared with the later, fresher, microgabbronorite (Fig. 7.31), there are clear geochemical similarities.

7.3 THE QUENCH-TEXTURED MICROPYROXENITES (QTM), MICROGABBRONORITE (MGN) AND QUARTZ-GABBRONORITE (QGN)

7.3.1 Introduction

Volumetrically these three rock types comprise the bulk of the unmetamorphosed sills (QTM) and marginal rocks (MGN and QGN). The quartz gabbronorite (QGN) is however considered to be contaminated (chapter 4.2), being geochemically similar to the meta quartz-dolerites discussed above in
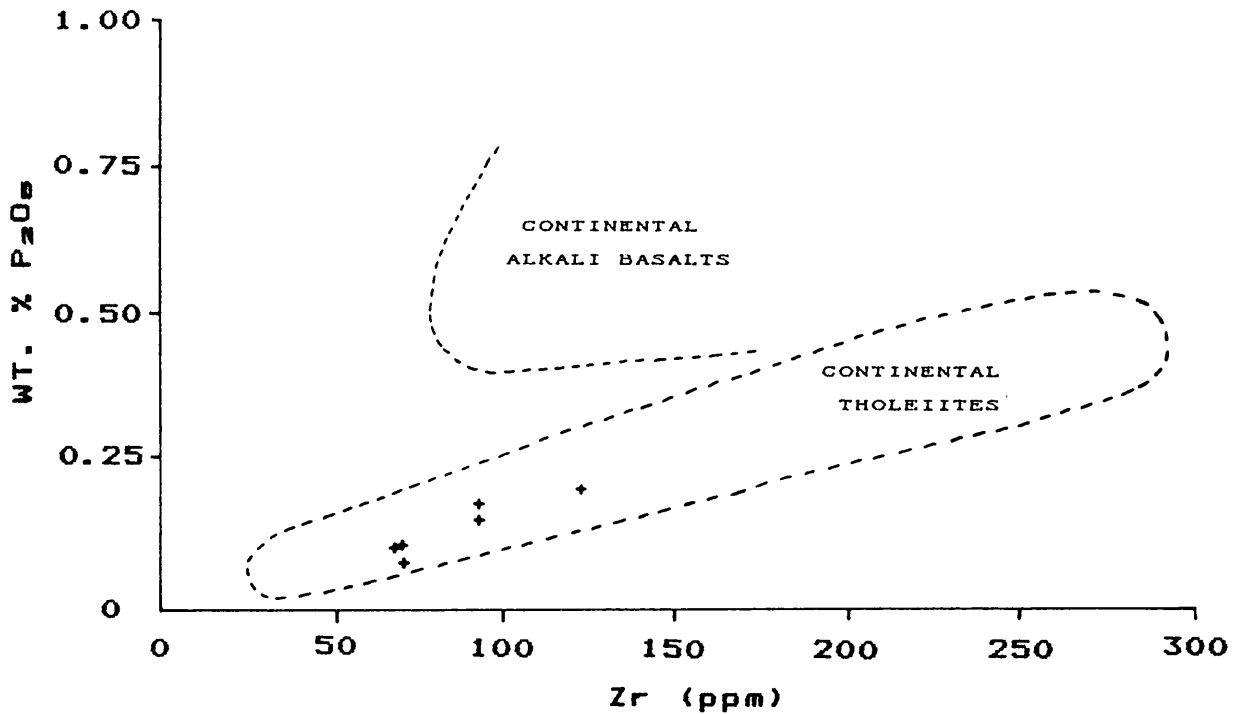
Fig. 7.6. The metadolerites plotted on the P_2O_5 vs. Zr discrimination diagram of Winchester and Floyd (1977).
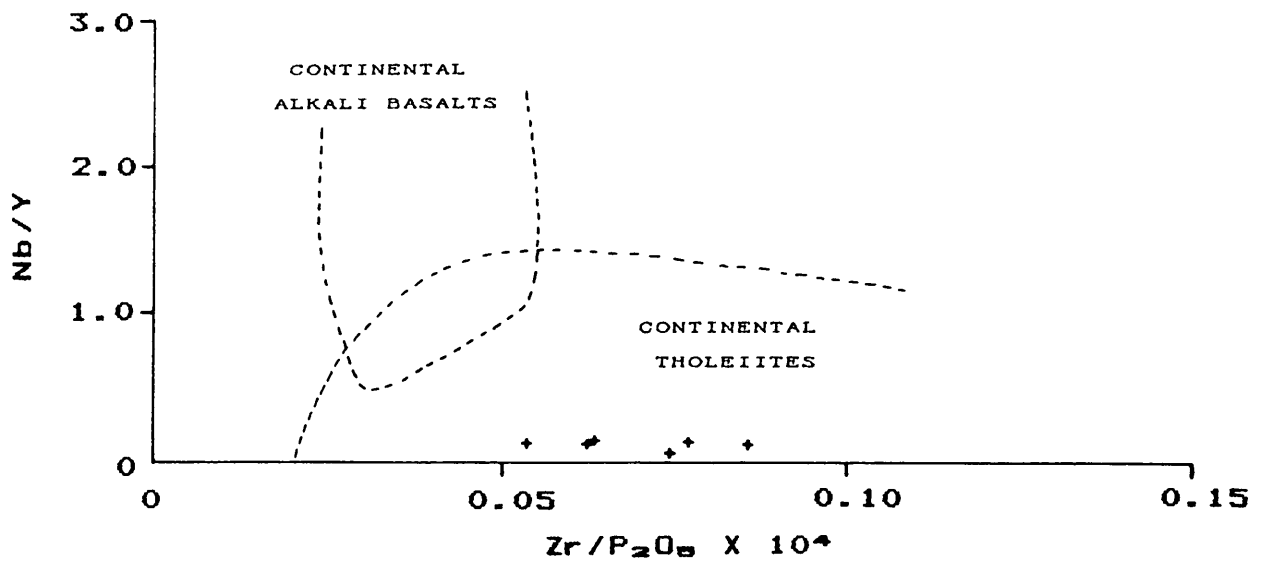
Fig. 7.7. The metadolerites plotted on the Nb/Y vs. Zr/P_2O_5 X 10^4 discrimination diagram of Winchester and Floyd (1977)
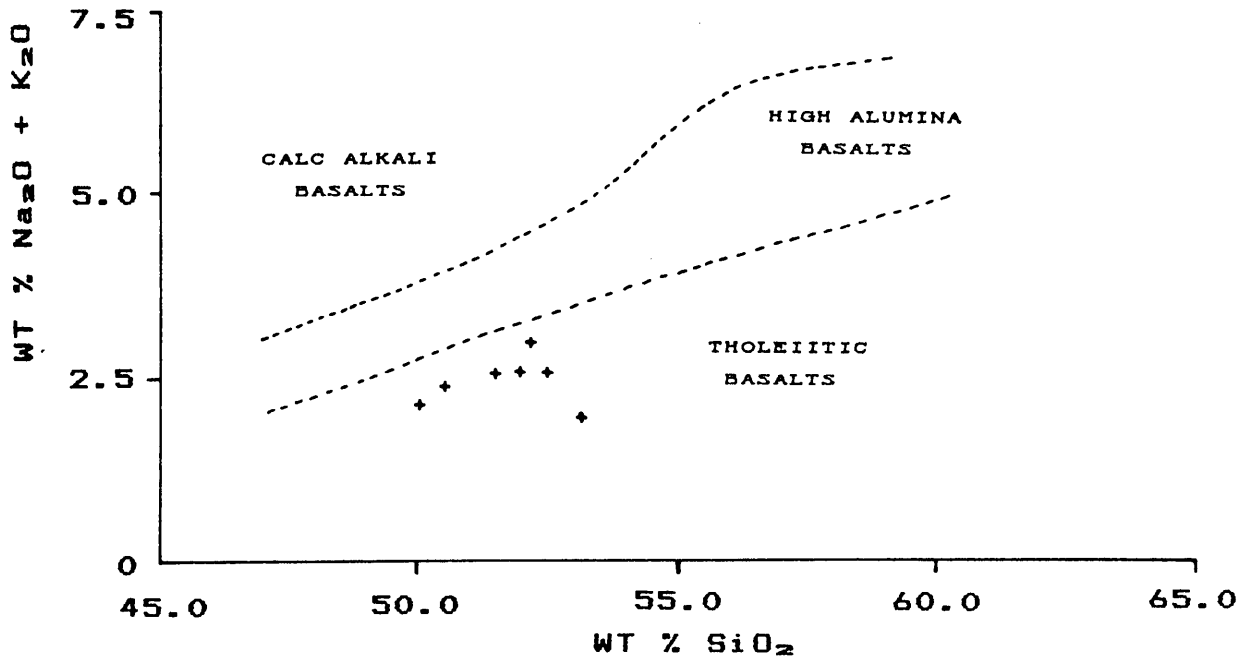
Fig. 7.8. The metadolerites plotted on the alkali - silica
diagram of Kuno (1966).
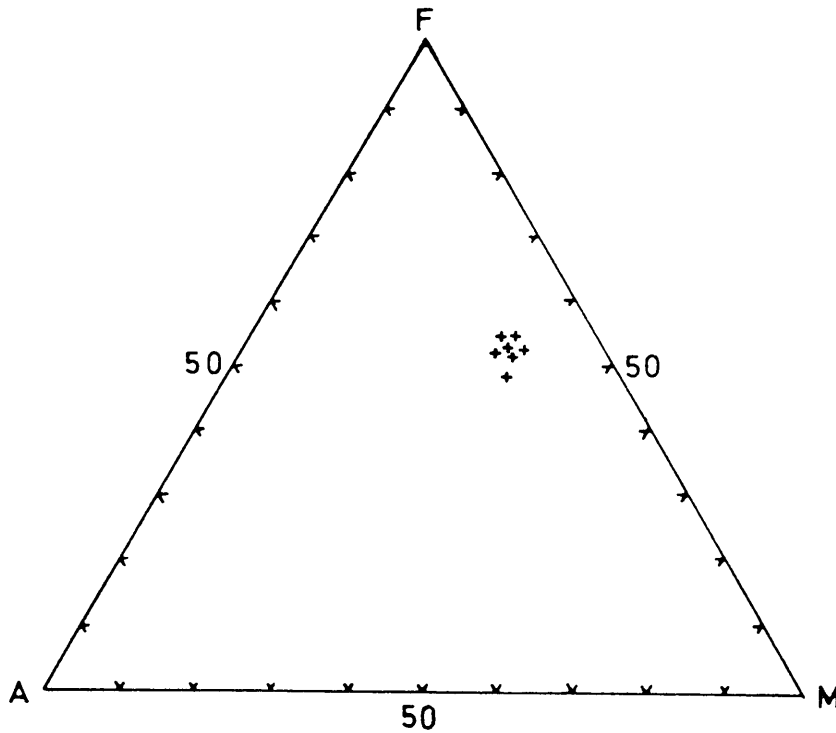
Fig. 7.9. The metadolerites plotted on the AFM diagram.

having a high SiO_2 content (±55 per cent, Appendix 1) and a somewhat lower but still significant, Rb content (±36 ppm, Appendix 2). This rock type is not considered further here but is discussed in terms of a mixing model in chapter 7.6.

7.3.2 The quench-textured micropyroxenites and the microgabbronorite

For 'basaltic' rocks the quench-textured micropyroxenites (QTM) are very distinctive geochemically, being characterised by high contents of SiO_2 (± 55.5 wt. per cent), K_2O (±0.9 wt. per cent) and MgO (±13.3 wt. per cent). Their high Ni (±300 ppm) and Cr (±1100 ppm) contents are also distinctive.

The presence of high SiO_2, K_2O and MgO in these rocks is unusual and was first noted by Willemse (1959) and further commented on by Sharpe (1978; 1981) and Cawthorn et al. (1981). Crustal contamination during ascent of a more basic magma has been appealed to as an explanation for their unusual geochemistry, including their high K/Rb (±200) and Rb/Sr (±0.2) ratios (Sharpe, 1980; 1981; Barnes, 1989). However, Harmer and Sharpe (1985), Hatton and Sharpe (1988) and Harmer and von Gruenewaldt (1991), argue that the geochemistry of these rocks is in fact largely unaffected by crustal contamination (chapter 7.9.3.).

Their unusual geochemistry makes it difficult to classify these rocks in the normal 'basaltic' schemes. However, they are quartz and hypersthene normative (Appendix 4) and fall well into the tholeiite field on Kuno's (1966) alkali-silica diagram (Fig. 7.10). They are however, somewhat surprisingly in view of their intra-cratonic setting, geochemically similar to boninites, (Hickey and Frey, 1982) which are high-Mg rocks usually found in island arc environments (see chapter 7.9.3. for further discussion).

The microgabbronorite (MGN) on the other hand, is geochemically a fairly typical, albeit slightly magnesium rich, continental tholeiite (cf. Tables 7.1, 7.2, Appendix 1, Appendix 2) with much lower Rb/Sr ratios (±0.02) and lower overall contents of SiO_2 (±50.50 wt. per cent), MgO (±8.40 wt. per cent), K_2O (±0.30 wt. per cent), Ni (±120 ppm) and Cr (±230 ppm) as compared to the QTM. Most examples, like the metadolerites can be classified as quartz-tholeiites (Yoder and Tilley, 1962) containing 0-2 per cent normative quartz (Appendix 3). Approximately 30 per cent of the MGN samples however, lie on the opposite side of the 'plane of silica saturation' and are therefore classified as olivine
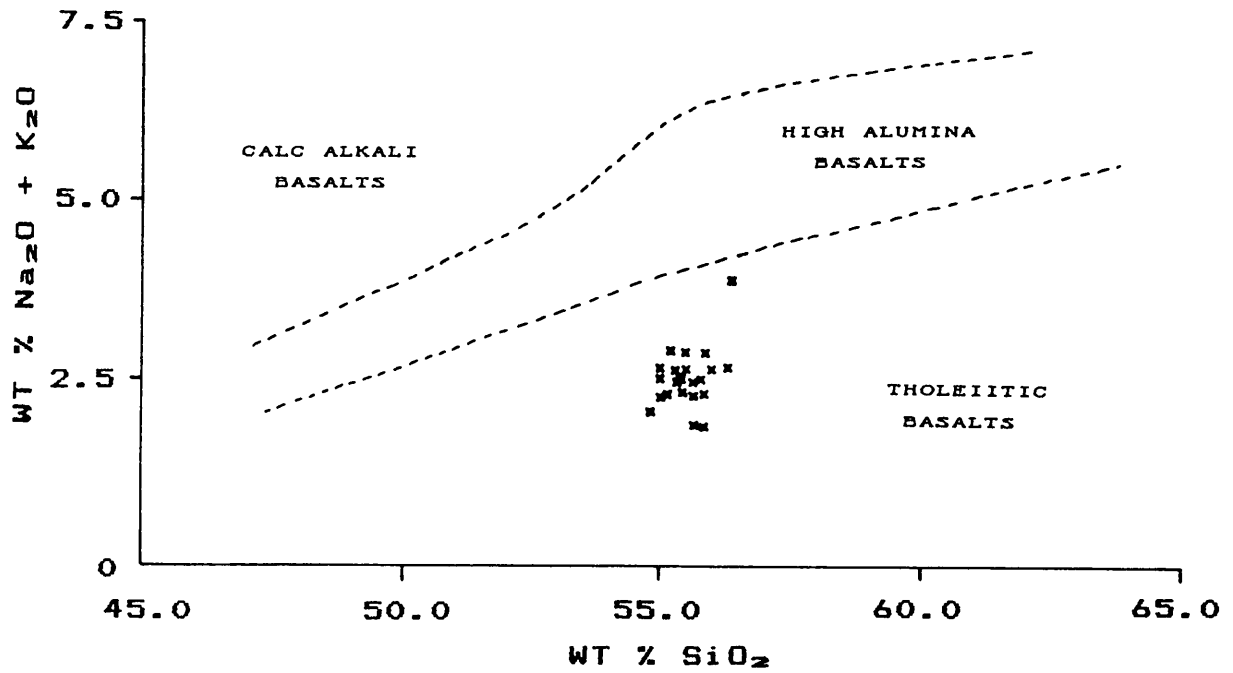
Fig. 7.10. The QTM plotted on the alkali – silica diagram of Kuno (1966).
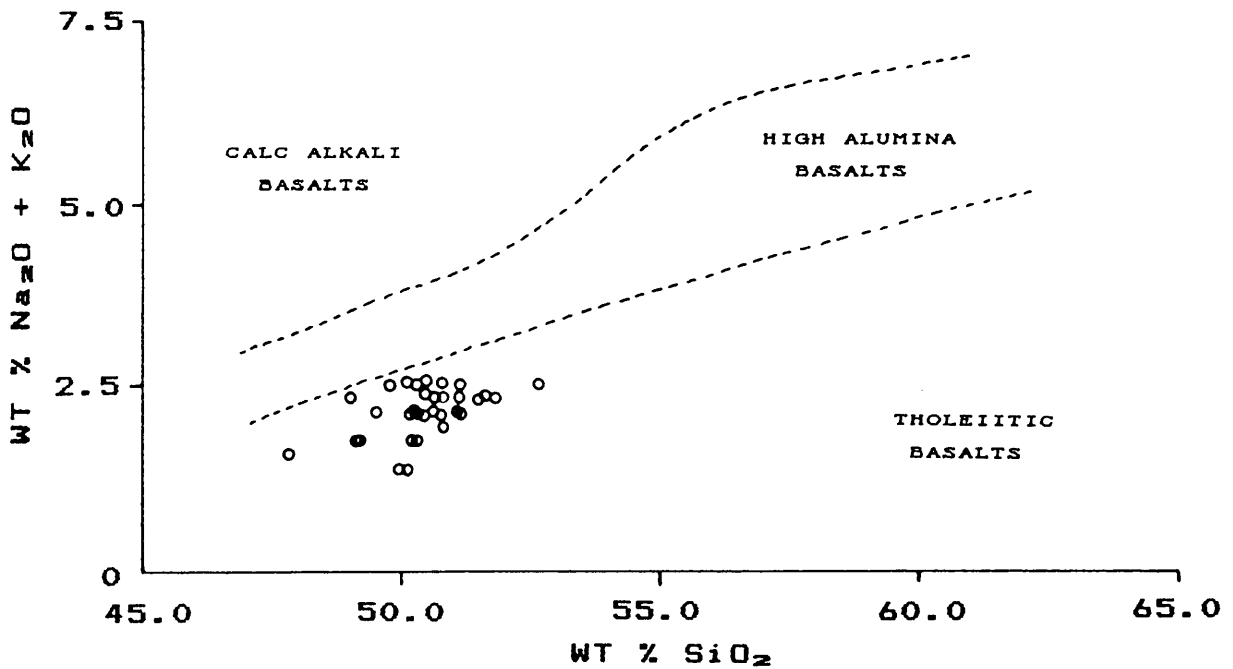
Fig. 7.11. The MGN plotted on the alkali – silica diagram of Kuno (1966)

tholeiites with small amounts of normative olivine. Like the MD and QTM, the MGN fall well within the tholeiite field on Kuno's alkali-silica diagram (Fig. 7.11).

Following the proposal of Wright (1974) meaningful visual comparisons of the MGN and QTM geochemistries were obtained by simple binary plots of major and trace elements vs. MgO as abscissa. Some of the more significant plots are presented in Figures 7.12 - 7.16. There is for most elements a clear separation of the fields of both rock groups. Moreover, there is commonly a difference in overall trend between the QTM and MGN suggesting that they may only be indirectly related, if at all.

Using two of the more widely used fractionation indices i.e. the Solidification Index (SI) of Kuno (1959) (where, SI = 100 MgO / MgO + FeO + Fe_2O_3 + Na_2O + K_2O) and the Differentiation Index, (DI), of Thornton and Tuttle (1960) (where, DI = normative Q + Or + Ab + Ne + Ks + Le) there is again, a generally clear separation of the QTM and MGN (Figs. 7.17 - 7.30). Here again the enigmatic geochemistry of the QTM is clearly illustrated; this rock type being more evolved than the MGN in terms of the DI, while it is more primitive in terms of the SI. However, in dealing with a basaltic system the SI is considered more applicable, since it is based largely on Fe/Mg relationships, as opposed to the essentially 'granitic' components of the DI. In view of this the position of the QTM on the DI diagrams must be ascribed to the anomalously high levels of SiO_2 and K_2O in these rocks. Even their primitive MgO content is insufficient to deplete the norm of this excess of silica, with the resultant formation of orthoclase and quartz. Such a relationship i.e. high weight per cent SiO_2, K_2O and MgO, also cannot be reconciled with the generally accepted rules of magmatic evolution, (Bowen 1928).

On the AFM diagram (Fig. 7.31) both the MGN and QTM define tholeiitic Fe-enrichment trends, with the MGN again being more evolved in terms of these apices. Note also the close similarity between the MGN and metadolerites as mentioned earlier.

Having established that the MGN is more evolved than the QTM in terms of several indices, it is pertinent to consider, despite the lack of intervening representatives, whether the MGN has evolved from the QTM or not. The most likely evolutionary mechanism is fractional crystallisation, for two obvious
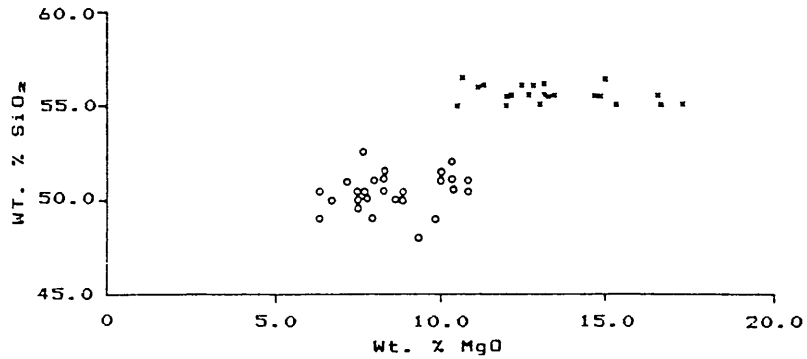
Fig. 7.12. Binary plot of SiO₂ vs. MgO for the QTM and MGN. Symbols as for Figs. 7.10 and 7.11.
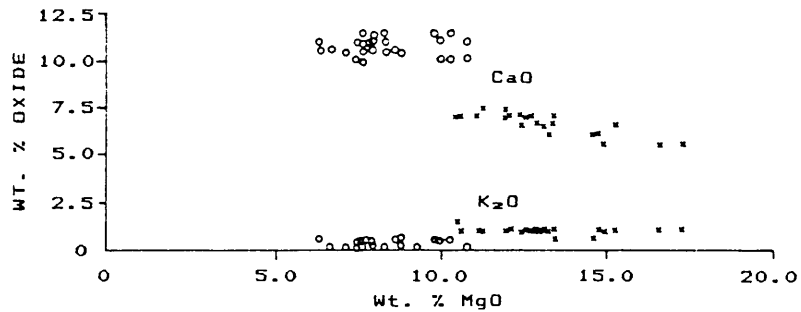
Fig. 7.13. Binary plot of CaO and K₂O vs. MgO for the QTM and MGN. Symbols as for Figs. 7.10 and 7.11.
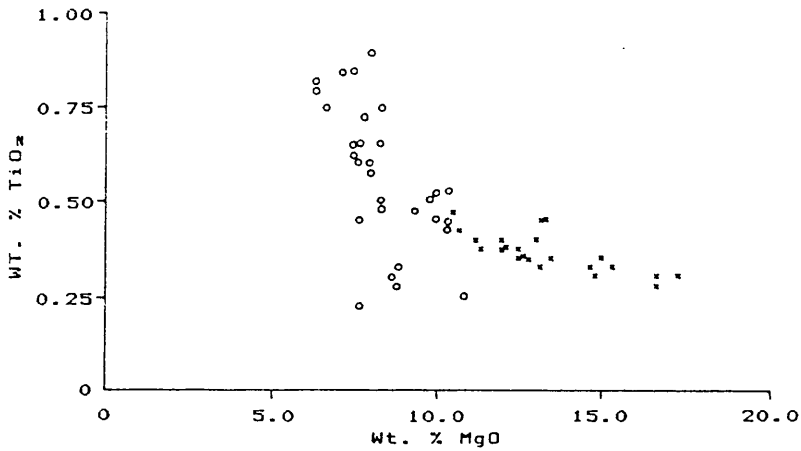
Fig. 7.14. Binary plot of TiO₂ vs. MgO for the QTM and MGN. Symbols as for Figs. 7.10 and 7.11.
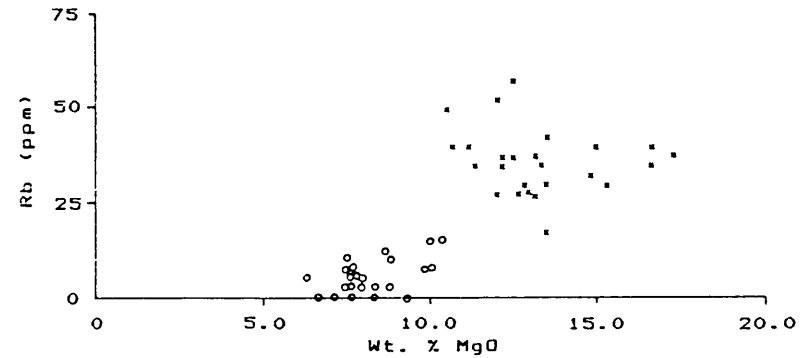
Fig. 7.15. Binary plot of Rb vs. MgO for the QTM and MGN. Symbols as for Figs. 7.10 and 7.11.
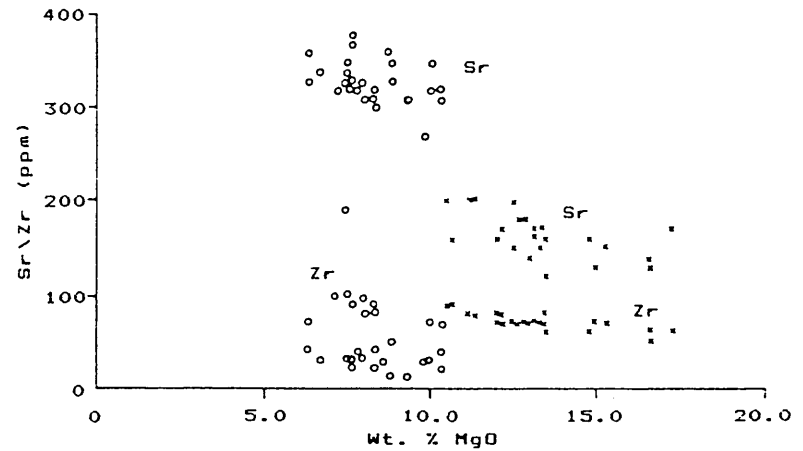
Fig. 7.16. Binary plot of Sr and Zr vs. MgO for the QTM and MGN. Symbols as for Figs. 7.10 and 7.11.
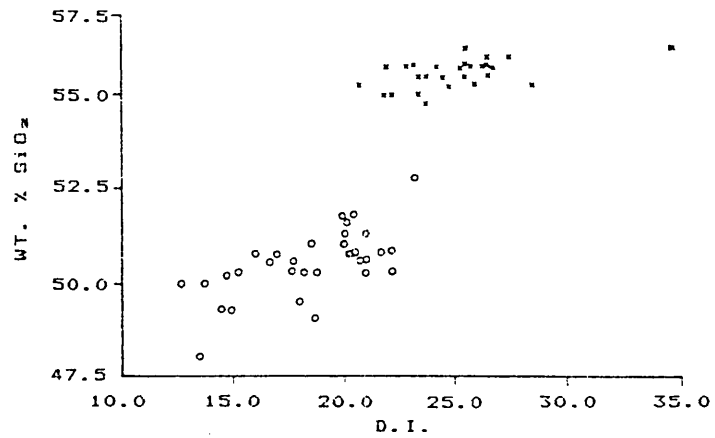
Fig. 7.17. Binary plot of SiO_2 vs. the D.I. for the QTM and MGN. Symbols as for Figs. 7.10 and 7.11.

Fig. 7.19. Binary plot of MgO vs. the D.I. for the QTM and MGN. Symbols as for Figs. 7.10 and 7.11.

Fig. 7.18. Binary plot of Al_2O_3 vs. the D.I. for the QTM and MGN. Symbols as for Figs. 7.10 and 7.11.
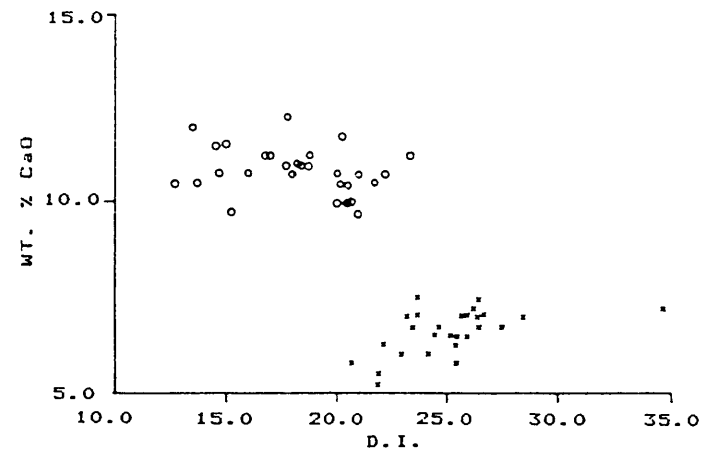
Fig. 7.20. Binary plot of CaO vs. the D.I. for the QTM and MGN. Symbols as for Figs. 7.10 and 7.11.
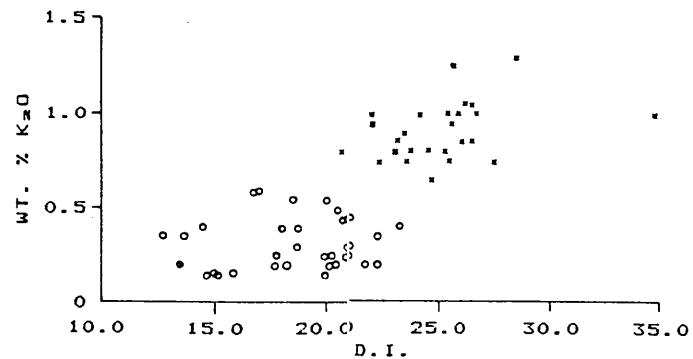
Fig. 7.21. Binary plot of K₂O vs. the D.I. for the QTM and MGN. Symbols as for Figs. 7.10 and 7.11.
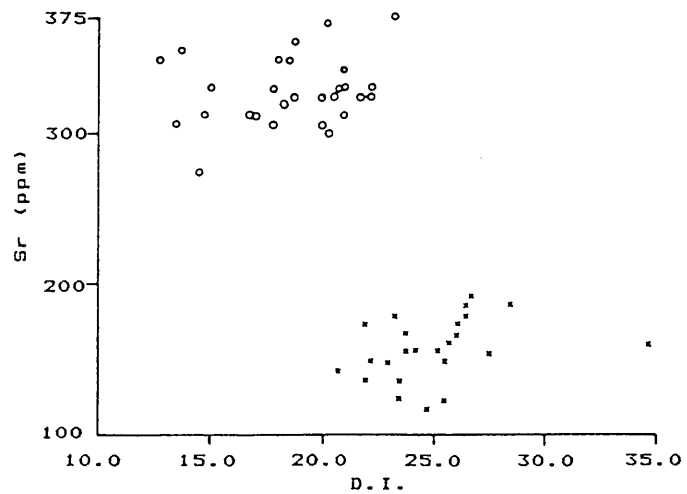
Fig. 7.22. Binary plot of Sr vs. the D.I. for the QTM and MGN. Symbols as for Figs. 7.10 and 7.11.
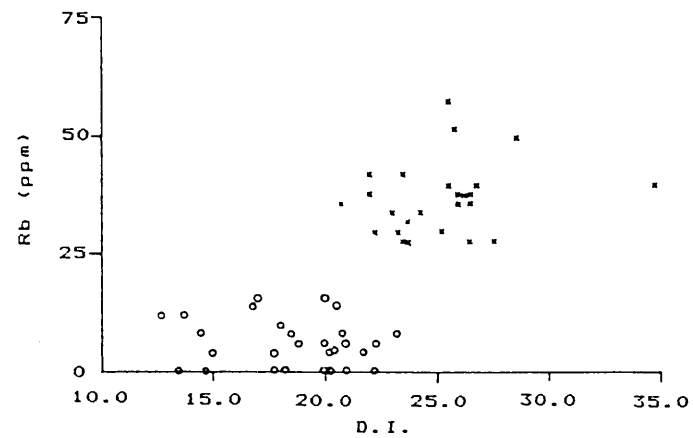
Fig. 7.23. Binary plot of Rb vs. the D.I. for the QTM and MGN. Symbols as for Figs. 7.10 and 7.11.
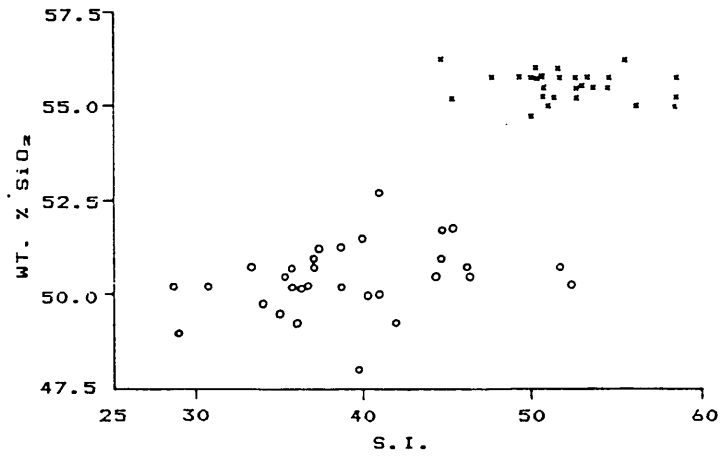
Fig. 7.24. Binary plot of SiO_2 vs. the S.I. for the QTM and MGN. Symbols as for Figs. 7.10 and 7.11.
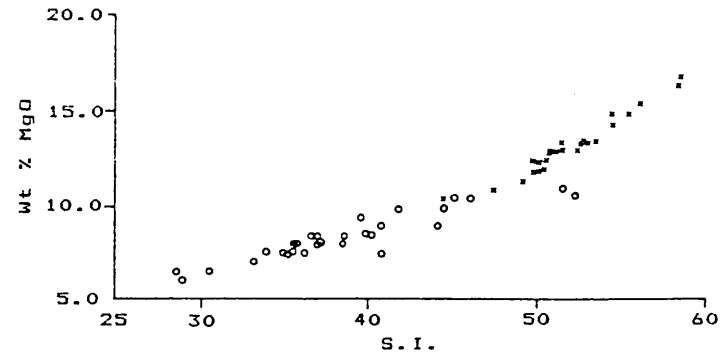
Fig. 7.26. Binary plot of MgO vs. the S.I. for the QTM and MGN. Symbols as for Figs. 7.10 and 7.11.
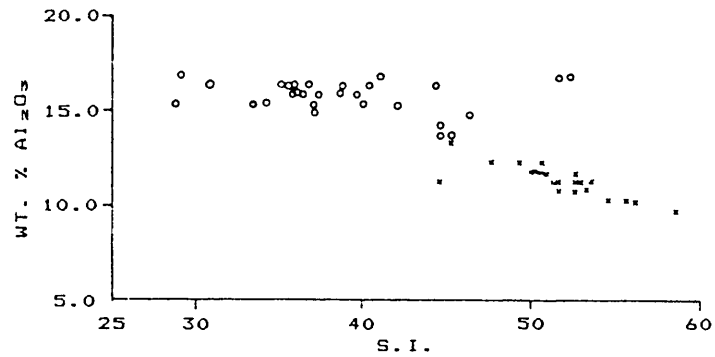
Fig. 7.25. Binary plot of Al_2O_3 vs. the S.I. for the QTM and MGN. Symbols as for Figs. 7.10 and 7.11.
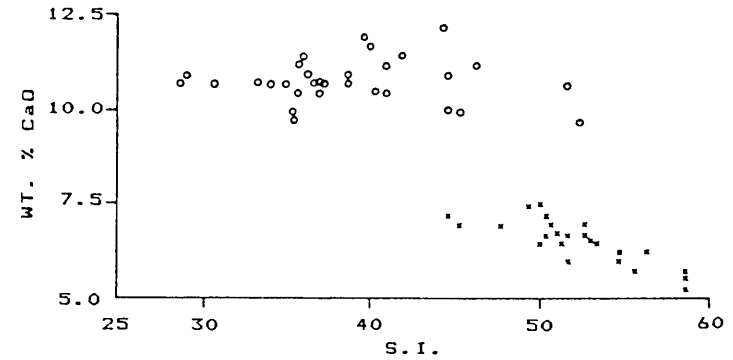
Fig. 7.27. Binary plot of CaO vs. the S.I. for the QTM and MGN. Symbols as for Figs. 7.10 and 7.11.
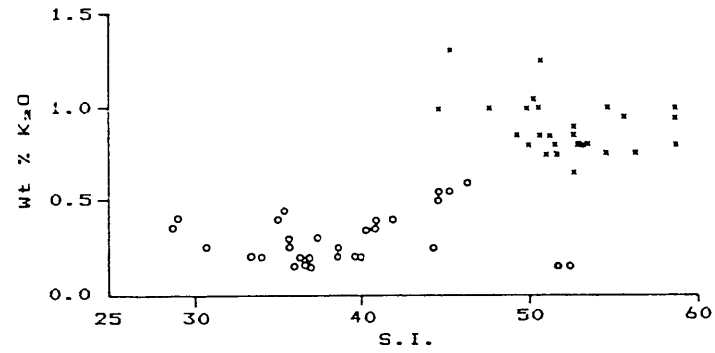
Fig. 7.28. Binary plot of K_2O vs. the S.I. for the QTM and MGN. Symbols as for Figs. 7.10 and 7.11.
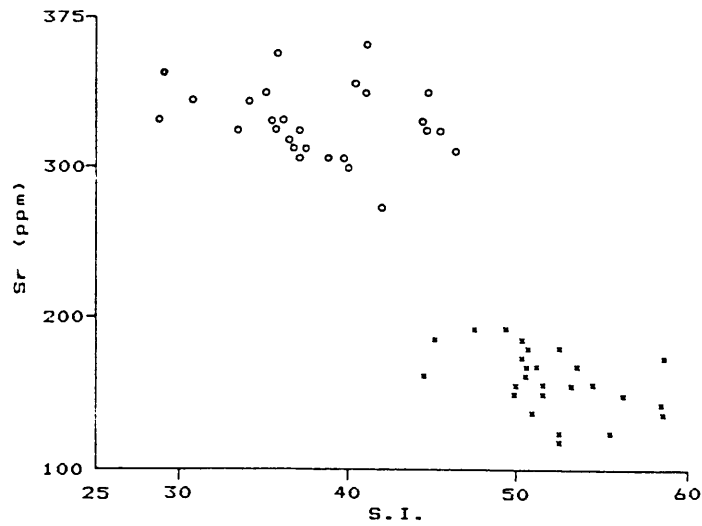
Fig. 7.29. Binary plot of Sr vs. the S.I. for the QTM and MGN. Symbols as for Figs. 7.10 and 7.11.
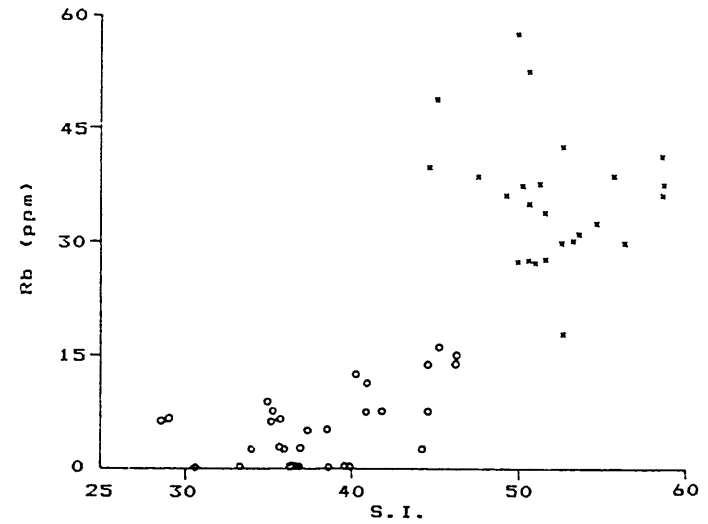
Fig. 7.30. Binary plot of Rb vs. the S.I. for the QTM and MGN. Symbols as for Figs. 7.10 and 7.11.
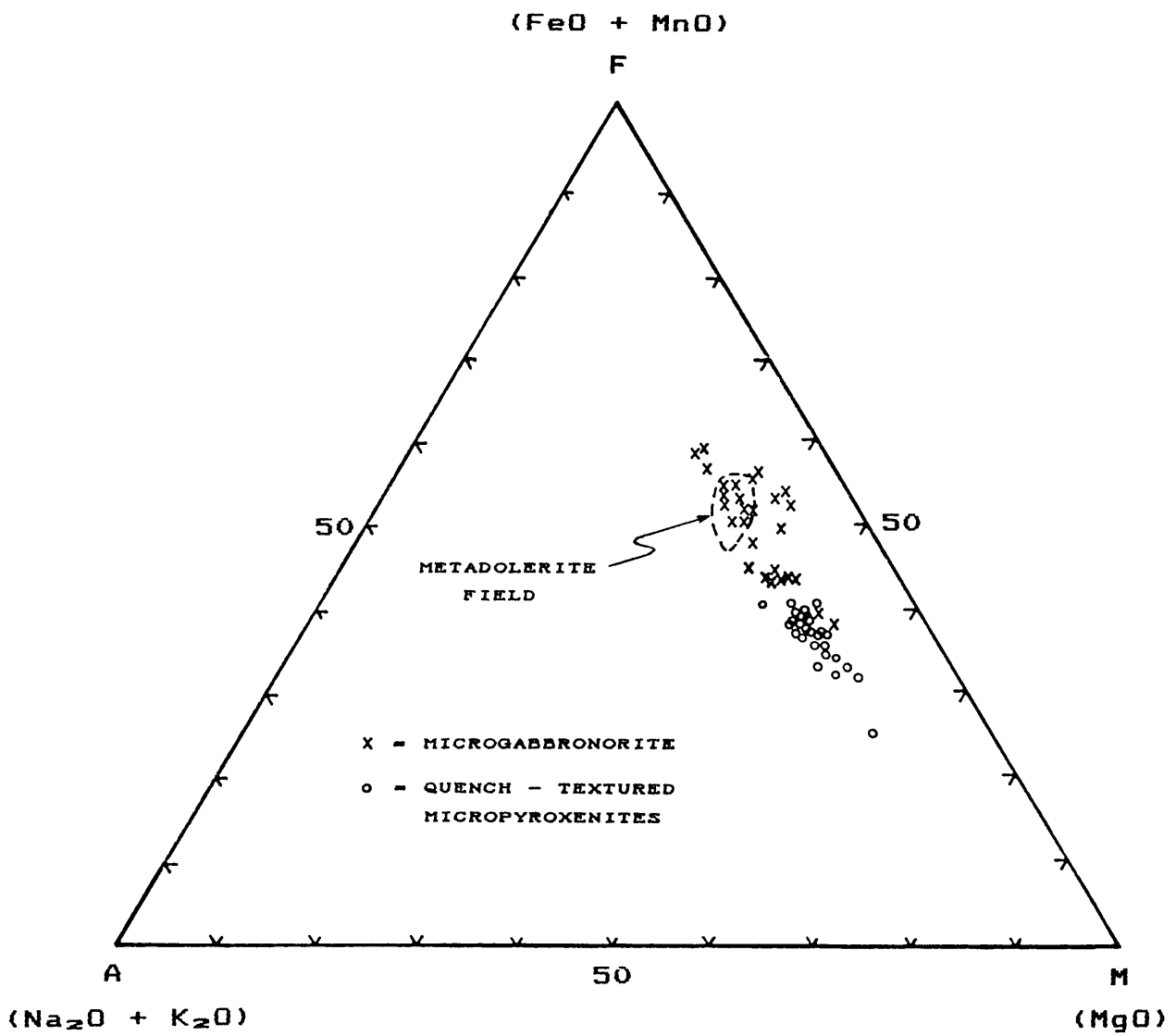
Fig. 7.31. AFM plot for the MGN and QTM.

reasons. Firstly for example as Cox et al. (1979, p.6) point out: all magmas at some stage consist of liquid plus crystals lying in the temperature interval between liquidus and solidus. Secondly, because "crystal-liquid separation mechanisms appear to operate frequently and rather efficiently in nature" (Cox et al., ibid, p.6). Nowhere else is the latter statement exemplified more pointedly, than in the adjacent cumulates of the Bushveld Complex!

Orthopyroxene is the most obvious candidate for involvement in any crystal-liquid fractionation hypothesis since it occurs as definite phenocrysts in the QTM. Also from the petrographic evidence (chapter 6) orthopyroxene is the first formed mineral during crystallisation of such rocks and it is therefore a logical choice for any crystal fractionation hypothesis.

To test graphically whether the MGN could have evolved from the QTM by removal (or addition) of orthopyroxene, mean values for analysed orthopyroxene, QTM and MGN were computed from the analyses in Appendices 1 and 2 as given in Table 7.3 and used in Figure 7.32 which is a simple 'extract' or 'subtraction' diagram (Wilcox, 1979).

TABLE 7.3

Mean compositions of the MGN, QTM and orthopyroxenes from the QTM

	MGN	QTM	OPX
SiO_2	50.46	55.56	54.88
TiO_2	0.55	0.36	0.23
Al_2O_3	15.97	11.39	1.42
FeO_{tot}	10.82	9.30	9.09
MgO	8.50	13.31	31.29
CaO	10.83	6.60	1.24
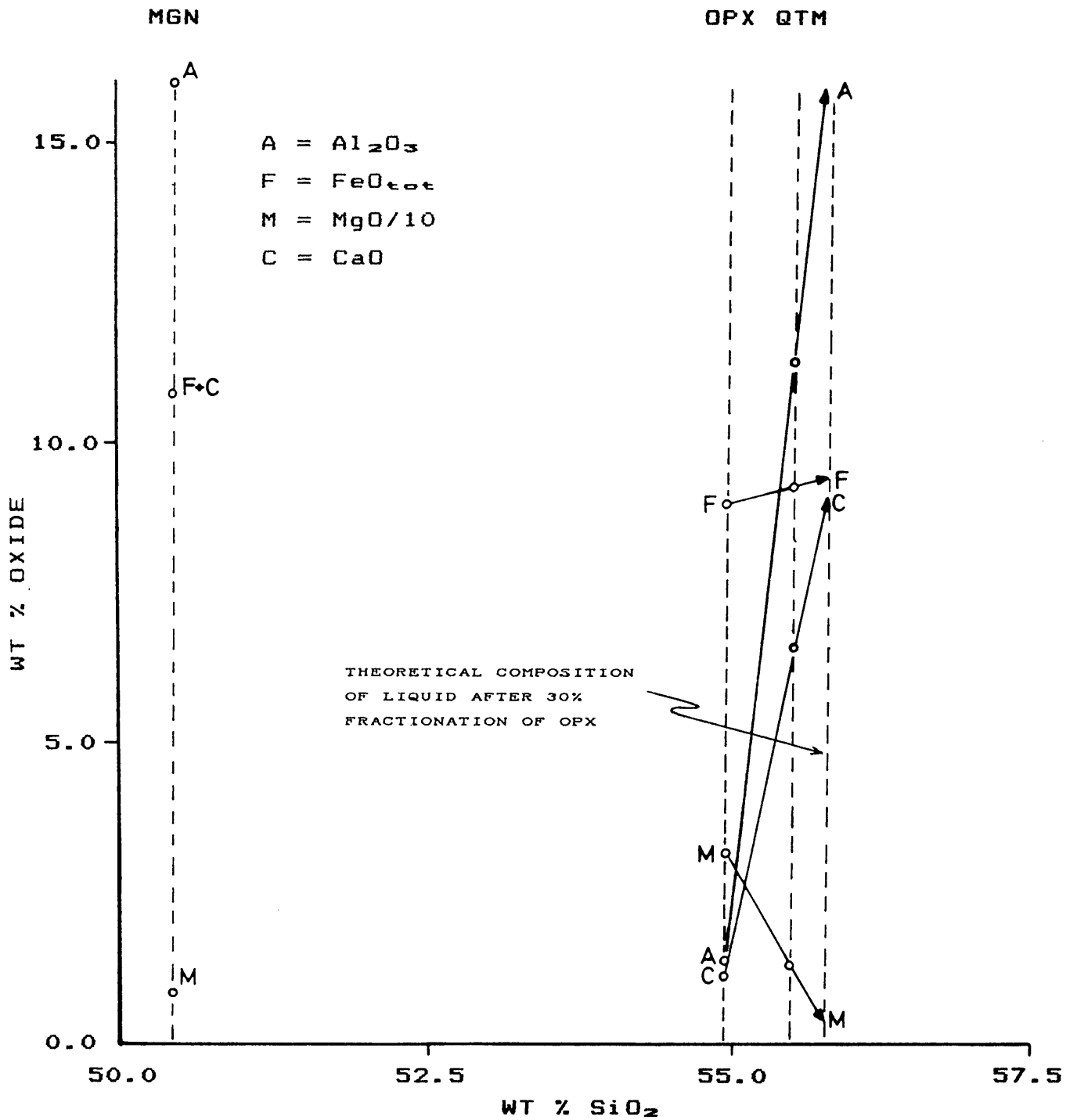
Fig. 7.32. Extract diagram for fractionation of
orthopyroxene from the QTM.

It is clear from Figure 7.32 that the removal of orthopyroxene, of the composition actually occurring in the QTM, cannot account for the generation of the MGN from the QTM (the diagram assumes a simplified constant composition for orthopyroxene). Removal of any such orthopyroxene can only shift the QTM composition further towards the silica-rich side of the diagram, i.e. away from the MGN composition. For example, if we assume that an arbitrary 30 per cent fraction is removed, then it is clear that the new liquid would have a composition of 55.8 wt per cent SiO_2, 16 wt per cent Al_2O_3 and 9 wt per cent CaO.

The only other mineral likely to be involved in such a process would be olivine, which was reported in some micropyroxenite samples of Sharpe (1981), but extraction of this would have a similar effect, because documented olivines (Deer, et al., 1978) all contain considerably less SiO_2 than the QTM (i.e. ±40 wt per cent SiO_2). Furthermore as Cawthorn, et al. (1979) point out from their investigation of similar rocks, fractionation of any reasonable 'extract' cannot decrease the K_2O content from ±1.00 wt per cent in the QTM to ±0.3 wt per cent in the MGN.

However, if it is assumed that the anomalously high SiO_2 and K_2O values of the QTM are the result of contamination, then the orthopyroxene composition lies to the right of the QTM and the situation is reversed. Therefore, as an initial approximation 'decontaminated' analyses (arrived at by iterative removal of possible granitic contaminants) of QTM type rocks from Sharpe (1980) were plotted on the same diagram (Fig. 7.33). In this diagram removal of the appropriate orthopyroxene composition does produce a trend from the QTM towards the MGN.

However, solely to reproduce the SiO_2 content of the MGN by such a process would require impossible amounts of extraction. For example the MgO content of the liquid would be reduced to zero before the appropriate value of SiO_2 was reached, while at the same time, the Al_2O_3 and CaO contents would far exceed those of the MGN.

In the case of olivine extraction the arguments presented above with regard to Figure 7.32, still apply. That is, because olivine compositions would still lie to the left of the QTM composition, the removal of olivine
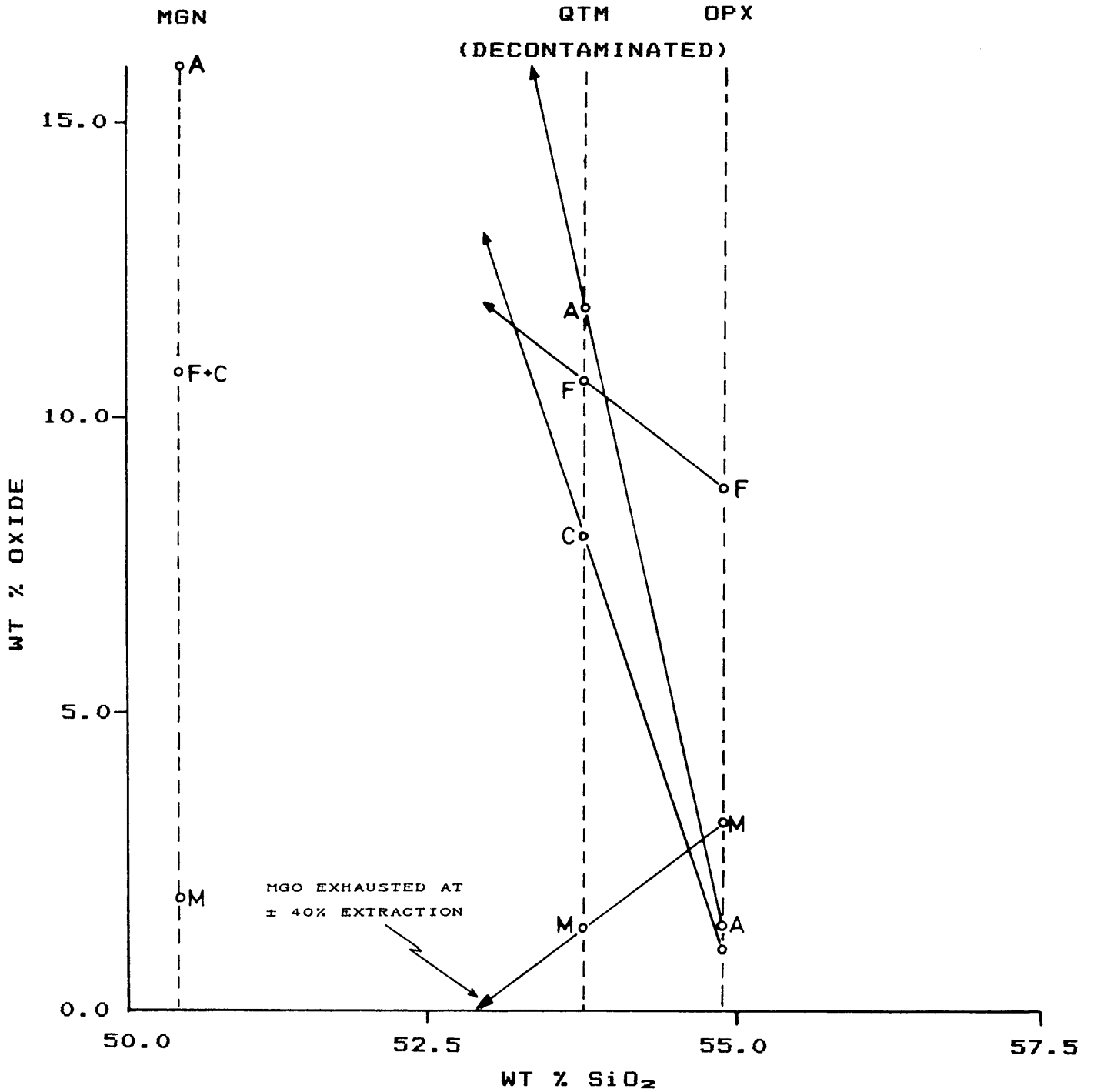
Fig. 7.33. Extract diagram for fractionation of orthopyroxene from "decontaminated" QTM. Symbols as for Fig.7.32.

would only lead to an increase in SiO_2 content and a consequent shift in composition away from the MGN.

Despite the simplicity of the above models, in view of the extreme disparity between observed and modelled behaviour it must be concluded that the MGN has not evolved from the QTM by simple fractional crystallisation.

Further attempts at understanding the petrogenesis of the MGN must take due regard of the findings of Harmer and Sharpe (1985) on similar rocks from the eastern lobe of the Bushveld Complex. These authors were the first to demonstrate that there is a considerable variation in initial $^{87}Sr/^{86}Sr$ ratios (R_o) for these rocks, that cannot be convincingly ascribed to crustal contamination, e.g. there is a lack of correlation between R_o and K_2O, SiO_2, Na_2O etc. In fact these authors note that there is a continuum of R_o values through both QTM- and MGN-type marginal rocks and conclude that such rocks "are the products of mixing between magmas from at least two mantle domains with distinct R_o compositions" (Harmer and Sharpe, 1985, p835). Initial ratios obtained during the present study confirm these results, with ranges of 0.7063-0.7084 for the MGN and 0.7024-0.7063 for the QTM (Appendix 5). The significance of these results is discussed further in chapter 7.9.3.

7.4 OLIVINE-BEARING PYROXENITES

The geochemistry of the two olivine-bearing pyroxenite bodies is closely similar, being very magnesium-rich (±23 wt. per cent MgO) reflecting their cumulate nature. Rock types from both occurrences are rich in incompatible elements, with Rb/Sr ratios of ±0.2 and they also possess high Ni (± 2500 ppm) and Cr contents (± 700 pm), (Appendices 1 and 2). Because of their cumulate nature most variation diagrams are not applicable but their high MgO and Ni contents indicate a fairly primitive origin.

Furthermore, the high modal percentage of cumulus orthopyroxene in these bodies (chapter 6.2.2.2.4) suggests that they were not intruded as true liquids. Hence it was originally considered that these bodies represented early formed cumulates of the main Complex which were subsequently squeezed out into the floor by tectonic instability. Such a process was suggested by Sharpe (1980) to explain the origin of certain olivine-bearing sills associated with the eastern lobe of the Bushveld Complex. Later quantitative work (Davies and

Tredoux, 1985; Sharpe and Hulbert, 1985) confirmed this origin, in that many of the olivine-bearing sills associated with the eastern lobe of the Bushveld Complex can be modelled by addition of olivine to QTM-type liquids. These authors thus conclude that these sills are actually solidified suspensions of olivine in QTM-type liquids. A similar origin for the investigated bodies was therefore considered. Since the proposed models involve straight addition of olivine to the liquid, then such an origin can easily be tested. The mean composition of olivine in the pyroxenites was determined (Table 7.4 and Appendix 4) and this mean value used, along with the QTM mean (Table 7.3) to test this hypothesis.

Although an extract/addition diagram (such as Fig. 7.32) could be used, it is a matter of simple arithmetic to illustrate that addition of any amount of olivine alone (SiO_2 38 wt. per cent, MgO 40 wt. per cent) to a QTM liquid cannot account for the genesis of the pyroxenite. For example, addition of 5 per cent olivine to the QTM would lower the SiO_2 value to that of the pyroxenite but would only increase the MgO content to 15.6 wt. per cent, i.e. considerably lower than the observed 23 wt. per cent in DI-75 (Table 7.4). Addition of larger amounts of olivine would raise the MgO value to that of the pyroxenite but would lower the SiO_2 content unacceptably. In any event both pyroxenite bodies contain less than 5 modal per cent olivine, so that addition of a large proportion of olivine is inconsistent with their petrography.

Ignoring for the moment the minor amount of olivine but still utilising the basic model of peridotite formation discussed above, the possibility of orthopyroxene (rather than olivine) addition to the QTM liquid was considered. Orthopyroxene-rich cumulates are at least as abundant as olivine-rich cumulates in the lower zone of the Bushveld Complex (Cameron, 1978) and the hypothesis is therefore feasible. Consequently, using the mean values given in Table 7.3, varying amounts of orthopyroxene were added to the QTM liquid (Table 7.4, Row 1). Since SiO_2 and total Fe are similar in all three compositions the model is largely constrained by the differences in Al_2O_3, MgO and CaO content. Again, simple arithmetic considerations indicate that approximately a 50:50 mix of QTM and orthopyroxene best fit the data for sample DI-75 (Table 7.4, Row 1). Lower and higher proportions of orthopyroxene increase the overall percentage error for MgO, CaO and Al_2O_3, relative to the olivine - pyroxenite composition. Similarly, slightly lower added proportions of orthopyroxene are indicated for

TABLE 7.4

Mixing calculation for the genesis of the olivine-bearing pyroxenites.

	QTM MEAN	ORTHOPYROXENE (OPX) MEAN	QTM:OPX 50 : 50	OLIVINE-BEARING PYROXENITE (DI-75)
SiO_2	55.56	54.88	55.22	54.44
TiO_2	0.36	0.23	0.30	0.22
Al_2O_3	11.39	1.42	6.41	6.74
FeO_{tot}	9.30	9.09	9.20	8.22
MgO	13.31	31.29	22.30	23.26
CaO	6.60	1.24	3.92	3.99

ROW 1

	OLIVINE MEAN (3 ANALYSES- APPENDIX 4)	OPX MEAN	OPX:OL 90:10	QTM MEAN	50:50 MIX OF COL 3+4	OL-PYROXENITE (DI-75)
SiO_2	38.32	54.88	53.22	55.56	54.39	54.44
TiO_2	0.20	0.23	0.23	0.36	0.30	0.22
Al_2O_3	0.20	1.42	1.30	11.39	6.35	6.74
FeO_{tot}	19.06	9.09	10.09	9.30	9.70	8.22
MgO	40.05	31.29	32.17	13.31	22.74	23.26
CaO	0.36	1.24	1.15	6.60	3.88	3.99

ROW 2

ERROR (% RELATIVE) FOR MIXTURES OF QTM AND ADDED COMPONENT, RELATIVE TO THE OLIVINE-BEARING PYROXENITE (DI-75).

	COMPOSITION OF ADDED COMPONENT MIXED IN THE PROPORTIONS QTM : COMPONENT 50:50			COMPOSITION OF ADDED COMPONENT MIXED IN THE PROPORTIONS QTM : COMPONENT 70:30		
	OPX:OL 100:0	OPX:OL 90:10	OPX:OL 80:20	OPX:OL 100:0	OPX:OL 90:10	OPX:OL 80:20
SiO_2	1.43	-0.9	-1.60	1.69	0.77	-0.15
TiO_2	36.4	31.82	31.82	45.45	45.45	45.45
Al_2O_3	-4.9	-5.79	-6.68	24.63	24.03	23.59
FeO_{tot}	11.9	18.00	23.97	12.41	16.06	19.59
MgO	-4.00	-2.24	-0.34	-19.60	-18.44	-17.33
CaO	-1.75	-2.76	-4.01	25.06	24.56	23.81

ROW 3

DI-76 (Appendix 1). Using other possible lower zone orthopyroxenes e.g. those of Cameron (1978, Table 1) indicates a similar degree of mixing because mean values for Al_2O_3, MgO and CaO for Cameron's data (8 analyses) are similar to those for orthopyroxene in Table 7.4, i.e. 1.68, 31.5 and 1.02 wt. per cent respectively. However, since the QTM contains no olivine in the norm, it is likely that the olivine present in the olivine-pyroxenite has also been added and it must therefore be taken into account in the mixing calculations. Nevertheless if the above model is used as a working hypothesis, then substitution of e.g. 10 per cent olivine in the added component can be easily reconciled with the available data. For example, if the added component contains 10 per cent olivine - 90 per cent orthopyroxene, and it is further assumed that a 50:50 mix of QTM liquid and added component has taken place, then this would explain the observed ±5 modal per cent olivine, and still be compatible with the bulk chemistry of the olivine pyroxenite (Table 7.4, Row 2).

Further stepwise calculations indicate that higher amounts of olivine in the added component leads to poorer agreement with the SiO_2, Al_2O_3 and FeO contents of the olivine pyroxenite. On the other hand, reduction of the overall proportion of added material e.g. to 30 per cent, to compensate for this, results in poorer agreement with the MgO and CaO. This feature can be best demonstrated by comparing a) the percentage error (relative) between the results obtained by mixing various porportions of QTM and added component (with varying olivine : orthopyroxene ratios) with b) the olivine - pyroxenite composition. In fact, the stepwise calculations indicate that all mixtures of QTM and added component, other than in a 50:50 ratio, have greater overall relative error, regardless of the olivine content of the added material. To illustrate this, the results of the error calculations for a 50:50 and an arbitrary 70:30 mixture of QTM liquid and added component, with varying olivine: orthopyroxene ratios, are shown in Table 7.4 (Row 3).

From these figures it is clear that a mixture comprising ±10 per cent olivine, and ±90 per cent orthopyroxene, mixed in equal proportions with QTM liquid, best fit the data for the olivine-bearing pyroxenite. Such a mixture, as noted above, is completely compatible with the observed ±5 modal per cent of olivine in the latter rock type. The closeness of the modelled and actual values are therefore considered strong evidence that these pyroxenitic bodies have originated in a similar fashion to the peridotite sills described by

previous authors. In this case however, they represent solidified crystal mushes of early, predominantly bronzititic, material suspended in micropyroxenitic liquid. Indeed the non-random, or clumped distribution of olivine within the the olivine-bearing pyroxenites (Fig. 6.39) might well result from the disruption and inclusion of minor dunitic layers associated with the bronzitites.

Further evidence is provided by the close similarity of incompatible element ratios for the QTM and olivine-bearing pyroxenites (Table 7.5).

Such a similarity is to be expected from the mixing model, since the addition of orthopyroxene would dilute the total concentration of such elements but their ratios should remain unchanged. Accordingly it is also notable that total contents of K_2O, Rb, Sr and Zr are significantly higher in the QTM than in the olivine-bearing pyroxenites (Table 7.5).

TABLE 7.5

Comparison of K_2O, trace elements and trace element ratios in the QTM and olivine-bearing pyroxenites.

	OLIVINE-BEARING PYROXENITES		OLIVINE-BEARING	QTM
	DI-75	DI-76	PYROXENITES (MEAN)	(MEAN)
K_2O	0.39	0.80	0.60	0.91
Rb	15	26	21	36
Sr	79	84	82	160
Zr	31	65	48	70
K/Rb	260	308	284	254
Rb/Sr	0.31	0.19	0.25	0.23
Rb/Zr	0.40	0.48	0.44	0.51

In conclusion, however, it must be noted that Sr isotope data (Harmer and Sharpe, 1985) show that, for the peridotite sills associated with the eastern lobe of the Bushveld Complex, simple addition of olivine to micropyroxenitic

(QTM) liquid does not entirely explain all the available data. These authors argue that at least two separate micropyroxenitic liquids (one with R_O = 0.7056 and one with R_O = 0.7034) existed simultaneously during the early development of the Bushveld Complex. Since both liquids have similar bulk compositions, mixing of one with the other has little effect on bulk geochemistry; however, it produces intermediate $^{87}Sr/^{86}Sr$ values for the hybrid liquid. The data of Harmer and Sharpe (ibid) indicate that the peridotites associated with the eastern lobe of the Complex result from cumulus olivine-enriched, high $R_O^{'}$ liquid being mixed with up to 30 per cent low R_O liquid.

Since the bulk chemistry of these peridotites is unaffected, the process merely appears to be straight addition of olivine to micropyroxenitic liquid. In the absence of isotope data for the olivine-bearing pyroxenites of the present study therefore, it may well be that a cumulus orthopyroxene (and minor olivine) – enriched liquid, has mixed with a micropyroxenitic liquid of different R_O in a similar fashion.

Note however that even broader ranges of $^{87}Sr/^{86}Sr$ ratios have been obtained for the micropyroxenites of the present study (i.e. 0.7024 – 0.7063), with intermediate values of 0.7041 and 0.7044 (Appendix 5). This suggests either that there is not necessarily distinct groupings or indeed unique R_O values for the micropyroxenites, or that magma mixing was important in producing the intermediate values (see Chapter 7.9.3.5. for further discussion).

7.5 THE QUARTZOFELDSPATHIC ROCKS

The chemistry of these rocks was not investigated in detail. It is notable however that, in normative content, the granophyric textured rocks generally fall closer to the ternary minimum in the Ab-Q-Or system (Tuttle and Bowen 1958) than the 'granoblastic' varieties, (Fig. 7.34). This observation is considered supportive of the suggestion that these rocks are derived from sediments, (chapter 2.2), for the following reason. Assuming appropriate metamorphic conditions, sediments with compositions closer to the ternary minimum should melt to a greater degree than those of less 'favourable' chemistry. Thus in a compositionally variable sequence of quartzofeldspathic sediments, certain layers may melt more extensively, subsequently giving rise to granophyric textures, while other layers may largely recrystallise
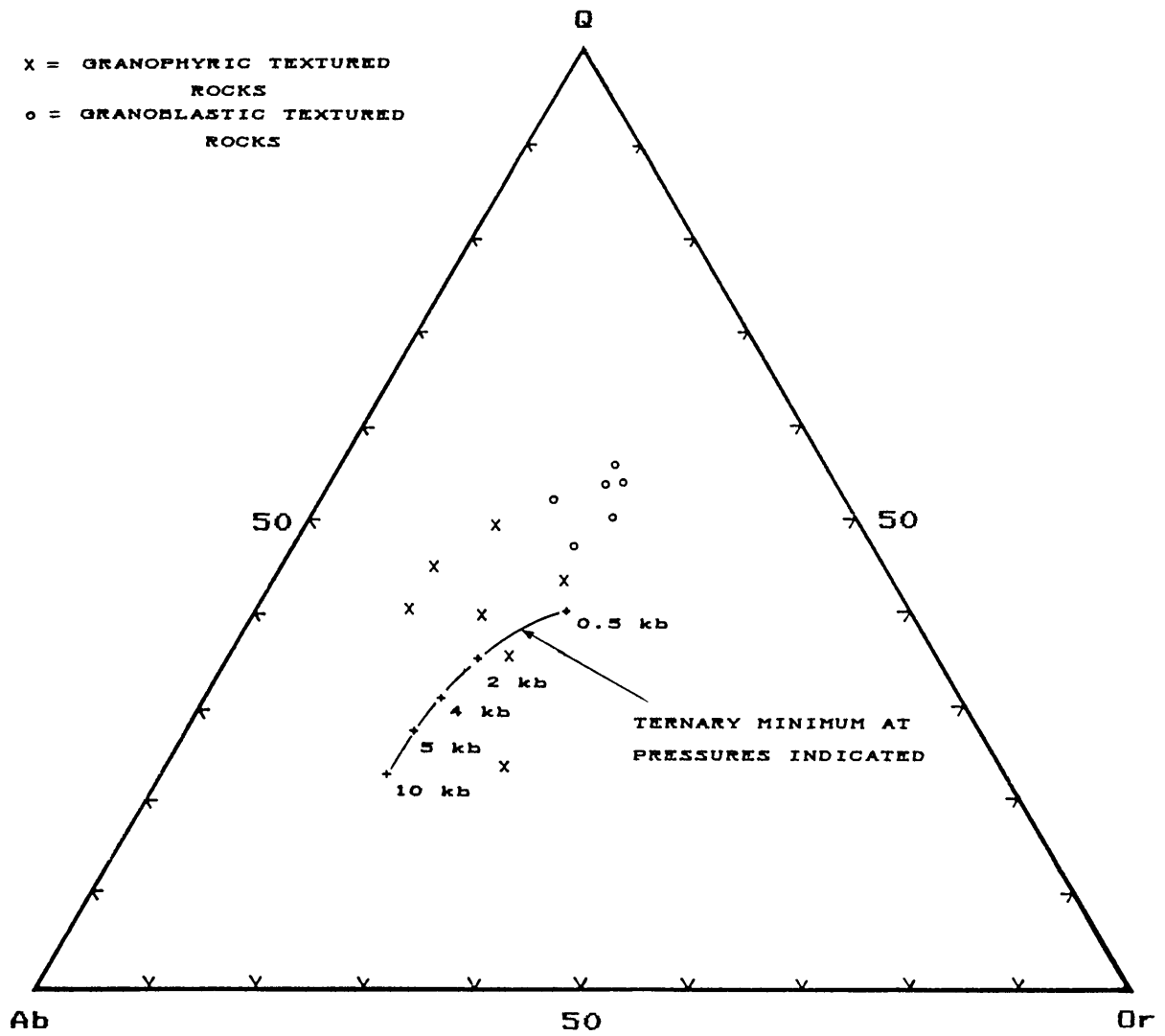
Fig. 7.34. Normative compositions of the quartzofeldspathic rocks plotted on the Ab-Q-Or diagram.

granoblastically. Such a process would readily explain the present spatial, compositional and textural variations of the quartzofeldspathic rocks, while it is difficult to conceive of other processes by which the observed variations could be produced.

In many respects the granophyric rocks resemble the Zwartbank pseudogranophyre of Walraven (1985), although in the present case they appear to be related to intrusion of the pre-Bushveld Middelwater Layered Sill (chapters 2 and 5.2.1) rather than due to intrusion of the main Complex.

The geochemically heterogeneous Zwartbank pseudogranophyre, is restricted in occurrence, being found only where the mafic rocks of the Bushveld Complex underlie sediments of the Pretoria Group. The latter occur either as interlayered or overlying units, as well as in the form of xenoliths within the pseudogranophyre. In view of the field relations and geochemical heterogeneity of the Zwartbank pseudogranophyre Walraven (ibid.) concluded that the pseudogranophyre formed by the metamorphism of preexisting country rocks. As already discussed, a similar origin for the granophyric quartzofeldspathic rocks of this study is also envisaged.

7.6 GEOCHEMICAL RELATIONSHIPS OF THE METADOLERITES (MD) META-QUARTZ DOLERITES (MQD) MICROGRABBRONORITE (MGN) AND QUARTZ GABBRONORITE (QGN)

From consideration of the variation diagrams for the metadolerites (MD) and microgabbronorite (MGN) presented in the previous chapters, it is apparent that there is a close geochemical similarity between these two rock types (see for example Figure 7.31). Furthermore, when major and trace element data for both sets of metamorphosed rocks i.e. MD and MQD are plotted on Harker diagrams (Fig. 7.35 and 7.36) and compared with similar plots for the MGN and QGN, the similarity is quite striking in that the MQD and QGN are also very similar geochemically. It was concluded (chapter 7.2) that Rb and Sr do not reflect original values in the metamorphosed rocks and these elements are consequently not shown.

These observations are somewhat surprising in view of the obvious mineralogical and textural differences between the rock groups.
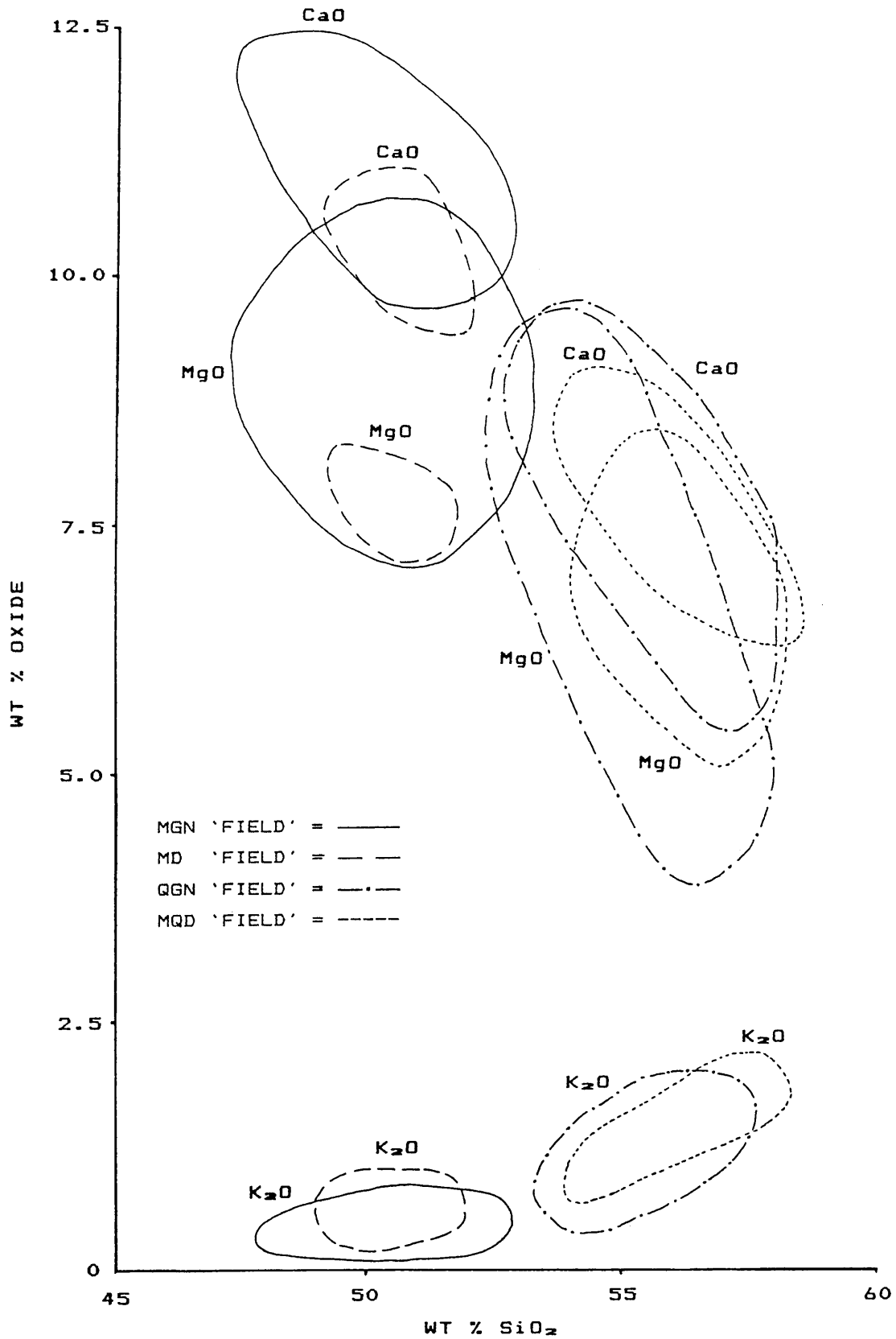
Fig. 7.35. Harker plot of CaO, MgO, and K₂O for the MGN, QGN, MD and MQD.

Fig. 7.36. Harker plot of Zr for the MGN AND QGN.
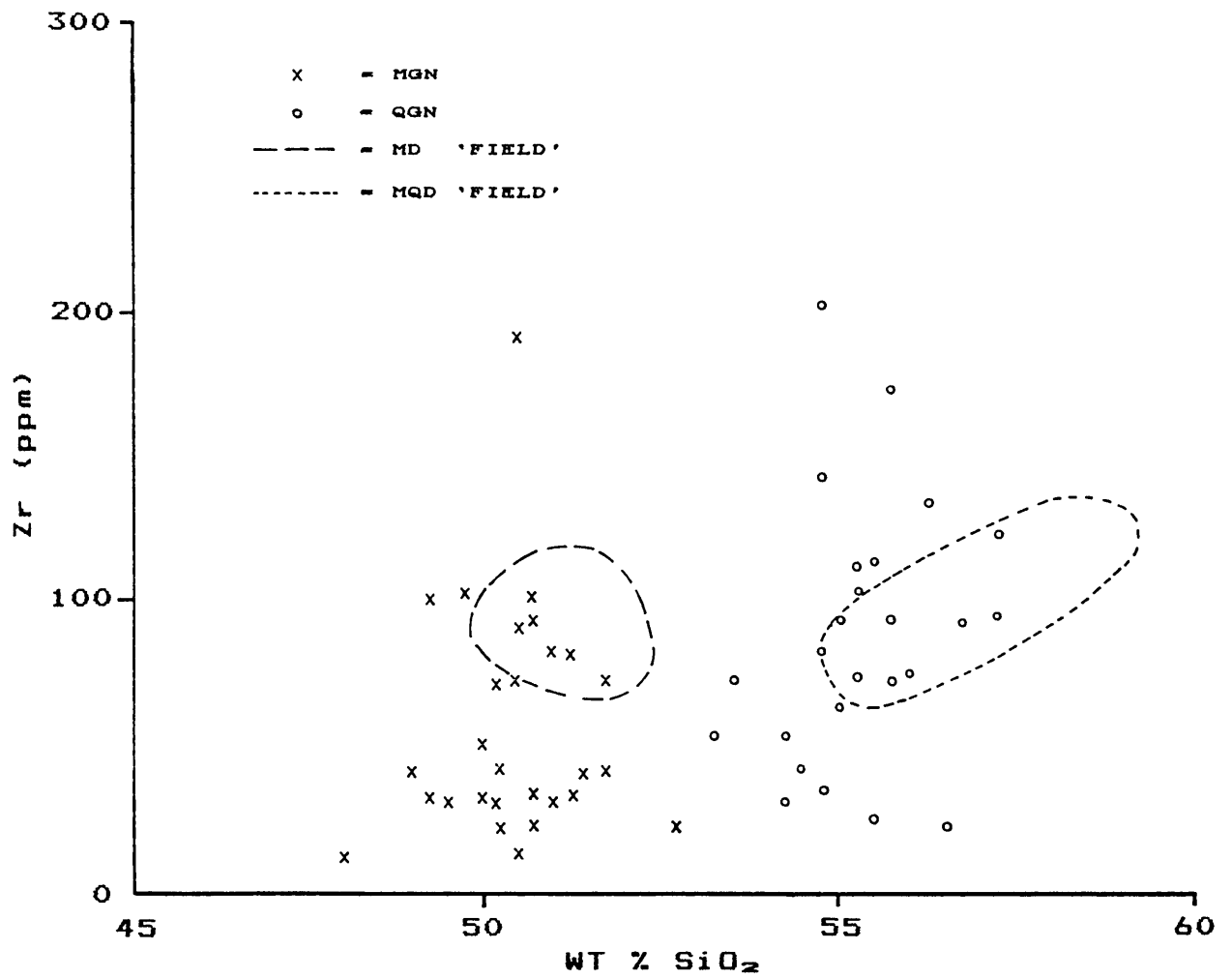
It was originally considered therefore that perhaps the geochemically similar rock types (e.g. MQD and QGN) were in fact part of the same intrusive event but that certain sills had been selectively metamorphosed. Such a process, effected by circulating groundwater, was proposed by Sharpe (1982) in order to explain the occurrence of both fresh and metamorphosed equivalents of the QTM. Essentially Sharpe (ibid.) envisaged that earlier sills, injected into the Transvaal Sequence, would set up a hydrothermal circulatory system which in turn would have an autometamorphic hydration effect on the accompanying intrusion. As a result of this autometamorphism and or the thermally driven escape of water from the system, later sills would be intruded into progressively drier host rocks. They would consequently remain relatively unaltered on consolidation. However this possibility must be rejected in the present case as it is inconsistent with observed field relationships and other geochemical data (chapters 2 and 7.7). For example, perfectly fresh micropyroxenite sills are interleaved with meta quartz-dolerite sills. If these meta quartz-dolerite sills are merely altered, earlier intrusions of the quartz gabbronorite magma it is difficult to envisage how the micropyroxenites, which are demonstrably older than the quartz gabbronorite[1], could have remained unaltered, while the early intrusions of quartz gabbronorite magma have been metamorphosed to meta quartz-dolerites.

Nevertheless the chemical similarity of the MD and MGN and their respective derivatives the MQD and QGN[2] is unquestionable and an explanation is required. The simple answer appears to be that rock types such as the MD and MGN (i.e. continental tholeiites) are common throughout the geological column. That is, as pointed out in chapters 7.2 and 7.3.2, although these rocks are very similar to each other, they are also very similar to geographically unrelated rocks of different ages, from elsewhere in the world (Tables 7.1 and 7.2). Furthermore as noted by Sharpe (1980) there is in fact a gross, overall

---

[1]Sharpe (1981) demonstrated that the QTM type sills predate intrusion of MGN type rocks in the eastern lobe of the Complex. In turn, the present investigation (chapter 7.7) indicates that intrusion of the MGN predates that of the QGN .

[2]Chapter 7.7.

similarity between many of the temporally unrelated igneous rock types that intrude the Transvaal Sequence.

The conclusion to be reached from the foregoing account is that two sets of geochemically similar rock types have been emplaced within the study area on two distinct occasions, being separated in time by intrusion of the QTM. In other words the MD and MQD equate with the pre-Bushveld sills of previous authors (e.g. Sharpe, 1981; Cawthorn et al. 1981) while the MGN and QGN are syn-Bushveld, being broadly coeval with the B2 rocks of Sharpe (ibid.) and the hypersthene microgabbro of Cawthorn et al. (ibid.).

Another significant feature of Figure 7.35. is that whereas the less silicic rocks tend to form groups, both sets of the more quartz-rich rocks tend to define trends, with their respective silica poor counterparts at one end. Since the latter (i.e. MD and MGN) are considered to be magmatic representatives (chapters 5.1.1 and 7.2) and the more silicic rocks (MQD and QGN) are considered to be contaminated (chapters 4.2 and 7.2) then there is a clear suggestion that the meta quartz-dolerite and quartz gabbronorite originated from their respective counterparts via a contamination process. Moreover this process appears to have been similar in both cases. On that premise, possible contaminants are considered and a discussion of mixing models is pursued in the next chapter.

7.7 MIXING MODELS AND THE ORIGIN OF THE META QUARTZ-DOLERITES AND QUARTZ GABBRONORITE

7.7.1 General

The previous chapters have established the geochemical similarity of the MD and MGN and of the MQD and QGN. To prevent repetition only the unmetamorphosed rocks, i.e. the MGN and QGN are discussed here but the modelling can be shown to apply to the metamorphosed rocks. In any event this will be apparent from comparison of Figures 7.35 and 7.36 with Figures 7.37 and 7.38.

7.7.2   Possible contaminants and a simple mixing model

Since portions of the QGN contain considerable quantities of hornfels xenoliths (chapter 5.1.2), the hornfels was considered as a possible contaminant. Initially only those hornfelses with a 'granophyric' texture (chapter 3.3.2) were included in the modelling, since these were presumed to have been close to melting and consequently more amenable to assimilation. This is in fact thought to be the reason that such rocks are always scarce within the QGN even when the laminated varieties are abundant (chapter 5.1.2). However, the addition of the laminated rocks to the modelling only increases the scatter of the data but does not unduly affect the overall position of the hornfels 'field' in Figures 7.37 – 7.40, or the conclusions reached below.

When major and trace element data for the hornfels are plotted on Harker diagrams, along with the MGN and QGN data (Figs. 7.37 – 7.40), all three rock groups lie along a straight line with the MGN and hornfels forming complementary end members. Such a relationship would be expected from simple assimilation (Wilcox, 1979), in this case, of hornfels by MGN magma but not if fractional crystallisation has accompanied this process (De Paolo, 1981). This is because in the latter case the one end member is continuously changing in composition, so that in effect, a more contaminated rock would have a different magmatic end-member to that of a less contaminated rock. It would be highly fortuitous for such mixtures to fall on a straight line between the two end members as it would require that the trend produced by fractionation would always parallel that produced by assimilation, which seems unlikely.

On the other hand in simple assimilation the end members are unchanged and mixtures between the two must therefore fall on a straight line joining the two end members. The composition of the QGN therefore appears to be the sum total of MGN magma plus assimilate, mixed in varying proportions. However, as Bowen (1928) showed many years ago, in a saturated liquid (magma), assimilation of a given amount of solid material can only be accomplished by the crystallisation, from the liquid, of an approximately equal amount of material. This relationship is a function of the large difference between the thermal capacities (0.2 – 0.3 cal/gm) and heats of solution or fusion (80 – 110 cal/gm) of silicates (Bowen, 1928; McBirney, 1979). It is clear from these figures that any drop in temperature would only release a small proportion of the heat necessary for assimilation and therefore the large amount of heat required for
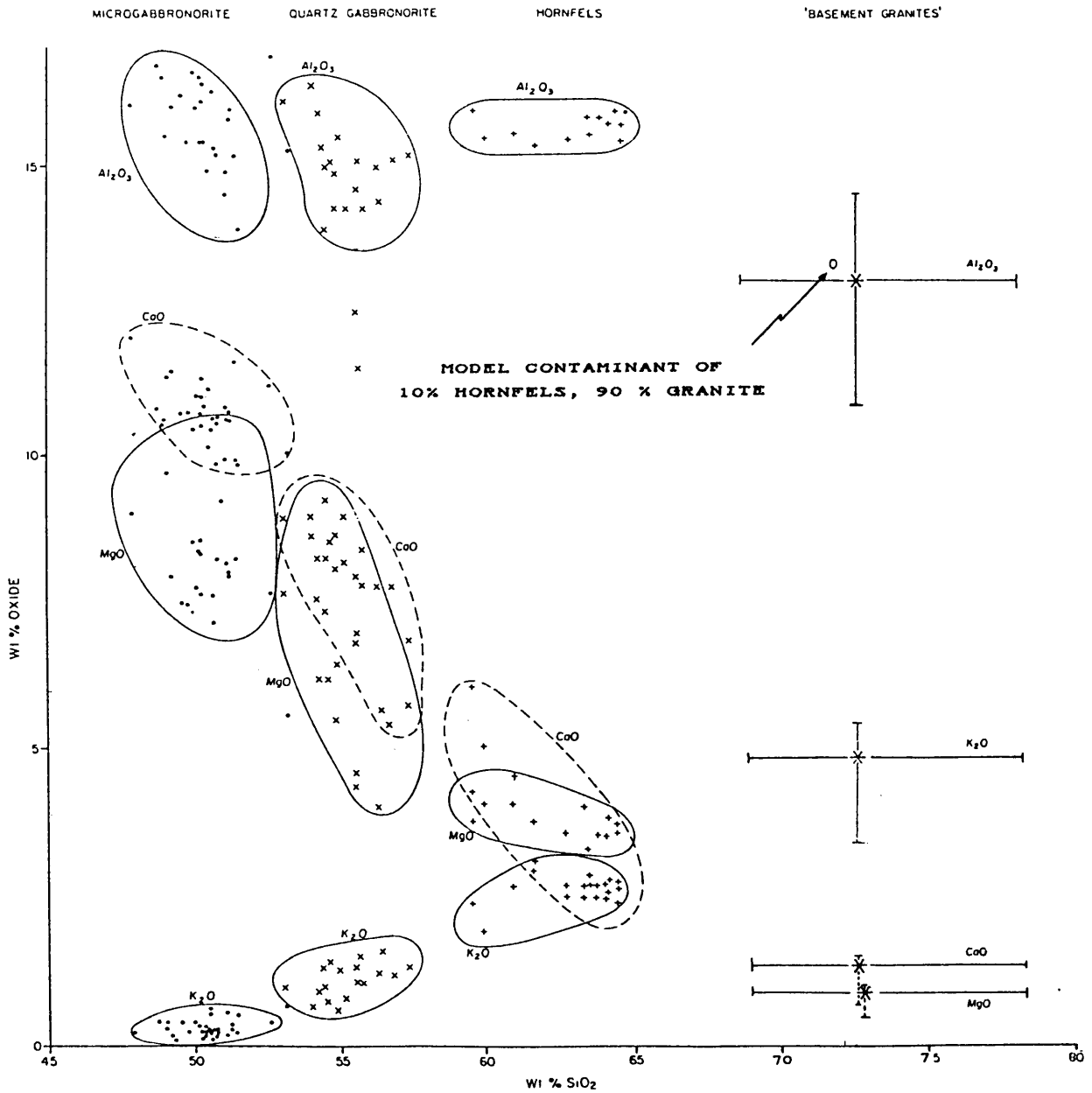
Fig. 7.37. Harker plot of Al₂O₃, CaO, MgO and K₂O for the MGN, QGN, hornfels and "basement granites".

X = MGN

O = QGN

+ = HORNFELS

'BASEMENT GRANITE' MEAN
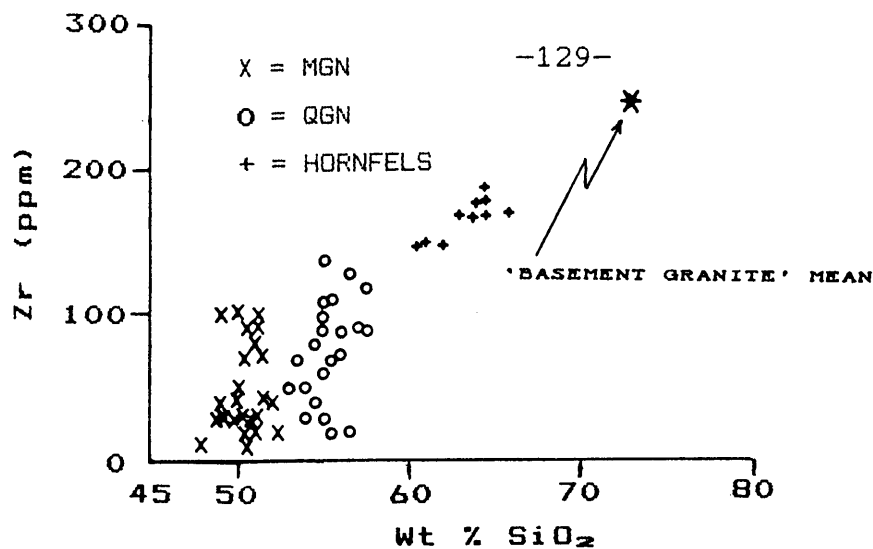
Fig. 7.38. Harker plot of Zr in the MGN, QGN, hornfels and 'basement granites'.
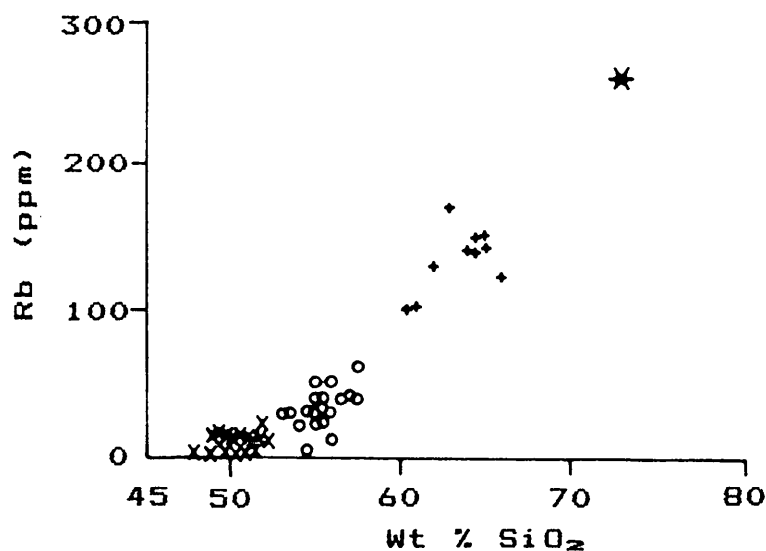
Fig. 7.39. Harker plot of Rb in the MGN, QGN, hornfels and 'basement granites'. Symbols as in Fig. 7.38.
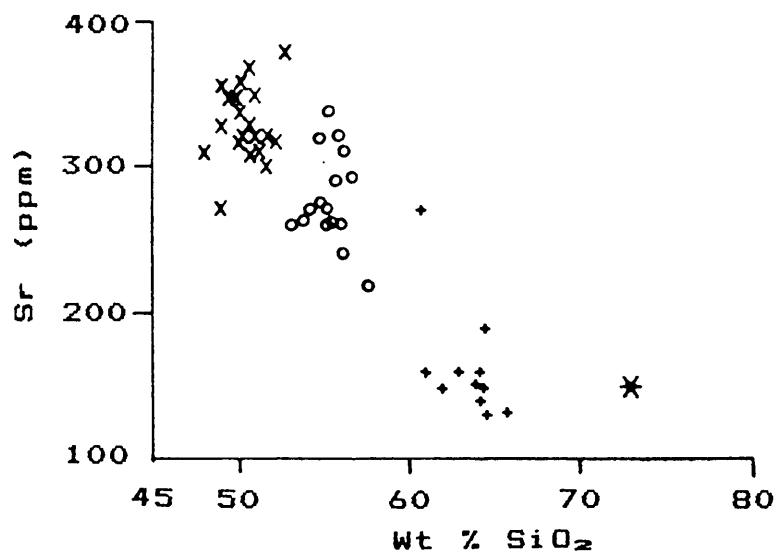
Fig. 7.40. Harker plot of Sr in the MGN, QGN, hornfels and 'basement granites . Symbols as in Fig. 7.38.

fusion could only be provided by a proportionately large amount of crystallisation.

Nevertheless, simultaneous crystallisation does not necessarily imply, or even require, crystal <u>fractionation</u>. In any event, the general heterogeneity of the QGN (chapter 5.1.2) indicates that at least some assimilation took place close to the site of emplacement, thus reducing the potential for such a process.

Bowen's observations (ibid.) are however of particular relevance if the 'lever rule' is applied for example to Figure 7.37. Clearly, for some compositions of QGN a 1:1 mix of MGN and hornfels is required and it is unlikely that such a mix could occur before the complete crystallisation of the liquid. This is because some heat would be lost by conduction, so that not all of the thermal capacity of the liquid would be available for melting entrained material. Consequently it could not assimilate its own weight of xenolithic material before completely crystallising and alternative contaminants must therefore be considered.

Sharpe (1981, p.316) argues that magmas reaching the crustal level at the base of the Bushveld Complex must have traversed <u>at least 25 km</u> of 'granitic' crust. Thus contamination by the basement is a distinct possibility.

From the data of Hunter (1974) for granites exposed in the Barberton – Swaziland area[1], Sharpe (1981) computed a mean 'granite' composition, assumed to represent that of a possible crustal contaminant (Sharpe, ibid., Table 1, col. 1). Although Sharpe (ibid.) used this composition to model possible effects on QTM type magmas, it is used here in assessing possible crustal contamination of the MGN. When this average 'granite' composition is also plotted on the Harker diagrams (Figs. 7.37 – 7.40) the general coincidence of the MGN, QGN, and 'granites' along a straight mixing line is apparent. There is therefore some indication that the basement 'granites' have been involved in the genesis of the QGN. Moreover the inclusion of granite components counters

---

[1]Presumed to be exposed representatives of the cratonic basement beneath the Complex.

the major objections raised above. Firstly because wall rock temperatures would be higher i.e. 400°C or possibly even greater, for the deep crust (35 - 40 km depth; Ringwood, 1975, p. 25) and secondly but more importantly, the maximum amount of assimilation required to produce the whole range of QGN compositions, as shown by the lever rule, would be less than 25 per cent.

It is also important to note that local contamination, by hornfels, consistent with the field evidence and arguments presented above could have occurred without influencing the trend of the mixing line for most elements. Since both hornfels and 'granites' generally lie along the same mixing line this ensures that any hornfels component would lie undetected in the final product i.e. the QGN (or MQD). Note however, that this relationship does not appear to apply to the Al_2O_3 data. In this case the hornfels data lie slightly above the mixing line for MGN-QGN-Granite. Nevertheless although this suggests that the hornfels may have played only a minor part in the contamination of the MGN, this does not completely rule out its role as an accessory contaminant. To illustrate that this is the case a 'model' contaminant consisting of 10 wt per cent hornfels and 90 wt per cent 'granite' is plotted in Figure 7.37. Mixing between this and the MGN could easily reproduce the Al_2O_3 content of the QGN.

Thus, the obvious conclusion to be drawn from this simple model is that the QGN originated via contamination of a microgabbronoritic magma by granitic crustal material. However localised assimilation of hornfels in the vicinity of the intrusion may have played a role in the final consolidation product. A more rigorous examination of the data for consistency with the hypothesis is discussed in the next chapter, and possible alternative contaminants are also considered.

7.7.3 A more complex mixing model and other possible contaminants

Langmuir et al. (1978) expanded on the mixing model of Vollmer (1976) to show that, for interelement ratio plots, a straight line relationship no longer prevails. They conclude that all mixing models can be described by a single hyperbolic equation of the form:

$$Ax + Bxy + Cy + D = 0$$

where x and y are the two ratios being considered and the coefficients are given by:

$$A = a_2 b_1 y_2 - a_1 b_2 y_1$$

$$B = a_1 b_2 - a_2 b_1$$

$$C = a_2 b_1 x_1 - a_1 b_2 x_2$$

$$D = a_1 b_2 x_2 y_1 - a_2 b_1 x_1 y_2$$

Where,

x_1, y_1 = co-ordinates of datapoint 1

a_1 = denominator of y_1

b_1 = denominator of X_1

Element ratios showing the greatest differences between the two postulated end members i.e. MGN and basement 'granites' are plotted in Figures 7.41 – 7.44. Furthermore coefficients for the above equation, calculated from the appropriate mean end member ratios, were used to derive general mixing curves between the MGN and Basement Granites. These mixing curves are superimposed on the actual data in Figures 7.41 – 7.44. There is clearly a close agreement of calculated values, expected from mixing of the two end members, and the actual data, thus corroborating the conclusion reached in the previous chapter. Note also that the mean hornfels value lies close to, or actually on, the calculated mixing curve, so that the arguments presented in chapter 7.6.2 still apply.

Despite the evidence presented however, some authors e.g. Patchett (1980) question whether bulk assimilation of crustal rocks is possible at all in nature. Patchett (ibid) argues that total melting of crustal material is possible only if it occurs within a short distance of the magma conduit. This results from the fact that although initial melts may be H_2O saturated, the
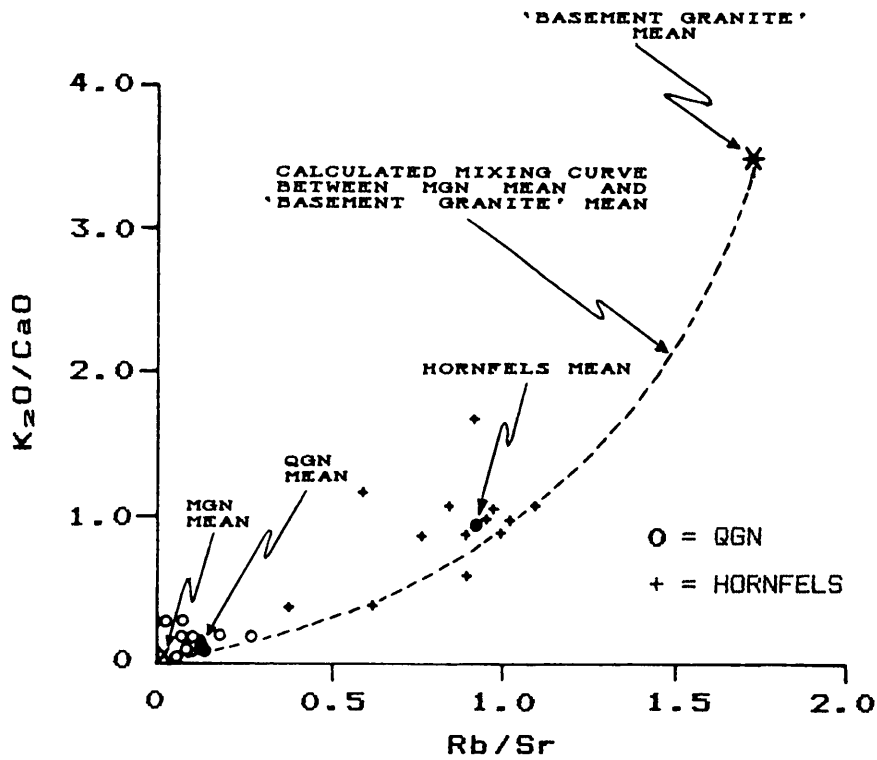
Fig. 7.41. Plot of K₂O/CaO vs. Rb/Sr for the MGN, QGN, hornfels and 'basement granites'.
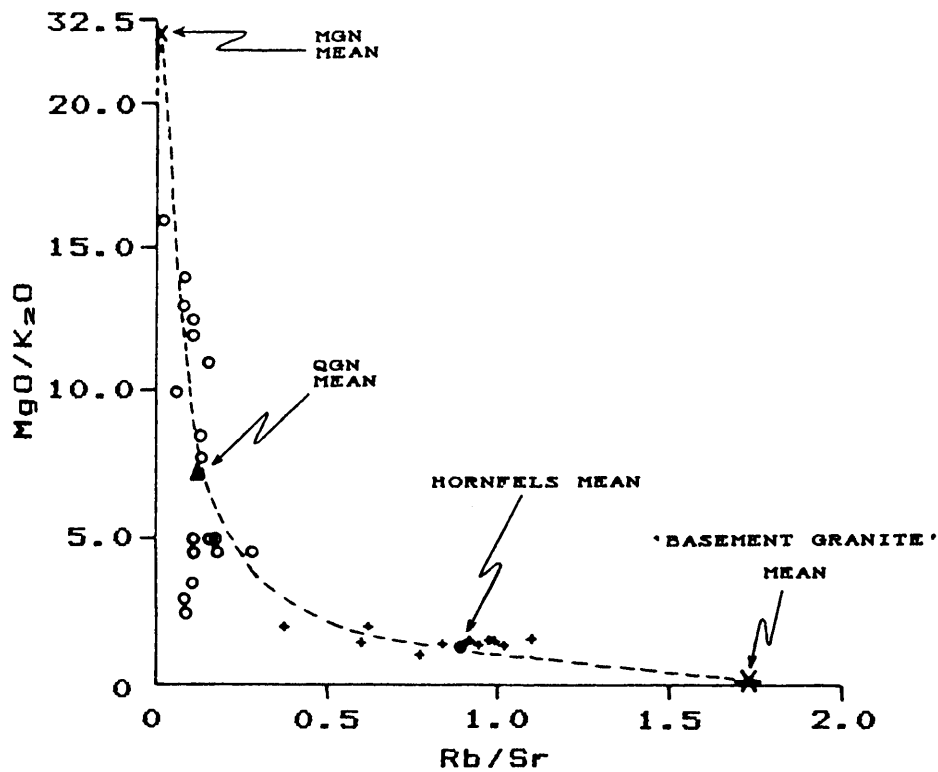
Fig. 7.42. Plot of MgO/K₂O vs. Rb/Sr for the MGN, QGN, hornfels and 'basement granites'. Unlabelled symbols as for Fig. 7.41.
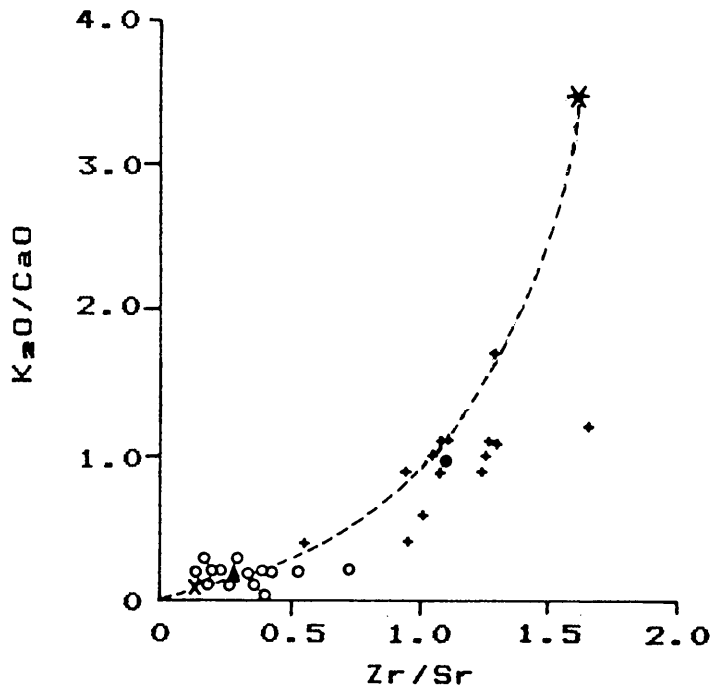
Fig. 7.43. Plot of K_2O/CaO vs. Zr/Sr for the MGN, QGN, hornfels and `basement granites`. Symbols as for Fig. 7.41.
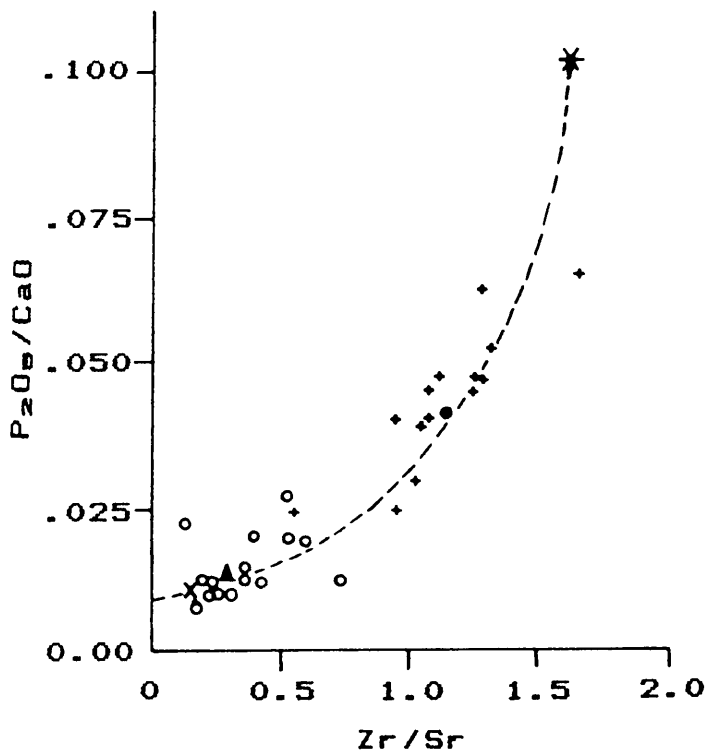
Fig. 7.44. Plot of P_2O_5/CaO vs. Zr/Sr for the MGN, QGN, hornfels and `basement granites`. Symbols as for Fig. 7.41.

overall H_2O content of the crustal rock is unlikely to be greater than 1 wt. per cent. This in turn requires that temperatures above 1 000°C are necessary for total melting i.e. at the 1 per cent H_2O granite liquidus (Wyllie, 1977).

Thus, although such temperatures may be attained within stoped material, it is unlikely that large amounts of bulk assimilation could occur in view of such relations. Nevertheless Patchett (1980), using a heat flow equation and appropriate thermal properties, calculates that partial melting should be widespread in the vicinity of basaltic magma conduits and contamination by such partial melts is therefore a viable alternative to bulk assimilation. Furthermore these zones of partial melting should be of the order of 10 - 20 per cent of the thickness of the magma conduit (Patchett, ibid.). Nell (1985) also argues that extraction of up to 65 per cent partial melt has occurred in some parts of the Bushveld aureole. In view of the above therefore, contamination by partial melts of both hornfels and granitic crustal material were also considered as alternatives to the bulk assimilation model.

In the absence of experimental or other data on partial melting of the hornfels, the residue-free, minimum melt composition of White and Chappell (1977) for their S-type granites was taken as representative of a hornfels melt.[1] (Table 7.6). These granites are considered to be the product of partial fusion of pelitic sedimentary rocks (White and Chappell, ibid). Similarly the

---

[1]Although Nell (1985) presents a composition for a partial melt considered to have been extracted from the Timeball Hill Shale Formation. It is questionable whether this is relevant to the present investigation. Firstly because of the chemical dissimilarity between this hornfels and those of the present study and secondly because the possible involvement of the intervening pelitic formation (Strubenkop) cannot be discounted. In any event, the chemistry of Nell's partial melt proves that it cannot have been important in the production of the QGN from the MGN since contents of Al_2O_3 (9wt. per cent) and Na_2O (1.5 wt. per cent) are too low at the appropriate level of silica saturation (71 wt. per cent). However, because of the considerable difference in chemistry between the Timeball Hill hornfels (Nell, ibid.) and those of the Silverton Shale - Magaliesberg quartzite, this does not prove that other possible melt compositions are not involved.

I-type minimum melt, considered to be the result of partial fusion of lower crustal material (White and Chappell, ibid) was taken as representative of a crustal partial melt (Table 7.6).

TABLE 7.6

Analyses of S- and I- type granites from White and Chappell (1977)

	S-TYPE	I-TYPE
SiO_2	75.07	76.21
TiO_2	0.28	0.06
Al_2O_3	12.85	12.89
FeO	0.24	0.29
Fe_2O_3	1.31	0.84
MnO	0.03	0.07
MgO	0.31	0.05
CaO	1.11	0.69
Na_2O	3.08	3.77
K_2O	4.81	4.72
P_2O_5	0.06	0.01
H_2O+	0.62	0.27
H_2O-	0.14	0.05
CO_2	0.14	0.12

The compositions of the potential contaminants are plotted on the Harker diagram in Figure 7.45. It is immediately apparent from this diagram that the separate involvement of either S-type or I-type 'partial melts' in the contamination process cannot be deduced, owing to their general similarity in major element content. Trace element data are unfortunately not available for these minimum melt compositions.

Nevertheless there is a clear suggestion that partial melts of similar composition were involved in the formation of the QGN from the MGN. Furthermore, applying the 'lever rule' to Figure 7.45 indicates that a mixture of 20 per cent or less, of contaminant with the MGN, would suffice to form QGN compositions and this accords well with the modelling of Patchett (ibid.).
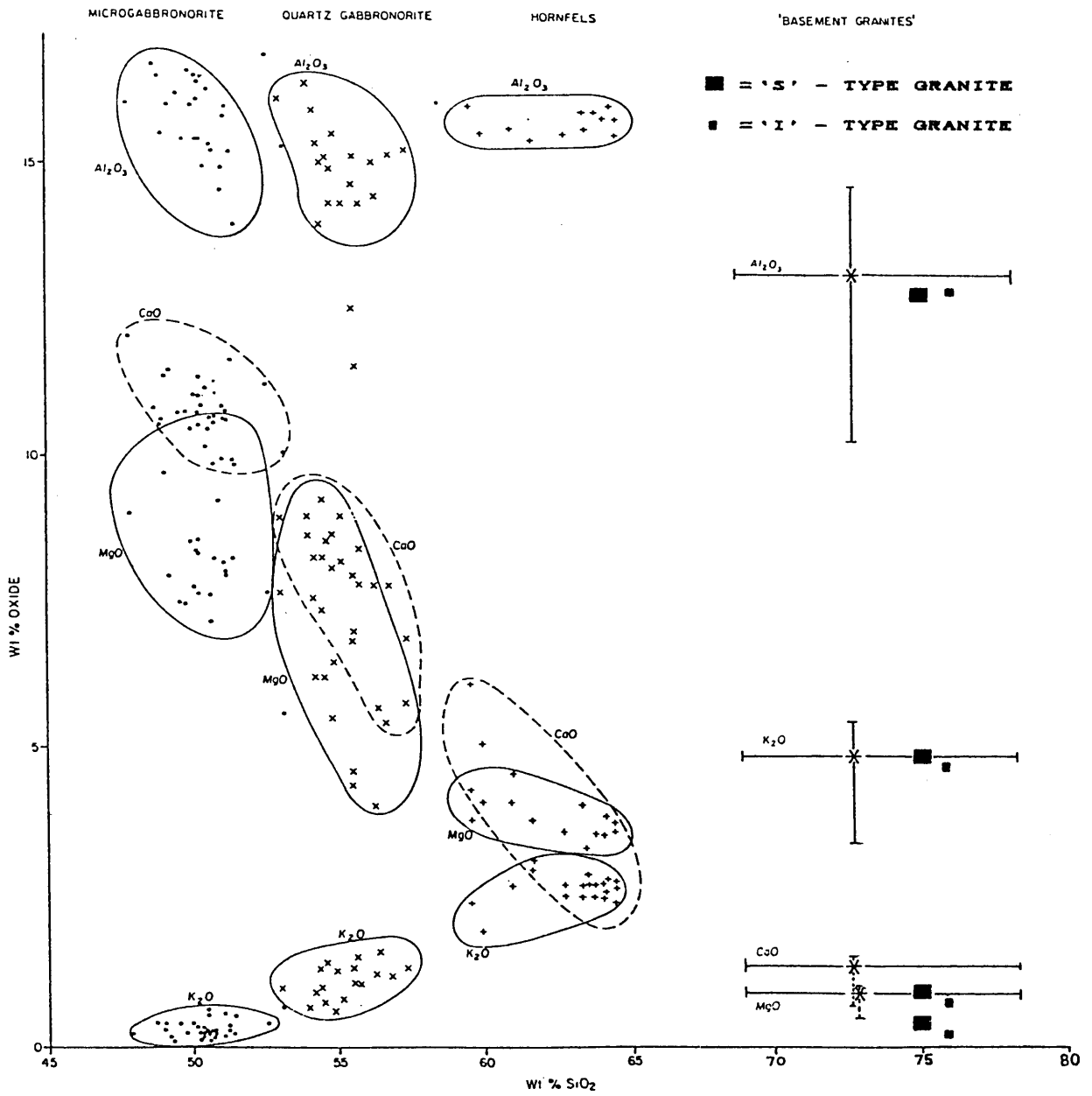
Fig. 7.45. Harker plot of Al_2O_3, CaO, MgO and K_2O for the MGN, QGN, hornfels, 'basement granites' and 'S' and 'I' — type granites.

The Langmuir et al. (ibid.) model is not readily applicable to this data as the choice of either S- or I-type melts as end member naturally ensures a better fit than the other. Use of the MGN and QGN compositions to attempt to define the other possible end member (end members do not necessarily have to be defined in this model) is also unacceptable because the hyperbola is poorly constrained by the relative proximity of MGN and QGN compositions. In order to be valid, the calculated curve must be constructed from two widely separated data points.

Although the use of Sr isotopes was considered in order to elucidate the possible contaminant(s), it was found that the MGN itself, like equivalent rocks from the eastern Bushveld, possesses variable initial ratios of $^{87}Sr/^{86}Sr$ (Harmer and Sharpe, 1985, and Appendix 5). Consequently it was felt unlikely that $^{87}Sr/^{86}Sr$ analysis alone would aid in unravelling the complex history of the QGN, particularly since there is evidence that crystal-liquid isotopic disequilibrium occurs in the crust over the time scale required for contamination (Pushkar et al, 1972; Betton, 1979; McBirney, 1979; Patchett, ibid). McBirney for example, suggests that partial melts could easily be enriched in K_2O, Rb and radiogenic Sr relative to the bulk crustal source, owing to the breakdown of minerals such as biotite and muscovite, which have high concentrations of K_2O, Rb and ^{87}Sr (McBirney, ibid). As a result, the geochemical patterns resulting from addition ... "of contaminants which are isotopically unrepresentative of their source rocks may be highly complex" (Patchett, ibid, p.561).

Nevertheless intrusion of such contaminated magma (presumably richer in radiogenic strontium) into the Bushveld Complex could explain the overall upward increase in $^{87}Sr/^{86}Sr$ values noted by Hamilton (1977). Such an upward increase in $^{87}Sr/^{86}Sr$ values is also common to several other layered intrusions (De Paolo, 1985) and has been interpreted as evidence of increasing contamination during their evolution (De Paolo, ibid.). However work by Kruger and Marsh (1982, 1985) and more recently by Eales et al. (1990), illustrates the wide small-scale variation of $^{87}Sr/^{86}Sr$ ratios that occur within the Bushveld Complex and this coupled with the isotopic variability of the MGN indicate that more data are clearly necessary to elucidate the contamination process.

It is probable that a multi-isotope approach, such as that used by Morrison et al, (1985) will be required to finally elucidate the contamination process. The latter authors were able to demonstrate, using Sr, O and Pb isotopic data, that the contamination process accompanying intrusion of the Mull (Scotland) basalts was complex, occurring at different crustal levels and involving differing country rocks.

In conclusion it must be stated that the QGN undoubtedly originated via contamination of the MGN-type magma.[1] However, the mechanism and amount of contaminant(s) is less clear. Latent heat considerations rule out bulk assimilation of hornfels and possibly even that of crustal 'granites' as the sole mechanism of contamination. The most reasonable explanation, in the light of the preceding discussion, is that of contamination by partial melts from the basement, similar in composition to S- or I-type melts, together with some component of partial melt extracted from the pelitic country rocks. Small amounts of bulk assimilation, both of basement rocks and pelitic hornfels could however, have occurred. Indeed the general heterogeneity of the QGN implies that at least some contamination took place close to the site of emplacement.

7.8   THE RELATIONSHIP OF THE QTM AND MGN TO THE RUSTENBURG LAYERED SUITE

7.8.1   General

The field relationships and volumetric abundances of the QTM and MGN implies that both 'magma types' are possible parents to the Rustenburg Layered Suite. It must be remembered, however, in the ensuing text that such rock types are only broadly representative of actual magmas.

Over the years considerable attention has been focussed on the topic of parental magmas to the Bushveld Complex, as reviewed in Sharpe (1981) and Von

---

[1]This conclusion incidentally, confirms the non-correlation of the 'Hendriksplaats norite' (Willemse, 1959) and the QGN, as noted in chapter 5.1.2. Sharpe (1980, 1981) concluded that this 'norite' was essentially a mixture of micropyroxenitic (i.e. QTM) magma plus contaminant(s), while the QGN is clearly a mixture of MGN plus contaminant(s).

Gruenewaldt et al. (1985) and a variety of parents have been proposed. These can be broadly divided into three categories:

1. <u>Ultramafic</u> (20 - 30 wt. per cent MgO) Vermaak (1976), Hamilton (1977), Van der Merwe (1976), Cameron (1978).

2. <u>High - magnesium basalt</u> (12 - 15 wt. per cent MgO) Gijbels et al. (1974), McCarthy and Cawthorn (1980), Cawthorn et al. (1981). These range from olivine tholeiite (Cameron, 1978) to contaminated komatiite representatives (Sharpe, 1981; Barnes, 1989) or boninites (Sharpe and Irvine, 1983; Cawthorn and Davies, 1983; Hatton and Sharpe, 1988).

3. <u>Tholeiite</u> (6 - 8 wt. per cent MgO) Von Gruenewaldt (1973), Vermaak (1976), Hamilton (1977), Cawthorn et al. (1981).

It was formerly considered (Sharpe, 1981) that the lower and critical zones evolved from a single parent (either of the type 1 or 2 above) while the main and upper zones were the product of a tholeiitic parent. However, more recent concepts invoke a more complex origin for the Rustenburg Layered Suite, involving mixing of two main magma types corresponding to the high-Mg and tholeiitic groups (Von Gruenewaldt et al., 1985).

The QTM clearly falls in the high-Mg category while the MGN is a typical tholeiite. This is hardly surprising since these rock types are similar to those described by many of the above-mentioned authors. However each is assessed on its own merits in the ensuing discussion, which explores the possible association of such magmas with the Rustenburg Layered Suite, using the relationships first described by Roeder and Emslie (1970). These authors investigated the equilibria between olivine and natural basaltic liquids in the temperature range 1150 - 1300°C. Total pressure was one atmosphere but oxygen fugacity was variable. From these investigations Roeder and Emslie derived an expression which may be written :

$$K_D = (FeO/MgO)^{Ol}/(FeO/MgO)^{Liq} \text{ (mol. ratios)}$$

which describes the partitioning of iron and magnesium between olivine and liquid based on the following reaction:

$$Mg_2SiO_4 \text{ (olivine)} + 2FeO(liquid) = Fe_2SiO_4(olivine) + 2MgO \text{ (liquid)}.$$
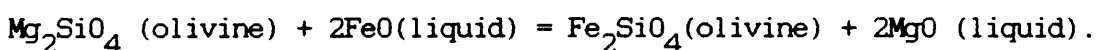
Roeder and Emslie (ibid.) found that the K_D value was independent of temperature and possibly pressure (p. 283) and had an average value of 0.30. Subsequent work by Roeder (1974) and several other workers. e.g. Walker et al. (1976); Bender et al. (1978); Longhi et al. (1978) confirmed this relationship although with some variation (i.e. 0.27 - 0.36). In addition Bender et al. (1978) found that at higher pressures the liquidus olivine was more iron rich, resulting in a systematic increase in K_D with pressure from 0.27 at 0 Kb to 0.31 at 10 Kb. Alternatively Longhi et al. (1978) considered this pressure effect negligible below 5 Kb and obtained K_D's in the range 0.28 - 0.33. Since the later work has not shown the K_D value of Roeder and Emslie (ibid.) to be seriously in error. although clearly there is some pressure dependence, the value 0.30 is retained here and used in the following chapters. This is considered appropriate for the probable pressure under which the Bushveld Complex crystallised. i.e. 1.1-1.6 Kb (Wallmach et al. 1989).

7.8.2. Ultramafic magma

Hulbert (1983) was able to show that an ultramafic magma was an unlikely parent to the Rustenburg Layered Suite and his arguments are briefly reiterated below to afford a complete treatment of the subject.

Most proposed ultramafic magmas average ±30 weight per cent MgO (chapter 7.8.1) and Hulbert (ibid.) used Cameron's (1978) estimated parental magma composition as a typical example. This composition was calculated from the bulk constitution of the lower zone and contains 31.72 per cent MgO with an Mg^* (see chapter 6.1.2.1)) of 0.855 (Hulbert, ibid.). Assuming a $K_D \, {}^{ol-liq}_{Fe-Mg_*}$ of 0.30 (chapter 7.8.1) such a magma should precipitate olivine with an Mg^* of 0.952 i.e. considerably more magnesian than any of the olivine found in the lowermost portions of the Bushveld Complex. For example, Cameron (ibid, Table 2) reports Mg^*'s for lower zone olivine ranging from 0.848 to 0.872, with a mean value of 0.865. Similarly Hulbert (ibid., Table 7, p. 222) also presents analyses of olivine from the lower zone of the Potgietersrus limb with a mean Mg^* of 0.875. Although the compositional range (0.900 - 0.845) is slightly greater for Hulbert's data, it is clear that none of this olivine crystallised from a liquid as magnesian as the postulated ultramafic parent.

Certain ultramafic sills found in the eastern portion of the Complex were also originally considered to be possible parental representatives. However,

Hulbert (1983) similarly showed that their high Mg^* (±0.86) precludes this possibility, while later work by Sharpe and Hulbert (1985) has demonstrated that these rocks do not represent true liquid compositions in any event.

There is therefore little evidence of an ultramafic parent to the lower portions of the Complex in view of the disparity between the expected and observed. olivine — liquid compositions.

7.8.3. High-Mg basalt

In the present study the mean of 20 quench-textured micropyroxenites was used as representative of this group (Table 7.7). This average composition is in fact very similar to one of the starting compositions used by Cawthorn and Davies (1983) in their melting experiments on postulated Bushveld Complex magmas (Table 7.7.). At the outset however, it must be mentioned that the ensuing argument cannot be directly related to the present area because of the absence of basal lower zone material.

Nevertheless following the same line of reasoning pursued in chapter 7.8.2., a liquid with the composition of the QTM mean would be in equilibrium with olivine of Mg^* 0.912. Although this is somewhat higher than the highest values of Cameron (ibid.), i.e. 0.872, it is very close to an olivine composition found by Hulbert (ibid) in the lowest exposed portion of the Rustenburg Layered Suite in the Potgietersrus area i.e. 0.90. Furthermore as the latter author points out (p.221) "rocks with olivines that have a higher Mg^* may be developed in the unexposed deeper succession, closer to the feeder of the ... funnel shaped intrusions".

In the melting experiments of Cawthorn and Davies (ibid.), on a slightly less magnesian composition than the QTM average (No. 4 in Table 7.7), liquidus olivine Mg^*'s lie in the range 0.88-0.89, clearly in close agreement with the calculated values for the QTM. Furthermore, the general crystallisation sequence obtained by Cawthorn and Davies (ibid.) and also Sharpe and Irvine (1983) for such compositions i.e. olivine-orthopyroxene-plagioclase-clinopyroxene, broadly resembles that found in the Rustenburg Layered Suite. The order of appearance of plagioclase and clinopyroxene is however reversed in more magnesian compositions (No. 1. Table 7.7) but olivine persists as liquidus mineral up to 6 Kb, when it is replaced by orthopyroxene. This replacement

TABLE 7.7

Comparison of the geochemistry of the QTM and the micropyroxenites used in the melting experiments of Cawthorn and Davies (1983).

	QTM (MEAN) (This study) (Anhydrous)	MICROPYROXENITES OF CAWTHORN AND DAVIES (1983) Table 1. (Anhydrous)	
		No. 4	No. 1
SiO_2	55.56	55.48	53.37
TiO_2	0.36	0.36	0.41
Al_2O_3	11.39	12.69	10.77
Fe_2O_3	1.86	1.78	2.02
FeO	7.63	7.77	8.08
MnO	0.18	0.9	0.19
MgO	13.31	12.39	15.41
CaO	6.60	6.93	6.27
Na_2O	1.71	2.01	1.77
K_2O	0.90	1.03	0.99
Mg^*	0.757	0.744	0.773

occurs at slightly lower pressures in the less magnesian composition (i.e. No.4, Table 7.7) but since the QTM average lies between these two, its crystallisation behaviour is reasonably predictable. Such a pressure – composition related crystallisation order also accords reasonably well with the observed bronzititic, harzburgitic and rare dunitic cumulates at the base of the Complex (Cameron, 1978) and with available estimates of pressures during crystallisation. These have previously ranged from ± 4.5 Kb (Sharpe and Snyman, 1980; Sharpe, 1981) to 1.5 Kb (Nell 1985) during formation of the lower zone, although more recent data indicates that the probable range is of the order 1.0-1.6 Kb, (Wallmach et al., 1989).

However an important point made by Irvine and Sharpe (1982) is that the crystallisation order (as e.g. predicted by the computer model of Nathan and v. Kirk (1978) and later determined by Sharpe and Irvine, 1983) of QTM-like compositions, even though broadly compatible with the Rustenburg Layered Suite does not in detail reproduce the observed cumulate sequence. From this they argue that such magmas cannot be truly parental and are considered to represent liquids derived from the original parent by olivine fractionation.

While it is true that the QTM are probably not primary liquids (chapter 7.9), if the term 'parental liquid' refers to the first liquid to enter the Bushveld chamber, then this argument is not necessarily valid and deserves further comment. For example, Irvine and Sharpe (ibid.) suggest that the QTM are derived liquids and that the true parent (Uo in their terminology) lies on a mixing line between the QTM and certain ultramafic rocks. These ultramafic rocks are considered to represent Uo liquid plus cumulus olivine and the QTM are considered to represent Uo minus olivine, i.e. the QTM represent Uo liquids that have undergone olivine fractionation.

Consequently if it is assumed that the hypothetical parent (Uo) was intruded into the initial Bushveld chamber and subsequently underwent closed system olivine fractionation, then the QTM composition, being derived from Uo, must lie somewhere on the fractionation path between Uo and its final, residual liquid. That is, at some stage the composition of the liquid in the chamber must have been equivalent to that of the QTM. Thereafter its fractionation path must have been the same as if only the QTM composition was initially introduced into the chamber.

On this assumption, it is clear that the earliest known (i.e. the lowest exposed) cumulates (olivine of Mg^{*} 0.900, Hulbert (ibid)) must have formed just after the stage at which the liquid in the chamber became equivalent to the composition of the QTM. This is because the predicted equilibrium olivine for the QTM (i.e. 0.912, see above) is slightly more primitive than that found at the base of the Rustenburg Layered Suite (i.e. 0.900; Hulbert, ibid.). In this case the subsequent behaviour of this liquid, as represented by the known cumulate lineage will be identical, irrespective of whether Uo or QTM-type compositions were its starting point. Consequently while the argument that the QTM are non-primary liquids is probably correct (chapter 7.9), postulating the existence of a more primitive parent (Irvine and Sharpe, ibid) cannot account

for the fact that the crystallisation <u>order</u> of the QTM does not reproduce the cumulate lineage of the Rustenburg Layered Suite.

However, the fact that the experimental crystallisation data do not in detail reproduce the order found in the Rustenburg Layered Suite still requires an explanation. It was considered possible, therefore, that the one atmosphere model of Nathan and van Kirk (1978) and the later (1 atm.) melting experiments of Sharpe and Irvine (1983) were not directly applicable to the cumulate sequence, which obviously crystallised under greater pressures. However, it must be noted that Cawthorn and Davies (1983) also obtained somewhat similar results for similar melt compositions at 3 Kb., so that this explanation is unlikely.

Another possibility is that in fact the experimental results do not apply to the whole of the Rustenburg Layered Suite. Clearly if "there are considerable differences in the nature and succession of rock types between the different lobes of the Complex, with the exception of the upper critical and lower main, zone" (Von Gruenewaldt et al., 1985, p. 807) then the experimental results must be inappropriate to some parts of the succession. For example, the lower zone of the Potgietersrus lobe is considerably richer in dunitic cumulates (and chromitites) than the eastern lobe of the Bushveld Complex (Van der Merwe, 1976; Cameron, 1978; Hulbert, 1983; Hulbert and Von Gruenewaldt, 1985). Unless differing parental compositions are postulated for the individual lobes then it is obvious that both successions cannot be precisely reconciled with the observed experimental behaviour. Such a concept would also be against the general consensus of many workers on the evolution of the Complex, as expressed in Sharpe (1981) and von Gruenewaldt et al. (1985). Hatton and von Gruenewaldt (1987) however, later speculated that in fact the initial magma emplaced into the southern lobe was more evolved than that in the north, although no chilled representatives of such a magma have been identified.

It is possible, however, that varying degrees of magma mixing were important in affecting the ultimate crystallisation sequence of individual lobes. In this sense the 'parental' magmas may have differed in different lobes. Hulbert and Von Gruenewaldt (1985) for example, explain the origin of the lower zone chromitites in the Potgietersrus limb by a process of mixing fresh QTM type magma with fractionated residual liquid of broadly basaltic composition. They also imply (p. 893) that the experimental data of Sharpe and

Irvine (1983) obtained from mixing MGN (basaltic) and QTM type compositions are of significance in the formation of these chromitites owing to the depression of silicate liquidi by the mixing process.

Since the MGN is a fairly typical 'basalt' (chapter 7.3.) the experimental data of Sharpe and Irvine (1983) may have even greater significance here, not only because it may have relevance to the formation of chromitite but because such a mixing process could also lead to formation of a larger proportion of dunitic cumulates than from crystallisation of QTM alone. This is because as the amount of basaltic component is increased, the temperature interval over which olivine is the sole silicate to crystallise from such mixed compositions is increased. For example, consideration of Figure 22. in Sharpe and Irvine (ibid) indicates that for pure QTM magmas, olivine is the sole silicate to crystallise only over a temperature interval of 5 - 10° C. However for mixtures of QTM and MGN, olivine is the sole silicate to crystallise over a temperature interval of ± 50° C.

Hence the larger proportion of dunitic material in the northern lobe of the Complex could be the result of a higher proportion of residual 'basaltic' component during mixing, relative to the other lobes, and it is not necessary to postulate a fundamentally different parent. Clearly however, if a process such as magma mixing has occurred, then the experimental crystallisation data on the QTM is no longer appropriate after the initial hybridisation. There is therefore no reason at all to expect the subsequent crystallisation sequence to accord with the experimental data.

Nevertheless, in conclusion, the fact remains that the first crystallised olivine (Mg^*=0.90) found at the base of the lower zone must have crystallised from a liquid of approximately Mg^* 0.73 to 0.75^1. Since these values are only slightly less than the Mg^* of the QTM mean (0.76) it is concluded that the QTM

---

[1]Assuming a $K_D \frac{ol-liq}{Fe-Mg}$ of 0.30 (Roeder and Emslie, 1970) or a $K_D \frac{ol-liq}{Fe-Mg}$ of 0.33 (Longhi et al., 1978), respectively.

is representative of the parental magma to the lowermost portion of the Bushveld Complex, thus reinforcing earlier conclusions by Davies et al. (1980), Sharpe (1981, 1982), Cawthorn et al. (ibid.).

7.8.4. Tholeiite magma

The MGN is representative of this group. However, the composition of the MGN is not necessarily representative of any actual liquid that existed within the magma chamber(s) of the Bushveld Complex, since presumably any MGN liquid would have mixed with residual magma on intrusion. Consequently it is not possible, using the geochemical data to directly link the MGN with particular portions of the Rustenburg Layered Suite as could be done for the QTM (chapter 7.8.2). In any event, many authors (Sharpe and Irvine, 1983; Hulbert and Von Gruenewaldt, 1985; Hatton 1985; Harmer and Sharpe, 1985, Von Gruenewaldt et al., 1985) present evidence that such liquids may well have been introduced into the fractionating chamber on several different occasions, further complicating interpretation. Such evidence, much of which was reviewed in Von Gruenewald+ et al. (1985), includes upwardly increasing amounts of radiogenic strontium[1] and intercumulus plagioclase (QTM averages ±35 wt. per cent normative plagioclase while the MGN averages ±50 wt. per cent (Appendix 3)) as well as reversals in cumulus mineral compositions. More recently, Reichardt (1989) has also documented pronounced changes in orthopyroxene composition (marked increase in Ti and a drop in Mg^*, Ca and Al across the pyroxenite subzone – anorthosite subzone boundary) which he attributed to intrusion of an MGN-type liquid at this level. On the other hand Eales et al. (1990) also found that while radiogenic strontium increased upwards within the MG 4 – UG 1 interval, the Cr content of pyroxene also increased upward and they disputed therefore whether the increase in radiogenic strontium was due to the intrusion of MGN-type liquids into the chamber. However, the extent to which their arguments are generally applicable to the whole critical zone would seem to require further confirmation and at present a general consensus, gleaned from the references cited above, is that a substantial individual addition of

---

[1]For the lower zone parental liquids (QTM type), R_o at 2.05 Ga equals approx. 0.704, while the MGN type liquids have R_o approx. 0.707 (Harmer and Sharpe, 1985) and Appendix 5.

MGN-type magma took place immediately prior to crystallisation of the anorthosite subzone.

Thus, in light of this extensive body of published data and consequent uncertainties in actual magma compositions within the intrusion, further discussion, along the lines pursued in chapter 7.8.3, is considered superfluous. However it must be concluded that the field evidence of the current study also provides strong support for an extensive intrusion of MGN type liquid immediately prior to crystallisation of the anorthosite subzone. Such a liquid, in itself may have been the product of mixing of two or more separate magmas, as pointed out by Harmer and Sharpe (1985) on the basis of variable $^{87}Sr/^{86}Sr$ ratios for this rock group. This contention is reinforced by the variable $^{87}Sr/^{86}Sr$ ratios obtained in the present study (Appendix 5).

7.9 PETROGENESIS OF THE QUENCH-TEXTURED MICROPYROXENITES (QTM)

7.9.1 Primary magmatic characteristics of the QTM.

Certain features of the QTM suggest that such rocks may be representative of a primary magma, i.e. liquid derived directly from the mantle with little modification en route to its level of emplacement. For example, Green et al. (1974) argued that primary magmas in equilibrium with mantle olivine (Fo_{90-92}) would have an Mg^* of ±0.70 (QTM = 0.76), on the same basis that the QTM equilibrium olivine was calculated in chapter 7.8. Furthermore, if we assume an equilibrium melting model (chapter 7.9.2), a reasonable residual mantle composition comprising olivine and orthopyroxene in a 4:1 ratio, and that for elements with a high D, the concentrations in the melt are almost independent of the degree of melting (Maaloe and Johnston, 1986), then with a total NiO content of 0.20 to 0.40 wt. per cent (Ringwood, 1975, Ch. 3), use of appropriate partition coefficients, i.e. D_{Ni}^{ol-liq} = 10 and $D_{Ni}^{opx-liq}$ = 4 (Cox et al., 1979, Table 14.1) indicates that between ±180 and ±400 ppm Ni should enter the equilibrium liquid. The average Ni content of the QTM, i.e. 300 ppm., clearly falls within this range, although this feature of the QTM is discussed further in the following chapter.

Although Cr is less refractory than Ni in mantle compositions the Cr content of the QTM (± 1100 ppm) also suggests an equilibrium relationship with the mantle, assuming reasonable degrees of melting, 2000-4000 ppm Cr in the residue (Ringwood, ibid., p. 165), and a bulk distribution coefficient of 2

(using the partition coefficients from Allegré et al. (1977), i.e. D_{Cr}^{ol-liq} = 1.8, $D_{Cr}^{opx-liq}$ = 2.8 and assuming a 4:1 olivine:orthopyroxene ratio in the residue).

If the QTM do represent a primary magma, then their high normative hypersthene content suggest that they are the result of extensive mantle melting. Orthopyroxene would be a residual phase at low degrees of melting so that increasing degrees of melting are necessary to incorporate increasingly greater amounts of this mineral into the final melt. The extremely low TiO_2 content of these rocks also endorses this view since TiO_2 is generally incompatible with residual mantle compositions comprising predominantly olivine and orthopyroxene (D_{Ti}^{ol-liq}=0.01, Langmuir et al., (1977); $D_{Ti}^{opx-liq}$ = 0.11, Irving, 1978, p. 743). Consequently given a fixed initial amount of TiO_2 this would be concentrated in the early fractions of the melt but would become progressively diluted as more and more of the compatible components were incorporated at increasingly higher degrees of melting. The QTM have TiO_2 contents (± 0.35 wt. per cent) comparable with komatiites, which have the lowest TiO_2 content of all mafic magmas (Hughes, 1982, p. 464). Komatiites are also considered to be generated by extensive mantle melting (Arndt and Nisbet, 1982).

In contrast to these indications that a high degree of melting is involved in the genesis of the QTM, is their anomalously high K_2O content (0.8-1.0 wt. per cent). This is anomalous, because K_2O is even more incompatible than TiO_2 in mantle compositions D_K^{ol-liq}=0.001 and $D_K^{opx-liq}$=0.001, Cox et al., 1979, Table 14.1) and should, for the same reason, be present in only small amounts in the final melt. The K_2O content of the QTM is however extremely high for a liquid thought to result from extensive mantle melting. Komatiites for example have K_2O contents in the range 0.0-0.07 wt. per cent (McIver et al., 1982, Table 5.2). This paradoxical situation could reasonably be ascribed to a later, fractional crystallisation episode involving, for example, olivine, or to contamination on passage through the crust, or it may indicate derivation from a mantle source enriched in K_2O. The possibility of olivine fractionation is discussed further in chapter 7.9.2.

Contamination is a reasonable explanation for the high K_2O content since K_2O is particularly mobile with respect to other major elements during continental contamination processes (Watson 1982). However, Harmer and Sharpe

(1985) consider that this explanation is unlikely. These authors demonstrate that micropyroxenitic rocks, similar to the QTM (from the eastern lobe of the Bushveld Complex), show no correlation between K_2O and $^{87}Sr/^{86}Sr$ initial ratios (R_O), as would be expected from crustal contamination. A similar relationship is shown by the QTM (see Fig. 7.49). Conversely Harmer and Sharpe (ibid.) argue that the variation in R_O must be original and that it is due to the mixing of magmas of similar bulk compositions but differing isotopic compositions. They also envisage that these micropyroxenitic rocks are the result of extensive mantle melting and conclude that since the high K_2O content is not due to contamination, then it must reflect an anomalously high K_2O content of the source. More recently however, this explanation has been disputed by Barnes (1989) who still favours the contamination process on other grounds. This argument, together with evidence for metasomatic enrichment of the QTM source region is discussed further in chapters 7.9.2 and 7.9.3.

7.9.2   Non-Primary characteristics of the QTM and the high SiO_2 problem.

As pointed out by Cawthorn and Davies (1983), any primary magma in equilibrium with peridotite mantle must have olivine as liquidus mineral. These authors' experimental melting data, on QTM-type compositions, indicate however that olivine ceases to be a liquidus mineral at pressures greater than 6 Kb, that is, such melts could not be in equilibrium with olivine at realistic mantle pressures. Cawthorn and Davies considered three possible explanations for these experimental results:-

1.   That volatiles (CO_2 and H_2O) were important in controlling melting relations.
2.   That assimilation of crustal material had occurred.
3.   That the magmas are not true primary liquids because olivine fractionation has occurred.

With regard to the first explanation Cawthorn and Davies (ibid.) point out that CO_2 would restrict the pressure range for olivine crystallisation even more than anhydrous conditions. On the other hand, hydrous melting would extend the incongruous melting interval of enstatite to considerable depths (Kushiro, 1969) and olivine would therefore be a liquidus mineral to greater pressures owing to contraction of the orthopyroxene stability field. Cawthorn and Davies, however, discount the possibility of hydrous melting on the basis that this

should theoretically cause the QTM composition both to crystallise hornblende before plagioclase and also to expand the olivine stability field, at lower pressures. Both of these considerations are incompatible with the observed mineralogy of the Rustenburg Layered Suite.

The second explanation, concerning assimilation was considered unlikely by Cawthorn and Davies (ibid.) because it requires the complete mixing of magmas on the scale of 150 000 km^3. Later work by Harmer and Sharpe (1985), confirmed by the present study, suggests that assimilation of crustal material is unlikely in view of the lack of correlation between $^{87}Sr/^{86}Sr$ ratios and e.g K_2O (see further discussion in Chapter 7.9.3.).

The third explanation was favoured by Cawthorn and Davies (ibid.) on the grounds that if olivine fractionation from a primary liquid has occurred, then its absence on the liquidus at mantle pressures is no longer a problem. They suggest that the QTM-type liquid had undergone up to 15 per cent fractionation of olivine since its separation from the mantle. This estimate was based on the maximum amount of olivine that could be added to the liquid, in order for the melt to be in equilibrium with mantle olivine compositions of Fo_{93}.

However, the high Ni content of the QTM (± 300ppm) is apparently inconsistent with this explanation, as the concentration of this refractory element would decrease rapidly during fractionation (Sato, 1977; Mysen, 1978; Maaloe and Johnston, 1986). For example Sato (ibid.) estimated that 6-12 per cent olivine fractionation would reduce the Ni content of a primary liquid by 50 per cent. As noted above, the QTM contain Ni contents closer to the higher limit of postulated primary liquids and thus the explanation offered by Cawthorn and Davies (ibid.) deserves further comment.

Cawthorn and Davies' estimate of 15 per cent fractionation from QTM compositions is based on the assumption that typical mantle olivines are as magnesian as Fo_{93}. However since the forsterite content of mantle olivines lie in the range Fo_{89-94} (Ringwood, 1975, Ch 3) there is clearly some latitude in the figure of 15 per cent fractionation calculated in this fashion. A much better indicator of the extent of olivine fractionation in basaltic magmas is their NiO content, as was shown by Sato (ibid.) for the following reasons:-

1. NiO content in mantle olivines is much more uniform (0.4 wt. per cent) than MgO content (thus placing more precise limits on the content in derived equilibrium liquids).

2. Ni has a greater preference for olivine than does Mg in basaltic systems ($K_{DNi-Mg}^{ol-liq} \pm 2.3$)

3. The Mg number of magma and olivine is more dependant on oxygen fugacity than is the Ni content.

Consequently although the high Ni content of the QTM apparently contradicts the conclusions of Cawthorn and Davies (ibid), it nevertheless allows a more rigorous quantitative testing of any olivine fractionation model.

Firstly we may assess whether the olivine fractionation hypothesis is compatible at all with the observed data for the QTM. This can be done by using appropriate olivine-liquid partition coefficients for Ni, in order to test whether the QTM composition would be in equilibrium with mantle olivine, a prerequisite for a primary unfractionated liquid. However this approach is complicated by the wide variation reported for D_{Ni}^{ol-liq} e.g. 13.5 - 16.8 (Häkli and Wright, 1967); 5 - 15 (Langmuir et al., 1977): 14.5 - 15.5 (Mysen, 1978); 10 (Cox et al., 1979, p. 344). While this variation does not appear significantly related to variations in pressure and temperature, Mysen (ibid) found that D_{Ni}^{ol-liq} decreased with increasing Ni content. Confirmation of this relationship, since Ni substitutes for Mg in olivine (Irvine, 1974; Sato, ibid.), was provided by Hart and Davis (1978) who found that D_{Ni}^{ol-liq} was strongly dependent on melt composition, varying linearly with 1/MgO at constant temperature. The latter authors derived an expression for D_{Ni}^{ol-liq} based on experiments in the Fo-Ab-An system such that:

$$D = (124/MgO) - 0.9$$

Since the coefficient is strongly composition dependent, the wide range in reported values is readily explained.

If we now apply the above relationship to the mean value for the QTM (MgO = 13.3 wt. per cent), we obtain a value for D of 8.42. Given that the QTM on average also contain 302 ppm Ni, then approximately 2540 ppm would be expected in the equilibrium olivine. This is in fact somewhat lower than typical mantle olivines which have very uniform Ni contents i.e. ±3150 ppm (Sato, ibid.).

The suggestion by Cawthorn and Davies (ibid.) that the QTM have evolved from a primary liquid via fractionation of olivine, therefore appears to be correct.

On the other hand, the actual <u>amount</u> of olivine removed, remains open to question and in order to resolve this, it is necessary to place an upper limit on the probable Ni content of the primary magma. To do this, however, it is also necessary to make certain assumptions concerning both D_{Ni}^{ol-liq} and the Ni content of the mantle.

Thus if we assume the primary magma of the QTM to contain ±15 wt. per cent MgO (since it must contain more than the QTM) then application of the Hart and Davies relationship indicates that a D_{Ni}^{ol-liq} of 7.37 is appropriate for use in calculating a bulk distribution coefficient. Furthermore, if we assume a $D_{Ni}^{opx-liq}$ as low as 4 (Cox et al., ibid, Table 14.1.) and a residual mantle comprising 80 per cent olivine and 20 per cent orthopyroxene (Ringwood, 1975, Ch. 3), then we obtain a bulk D of 6.70. Using other reasonable estimates of residual mantle composition and partition coefficients would give similar or <u>higher</u> values for bulk D_{Ni}.

Although estimates of nickel content in the upper mantle vary (Mysen, 1978), 2000 ppm is considered appropriate for pristine mantle, while up to 3500 ppm may be appropriate for residual compositions (Mysen, ibid.). Using the latter figure for residual mantle and a bulk D of 6.70 as calculated above gives an upper limit of concentration in the derived primary liquid of 522 ppm. Note, however, that this is considerably higher than that of unfractionated oceanic tholeiites i.e. 250 - 300 ppm, which are considered to represent primary magmas (Frey et al., 1974).

As a further check on the above estimate we can also use the exchange partition coefficient, $K_{D\ Ni-Mg}^{ol-liq}$, as derived by Sato (ibid.) and which has a value of ±2.3. On the basis that mantle olivines typically contain some 50 per cent MgO and ±3200 ppm Ni (Table 7.8), then for a primary liquid containing 15 wt. per cent MgO some 417 ppm would be required in the liquid to maintain equilibrium. Higher values could be obtained by postulating a higher MgO content in the liquid and or slightly lower values for $K_{D\ Ni-Mg}^{ol-liq}$ but even the lowest value for the latter, i.e. ±2.0 (Sato, ibid.), would only require a concentration of ±480 ppm Ni in the liquid. Alternatively an MgO content of 18

wt. per cent would require some 500 ppm Ni in the equilibrium liquid. Given the general range of estimates discussed above, the latter figure i.e. 500 ppm, is considered a reasonable value for the upper limit of concentration of Ni in primary magma. While accepting that this estimate is probably much too high, in view of the evidence from oceanic tholeiites, it nevertheless allows more stringent testing of the olivine fractionation hypothesis (Cawthorn and Davies, 1983) for the reasons discussed above.

In a similar fashion to the above authors, calculations were performed by adding olivine of the appropriate composition to the QTM liquid, in order to raise its Ni content from 300 to 500 ppm. Calculations for other elements of interest, namely SiO_2, MgO and K_2O, were also performed and are presented along with the Ni data in Table 7.8. Olivine with $Mg^{2+}/(Mg^{2+}+Fe^{2+})$ of 0.92 was used as 'extract' mineral (Deer et al., 1962, p.10 analysis 5). This analysis was chosen in order to maximise MgO removal effects, although the data of Sato (ibid.) indicates a median Mg^* of 0.90 is more appropriate. Similarly a Ni content of 3200 ppm was substituted in the original analysis, which is also in line with Sato's data on 'mantle' olivines.

The results presented in Table 7.8 indicate that the QTM is probably not a primary magma but is the result of fractionation of some 6 – 8 per cent olivine from such a liquid. The parent primary magma to the QTM had a major element chemistry of ±54.5 wt. per cent SiO_2, ±15.9 wt. per cent MgO and ±0.84 wt. per cent K_2O, assuming that it initially contained 500 ppm Ni.

Several other conclusions may be drawn from the results in Table 7.8. Firstly, the degree of olivine fractionation, in the genesis of the QTM from a primary liquid, is unlikely to have been as high as 15 per cent, as was proposed by Cawthorn and Davies (1983). Even assuming a much lower Ni content in the extract olivine (e.g. ±2500 ppm), less than 10 per cent could be removed without raising the Ni content of the QTM above 500 ppm.

Secondly, even if the limiting factor of 500 ppm for primary magmas is incorrect and they may contain higher proportions of Ni, it is still quite evident that the primary magma to the QTM was considerably more SiO_2-rich than might be expected for a mantle – derived liquid under anhydrous conditions. For

TABLE 7.8

Estimates of primary magma composition for the QTM, prior to olivine
fractionation

	OLIVINE	QTM MEAN	PRIMARY COMPOSITION AT INDICATED DEGREE OF FRACTIONATION						
			5%	6%	7%	8%	9%	10%	15%
Wt% SiO_2	40.96	55.56	54.77	54.63	54.48	54.34	54.19	54.05	53.32
Wt% MgO	50.45	13.31	15.17	15.54	15.91	16.28	16.65	17.02	18.88
Wt% K_2O	0.0	0.91	0.86	0.85	0.84	0.83	0.82	0.81	0.77
ppm Ni	3200	302	447	476	505	533	562	591	737

example, even assuming 15 per cent fractionation of olivine has occurred then
the primary liquid would still have contained approximately ±53.00 wt. per cent
SiO_2.

Thirdly, not only do the above conclusions weaken the argument that
olivine is absent in experimental melts at mantle pressures, because of
fractionation (Cawthorn and Davies, ibid.) but without extensive fractionation
it also becomes increasingly difficult to explain the high SiO_2 content of the
primary liquid without invoking some degree of hydrous melting. However, as
noted earlier in this chapter, Cawthorn and Davies (ibid.) argue against this
possibility on the basis of experimental data which suggest that the stability
field of olivine is expanded at lower pressure under hydrous conditions. The
same experimental data also indicate that hornblende should crystallise before
plagioclase for hydrous QTM-type compositions at crustal levels. Both of these
features "contradict the observed mineral proportions in the Bushveld Complex"
(Cawthorn and Davies, ibid., p. 133).

Nevertheless, in view of the discussion presented in chapter 7.8.3. it is
clear that these arguments are not necessarily valid. Firstly because, as noted
in chapter. 7.8.3, there is a considerable variation in the cumulate succession
between individual lobes of the Bushveld Complex and secondly because the
expected crystallisation of hornblende assumes that the initial magma was

allowed to undergo uninterrupted fractionation in situ. As discussed in chapter 7.8.3 there is strong evidence for the addition of fresh liquids, even during the early evolution of the Rustenburg Layered Suite (Hulbert and Von Gruenewaldt, ibid.) and consequently there is no reason why the resultant hybrid liquid(s) should crystallise in the same fashion as that of the QTM alone.

Thus the lack of correlation between the observed cumulate sequence and the postulated behaviour of hydrous QTM-type compositions cannot be used as evidence against a hydrous melting origin for the primary magma.

If some degree of hydrous melting is not invoked for the genesis of the QTM parent, then the high SiO_2 content of such a magma is enigmatic. Such a process, albeit at relatively low pressures readily explains the unusual high-MgO, high-SiO_2 compositions of boninites, rocks whose chemistry the QTM closely resemble (Cameron et al., 1979; Hickey and Frey, 1982; Walker and Cameron, 1983; Hatton and Sharpe, 1988; Barnes, 1989). This similarity and its implications are discussed in more detail in chapter 7.9.3.

7.9.3 The genesis of the QTM

7.9.3.1. Melting Models and Processes.

The general approach in modelling the genesis of magmas is to assume a certain process and starting composition. This composition is then used in one of a series of theoretical melting equations to deduce hypothetical liquid derivatives (e.g. Gast, 1968; Shaw, 1970; O'Nions and Clarke, 1972; Hertogen and Gijbels, 1976; Langmuir, 1977). Comparison of these derived liquids with actual rock types in turn, allows conclusions to be drawn concerning the ultimate origin of the rocks in question. While there is considerable uncertainty about the way in which melting actually occurs (e.g. Maaloe and Johnston, 1986), two distinct models are usually considered as representative, namely fractional and equilibrium (or batch) melting (Cox et al., 1979, p. 338; Hughes, 1982, p. 451).

Fractional melting supposes that infinitesimally small amounts of melt form in equilibrium with the residue and simultaneously escape from the system. In equilibruim melting the melt remains in contact (equilibrium) with the

residual material until physical conditions allow it to escape as a single batch. Wood and Fraser (1976) conclude that the removal of infinitesimally small amounts of melt is unlikely in nature and that in geologically reasonable cases it is likely that an appreciable batch of magma must accumulate before its separation from residual phases. Maaloe and Johnston (1986) similarly consider fractional melting to be an unrealistic model, because it implies that there is no melt in the source, while Hart and Allegré (1980) also conclude that on kinetic grounds an equilibrium approximation is more reasonable. Furthermore Richter (1986) using a complex dynamic formulation and a set of synthetic data concludes that actual results of melting are better described by an equilibrium model, irrespective of the process involved. Other diverse papers also indicate that equilibrium melting is generally considered more valid as a model for melting processes than is fractional melting (e.g. Warner et al., 1985; Weber et al., 1985). It is concluded therefore, that the process of partial melting in the mantle is better described by an equilibrium, rather than a fractional melting model.

7.9.3.2 Melting equations for describing equilibrium melting and experimental determinations

Consolmagno and Drake (1976) have shown that several of the more complex equations used to describe equilibrium melting do in fact reduce to a simple form:-

$$C_1/C_o = \frac{1}{F+D(1-F)}$$

Where C_1 = Conc. of element in liquid.
C_o = Conc. of element in original starting composition.
F = Mass fraction of melt.
D = Bulk distribution coefficient for the residue (at the time of melt separation).

Other equations e.g. Wood and Fraser (1976) are formulated in terms of relative melting rates and take into account the fractions of liquid contributed by each phase, i.e.

$$C_1/C_o = \frac{1}{D_o+F(1-P)}$$

Where, D_0 = Bulk distribution coefficient for starting composition,

and $P = (P^\alpha K^{\alpha/liq} + P^\beta K^{\beta/liq} + etc.)$,

in which P^α, P^β , etc. are the mass fractions of liquid contributed by each phase.

The major drawback with either of these equations and indeed with other, more complex formulations (e.g. Maaloe 1982; O'Hara 1985), is that much of the data necessary for their use is at best imperfectly known. Firstly, there is a considerable array of varied partition coefficients, not only for individual minerals but also with respect to each element. (e.g. Allegré et al., 1977; Hanson, 1977; Langmuir et al., 1977; Irving, 1978; Irving and Frey, 1978). Secondly because physical conditions and phase compositions change during a melting event (Mysen and Kushiro, 1977), it is unlikely that such partition coefficients remain constant during melting. Furthermore given the complexity of actually determined melting reactions (Mysen, 1977), the true phase proportions entering the liquid and hence those left in the residue remain unknown for the vast majority of such reactions.

The usual approach however, in the use of these equations appears to be an 'educated guess' (C.J. Hatton, pers. comm.) as to the actual proportions involved, either entering the melt or left behind in the residue (O'Nions and Clarke, 1972; Hanson, 1977; Pearce and Flower, 1977; Warner et al., 1985). Given the latitude already involved in the choice of distribution coefficients, the possibilities for error are clearly compounded, even assuming that estimates of the starting (mantle) composition are approximately correct. Given this state of affairs, a more empirical approach was adopted in the present investigation and although this approach, as will be apparent from the ensuing text, is also speculative, it nevertheless provides a different perspective on the possible genesis of the QTM.

This study utilised the experimentally determined data of Harrison (1981). This work, conducted at mantle pressures (35 Kb), involved equilibrium melting of a 'spiked' sample of garnet lherzolite i.e. PHN1611 (Nixon and Boyd, 1973), in which the concentration of the rare earth elements (REE) could be measured in the resultant liquid by means of a radioactive REE spike. REE concentrations in the liquid at various degrees (mass fractions) of melting were thus directly

measured and allowed an 'enrichment factor' (E.F.) to be calculated for differing degrees of melting, such that:-

$$E.\ F.= \frac{\text{Radioactive REE in liquid}}{\text{Radioactive REE in starting mix}}$$

These experimental results are clearly independent of the actual mechanisms involved and they eliminate the need for any 'guesswork' involving possible distribution coefficients, phase proportions, etc., which is inherent in the use of the equations discussed above. Note also that comparison of these enrichment factors with the data of Mysen and Holloway (1977) obtained at 20 Kb, indicates that there is little pressure dependence of these values (Harrison, ibid., Fig. 7).

Although PHN1611 approaches the theoretical pyrolite (Green and Ringwood, 1967) in composition and thus may be considered 'fertile' mantle in the sense that it has the capacity to generate a wide variety of basaltic melts (Hughes, 1982; Dawson, 1984) it could be argued that its use may not be appropriate to the present study, particularly in view of the more recent debate on the possible origins of the Bushveld Complex, (chapter 7.9.3.4.). However Harrison (ibid.) suggests that the E.F. may be used to determine REE contents in derived liquids for variously enriched source regions because the E.F. is only dependent on the degree of melting. Furthermore given that there are indications that the QTM were generated by high degrees of mantle melting (chapters 7.9.1. and 7.9.3.3.), then irrespective of precise starting composition, any reasonable residuum could be expected to approximate an overall 'harzburgitic' composition as melting increased. Since clinopyroxene is completely melted at 40 per cent melting (Harrison, ibid.) the use of Harrison's enrichment factors were therefore thought to be relevant to the present study, given that this level of melting may have been approached during generation of the QTM (chapter 7.9.3.3.). Results from the application of the E.F.s to the QTM are therefore presented and discussed in the ensuing chapter.

7.9.3.3 REE content of the QTM and a comparison with probable mantle melts.

REE contents of five QTM samples were analysed by ICP-AES at the the Dept. of Geology, University of Stellenbosch, and results normalised to the C1 values

of Evensen (1978) (Table 7.9.). The five samples chosen span a broad cross-section of the textures shown by the QTM (chapter 6), although all were considered as approximating 'liquid' compositions. In this regard, porphyritic textures were not considered incompatible per se, as many of the phenocrysts are skeletal and may well have originated essentially in situ.

All five samples however, show similar, rather steep, chondrite normalised patterns on conventional diagrams, with Ce_n/Yb_n ratios of ±7.5 and ±48X chondritic abundances at Ce (Fig. 7.46). These patterns, although slightly less fractionated, are similar to those obtained by Harmer and Sharpe (1985) for micropyroxenites from the eastern lobe of the Complex and it is concluded that they and the QTM are consanguineous.

Furthermore, as pointed out by Harmer and Sharpe (1985) the LREE enriched nature of these patterns reinforces the view that the micropyroxenites (QTM) are parental liquids to the lower zone because lower zone bronzitites have flat REE patterns, with 1 to 3 times chondritic abundances. Since orthopyroxene has a strong preference for the HREE and the lower zone patterns are not depleted in LREE then it seems likely that they were derived from liquids with strongly fractionated patterns like the QTM. However before proceeding to interpret the REE patterns in terms of primary melt composition it is important to assess the effect that any olivine fractionation may have had on the primary REE content.

The probable degree of olivine fractionation, involved in the genesis of the QTM from a primary liquid, was concluded to be approximately 7 per cent (chapter 7.8.2). In the following calculations up to 10 per cent olivine fractionation was assumed, both in order to exaggerate any effects due to such a process and also to accommodate any errors in the fractionation calculation. Two possible effects are considered, firstly the effect on LREE/HREE (Ce/Tm) ratios and secondly the effect on the total REE content. Unfortunately because the REE content of the olivine extract is unknown it is not possible to simply add additional components, as was done in the determination of the degree of olivine fractionation using Ni content. However, the behaviour of REE during fractional crystallisation may be assessed using the Rayleigh fractionation law for trace elements where:-

TABLE 7.9.

Chondrite normalised REE contents of selected QTM samples (REEn).

SAMPLE NO.

	DI-7B	DI-36	DI-53	DI-59C	DI-74
La_n	57.8	63.5	59.8	56.0	54.9
Ce_n*	47.6	52.1	52.1	46.0	42.9
Pr_n	37.4	40.8	44.4	35.9	30.9
Nd_n	29.0	30.9	27.2	26.0	25.2
Sm_n	14.0	15.5	14.8	13.6	13.3
Eu_n	9.5	10.7	9.9	9.4	10.1
Gd_n	9.2	10.3	9.4	9.4	10.1
Dy_n	7.0	8.1	7.5	7.1	7.5
Ho_n	7.5	8.6	7.7	7.2	7.7
Er_n	7.4	8.5	7.3	7.5	8.6
Tm_n*	6.8	7.8	6.9	6.8	7.5
Yb_n	6.2	7.1	6.5	6.1	6.4

Ce_n* and Tm_n* are interpolated values.
(Normalising values taken from Evensen et al., 1978)
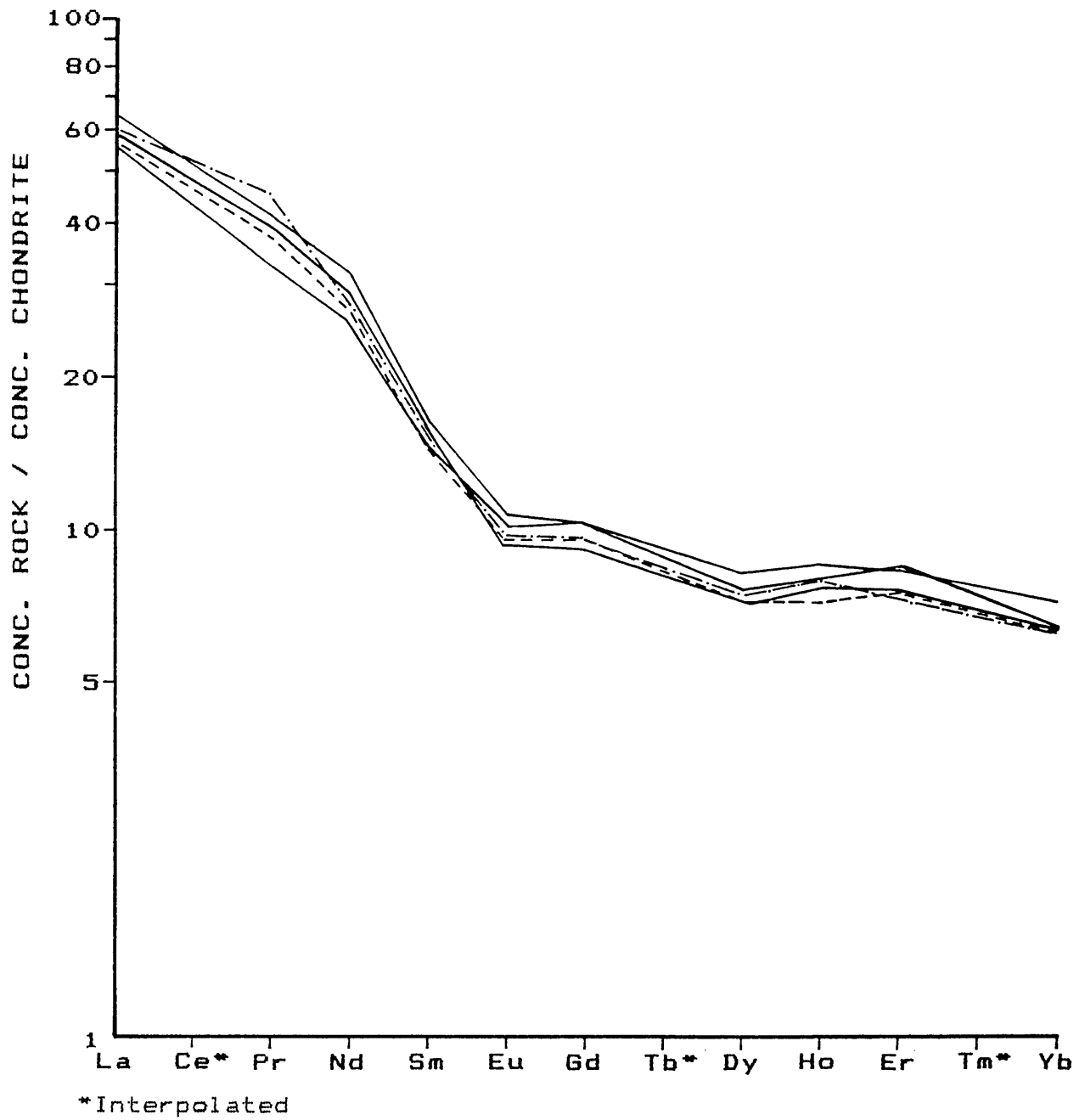
Fig. 7.46. Chondrite-normalised plot of REE data for five samples of the QTM.

$$C_1/C_0 = (F)^{D-1}$$

and C_1 = Final conc. in liquid.

C_0 = Initial conc. in liquid.

F = Fraction of liquid remaining.

D = Bulk partition coefficient for precipitating phases

Wood and Fraser (1976).

Since olivine is the only precipitating phase then D is equal to D_{REEn}^{ol-liq} for the appropriate element. In addition, although D values are fairly low for REE in olivine (Irving, 1978; Wood, 1979), the highest values recorded were used, (Harrison, 1981) so as to maximise any fractionation effect on the REE pattern and total content. Results of the calculations are presented in Table 7.10.

TABLE 7.10.

Calculation of the effects of olivine fractionation on the primary
REE content of the QTM

REE	D_{REEn}^{ol-liq}	CHANGE IN C_1/C_0 AT GIVEN PERCENT OLIVINE FRACTIONATION	
		7%	10%
Ce	0.049	1.07	1.11
Sm	0.070	1.07	1.10
Tm	0.046	1.07	1.11

Two conclusions are immediately obvious from these results:-

1. That the pattern of REE distribution is unaffected by up to 10 per cent olivine fractionation.

2. That the total content of REE could only have been marginally increased in the liquid by small amounts of olivine fractionation. For example, since the average content of the five QTM samples is 48 times chondritic

abundances for Ce, then the parental primary liquid would have contained 44.9 times and 43.2 times chondritic abundances, prior to 7 per cent and 10 per cent fractionation respectively. Similar calculations for Sm and (interpolated) Tm, indicate that such an effect is insufficient to shift the primary liquid pattern out of the QTM envelope (Fig. 7.47). The REE content and resulting patterns of the QTM must therefore be very similar to that of the primary liquid. On this premise, the QTM results were directly compared with the melting data of Harrison (1981) in order to assess the possible genesis of the QTM.

Using the enrichment factors (E.F.) measured by Harrison for Ce, Sm and Tm in partial melts for PHN1611 at differing degrees of melting, the REE patterns shown in Figure 7.48 were constructed and compared with the QTM data.

It is clear from Figure 7.48 that the REE concentrations produced by various degrees of partial melting of PHN1611 at 35Kb are not very similar to that of the parent liquid to the QTM. Thus we may reasonably conclude that the QTM were not derived from a source with REE contents similar to PHN1611, i.e. 'fertile' mantle.

Nevertheless there are indications that the QTM have been generated by extensive mantle melting, as evidenced for example by the high MgO contents of these rocks (the significance of the extremely low TiO_2 content is discussed further in chapter 7.9.3.4.).

Furthermore, the melting data of Jaques and Green (1980) indicate that the QTM resemble liquids produced at 30 - 40 per cent melting of a pyrolitic source, while Cameron and Nisbet (1982) also indicate that up to 35 per cent melting would be compatible with the MgO content of similar liquids. Although the data of Jaques and Green (ibid.) were obtained under anhydrous conditions, they conclude that comparison of their data with other data obtained for hydrous systems indicates that for similar degrees of melting (of pyrolite), the hydrous melts are distinctly more siliceous and lower in CaO, MgO and FeO.

Consequently with respect to MgO, the above estimates of the degree of melting can be considered as minimum values. This is because the high SiO_2 content of
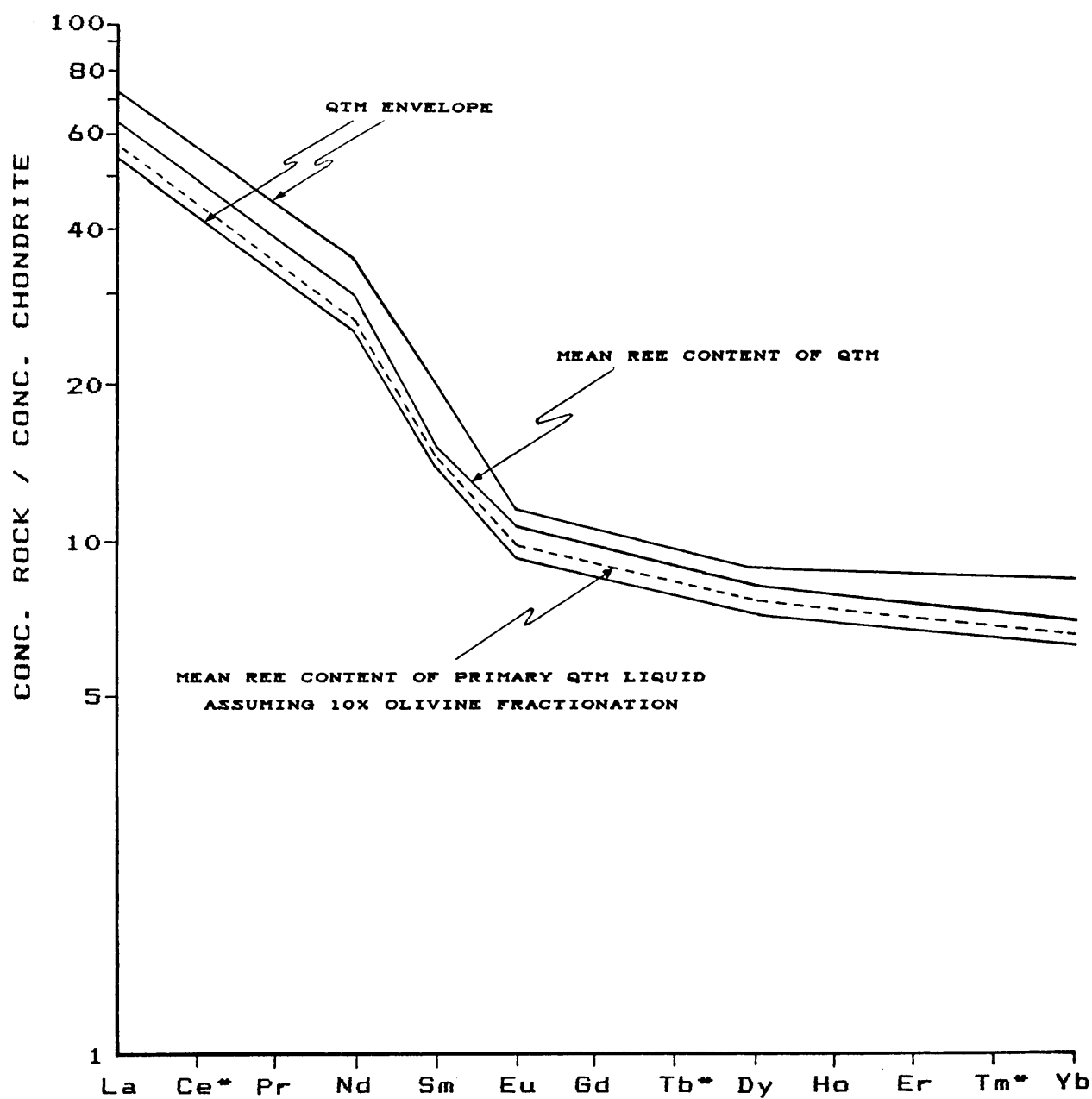
Fig. 7.47. The effect of 10% olivine fractionation on the REE content of the QTM primary liquid.
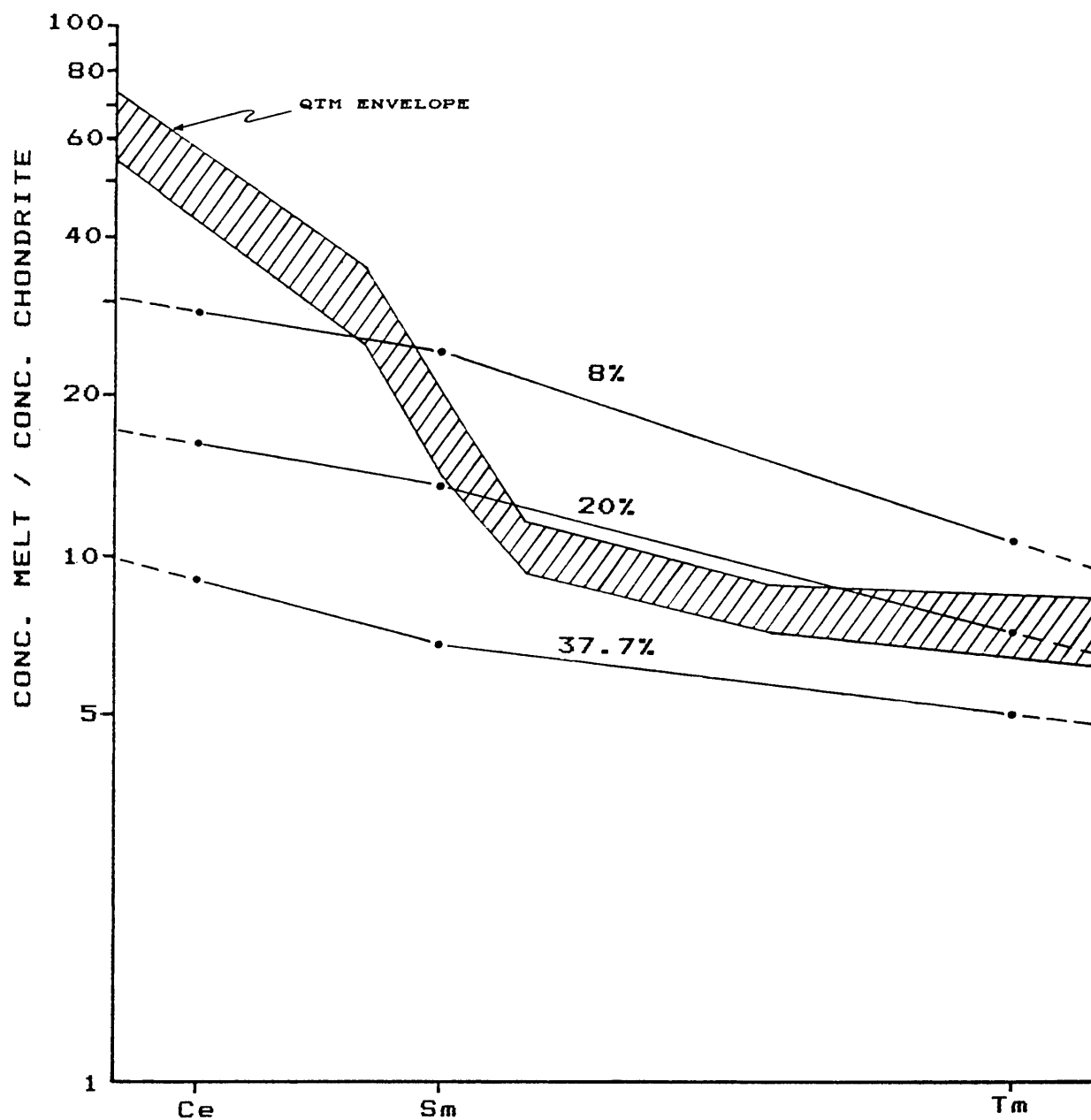
Fig. 7.48. Comparison of the REE contents of the QTM with those of liquids obtained by varying degrees of partial melting of nodule PHN1611.

the QTM implies some degree of hydrous melting in its genesis (chapter 7.9.2.) and consequently a higher degree of melting would be required to reproduce the equivalent MgO content in a hydrous melt. Furthermore, although Harrison's (ibid.) data was also obtained under anhydrous conditions, she notes (p. 255) that at high percentages of melting "volatiles are diluted in the melts and their effects on partitioning may be much reduced".

In view of the arguments presented above, (i.e. that Harrison (ibid.) considers that the enrichment factors are appropriate for various source compositions because they are only dependent on the extent of melting, and because at high degrees of melting the residuum would approximate a harzburgitic composition, irrespective of any reasonable starting composition) we can invert the problem and by using the REE content of the QTM we can attempt to constrain the REE content of the source. As a first approximation use of the E.F.'s for 37.7 per cent melting and the REE content of the QTM (Prior to 7 per cent fractionation of olivine) indicates that the source region must have contained ±18.2, ±6.3 and ±2.8 times chondrite normalised contents of Ce, Sm and Tm respectively.

This conclusion is based only on the assumptions that nodule PHN1611 is reasonably representative of the mantle source region, with the obvious exception of its REE content, and that the QTM were generated by extensive (± 37 per cent) equilibrium partial melting. Such a conclusion does not depend on further assumptions regarding phase proportions in the residue or those entering the melt, or indeed on assumptions regarding partition coefficients during melting, as is necessary for analysis using the melting equations previously discussed.

Furthermore, while this sort of enrichment might appear unlikely, it is worth noting that if Harrison's enrichment factors are generally applicable, then the range of LREE's found in alkali basalts (i.e. 40 - 200 times chondrites (Schilling and Winchester, 1969; Kay and Gast, 1973; Shimizu and Arculus, 1975; Frey et al.,(1978)) would require enrichment of the source region of up to 50 per cent of that calculated above for the QTM source . Furthermore the high K_2O content of the QTM may well indicate excessive enrichment of the source region, particularly when the probable degree of melting is taken into account. For example, even the high K_2O content of PHN1611, which is itself enriched some 2.3 times relative to chondrites

(Wedepohl, 1971; Ringwood, 1975) is insufficient to have generated liquids with K_2O contents as high as those of the QTM. To illustrate this however, it is necessary to rely on melting equations and their inherent assumptions. Nevertheless we may use, as a first approximation, the equilibrium melting equation of Shaw (1970), i.e.

$$C_1/C_o = \frac{1}{F + D (1 - F)}$$

which reduces to

$$C_1/C_o = 1/F$$

as the bulk distribution coefficient (D) approaches zero (Arth, 1976). From this relationship it follows that for elements with a low D, the degree of melting effectively controls the final content of the element in the liquid.

For K_2O as noted previously (chapter 7.9.1), D's are very low for both olivine and pyroxene, the major residual minerals at high degrees of mantle melting (Harrison, ibid.). Consequently, given an initial content of 0.14 wt. per cent in PHN 1611 and assuming ± 37 per cent melting, in keeping with the above REE calculations, the derived liquid should contain ± 0.37 wt. per cent K_2O. However if the QTM originally contained ±0.84 wt. per cent K_2O^1 then the source must have been even more enriched relative to PHN 1611. Using the above relationship it is apparent that at 37 per cent melting the initial content of the source region must have been ± 0.32 wt. per cent K_2O, i.e. ±5 times chondrites, in order to have given rise to the concentration in the QTM.

Although there is some latitude in these figures as the precise amount of melting is not known, it would be reasonable to assume that Ce, being similarly incompatible, should have been enriched in a similar manner. In this case there is clearly a lack of correlation between the estimated ±5 times chondrite enrichment in K_2O and the ±18 times chondrite enrichment in Ce as estimated above. Consequently even though there is independent evidence for enrichment of the source region, there appears to be little correlation between chondritic abundances and the concentration of individual elements in the source region.

---

[1]This estimate allows for the effect of 7 per cent olivine fractionation from the primary liquid.

The possible origin of these features and the latest hypotheses for the origin of the QTM are discussed further in the following Chapter.

7.9.3.4. The boninitic affinities of the QTM as indicators of their genesis.

As noted earlier the geochemical composition of the QTM is similar in many respects to boninites, which are volcanic rocks associated with island arc environments (Cameron et al., 1979; Hickey and Frey 1982; Bloomer and Hawkins, 1987; Hatton and Sharpe, 1988; Barnes, 1989). The unusual chemistry of boninites suggests derivation from both a depleted (low TiO_2 and high Mg^*) and at the same time enriched (high LREE, high K_2O) mantle source. These characteristic features are generally considered to reflect generation from a mantle source depleted by MORB generation but enriched by a hydrous, LREE-enriched minor component that may be derived from either subducted crust or metasomatic fluids from undepleted portions of the mantle (Hickey and Frey, ibid.; Cameron et al. 1983; Kyser et al. 1986).

Hamlyn and Keays (1986) note that in addition to the abovementioned geochemical features, such second stage melts should also have enhanced platinum-group element (PGE) abundances relative to e.g. MORB, because of the strong partitioning of PGE's into residual sulphide during the primary melting event. Magmas generated from the melting of such a residuum, in which the sulphide component is enriched in PGE's but poor in sulphur, leads to complete dissolution of the sulphide component and consequently to second stage magmas enriched in PGE's relative to those derived from an undepleted source region. In this regard they note that the average Pd content for second stage (boninitic) melts is 15 ppb, i.e. ±18 times the value for MORBs. It is also similar to the Pd content in the Bushveld quenched micropyroxenite analysed by Sharpe (1982) i.e. 20 ppb, and Hamlyn and Keays (ibid., p 1432) therefore speculate that the source region for the micropyroxenites (QTM) has undergone a similar evolution to that of boninites.

The LREE enriched component of boninites also has a low Ti/Zr ratio relative to undepleted mantle (Hatton and Sharpe, 1988) and it is this feature that allowed these authors to propose a comprehensive model for the possible generation of the QTM-type magma. This model and their arguments are summarised below.

Hatton and Sharpe (ibid.) note that the Ti/Zr ratio is largely unaffected by extraction of MORB from the mantle, since both elements have identical bulk distribution coefficients for probable mantle compositions (Le Roex, 1987). Consequently, both primitive mantle and MORBs have ratios close to 100 (Frey et al., 1974; Sun et al., 1979; Taylor and McLennan 1985) and therefore the origin of the LREE enriched, low Ti/Zr component of boninites cannot be deep, undepleted mantle. However Hatton and Sharpe (ibid.) argue that during crustal formation and melting, with magnetite or ilmenite as a residual phase, Ti would behave as a compatible element while Zr would behave incompatibly. Hence crustal melting would result in a lowering of the Ti/Zr ratio, in contrast to mantle melting, and the source of the LREE enriched, low Ti/Zr component of boninites therefore appears to be crustal in origin.

The addition of this component during magma ascent is discounted by Hatton and Sharpe (ibid.) predominantly on the basis that the degree of contamination required to generate the high silica content of the micropyroxenites from primary magnesian (komatiitic) liquid is unlikely for physical reasons. More specifically because the formation of a viscous margin against the conduit walls during any initial contamination phase would effectively prevent assimilation of the quantity of material required.[1] To digress briefly, this argument has more recently been questioned by Barnes, (1989) who argues, on the basis of elevated $^{87}Sr/^{86}Sr$ ratios in the QTM, for an assimilation – fractional crystallisation (AFC) model involving 30 – 50 per cent contamination of a komatiitic liquid by Archean crust, accompanied by about 35 per cent olivine fractionation. However, notwithstanding the physical arguments against the AFC model it seems incompatible with the high Ni content of the QTM (see e.g. chapter 7.9.2) and as pointed out by Hatton and Sharpe (ibid.) it is also

---

[1] Note incidentally that this is not considered to invalidate the earlier conclusion that the MGN has been contaminated by wall rock assimilation (chapter 7.6.) for several reasons. These include the fact that the MGN is basaltic and therefore would 'chill' less effectively against the walls than a komatiite magma, it is also envisaged that later pulses of the MGN would pass through increasingly hotter country rocks, preheated by earlier pulses of QTM and MGN magma and finally it must be remembered that there is abundant field and petrographic evidence for contamination of the MGN to produce the QGN (Figs. 5.5. and 6.18.).

inconsistent with the reverse zoning of orthopyroxene phenocrysts in these micropyroxenites. Other arguments against such an origin are presented below and in chapter 7.9.3.5. Since crustal comtamination was ruled out Hatton and Sharpe (ibid.), although not considering the tectonic setting in detail, argued that the incorporation of crustal material must therefore have taken place in the source region. Consequently they concluded that subduction of continental crust in the form of sediment and subsequent melting/mixing with overlying (depleted) subcontinental upper mantle was a viable model for the genesis of the micropyroxenites.

With regard to the likely scale of such a process, Hatton and Sharpe point to the immense erupted volume ($\pm$ 300.000 km^3) of pre-Bushveld acid volcanics (Twist and French, 1983) which include a component (i.e. high-magnesium felsite) with major element content and trace element patterns similar to precambrian sediments (Hatton and Sharpe, ibid.). Patterns for Rb, K, La, Zr, Sm, Ti, Y,and Yb in the high magnesium felsite are also systematically higher, but subparallel to trace element patterns for the QTM and this strongly suggests that one of the components in the QTM was derived from the high-magnesium felsite (Hatton and Sharpe, ibid).

Despite its attraction however, the intra-cratonic nature of the Bushveld Complex seems at odds with a model similar to that for island- arc boninites, although Hall and Hughes (1987), in a discussion of intra-cratonic, boninitic dykes from Greenland which are of similar age to the Bushveld Complex, note that similar Proterozoic intrusives are distributed world-wide. They question therefore whether the similarity of modern boninites and Proterozoic intrusives require similar petrogenetic models. They suggest that this widespread distribution of 'boninitic' rock types may reflect a major stage in continental crust formation during a period of high heat flow and increased convection in the mantle. During this period oceanic crust and residual harzburgite depleted by Archean komatiitic-tholeiitic volcanism may have been returned deep into the mantle. Furthermore "heterogeneity may have been greatly increased .... by the foundering of blocks of the lower crust into the sub - continental mantle during the frequent collision and thrusting events" (Hall and Hughes, ibid., p179). LREE and large ion lithophile elements "derived from the partial melting of either underlying mantle or xenolithic blocks of dense, lower crustal material within the mantle could have provided a source of contamination of the harzburgitic component. The remelting of this replenished, or enriched

metasomatised harzburgite produced high-Mg, high-Si, high-LIL element noritic (boninitic) liquids" (Hall and Hughes, ibid., p179).

More specifically however, Harmer and von Gruenewaldt (1991) have recently expanded on the model of Hatton and Sharpe (ibid.) and have assessed in broader terms the tectonic-magmatic setting of the Transvaal Basin, of which the Bushveld Complex magmatism is an intimate component. They point out that an apparent subduction zone component is recognisable in pre-Bushveld and even pre-Transvaal volcanics (Crow and Condie, 1988; 1990). A feature that would require that any proposed subduction zone would have been in operation for many 100 Ma prior to 2.05 Ga., which seems unlikely. On the other hand, Harmer and von Gruenewaldt (ibid.) argue that this feature is equally unlikely to be due to crustal contamination, as the incompatible trace element signatures of laterally extensive magmatic units, such as the Hekpoort volcanics and the boninitic QTM, "would require unrealistically uniform combinations of crustal composition and structure, primary magma composition, and degree of assimilation", in order to reproduce the observed patterns (Harmer and von Gruenewaldt, ibid. p119). Furthermore, the similarities (in trace element patterns) between the geographically and temporally unrelated Dullstroom and Hekpoort Andesite Formations militates against such an origin for the 'subduction zone' component.

Harmer and von Gruenewaldt (ibid.) therefore suggest that the 'subduction zone' component of the melts generated in the sub-Kaapvaal Craton must have been a widespread feature of the lower crust or uppermost mantle, for an extended period of time. Consequently in contrast to the active subduction model of Hatton and Sharpe (ibid.) they propose that the 'subduction zone' signature was imprinted on the sub-Kaapvaal lithosphere through processes, possibly including subduction, during accretion and stabilisation of the Kaapvaal craton crust at a much earlier time, possibly as early as 3.45 Ga. Harmer and von Gruenewaldt (ibid.) envisage that during the earlier evolution of the craton, significant magmatic underplating occurred, perhaps along the lines of the model of Hildreth and Moorbath (1988) in which a zone of melting, assimilation, storage and homogenisation (MASH) develops in the lowermost crust or crust-mantle transition. This occurs in response to the ascent of basaltic magmas, generated in the mantle wedge above the subduction zone, which rise to a neutrally buoyant level at which they induce local melting, assimilate and mix extensively.

Harmer and von Gruenewaldt (ibid.) contend that subsequent reactivation of this zone, even at much later times, must generate magmas with the imprint of earlier subduction-related processes and it is unnecessary therefore to invoke an active subduction model to explain the formation of the QTM.

7.9.3.5. $^{87}Sr/^{86}Sr$ systematics of the QTM as indicators of their genesis

$^{87}Sr/^{86}Sr$ initial ratios (R_o's) were determined for the same five samples used in the REE analyses. The work was undertaken by R.E Harmer and B.M. Eglington, of the CSIR's division for Earth, Marine and Atmospheric Science and Technology and results and analytical details are given in Appendix 5.

Results for the QTM are fairly similar to those obtained by Harmer and Sharpe (1985) for the micropyroxenites of the eastern Bushveld, although the range is slightly greater for the QTM, i.e. ‹0.7024 to 0.7063. Harmer and Sharpe (ibid.) concluded that their range of values could not easily be ascribed to contamination during emplacement because there is a lack of correlation between R_o and elements expected to be incorporated during such a process. Although there is for the present data set some indication of a trend for some of these elements, (Figs. 7.49, 7.50), comparison of these results with those of Harmer and Sharpe (ibid.) indicates that such a trend is probably the result of limited data coverage. The data of Harmer and Sharpe are therefore also plotted on Figures 7.49. and 7.50. and it is concluded that the present data do not invalidate their contention that there is a lack of correlation between R_o and e.g. K_2O.

Nevertheless, like the micropyroxenites, all the QTM samples are enriched relative to the 'Bulk Earth' composition at 2.05 Ga of 0.7022 (Hatton and Sharpe, 1988; Harmer and von Gruenewaldt, 1991) and this accords with the latter authors' model (see chapter 7.9.3.4.) involving enrichment of the source region by subduction related processes. However the lack of correlation between the Sr isotope data and e.g. K_2O, is also not readily explained by this model, any more than by contamination during emplacement, unless a multicomponent source is postulated. Given the overall uniformity of bulk chemistry for the QTM (Appendices 1 and 2) — which suggests either a single enriched source and/or complete melt homogenisation, and the variability in R_o — which suggests several sources and/or incomplete homogenisation, then some sort of decoupling mechanism is required between the source of the radiogenic Sr and the source of other major and trace element components of the melt.
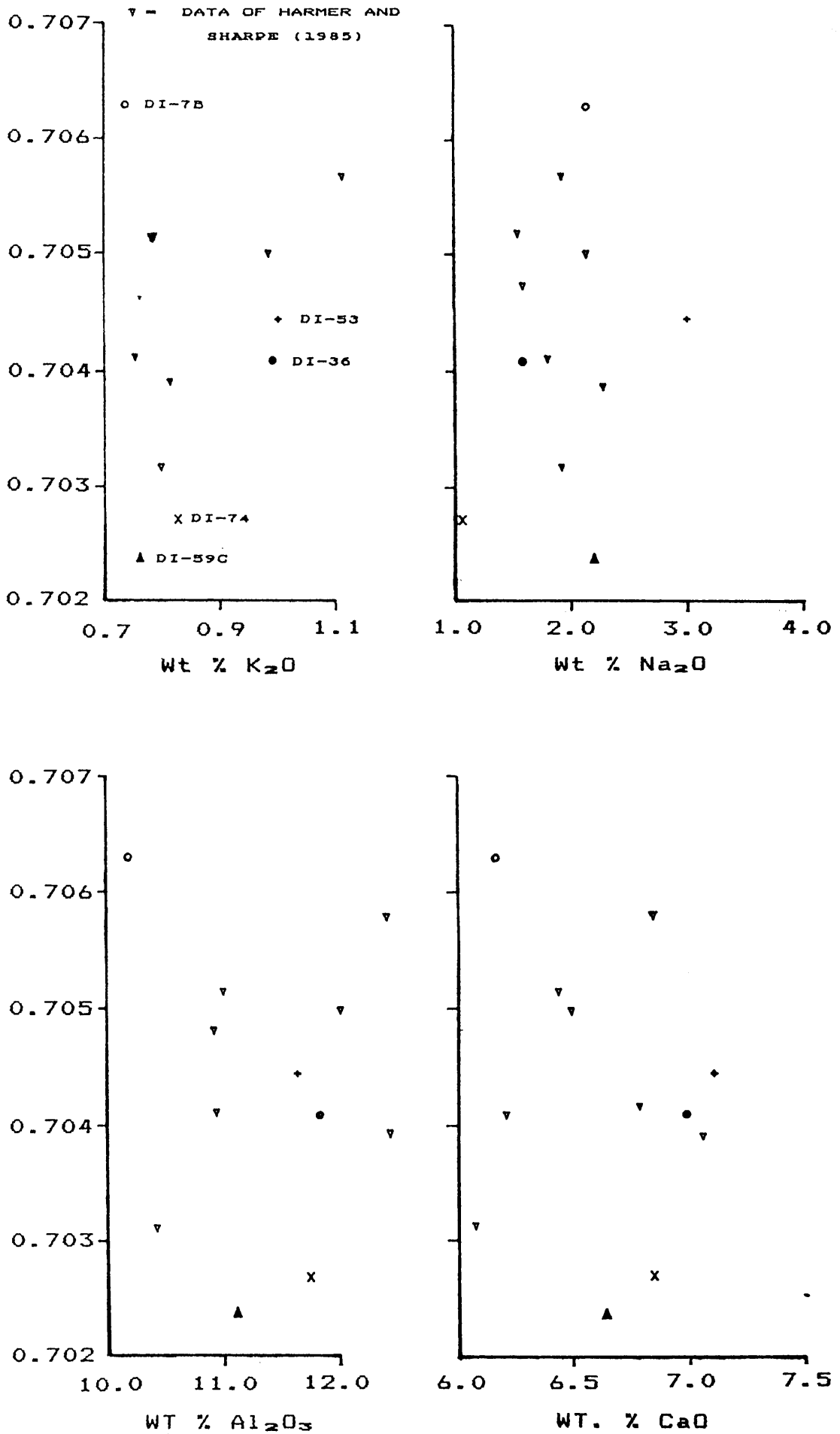
Fig. 7.49. Plot of R_o vs. major elements K_2O, Na_2O, Al_2O_3 and CaO for the QTM. Symbols correspond to sample numbers indicated in K_2O plot.
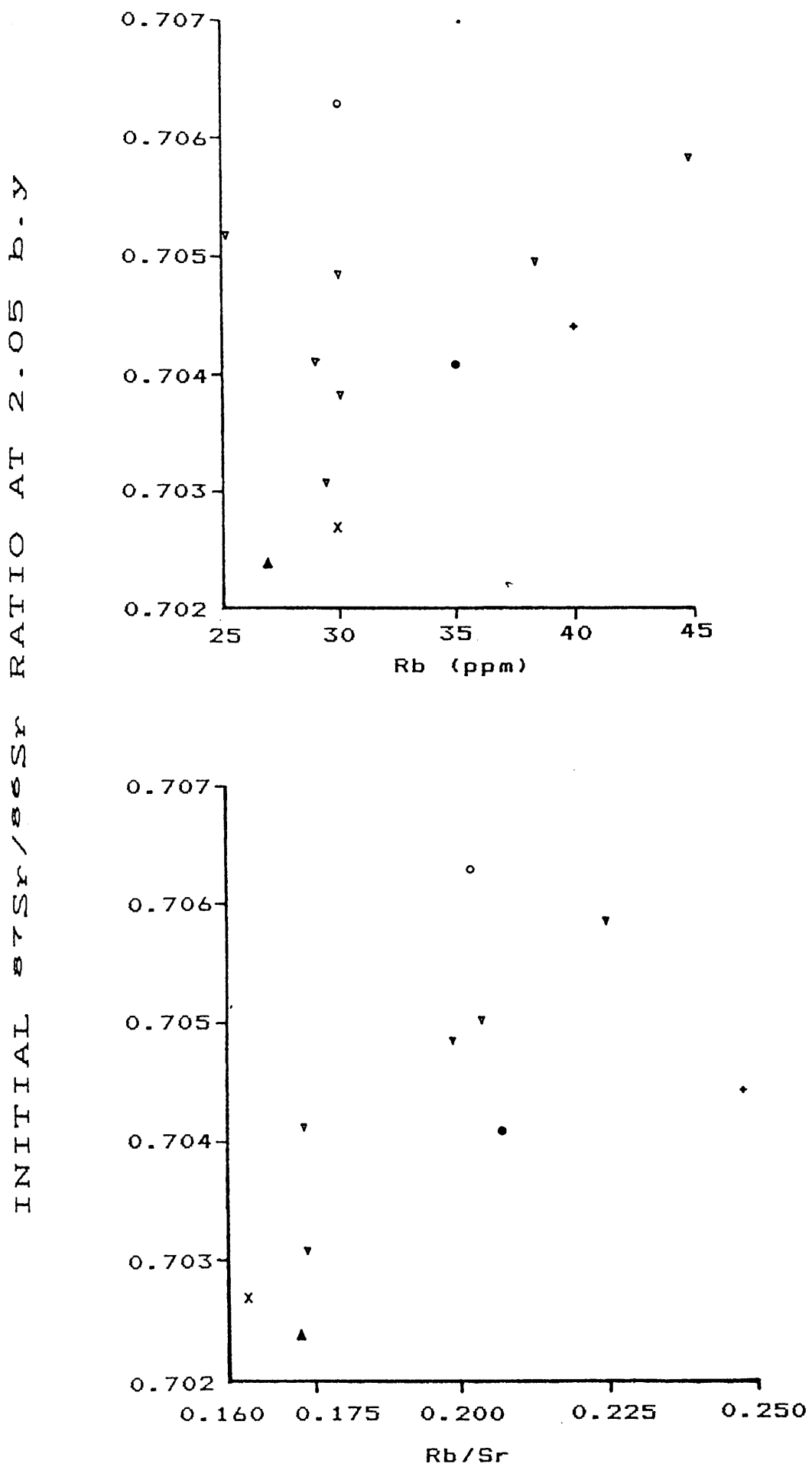
Fig. 7.50. Plot of R_o vs. Rb and Rb/Sr for the QTM. Symbols as indicated in Fig. 7.49.

The precise mechanism is clearly open to debate, however such a decoupling would seem more likely to occur during a complex multistage evolution, such as that advanced by Harmer and von Gruenewaldt (ibid.), rather than during a simple contamination event accompanying emplacement (Barnes, 1989).

One possibility is that Sr, derived from seawater altered ocean floor during subduction, could have been variably introduced into the overlying mantle wedge. Since Sr derived in this fashion from subducted sea floor basalts could be expected to be enriched in radiogenic Sr (O'Nions et al. 1977), incomplete homogenisation would give rise to R_O variation in melts derived from the overlying material.

Another possibility is that crustal material of similar bulk chemistry but of different age was involved in the complex underplating process envisaged by Harmer and von Gruenewaldt (ibid.), (see chapter 7.9.3.4.). Such a process could subsequently have given rise to melts of similar bulk chemistry but variable R_O's if incomplete isotopic homogenisation of the MASH zone occurred.

Clearly the above hypotheses require further isotope studies in order to constrain the various ambiguities posed by the Sr data. The determination of initial $^{143}Nd/^{144}Nd$ ratios, as emphasised by Harmer and von Gruenewaldt, (ibid.) would be particularly fruitful in this regard.

Nevertheless it is concluded that, whatever the precise origin of the increase in R_O for the QTM, relative to 'Bulk Earth', it is due to enrichment at source rather than contamination during emplacement. In support of this the relevant arguments are briefly reiterated below:-

1. Hatton and Sharpe (ibid.) conclude that the generation of QTM – type liquids from komatiitic magmas is unlikely on physical grounds, because of the large degree of wall rock assimilation required. They argue that any assimilation of cold, silica-rich wall rock would effectively give rise to a viscous margin preventing further assimilation and they question whether contamination of komatiite could ever proceed far enough to produce such a siliceous magma as the QTM.

2. The reverse zoning of orthopyroxene phenocrysts (i.e. rims are more magnesium-rich than cores) seems incompatible with the crystallisation of a magma undergoing contamination.

3. The high Ni content of the QTM is incompatible with an assimilation – fractionation model involving olivine.

In addition, as pointed out by Hall and Hughes (ibid. p179) "most komatiites erupted through and onto sialic crust appear to have arrived geochemically unscathed (Claoue-long and Nesbitt, 1985; Arndt et al. 1986)" which is further evidence against a contamination model.

Finally an important, and to some extent overlooked point, first made by Cawthorn and Davies (1983), is that of the conceptual difficulty in generating approximately 150 000 km^3 of QTM-type magma (with similar bulk chemistry) by contamination during emplacement. As discussed in chapter 7.9.3.4, Harmer and von Gruenewaldt (ibid.) have recently reiterated similar arguments for much of the magmatism associated with the Transvaal Basin.

8.   GEOTHERMOMETRY

8.1   INTRODUCTION

The initial aim of the geothermometry study was to attempt to determine actual temperatures of crystallisation of the marginal rocks (QTM and MGN) and of the Rustenburg Layered Suite, using the thermometers of Wood and Banno (1973) and Wells (1977). It was considered that the use of such methods would place further constraints on the marginal rocks vis a vis their relationships to the Layered Suite. The two above mentioned methods were initially considered appropriate since they are based on pyroxene equilibria and both the marginal rocks and portions of the Rustenburg Layered Suite are therefore amenable to analysis. Although the magnetite-ilmenite thermometer of Buddington and Lindsley (1964) could also be applied to the marginal rocks, both Davies (pers. comm. and 1982) and Hulbert (pers. comm.) found that realistic magmatic temperatures are not obtained using this method. Consequently this thermometer was not considered. Unfortunately, with regard to the QTM and MGN, more recent work by Sharpe and Hulbert (1985) also found that the Wood-Banno method is inapplicable to these rocks, possibly due to resetting in the thermal aureole. Thus, although calculated temperatures are broadly consistent with expected liquidi, Sharpe and Hulbert (ibid) found that there was no consistent correlation of the Wood-Banno temperatures with temperatures calculated from the computer program of Nathan and Van Kirk (1978). The latter however closely approximate actual temperatures measured in melting experiments (Sharpe and Irvine, 1983). Lindsley (1983), also noted (p. 478) that the Wood-Banno and Wells thermometers are based on erroneous assumptions and their use "is an anachronism that should be avoided." However, on the other hand the pyroxene thermometer of Lindsley (1983) may also not be generally applicable to orthopyroxenes as is discussed later. Nevertheless an attempt was made, using geothermometric methods, to try and relate the marginal rocks to the Rustenburg Layered Suite.

8.2   THE RUSTENBURG LAYERED SUITE

Since the earliest cumulates of the Complex are not exposed in the study area, it was necessary to rely on previously published mineral data for geothermometry of the lower zone. Using the data of Atkins (1969), Wood and Banno (ibid) calculated temperatures for the lower part of the lower zone of

1100° C and 1150° C, based on analyses of coexisting clino- and orthopyroxene. Using these same pyroxene analyses, recalculated and plotted according to the Lindsley method, gives temperatures of 1025° C and 1125° C for clinopyroxene and 1100° - 1150° C for coexisting orthopyroxenes (Fig. 8.1), which are in reasonable agreement with the Wood-Banno results. However, from consideration of Figure 8.1 it is clear that even small variations in the Wo content of orthopyroxene can lead to large variations in predicted temperature (in excess of 100° C/mol. Wo), owing to the closely spaced temperature contours in the orthopyroxene 'field'. In view of this the orthopyroxene data is clearly dependent on extremely accurate analysis and its general application is suspect. However the general agreement with the clinopyroxene temperatures suggests that an average temperature of 1100° C is appropriate for the consolidation of the lower part of the lower zone. However since the orthopyroxene and clinopyroxene temperatures are similar and since the clinopyroxene is intercumulus, then this temperature will be considerably below that of the liquidus.

To further attempt to estimate the liquidus temperature, the relationship derived by Hulbert (1983) was used. Briefly, this relationship was obtained by using the program of Nathan and van Kirk (ibid) to model the (1 atm) fractional crystallisation of QTM and MGN type rocks. Respective calculated liquid temperatures were then plotted against predicted olivine compositions and a regression line fitted to the data. The expression derived from this i.e.,

$$T° C = 1370.9 \ (X_{Mg}^{ol})^{0.6776}$$

where, $X_{Mg}^{ol} = Mg^{2+}/(Mg^{2+} + Fe^{2+})$ in olivine,

relates temperatures to olivine composition. This relationship was shown by Hulbert (ibid.) to be accurate to within 25° C of reported values when tested against known composition-temperature data. Using this expression and applying it to the lower zone olivines (Mg* = 0.87) of Cameron (1978), gives a liquidus temperature of 1247° C for the lower zone liquid. Thus a reasonable estimate for the temperature interval between onset of crystallisation (1247° C), and crystallisation of intercumulus clinopyroxene (1100° C) in the lower zone, is ±150° C.
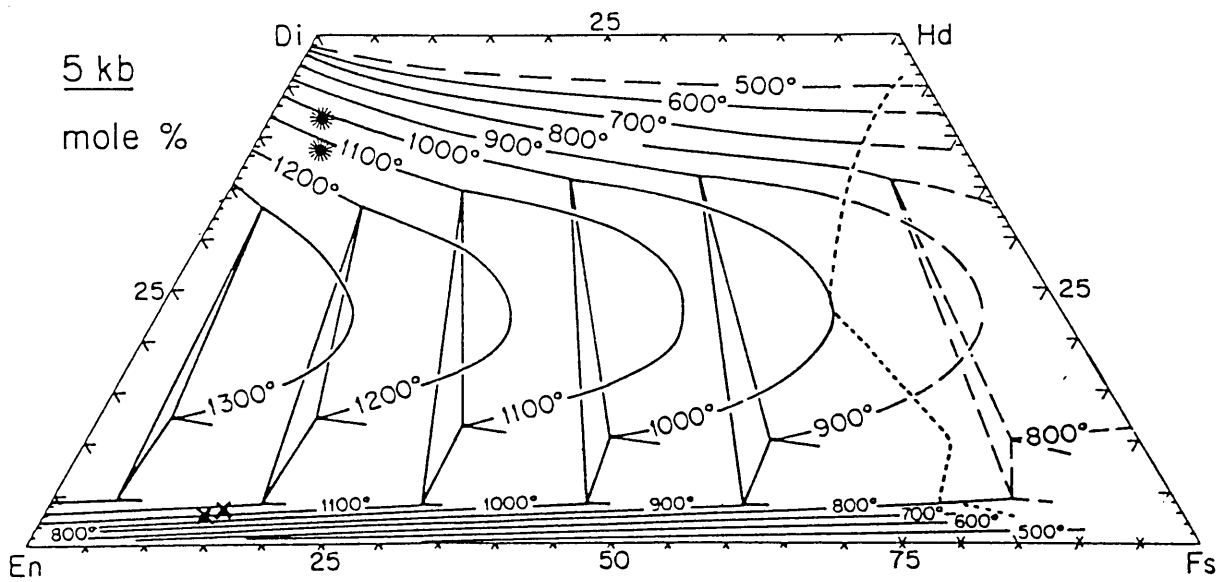
Fig. 8.1. Analyses 1, 2, 1a and 1b of Atkins (1969), recalculated and plotted on the graphical thermometer of Lindsley (1983).

On the other hand in their 3 Kb melting experiments on a composition close to the QTM mean (Table 7.3) Cawthorn and Davies (1983) recorded temperatures of ±1300° C for the onset of olivine crystallisation and ±1150° C for the first appearance of clinopyroxene. Although these temperatures are somewhat higher than the liquidus and clinopyroxene values calculated above, the temperature interval between the initial liquidus and that of clinopyroxene crystallisation i.e. ±150° C, is similar in both modelled and experimental systems. Furthermore use in the expression above, of the most magnesian olivine yet found in the Complex (Mg* 0.90 – Hulbert, 1983) yields a temperature of 1276° C, which is not far below the experimental liquidus for the QTM liquid.

8.3 THE MARGINAL ROCKS

In addition to the melting experiments referred to above, QTM and MGN type compositions have also been extensively investigated by Irvine and Sharpe (1982) and Sharpe and Irvine (1983), so that calculations of crystallisation temperatures are perhaps superfluous. Nonetheless liquidus temperatures were calculated for the marginal rocks of the present study area using major element means and a FORTRAN[1] version of the Nathan and Van Kirk (ibid) crystallisation program. These temperatures are indeed quite close to experimental values (Table 8.1) thus confirming the findings of Sharpe and Hulbert (ibid.)

TABLE 8.1

Comparison of calculated liquidus temperatures for the QTM
and MGN with those obtained in melting experiments

	PRESENT WORK	CAWTHORN AND DAVIES (1983)	SHARPE AND IRVINE (1983)
QTM-type	1294° C	±1300° C	1280–1290° C
MGN-type	1230° C	1166° C	1200° C

As a further check on this, clinopyroxenes from two samples of the QTM were analysed and recalculated according to the Lindsley method. Temperatures indicated for crystallisation of these pyroxenes are approximately 1150° C (Fig. 8.2), in close agreement with the quenched experimental charges of Cawthorn and Davies (ibid.)

---

[1]Translated from the original Algol by M.R. Sharpe.
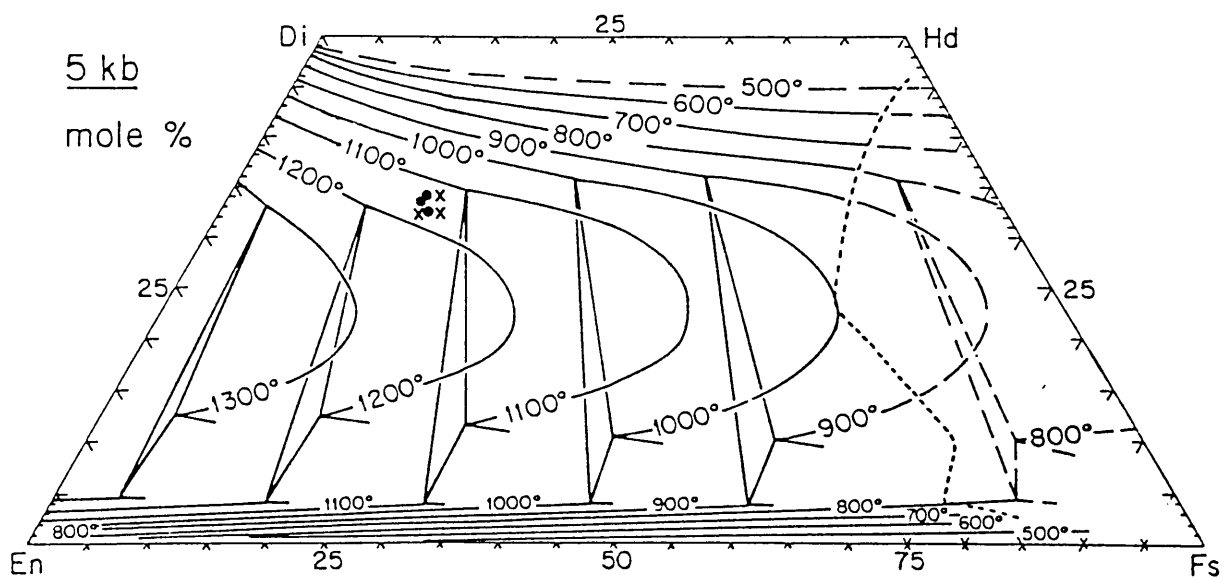
Fig. 8.2. Clinopyroxene analyses from the QTM (samples DI-56 and DI-74), recalculated and plotted on the graphical thermometer of Lindsley (1983).

8.4 DISCUSSION AND CONCLUSIONS

Comparison of the experimental liquidus temperatures for the QTM (±1290° C) with the estimated minimum liquidus temperature (±1250° - 1275° C) for the lower zone magma, clearly agrees with the proposal (chapter 7.8.3) that the QTM are chilled representatives of the parental liquids to the lowermost portion of the Bushveld Complex. In fact the slight discrepancy between the QTM liquidus and that estimated for the lower zone magma is in complete agreement with the suggestion (chapter 7.8.3) that the lowest exposed cumulates crystallised from a QTM magma which had already undergone a small amount of fractionation. Note also that this suggestion is supported by the clinopyroxene crystallisation data with ±1100° C being indicated for the lower zone and ±1150° C for the QTM.

The relationship of the MGN to the Rustenburg Layered Suite is however, more difficult to assess using the above approach. Wood and Banno (ibid.), again using Atkins' (ibid) data, calculated a temperature near the base of the anorthosite subzone of 1015° C. Notwithstanding the inaccuracy of the thermometer, this temperature is based on cumulus phases and therefore presumably should reflect the liquidus temperature, although intuitively it seems rather low. On the other hand Flynn et al. (1978) obtained an equilibrium crystallisation temperature of 1091° C ±35° C for a bronzite - chromite - anorthosite cumulate at the base of the anorthosite subzone, so perhaps the Wood-Banno result is approximately correct. While these values could be considered broadly consistent with a major addition of MGN immediately prior to formation of the subzone (chapter 7), definitive conclusions are unwarranted. Furthermore, the field evidence of the present study indicates that at least two and probably several, episodes of MGN intrusion occurred, while the review by Von Gruenewaldt et al.,(1985) indicated that many workers on the Bushveld Complex consider that numerous injections of MGN-type magma occurred throughout the development of the critical zone. Notwithstanding more recent and somewhat conflicting views as to when, or indeed whether, major influxes of MGN occurred, (e.g. Reichardt 1989; Eales et al. 1990), when the dynamic processes inherent in the formation and subsequent crystallisation of a magma body are also taken into account (e.g. Irvine, 1980b; Irvine et al, 1983, Sparks et al. 1985; Shirley, 1986; Weinstein et al. 1988), then it is clear that the applicability of the above approach to the later stages of intrusion is questionable. The usefulness of this approach therefore appears restricted to the initial stages of intrusion, for which a close correspondence between observed and modelled behaviour of the QTM has already been demonstrated.

9. SUMMARY

Mapping of an area roughly bounded by Rosslyn, Brits, Hartbeespoort Dam and Pretoria has identified three broad geological divisions within the area, namely: floor rocks, layered rocks (the Rustenburg Layered Suite) and marginal rocks, of the Bushveld Complex.

The floor rocks consist of the Magaliesberg Quartzite and underlying Silverton Shale. The former, comprising predominantly massive orthoquartzite, is lithologically uniform throughout the study area, although discontinuous beds of pelitic hornfels and calc silicates occur near the top of the sequence. The Silverton Shale, although poorly exposed and deeply weathered in the eastern part of the area is largely unmetamorphosed whereas in the west it consists of fresh, banded hornfels. This eastward decrease in grade is thought to be due to the increase in stratigraphic distance between the Layered Suite and the shale owing to the pre-Bushveld intrusion of the Middelwater layered Sill. Both units of the floor are intruded by numerous thin sills.

The Rustenburg Layered Suite has, in part, a transgressive relationship with the floor and is not comformable throughout the study area, as shown on previous maps. Thus, in the western portion of the area the Ruighoek Pyroxenite (lower subzone of the critical zone) forms the base of the Complex while further east the Pyramid Gabbro - Norite (lower portion of the main zone) is the lowermost unit. That is, the base of the Bushveld Complex rises in an easterly direction. The Rustenburg Layered Suite therefore has its maximum development in the western part of the area, where the Ruighoek Pyroxenite, Mathlagame Norite-Anorthosite (upper subzone of the critical zone) and Pyramid Gabbro-Norite crop out. Borehole data from this region indicate that the overall succession is similar to the eastern and western lobes of the Bushveld Complex, except for the absence of the Lower Group chromitites, the occurrence of cumulus plagioclase below the Middle Group chromitites, and the unusual thickness (12 m) of the Merensky Reef.

The marginal rocks, sensu lato, form a diverse group which include metamorphosed (pre-Bushveld Complex) sills in the floor, as well as rocks which were intruded during the formation of the Rustenburg Layered Suite. Pre-Bushveld sills that intrude the Magaliesberg Quartzite and Silverton Shale are of two distinct types, namely metadolerite and meta quartz-dolerite. The latter is volumetrically more abundant and comprises approximately 50 per

cent of the sills in the study area. Petrographically, little of the primary mineralogy is preserved in either of these sill types, both consisting predominantly of saussuritised plagioclase and amphibole, although in some of the meta quartz-dolerite sills up to 20 modal per cent quartz occurs. Geochemically, the metadolerites are fairly typical continental tholeiites, with up to 3 per cent normative quartz and up to 25 per cent normative hypersthene. The meta quartz-dolerites, on the other hand are characterised by high weight per cent contents of SiO_2 (55.5) and Rb contents of 45-50 ppm, as compared with other continental tholeiites. They are undoubtedly contaminated and geochemical modelling suggests that they are the result of assimilation of crustal material by the metadolerite magma.

Above the Magaliesberg Quartzite, intrusion of metadolerite magma prised off rafts and screens of metasediment and gave rise to a 350 m thick layered sill, (the Middelwater Layered Sill). Within this sill, which is sheathed by contaminated meta quartz-dolerites, noritic and anorthositic cumulates occur. Metamorphism within this sill is also common and petrographically it is characterised by oscillatory zoned plagioclase feldspars. Both of these features distinguish it from rocks of the Rustenburg Layered Suite, which together with their marginal facies cross cut the Middelwater Layered Sill in the central portion of the area. Thus these predominantly noritic cumulates are not a lateral extension of the Rustenburg Layered Suite, as shown on earlier maps, but belong to a previous magmatic episode.

The second major suite of sills, the micropyroxenites, comprise approximately 30 per cent, by volume, of the sills in the study area. In outcrop, textural types vary but in places spinifex-like textures occur. More rarely the texture known as cone-diabase texture is seen. Such textures are considered to be the result of rapid cooling or quenching and petrographic evidence of such a process is abundant. This evidence includes comb-textured plagioclase, hopper-shaped to acicular orthopyroxene and sheaf-like or plumose intergrowths of plagioclase, orthopyroxene and biotite. Geochemically these quench-textured micropyroxenites are very distinctive for basaltic rocks in having high weight per cent contents of SiO_2 (55.5), K_2O (0.9) and MgO (13.3) as well as containing ±300 ppm Ni and ±1100 ppm Cr. They are similar to rocks described from elsewhere in the Bushveld Complex and geochemically, in many respects, they resemble boninites.

Like the micropyroxenites from the eastern Bushveld, these rocks have high initial $^{87}Sr/^{86}Sr$ ratios (i.e. ±0.703 - ±0.706 at 2.05 Ga) and similarly the lack of correlation between these and e.g. K_2O or SiO_2 content is interpreted as evidence against contamination on passage through the crust. Moreover, although enriched in K_2O and LREE, the micropyroxenites do not appear to be the product of low degrees of mantle melting as their high MgO and Ni contents cannot be reconciled with such an explanation. Thus, while there is still some uncertainty about their precise origin, it is concluded that the micropyroxenites result primarily from the extensive (±35 per cent) partial melting of mantle material. However, whether their high K_2O and LREE contents are due to enrichment of the source region or whether, as has recently been proposed, these components are derived from a metasomatised zone close to the source (e.g. at the crust-mantle transition), cannot be elucidated from the presently available data. The high SiO_2 content of the micropyroxenites is also difficult to explain without invoking some degree of enrichment at, or close to, the source and/or hydrous melting. Although this feature has been ascribed to early fractionation of olivine from a more basic magma, (possibly coupled with assimilation of crustal material) the degree of fractionation required to produce the observed SiO_2 content (i.e. 55.5 wt. per cent) is not compatible with the high Ni values (i.e. ±300 ppm) of the micropyroxenites.

Geochemical and mineralogical data indicate that the micropyroxenites are representative of the parental magma to the lower portions of the Rustenburg Layered Suite.

Of the remaining sills in the area, the origin of the sparse norites and a feldspathic pyroxenite sill are enigmatic. Most norites are cumulate textured and or contaminated, whilst the feldspathic pyroxenite closely resembles rocks of the Ruighoek Pyroxenite. These rocks are probably offshoots of the Rustenburg Layered Suite, although some norites may be related to chilled marginal phases of the latter. Two distinctive olivine and chromite bearing pyroxenite bodies appear to be squeezed out cumulates from a lower, unexposed portion of the Rustenburg Layered Suite. This is thought to be the case because geochemical modelling indicates that they represent solidified suspensions of cumulate crystal mushes in micropyroxenitic liquid. Since no olivine occurs in the lowest portion of the Rustenburg Layered Suite exposed in the study area, then these cumulates must have originated at levels below this. The occurrence

of these rocks consequently indicates the presence of olivine bearing cumulates at greater depths.

The remainder of the marginal rocks in the study area comprise a fine to medium grained microgabbronoritic phase and a younger, coarser grained, partly heterogeneous, quartz gabbronorite. The microgabbronorite originally formed a chilled marginal zone adjacent to the Rustenburg Layered Suite, however it is now separated from the latter by the quartz gabbronorite. The extensive development of this chilled marginal zone is nevertheless restricted to levels above the Ruighoek Pyroxenite - Mathlagame Norite-Anorthosite junction (i.e. above the junction between the lower and upper subzones of the critical zone) and field relations indicate that at least two and probably several, phases of intrusion occurred. However, the abrupt appearance of significant volumes of this rock type at the Ruighoek Pyroxenite-Mathlagame Norite-Anorthosite junction is considered to be evidence of a major intrusion of microgabbronoritic magma into the Bushveld Complex at this level.

Geochemically the microgabbronorite is a fairly typical, albeit slightly magnesium-rich, continental tholeiite with overall weight per cent contents of SiO_2, MgO and K_2O of 50.50, 8.40 and 0.30 respectively. Rb/Sr ratios are typically 0.02 and, although somewhat variable, like many other continental tholeiites they possess high initial ratios of $^{87}Sr/^{86}Sr$ (i.e. ±0.706 - ±0.708 at 2.05 Ga)). Normatively, samples of the microgabbronorite straddle the plane of silica saturation with individual samples containing up to several per cent quartz (quartz tholeiites) or up to several per cent olivine (olivine tholeiites).

The quartz gabbronorite is a variably contaminated rock that, throughout the study area, forms a heterogeneous basal zone between the Rustenburg Layered Suite and the floor, or other marginal rocks. It is gradational upwards into the cumulates and in places intermediate rock types between the microgabbronorite and the more normal coarser-grained varieties of the quartz gabbronorite occur. In other places it includes microgabbronorite xenoliths. Geochemical modelling indicates that the quartz gabbronorite is largely a mixture of microgabbronorite and crustal (granitic) material, possibly with varying proportions of hornfels also being included in the final consolidation product.

The formation of the quartz gabbronorite is viewed as the natural consequence of the extended intrusion of the microgabbronorite. This is because later pulses would pass through increasingly heated crustal rocks and it seems likely therefore that later pulses would become increasingly contaminated. However, it is uncertain to what extent this contaminated material entered the magma chamber or was confined to the structural weakness along the contact of the Rustenburg Layered Suite and floor. Certainly some upward infiltration into the hot cumulate pile is suggested by the gradational contact of the quartz gabbronorite with the overlying cumulates of the critical zone and lowermost main zone.

ACKNOWLEDGEMENTS

Firstly I would like to thank my wife, Chrissie, without whose constant support, both moral and latterly financial, this project would not have been completed. The continued interest shown by Prof. G. von Gruenewaldt, particularly at times when other work commitments stalled the project, also played a major role in completion of this thesis, and his assistance is gratefully acknowledged. This project was initiated at his suggestion and financial assistance both from the Institute for Geological Research on the Bushveld Complex and the CSIR was most generous.

Dr Martin Sharpe and Dr Chris Hatton, also provided material assistance, guidance and a number of helpful suggestions and criticisms during the course of this work and their input is also gratefully acknowledged.

Dr Bruce Eglington and Jock Harmer of the CSIR's Division of Earth, Marine and Atmospheric Science and Technology kindly undertook the Sr isotopic analyses on my behalf and their contribution is also much appreciated.

Much of this work was compiled on a part-time basis while I was employed at the Geological Survey of South Africa and I am grateful to numerous people from the Survey who provided assistance at one stage or another. In particular to the Chief Director, Dr C. Frick and to deputy Director L.S. Labuschagne, for allowing me the time, and providing the facilities, for research. I would also like to thank Thinus Cloete for providing excellent thin sections and particularly for arranging to have the REE analyses done at the University of Stellenbosch while I was overseas. For providing photographic services and for assistance with the microprobe I would like to thank Martin Kohler and Gerhard Du Plessis respectively.

A number of photomicrographs were also taken using facilities at the West Australian Museum in Perth and I am grateful to Dr Alex Bevan for his assistance in this regard. Finally I would like to thank Ian Houston of the Dept. of Geology and Applied Geology, University of Natal-Durban, for technical assistance and for allowing me to use his darkroom facilities in order to print the final text photographs.

REFERENCES

ALLEGRE, C.J., TREUILL, M., MINSTER, J.F., MINSTER, B. and ALBAREDE., 1977. Systematic use of trace elements in igneous processes. Part 1. Fractional crystallization in volcanic suites. Contrib. Mineral. Petrol v60 p57-75.

ARMBRUSTMACHER, T.J. and BANKS, N.G., 1974. Clouded plagioclase in metadolerite dikes, Southeastern Bighorn Mountains, Wyoming. Am. Miner., 59, p. 656-665.

ARNDT, N.T., NALDRETT, A.J. and PYKE, D.R., 1977. Komatiitic and iron-rich tholeiitic lavas of Munro Township, Ontario. J. Petrol., v. 18, p.318-369.

ARNDT, N.T. and NISBET, E.G. 1982. (Eds.) Komatiites, George Allen and Unwin, London. 526pp.

ARNDT, N.T., JENNER, G.A., NISBET, E.G. and ZINDLER, A., 1986. The nature and composition of the archaean mantle. Eos, v.67 p.172-174.

ARTH, J.G. 1976. Behaviour of trace elements during magmatic processes – a summary of theoretical models and their applications. Journ. Research, U.S. Geol Surv. v4(1) p 41-47.

ATKINS, F.B., 1969. Pyroxenes of the Bushveld Intrusion, South Africa. J. Petrol., 10, p. 222-249.

BARNES, S.J., 1989. Are Bushveld U-type parent magmas boninites or contaminated komatiites? Contrib. Mineral. and Petrol. v101 p. 447-457.

BENDER, J.F., HODGES, F.N., and BENCE, A.E. 1978. Petrogenesis of basalts from the project FAMOUS area, experimental study from 0 to 15 kbars. Earth and Plan. Sci. Letters v41 p. 277-302.

BLOOMER, S.H., and HAWKINS, J.W., 1987. Petrology and geochemistry of boninite series volcanic rocks from the Mariana trench. Contrib. Mineral. and Petrol. v97, p. 361-377.

BOWEN, N.L. 1928. The evolution of the Igneous Rocks, Princeton University Press, Princeton, New Jersey 332pp.

BOYD, F.R. and NIXON, P.H. 1973. Carnegie Inst. Washington. Yearbook 72.

BUDDINGTON, A.F., and LINDSLEY, D.L. 1964. Iron-Titanium Oxide Minerals and synthetic equivalents. Journ. Petrol. v5 p. 310.357.

BUTTON, A., 1976. Stratigraphy and relations of the Bushveld floor in the Eastern Transvaal. Trans. geol. Soc. S. Afr., v. 79, p. 3-12.

CAMPBELL, I. H., ROEDER, P. L. and DIXON, J.M. 1978. Plagioclase buoyancy in basaltic liquids as determined with a centrifuge furnace. Contrib. Mineral. Petrol. v67 p.369-377

CAMERON, E.N., 1963. Structure and rock sequences of the critical zone of the

eastern Bushveld Complex. Miner. Soc. America, Spec. Paper 1, p.93-107.

CAMERON, E.N., 1964. Chromite deposits of the eastern part of the Bushveld Complex In: Haughton, S.H. (Ed.). The Geology of some ore deposits in Southern Africa II, Geol. Soc. S.Afr. p.131-168.

CAMERON, E.N., 1975. Postcumulus and sub solidus equilibration of chromite and co-existing silicates in the Eastern Bushveld Complex. Geochim. Cosmochim. Acta. v39, p.1021-1033.

CAMERON, E.N., 1978. The lower zone of the eastern Bushveld in the Olifants River Trough. J. Petrol., v19 (3), p.437-462.

CAMERON, E.N., and DESBOROUGH, G.A., 1969. Occurrence and characteristics of chromite deposits - Eastern Bushveld Complex. Econ. Geol. Monograph v4, p.23-40.

CAMERON, W.E., and NISBET, E.G., 1982. Phanerozoic analogues of Komatiitic basalts. In: Arndt, N.T. and Nisbet, E.G., (Eds.) Komatiites. George Allen and Unwin London. 526pp.

CAMERON, W.E., NISBET, E.G., and DIETRICH, V.J., 1979. Boninites, Komatiites and ophiolitic basalts. Nature, v280, p.550-553.

CAWTHORN, R.G., and DAVIES, G. 1983. Experimental data at 3kbars pressure on parental magma to the Bushveld Complex. Contrib. Mineral. Petrol. v83, p.128-135.

CAWTHORN, R.G., and McCARTHY, T.S., 1985. Incompatible trace element behaviour in the Bushveld Complex. Econ. Geol. v80, p.1016-1026.

CAWTHORN, R.G., BIGGAR, G.M., GRAHAM, A., FORD, C.E., SHARPE, M.R. and DAVIES, G., 1979. Experimental petrological data on the parental magmas to the Bushveld Complex. Res. Rept. no. 18, Inst. geol. Res. Bushveld Complex, University of Pretoria, 27pp.

CAWTHORN, R.G., DAVIES, G., CLUBLEY-ARMSTRONG, A. and McCARTHY, T.S., 1981. Sills associated with the Bushveld Complex, S. Africa: an estimate of the parental magma composition. Lithos, v14, p.1-16.

CHAYES, F., 1956. Petrographic modal analysis, an elementary statistical appraisal. John Wiley and Sons, New York, 113pp.

CHAYES, F., 1964. Variance - covariance relations in Harker diagrams of volcanic suites. Journ. Petrol. v5, p.215-237.

CLAOUE-LONG, J.C. and NESBITT, R.W. 1985. Contaminated komatiites. Nature, v313, p.247.

COERTZE, F.J., 1970. The geology of the western part of the Bushveld Igneous Complex. Geol. Soc. S. Afr., Spec. Publn. 1, p.1-20.

———————————— 1974. The geology of the Basic Portion of the western Bushveld Igneous Complex. Geol. Surv. S. Afr., Mem. 66, 148pp.

CONSOLMAGNO, G.J., and DRAKE, M.J., 1976. Equivalence of equations describing trace element distribution during equilibrium partial melting. Geochim. Cosmochim. Acta. v40, p.1421–1422.

COUSINS, C.A., 1969. The Merensky Reef of the Bushveld Igneous Complex. Econ. Geol. Mon. 4, p.239–251.

———————————— and FERINGA, G., 1964. The chromite deposits of the western belt of the Bushveld Complex. In: Haughton, S.M. (Ed.) The geology of some ore deposits in Southern Africa, II. Geol. Soc. S. Africa, p.183–202.

COX, K.G., 1972. The Karroo volcanic cycle. Journ. Geol. Soc. London. v128, p.311–336.

————————, BELL, J.D., and PANKHURST, R.J., 1979. The interpretation of Igneous Rocks. George Allen and Unwin Ltd. London 450pp.

DAVIES, G., 1982. The petrogenesis of the marginal rocks and sills associated with the Rustenburg Layered Suite between Hartebeespoort and Buffelspoort dams, western Bushveld Complex. Unpub. Phd. thesis, Univ. of the Witwatersrand, 450pp.

————————, CAWTHORN, R.G., BARTON, J.M., Jr. and MORTON, M., 1980. Parental magma to the Bushveld Complex. Nature, v287, p.33–35.

————————, and TREDOUX, M., 1985. The platinum group element and gold contents of the marginal rocks and sills of the Bushveld Complex. Econ. Geol. v80, p.838–848.

DAWSON, J.B., 1984. Contrasting types of upper mantle metasomatism? In: Kornprobst J. (Ed.). Kimberlites II. The mantle and crust–mantle relationships. Elsevier Amsterdam, 393pp.

DEER, W.A., HOWIE, R.A., and ZUSSMAN, J., 1962. Rock forming minerals, William Clowes and Sons Ltd. London.

————————, HOWIE, R.A., and ZUSSMAN, J., 1978 Rock forming minerals. 2nd ed. Longman, London.

DE PAULO, D.J., 1981. Trace element and isotopic effects of combined wallrock assimilation and fractional crystallization Earth and Plan. Sci. Letters, v53, p.189–202.

————————, 1985. Isotopic studies of processes in mafic magma chambers I. The Kiglapait Intrusion, Labrador, Journ. Petrol. v26, p.925–951.

DONALDSON, C.H., 1977. Laboratory duplication of comb–layering in the Rhum Pluton. Mineral. Mag. v41, p.323 – 336.

EALES, H.V., DE KLERK, W.J., BUTCHER, A.R., and KRUGER, F.J., 1990. The cyclic unit beneath the UG1 chromitite (UG1FW unit) at RPM Union Section Platinum Mine-Rosetta Stone of the Bushveld Upper Critical Zone? Mineral. Mag. v54 p. 23-43.

———————, MARSH, J.S., MITCHELL, A.A., DE KLERK, W.J., KRUGER, F.J. and FIELD, M. 1986. Some geochemical constraints upon models for the crystallisation of the upper critical zone-main zone interval, northwestern Bushveld Complex. Mineral. Mag. v50, p.567-582.

EGLINGTON, B.M. and HARMER, R.E. 1989. GEODATE: A program for the processing and regression of isotope data using IBM-compatible microcomputers. CSIR Manual EMA-H8901. Division of Earth, Marine and Atmospheric Sciences and Technology, CSIR, Pretoria, S. Africa, 58pp.

ELLIOTT, R.B., 1973. The chemistry of Gabbro/Amphibolite transitions in South Norway. Contrib. Mineral. Petrol v38, p. 721 - 79.

EVENSEN, N.M., HAMILTON, P.J. and O'NIONS, R.K., 1978. Rare earth abundances in chondritic meteorites. Geochim. Cosmochim Acta. v42 p. 1199. 1212.

FERGUSON, J. and WRIGHT, L.H., 1970. Compositional variation of plagioclases in the Critical Series, Bushveld Complex. Spec. Publ. No. 1 Geol. Soc. S. Africa.

FREY, F.A., BRYAN, W.B. and THOMPSON, G. 1974. Atlantic ocean floor. Geochemistry and petrology of basalts from Legs 2 and 3 in the deep sea drilling project. Journ. Geophys. Res. v79, p. 5507-5527.

———————, GREEN , D.H. and ROY, S.D. 1978. Integrated models of basalt petrogenesis: A study of quartz tholeiites to olivine melilites from south eastern Australia, utilizing geochemical and experimental petrological data. Journ. Petrol. v19, p. 463-513.

FLYNN, R.T., ULMER, G.C and SUTPHEN, C.F., 1978. Petrogenesis of the eastern Bushveld Complex : Crystallization of the middle Critical Zone. Journ. Petrol v19, p. 136-152.

GAIN, S.B. 1985. The geological setting of the platiniferous UG-2 chromitite layer on Maandagshoek, eastern Bushveld Complex. Econ. Geol. v80, p.925-943.

GAST, P.W., 1968. Trace element fractionation and the origin of tholeiitic and alkaline magma types. Geochim. Cosmochim Acta v32, p. 1057-1086.

GIBB, F.G.F., 1974. Supercooling and the crystallization of plagioclase from a basaltic magma. Mineral. Mag. v39, p. 641-653.

GIJBELS, R.H., MILLARD, H.T. Jr., DESBOROUGH, G.A. and BARTEL, A.J., 1974. Osmium, ruthenium, iridium and uranium in silicates and chromite from the eastern Bushveld Complex, South Africa. Geochim. Cosmochim Acta. v38 p.319-337.

GREEN, D.H., EDGAR, A.D., BEASLEY, P., KISS, E. and WARE, N.G. 1974. Upper mantle source for some hawaiites, mugearites and benmoreites. Contrib. Mineral Petrol. v48, p.33-43.

—————————, and RINGWOOD, A.E. 1967. The genesis of basaltic magmas. Contrib. Mineral. Petrol. v15, p.103-190.

GURNEY, J.J. and HARTE, B., 1980. Chemical variations in upper mantle nodules from Southern African Kimberlites. Phil. Trans. Roy. Soc. Lond. A297, p.273-293.

HäKLI, T.A. and WRIGHT, T.L., 1967. The fractionation of nickel between olivine and augite as a geothermometer. Geochim. Cosmochim. Acta v31, p.877-884.

HALL, A.L., 1932 The Bushveld Igneous Complex of Central Transvaal. Geol. Surv. S. Afr., Mem. 28.

—————————. and DU TOIT, A.L., 1923. On the section across the floor of the Bushveld Complex at Hartebeespoort Dam. Trans. geol. Soc. S. Afr., v26, p.69-97

HALL, R.P., and HUGHES, D.J., 1987. Noritic dykes of southern West Greenland: early Proterozoic boninitic magmatism. Contrib. Mineral. Petrol. v97, p.169-182.

HAMILTON, J., 1977. Sr-isotope and trace element studies of the Great Dyke and Bushveld mafic phase and their relation to early Proterozoic magma genesis in Southern Africa. Journ. Petrol., v18, p.24-52.

HAMLYN, P.R. AND KEAYS, R.R., 1986. Sulfur saturation and second-stage melts: application to the Bushveld platinum metal deposits. Econ. Geol. v81, p.1431-1445.

HANSON, G.N., 1977. Geochemical evolution of the sub-oceanic mantle. Journ. Geol. Soc. Lond. v134, p.235-253.

HARKER, A., 1932. Metamorphism. A study of the transformation of Rock-masses Chapman and Hall, London., 362pp.

HARMER, R.E. and VON GRUENEWALDT, G., 1990. A review of magmatism associated with the Transvaal Basin - implications for its tectonic setting. South Afr. J. Geol. v94, p.104-122.

HARMER, R.E. and SHARPE, M.R., 1985. Field Relations and Strontium Isotope Systematics of the Marginal Rocks of the Eastern Bushveld Complex. Econ. Geol. v80, p.813-837.

HARRISON, W.J., 1981. Partitioning of REE between minerals and coexisting melts during partial melting of a garnet lherzolite. Am. Mineralogist v66, p.242-259.

HART, S.R. and ALLEGRE, C.J., 1980. Trace element constraints on magma genesis,

p.121-160. In: Hargraves, R.B. (Ed.) Physics of Magmatic Processes, Princeton University Press. 585pp.

——————, and DAVIS, K.E., 1978. Nickel partitioning between olivine and silicate melt. Earth and Plan. Sci. Letters, v40, p.203-219.

——————, ERLANK, A.J. and KABLE, E.J.D., 1974. Sea floor basalt alteration: some chemical and Sr. isotopic effects. Contrib. Mineral Petrol. v44, p.219-230.

HATTON, C.J. and VON GRUENEWALDT, G., 1985. Chromite from the Swartkop chrome mine - an estimate of the effects of sub solidus re-equilibration. Econ. Geol. v80, p.813 - 837.

HATTON, C.J. and VON GRUENEWALDT, G. 1987. The geological setting and petrogenesis of the Bushveld Chromitite layers. In Stowe, C.W., (ed.). Evolution of chromium ore fields, van Nostrand Rheinhold, New York, p109-143.

HATTON, C.J. and SHARPE, M.R., 1988. Significance and origin of boninite-like rocks associated with the Bushveld Complex, p.174-207, In: Crawford, A.J., (Ed), Boninites. Unwyn Hyman Ltd., London.

HERTOGEN, J. and GIJBELS, R., 1976. Calculation of trace element fractionation during partial melting. Geochim. Cosmochim. Acta. v40, p.313-322.

HICKEY, R.L. and FREY, F.A., 1982. Geochemical characteristics of boninite series volcanics : implications for their source. Geochim. Cosmochim. Acta v46, p.2099-2115.

HIEMSTRA, S.A., and VAN BILJON, W.J., 1959. The geology of the Upper Magaliesberg Stage and the Lower Bushveld Complex in the vicinity of Steelpoort. Trans., geo. S. Afr., v62, p.239-225.

HOLM, P.E., 1982. Non-recognition of Continental Tholeiites using the Ti-Y-Zr diagram. Contrib. Mineral Petrol. v79, p.308-310.

HUGHES, C.J., 1982. Igneous Petrology. Elsevier, Amsterdam, 551pp.

HULBERT, L., 1983. A petrological investigation of the Rustenburg Layered Suite and associated mineralization south of Potgietersrus. D.Sc. thesis, Univ. of Pretoria 511pp. (unpubl.).

HULBERT, L.J. and VON GRUENEWALDT, G. 1985. Textural and Compositional features of chromite in the lower and critical zones of the Bushveld Complex, South of Potgietersrus. Econ. Geol. v80, p.872-895.

HUNTER, D.R., 1974. Crustal development in the Kaapvaal craton, II. The Proterozoic. Precamb. Res., v1, p.295-326.

——————, and HAMILTON, P.J., 1978. The Bushveld Complex , p.107-165 In: Tarling, D.H. (Editor). Evolution of the Earth's Crust. Academic Press, London.

HUTCHISON, C.S., 1974. Laboratory handbook of Petrographic Techniques. John Wiley and Sons, New York, 527pp.

IRVINE, T.N., 1974. Fractionation of chromium and nickel from silicate melts, Carnegie Inst. Washington, Year book 73, p.306-307.

——————, 1980a. Magmatic density currents and cumulus processes. Am. Jour. Sci., v280-A, p.1-58.

——————, 1980b. Magmatic infiltration metasomatism, double diffusive fractional crystallisation and adcumulus growth in the Muskox intrusion and other Layered Intrusions. In: Hargraves, R.B., (Ed.) Physics of Magmatic Processes. Princeton Univ. Press. 585pp.

——————, and BARAGAR, W. R. A., 1971. A guide to the classification of the common volcanic rocks. Can. Journ. Earth Sci. v8, p.523-548.

——————, and SHARPE, M.R., 1982. Source rock composition and depths of origin of Bushveld and Stillwater magmas. Carnegie Inst. Washington. Yearbook 81, p.294-303.

——————, KEITH, D.W. and TODD, S.G., 1983. The J-M platinum-palladium reef of the Stillwater Complex, Montana: II. Origin by double diffusive convective magma mixing and implications for the Bushveld Complex. Econ. Geol. v78, p.1287-1334.

IRVING, A.J., 1978. A review of experimental studies of crystal/liquid trace element partitioning. Geochim. Cosmochim. Acta. v42, p.743-770.

JAQUES, A.L. and GREEN, D.H., 1980. Anhydrous melting of peridotite at 0-15Kb pressure and the genesis of tholeiitic basalts. Contrib. Mineral. Petrol. v73, p.287-310.

KAY, R.W. and GAST, P.W., 1973. The rare earth content and origin of alkali-rich basalts. Journ. of Geology, V81, p.653-682.

KRUGER, F.J., 1990. The stratigraphy of the Bushveld Complex: a reappraisal and relocation of the Main Zone boundaries. S. Afr. J. Geol., v93, p.376-381.

——————, 1991. Author's reply to discussion, S. Afr. J. Geol. v94, p.187-190.

—————— and MARSH, J.S., 1982. Significance of $^{87}Sr/^{86}Sr$ ratios in the Merensky cyclic unit of the Bushveld Complex. Nature, v298, p.53-55.

—————— and MARSH, J.S., 1985. The mineralogy, petrology and origin of the Merensky cyclic unit of the Bushveld Complex. Econ. Geol. v80, p.958-974.

KUNO, H., 1959. Origin of Cenozoic petrographic provinces of Japan and surrounding areas. Bull Volcanol. v20, p.37-76.

————————, 1966. Lateral variation of basaltic magma type across continental margins and island arcs. Bull Volcanol. XXIX, p.195-222.

KUSHIRO, I., 1969. The system forsterite-diopside - silica with and without water at high pressures. Am. J. Sci. v267A, p.269-294.

KYNASTON, H., 1904. On the area lying north-west of Pretoria between the Magaliesberg Range and the Salt Pan. Ann. Rept. Geol. Surv. Transvaal, p.71-74.

————————, 1907. The geology of the country round Pretoria. Explan. Sheet 1 (Pretoria), Geol. Surv. Transvaal, 38pp.

————————, KRIGE, L.J. and LOMBAARD, B.V., 1929. The geology of the country round Pretoria. Explan. Sheet 1 (Pretoria, Revised Edition), Geol. Surv. S. Africa.

KYSER, T.K., CAMERON, W.E., and NISBET, E.G., 1986. Boninite petrogenesis and alteration history: constraints from stable isotope compositions of boninites from Cape Vogel, New Caledonia and Cyprus. Contrib. Mineral. Petrol. v93, p222-226

LANGMUIR, C.H., BENDER, J.F., BENCE, A.E., HANSON, G.N. and TAYLOR, S.R., 1977. Petrogenesis of basalts from the Famous area: Mid-Atlantic Ridge. Earth Plan. Sci. Letters v36, p.133-156.

————————, VOLKE, R.D. Jr., HANSON, G.N. and HART, S.R., 1978. A general mixing equation with applications to Icelandic basalts. Earth and Plan. Sci. Letters, v37, p.380-392.

LE ROEX, A.P. 1987. Source regions of mid-ocean ridge basalts; evidence for enrichment processes. In Menzies, M.A. and Hawkesworth, C.J. (eds.), Mantle Metasomatism. Academic Press, London, p.389-422.

LINDSLEY, D.H., 1983. Pyroxene thermometry. Amer. Mineralogist. v68, p.477-493.

LOFGREN, G., 1980. Experimental studies on the dynamic crystallization of silicate melts, p.487-551. In: HARGRAVES, R.B., Physics of Magmatic Processes. Princeton Univ. Press, N. Jersey. 585pp.

————————, DONALDSON, C.H., WILLIAMS, R.J., MULLINS, O. Jr. and USSELMAN, T.M., 1974. Experimentally reproduced textures and mineral chemistry of Apollo 15 quartz normative basalts. Proc. 5th. Lunar Sci. Conf., Geoch. Cosmochim. Acta, v1, p.549-568.

LONGHI, J., WALKER, D and HAYS, J.F., 1978. The distribution of Fe and Mg between olivine and lunar basaltic liquids. Geochim. Cosmochim. Acta. v12, p.1545-1558.

MAALOE, S., 1982. Geochemical aspects of permeability controlled partial melting and fractional crystallisation. Geochim. Cosmochim. Acta. v46, p.43-57.

with degree of melting of peridotite in the upper mantle. Am. Mineralogist, v62, p.843-865.

NATHAN, H.D. and VAN KIRK, C.K., 1978. A model of magmatic crystallisation. Journ. Petrol. v19, p.66-94.

NEL, H.K., 1940. The basal rocks of the Bushveld Igneous Complex, north of Pretoria. Trans. geol. Soc. S. Afr. v43, p.37-68.

NELL, J., 1985. The Bushveld metamorphic aureole in the Potgietersrus area: Evidence for a two stage metamorphic event. Econ. Geol. v80, p.1129-1152.

NESBITT, R.W., 1971. Skeletal crystal forms in the ultramafic rocks of the Yilgarn Block, Western Australia: Evidence for an Archean ultramafic liquid. Spec. Publ. of the Geol. Soc. Australia v3, p.331-348.

NIXON, P.H. and BOYD, F.R., 1973. Petrogenesis of the granular and sheared ultrabasic nodule suite in Kimberlites p.48-56. In: Nixon, P.H. (Ed.) Lesotho Kimberlites. Lesotho National Development Corporation, Maseru, Lesotho.

NORRISH, K. and HUTTON, J.J., 1969. An accurate X-Ray spectrographic method for analysis of a wide range of geological samples. Geoch. Cosmochim. Acta v43, p.431-453.

O'HARA, M.J., 1985. Importance of the shape of the melting regime during partial melting of the mantle. Nature v314, p.58-62.

O'NIONS, R.K. and CLARKE, D.B., 1972. Comparative trace element geochemistry of Tertiary basalts from Baffin Bay. Earth Plan. Sci. Letters v15, p.436-446.

O'NIONS, R.K., HAMILTON, P.J. and EVENSEN, N.M., 1977. Variations in $^{143}Nd/^{144}Nd$ and $^{87}Sr/^{86}Sr$ ratios in oceanic basalts. Earth Plan. Sci. Letters, v34, p.13-22.

PATCHETT, P.J., 1980. Thermal effects of basalt on continental crust and crustal contamination of magmas. Nature v283, p.559-561.

PEARCE, J.A., 1975. Basalt geochemistry used to investigate past tectonic environments on Cyprus. Tectonophysics v25, p.41-67.

—————————, J.A. and CANN, J.R., 1973. Tectonic setting of basic volcanic rocks determined using trace element analysis. Earth Plan. Sci. Letters, v19, p.290-300.

—————————, and FLOWER, M.F.J., 1977. The relative importance of petrogenetic variables in magma genesis at accreting plate margins: a preliminary investigation. Journ. Geol. Soc. Lond. v134, p.108-127.

POLDERVAART, A. and GILKEY, A.F., 1954. On clouded plagioclase. Amer. Mineralogist v39, p.75-91.

PUSHKAR, P., McBIRNEY, A.R. and KUDO, A.M., 1972. The isotopic composition of strontium in Central American ignimbrites. Bull. volcanol. v35, p.265-294.

PYKE, D.R., NALDRETT, A.J. and ECKSTRAND, O.R., 1973. Archaean ultramafic flows in Munro Township, Ontario. Bull. Geol. Soc. America. v84, p.955-978.

REICHARDT, F.J., 1989. A petrological investigation of the transition from the lower to the upper critical zone in the central sector of the eastern Bushveld Complex. Phd thesis (unpubl.) Univ. of Pretoria, 238pp.

RICHTER, R, 1986. Simple models for trace element fractionation during melt segregation. Earth Plan. Sci. Letters v77, p.333.

RINGWOOD, A.E., 1975. Composition and Petrology of the Earth's Mantle. McGraw - Hill, New York, N.Y. 618pp.

ROEDER, P.L., 1974. Activity of iron and olivine solubility in basaltic liquids. Earth Plan. Sci. Letters, v23, p.397-410.

ROEDER, P.L. and EMSLIE, R.F., 1970. Olivine-liquid equilibrium. Contrib. Mineral. Petrol. v29, p.275-289.

SACS, 1980. South African Committee for Stratigraphy. Stratigraphy of South Africa. Part 1 (Comp. L.E. Kent). Lithostratigraphy of the Republic of South Africa, South West Africa/Namibia and the Republics of Bophutatswana, Transkei and Venda. Handb. Geol. Surv. S. Africa, 8.

SATO, H., 1977. Nickel content in basaltic magmas: identification of primary magmas and a measure of the degree of olivine fractionation. Lithos v10, p.113-120.

SCHILLING, J.G. and WINCHESTER, J.W., 1969. Rare earth contribution to the origin of Hawaiian lavas. Contrib. Mineral. Petrol. v23, p.22-37.

SCHWELLNUS, J.S.I., ENGELBRECHT, L.N.J. COERTZE, F.S., RUSSELL, H.D., MALHERBE, S.J. VAN ROOYEN, D.P. and R. COOKE., 1962. The geology of the Olifants River Area, Transvaal: Explan. Sheets 2429B (Chuniespoort) and 2430A (Wolkberg), Geol. Surv. S.Africa 87pp.

SHARPE, M.R., 1978. 'Cone-type' diabases from the Eastern Transvaal - Representatives of a quenched magma. Trans. Geol. Soc. S. Africa. v81, p.373-378.

—————————, 1980. Evolution of the Bushveld Magma chambers. Inst. for Geological Research on the Bushveld Complex. Univ. of Pretoria. Res. Rept. No. 20, 57pp.

—————————, 1981. The chronology of magma influxes to the eastern compartment of the Bushveld Complex as exemplified by its marginal border groups. Journ. Geol. Soc. Lond. v138, p.307-326.

—————————, 1982. Noble metals in the marginal rocks of the Bushveld Complex. Econ. Geol. v77, p.1286-1295.

—————————, 1982. Petrography, classification and chronology of mafic sills beneath the Eastern Bushveld Complex. Inst. for Geol. Res. on the Bushveld Complex, Univ. of Pretoria, Res. Rept. No.37, 51pp.

—————————, BAHAT, D. and VON GRUENEWALDT, G., 1981. The concentric elliptical structure of feeder sites to the Bushveld Complex and possible economic implications. Trans. Geol. Soc. S. Africa v84, p.239-244.

————————— and CHADWICK, B., 1982. Structures in Transvaal Sequence rocks within and adjacent to the eastern compartment of the Bushveld Complex. Trans. Geol. Soc. S. Africa v85, p.29-41.

————————— and HULBERT, L.J., 1985. Ultramafic sills beneath the eastern Bushveld Complex: Mobilized suspensions of early lower zone cumulates in a parental liquid with boninitic affinities. Econ. Geol. v80, p.849-871.

————————— and IRVINE, T.N., 1983. Melting relations of two Bushveld chilled marginal rocks and implications for the origin of chromitite. Carnegie Inst. Washington, Yearbook 82, p.295-300.

————————— and SNYMAN, J.A., 1980. A model for the emplacement of the eastern compartment of the Bushveld Complex. Tectonophysics v65, p.85-110.

SHAW, D.M., 1970. Trace element fractionation during anatexis. Geochim. Cosmochim. Acta v34, p.237-243.

SHIMIZU, N. and ARCULUS, R.J., 1975. Rare earth element concentrations in a suite of basanitoids and alkali olivine basalts from Grenada, Lesser Antilles. Contrib. Mineral Petrol. v50, p.231-240.

SHIRLEY, D. N., 1986. Compaction of igneous cumulates. Journ. of Geology v94, p.795-809.

SOHL, N., 1977. Application for amendment concerning terminology for igneous and high grade metamorphic rocks. Bull. Am. Ass. Petrol. Geol. v61, p.248-252.

SPRY, A., 1967. Metamorphic Textures. 1st ed. Pergamon Press, Oxford, 350pp.

STRECKEISEN, A., 1976. To each plutonic rock its proper name. Earth Sci. Reviews v12, p.1-33.

SUN, S., NESBITT, R.W., and SHARASKIN, A.Y., 1979. Geochemical characteristics of mid-ocean ridge basalts. Earth and Plan. Sci. Letters v44, p.119-138.

SUN, S. and HANSON, G.N., 1975. Origin of Ross Island basanitoids and limitations on the heterogeneity of mantle sources for alkali basalts and nephelinites. Contrib. Mineral. Petrol. v52, p.77-106.

TANKARD, A.J., JACKSON, M. P. A., ERIKSSON, K.A., HOBDAY, D.K., HUNTER, D.R. and MINTER, W.E.L., 1982. Crustal evolution of southern Africa, 3.8 billion years of earth history. Springer-Verlag, New York, Heidelberg, Berlin, 523pp.

TAYLOR, S.R. and McCLENNAN, S., 1985. The Continental Crust: its Composition and Evolution. Blackwell Scientific Publications, Oxford, 312 pp.

TAIT, S.R., HUPPERT, H.E. and SPARKS, R.S.J., 1984. The role of compositional convection in the formation of adcumulus rocks. Lithos v17, p.139-146.

THORNTON, C.P. and TUTTLE, O.F., 1960. Chemistry of igneous rocks, 1. Differentiation Index. Am. J. Sci. v258, p.664-684.

TUTTLE, O.F. and BOWEN, N.L., 1958. Origin of granite in the light of experimental studies in the system $NaAlSi_2O_8$ - $KAlSi_2O_8$ - H_2O. Geol. Soc. America, Mem.74.

TWIST, D. and FRENCH, B.M., 1983. Voluminous acid volcanism in the Bushveld Complex: A review of the Rooiberg felsite. Bull. volcanol. v46, p.225-242.

TWIST, D. and HARMER, R.E., 1987. Geochemistry of contrasting siliceous magmatic suites in the Bushveld Complex: Genetic aspects and implications for tectonic discrimination diagrams. Journ. of volcanol. and geotherm. res. v32, p.83-98.

VAN DER MERWE, M.J., 1976. The layered sequence of the Potgietersrus limb of the Bushveld Complex. Econ. Geol. v71, p.1337-1351.

VERMAAK, C.F., 1976. The Merensky Reef - thoughts on its environment and genesis. Econ. Geol. v71, p.261-285.

VILJOEN, M.J. and SCOON, R.J., 1985. The distribution and main geologic features of discordant bodies of iron-rich ultramafic pegamatite in the Bushveld Complex. Econ. Geol. v80, p.1109-1128.

VOLLMER, R., 1976. Rb-Sr and U-Th-Pb systematics of alkaline rocks: Geochim. Cosmochim. Acta v40, p.283-295.

VON GRUENEWALDT, G., 1971. A petrographical and mineralogical investigation of the rocks of the Bushveld Igneous Complex in the Tauteshoogte-Roossenekal area of the Eastern Transvaal. Unpub. DSc. thesis, Univ. of Pretoria, 228pp.

——————————, 1973. The Main and Upper Zones of the Bushveld Complex in the Roossenekal area, Eastern Transvaal. Trans. Geol. Soc. S. Africa v76, p.207-227.

——————————, SHARPE, M.R. and HATTON, C.J., 1985. The Bushveld Complex: Introduction and Review. Econ. Geol. v80, p.803-812.

WADSWORTH, W.J., 1985. Terminology of postcumulus processes and products in the Rhum layered intrusion. Geol. Mag. v122, p.549-54.

WAGER, L.R. and BROWN, G.M., 1968. Layered Igneous Rocks. Oliver and Boyd, Edinburgh and London, Chapter XIV. The Bushveld Intrusion, South Africa p.343-407.

——————————————, and WADSWORTH, W.J., 1960. Types of igneous cumulates. Journ. Petrol. vl, p.73-85.

WAGNER, P.A., 1929. The platinum deposits and mines of South Africa. Oliver and Boyd, Edinburgh and London, 326pp.

——————————, and MELLOR, E.T., 1925. On platinum - bearing hortonolite dunite of the Lydenburg district, Transvaal. Trans. Geol. Soc. S. Africa v28, p.1-18.

WALKER, D., KIRKPATRICK, R.J., LONGHI, J. and HAYS, J.F., 1976. Crystallisation history of lunar picritic basalt sample 12002: phase equilibria and cooling rate studies. Geol. Soc. Amer. Bull. 87, p.646-656.

WALKER D.A. and CAMERON, W.E., 1983. Boninite primary magmas: evidence from the Cape Vogel peninsula, PNG. Contrib. Mineral. Petrol. v83, p.150-158.

WALLMACH, T., HATTON, C.J. and DROOP, G.T.R., 1989. Extreme facies of contact metamorphism developed in calc-silicate xenoliths in the eastern Bushveld Complex. Can. Mineralogist v27, p.509-523.

WALRAVEN, F., 1974. Tectonism during the emplacement of the Bushveld Complex and the resulting fold structures. Trans. Geol. Soc. S. Africa v77, p.323-328.

WARNER, R.D., SNIPES, D.S., HUGHES, S.S., STEINER, J.C., DAVIS, M.W., MANOOGIAN, P.R. and SCHMITT, R.A. 1985. Olivine-normative dolerite dikes from western South Carolina: Mineralogy, chemical composition and petrogenesis. Contrib. Mineral. Petrol. v90, p.386.

WATSON, E.B., 1982. Basalt contamination by continental crust: some experiments and models. Contrib. Mineral. Petrol. v80, p.73-87.

WEBER C., BARBEY, P., CUNEY, M.J., MARTIN, H. Trace element behaviour during migmatization. Evidence for a complex melt-residuum-fluid interaction in the St. Malo migmatitic dome (France). 1985. Contrib. Mineral. Petrol. v90, p.52-62.

WEDEPOHL, K.H., 1972. (ed.) Handbook of Geochemistry 11/2. B1-N9. Springer - verlag Berlin.

WEINSTEIN, S.A., YUEN, D.A. and OLSON, P.J., 1988. Evolution of crystal - settling in magma-chamber convection. Earth and Plan. Sci. Letters v87, p.237-248.

WELLS, P.R.A., 1977. Pyroxene thermometry in simple and complex systems. Contrib. Mineral Petrol. v62, p.129-139.

WHITE, A.J.R. and CHAPPELL, B.W., 1977. Ultrametamorphism and granitoid genesis. Tectonophysics v43, p.7-22.

WILCOX, R.E., 1979. The liquid line of descent and variation diagrams. p.205-224. In Yoder, H.S. (Ed.). The evolution of the Igneous Rocks (Fiftieth Anniversary Perspectives). Princeton University Press, Princeton, New Jersey. 588pp.

WILLEMSE, J., 1959. The 'floor' of the Bushveld Igneous Complex and its relationships, with special reference to the eastern Transvaal Trans. Geol. Soc. S. Africa v62, p.21-83.

———————, 1969. The geology of the Bushveld Igneous Complex, the largest repository of magmatic ore deposits in the world. Econ. Geol. Monograph v4, p.1-22.

———————, and BENSCH, J.J., 1964. Inclusions of original carbonate rocks in gabbro and norite of the eastern part of the Bushveld Complex. Trans. Geol. Soc. S. Africa v67, p.1-84.

WINCHESTER, J.A., and FLOYD, P.A., 1976. Geochemical magma type discrimination; application to altered and metamorphosed basic igneous rocks. Earth and Plan. Sci. Letters, v28, p.459-469.

WOOD, B.J., and BANNO, S., 1973. Garnet-orthopyroxene and orthopyroxene-clinopyroxene relationships in simple and complex systems. Contrib. Mineral. Petrol. v42, p.109-124.

———————, and FRASER, D.G., 1976. Elementary thermodynamics for geologists. Oxford University Press, Oxford, 303pp.

WOOD, D.A., 1979. Dynamic partial melting: its application to the petrogenesis of basalts erupted in Iceland, the Faeroe Islands, the Isle of Skye (Scotland) and the Troodos Massif (Cyprus). Geochim. Cosmochim. Acta v43, p.1031-1046.

WRIGHT, T.L., 1974. Presentation and interpretation of chemical data for igneous rocks. Contrib. Mineral. Petrol. v48, p.233-248.

WYLLIE, P.J., 1977. Crustal anatexis: an experimental review. Tectonophysics, V43, p.42-72.

YODER, H.S. and TILLEY, C.E., 1962. Origin of basalt magmas: an experimental study of natural and synthetic rock systems. Journ. Petrol. v3, p.342-532.

ANALYTICAL PROCEDURES

For each sample, approximately 4 kg of fresh material was collected by hammer, with weathered surfaces being removed as far as possible in the field. These samples were then crushed to ±40 mm chips and any remaining weathered surfaces and or veins etc. removed by hand picking. Further crushing reduced the material to ±5 mm chips from which the fines were discarded. These chips were then split by use of a riffle box and powdered in a tungsten carbide Beuhler swing mill. (Samples used in the REE and isotope analyses were prepared by collecting a further ±10 kg of sample from the appropriate outcrop. This was crushed and split in the same fashion except that approximately 1 kg of the 5 mm chips were powdered in carbon steel mills).

All samples were analysed in duplicate on a Siemens SRS-1 XRF spectrometer, with major elements SiO_2, TiO_2, Al_2O_3, total iron as Fe_2O_3, MnO, MgO, CaO, K_2O, P_2O_5, Cr_2O_3 and NiO being determined on glass discs, using a method developed by the University of Cape Town based on that of Norrish and Hutton (1969). Trace elements and Na_2O were determined on pressed powder pellets.

Using standards JG-1, JB-1, AGV-1, BCR-1, G-2, PCC-1, GSP-1, MRG-1, NIM-N, NIM-P and NIM-D, maximum absolute errors in accuracy (weight per cent) were at the following levels: SiO_2 ±0.372, TiO_2 ±0.019, Al_2O_3 ±0.126, Fe_2O_3 ±0.075, MnO ±0.003, MgO ±0.035, CaO ±0.060, K_2O ±0.021, P_2O_5 ±0.011, Cr_2O_3 ±0.009 and NiO ±0.010. Similarly for trace elements, values (ppm) were as follows: Cr ±4, Cu ±2, Ni ±3, Zn ±1, Rb ±2, Sr ±2, Y ±2, and Zr ± 4. Precision (1 std. dev.) in all cases was better than ±40 per cent of the absolute error. FeO was calculated by setting Fe_2O_3 equal to TiO_2 + 1.5, following the convention of Irvine and Baragar (1971), and adjusting the remaining value such that FeO = Fe_2O_3 X 0.8998.

<u>N.B.</u> Values given in Appendix 1 have not been normalised to the respective hydrous total because LOI values are used in the text (chapter 7.2.). However all other values referred to in the text are expressed LOI and H_2O- free, where the major element chemistry has been normalised to the hydrous total.

APPENDIX 1
MAJOR ELEMENT ANALYSES
(QUENCH-TEXTURED MICROPYROXENITES)

SAMPLE NO.	DI-5	DI-6	DI-7A	DI-7B	DI-8C	DI-8H	DI-19
SiO_2	55.17	55.32	54.46	55.02	55.20	55.20	55.38
TiO_2	0.31	0.39	0.32	0.32	0.34	0.34	0.37
Al_2O_3	10.42	12.39	10.31	10.20	11.27	11.06	12.54
Fe_2O_3	1.81	1.89	1.82	1.82	1.84	1.84	1.87
FeO	7.70	7.77	7.46	7.32	7.54	7.27	7.22
MnO	0.16	0.17	0.18	0.17	0.17	0.17	0.18
MgO	14.66	11.03	15.15	14.51	13.42	13.33	11.33
CaO	5.92	7.02	6.22	6.17	6.56	6.55	7.47
Na_2O	1.66	1.44	1.74	2.14	1.67	1.77	1.64
K_2O	0.98	0.99	0.75	0.74	0.81	0.78	0.86
P_2O_5	0.08	0.10	0.07	0.07	0.09	0.08	0.09
H_2O-	0.01	0.06	0.11	0.18	0.10	0.19	0.05
LOI	0.87	0.79	0.85	0.72	0.65	0.67	0.69
TOTAL	99.75	99.36	99.44	99.38	99.66	99.25	99.69

SAMPLE NO.	DI-22	DI-23	DI-24	DI-25	DI-28	DI-29	DI-30
SiO_2	54.74	54.20	55.16	55.35	54.82	55.20	55.47
TiO_2	0.28	0.46	0.31	0.37	0.37	0.40	0.35
Al_2O_3	9.76	13.40	9.37	11.91	11.91	12.39	11.93
Fe_2O_3	1.78	1.96	1.81	1.87	1.87	1.90	1.86
FeO	7.49	7.52	7.39	7.46	7.94	7.27	7.52
MnO	0.17	0.19	0.17	0.17	0.19	0.17	0.17
MgO	16.49	10.38	16.56	12.12	12.00	11.96	12.31
CaO	6.71	6.94	5.33	7.09	7.46	6.88	6.81
Na_2O	1.57	1.73	1.45	1.60	1.51	1.29	1.67
K_2O	0.81	1.29	0.97	1.04	0.78	1.23	1.03
P_2O_5	0.06	0.10	0.06	0.09	0.09	0.09	0.08
H_2O-	0.01	0.04	0.18	0.09	0.06	0.00	0.18
LOI	0.70	1.75	0.66	0.61	0.00	0.86	0.70
TOTAL	99.57	99.96	99.42	99.77	98.97	99.64	100.08

APPENDIX 1
MAJOR ELEMENT ANALYSES
(QUENCH-TEXTURED MICROPYROXENITES)

SAMPLE NO.	DI-31	DI-34	DI-36	DI-42C	DI-45	DI-53	DI-56
SiO_2	54.20	54.00	55.22	55.60	55.60	56.18	55.43
TiO_2	0.36	0.39	0.37	0.44	0.36	0.43	0.36
Al_2O_3	11.52	11.62	11.85	11.26	10.36	11.63	11.95
Fe_2O_3	1.86	1.89	1.87	1.94	1.86	1.93	1.86
FeO	7.92	7.98	7.36	8.52	7.17	7.27	7.54
MnO	0.18	0.20	0.26	0.19	0.18	0.17	0.17
MgO	12.16	12.72	12.11	13.25	14.72	10.67	12.59
CaO	6.21	6.59	6.98	5.96	5.64	7.11	6.97
Na_2O	1.45	1.55	1.59	1.10	1.73	3.06	2.04
K_2O	0.96	0.76	0.99	0.81	0.95	1.01	0.83
P_2O_5	0.08	0.08	0.09	0.10	0.07	0.09	0.08
H_2O-	0.00	0.13	0.09	0.06	0.12	0.11	0.10
LOI	2.88	1.71	0.17	0.00	1.23	0.15	0.00
TOTAL	99.78	99.62	98.95	99.23	99.99	99.81	99.92

SAMPLE NO.	DI-57A	DI-59B	DI-59C	DI-61	DI-70	DI-74	DI-77
SiO_2	55.22	55.28	55.84	55.23	54.67	55.55	55.37
TiO_2	0.44	0.36	0.33	0.34	0.31	0.36	0.35
Al_2O_3	11.68	11.30	11.13	11.03	9.39	11.75	11.22
Fe_2O_3	1.94	1.86	1.83	1.84	1.81	1.86	1.85
FeO	7.61	7.43	7.45	7.70	7.49	7.61	7.90
MnO	0.17	0.17	0.17	0.18	0.18	0.17	0.19
MgO	13.10	13.47	13.10	13.56	17.13	12.72	13.43
CaO	6.53	7.01	6.66	6.78	5.25	6.85	6.83
Na_2O	1.95	1.60	2.23	1.98	1.85	1.09	1.47
K_2O	0.86	0.81	0.76	0.66	0.95	0.83	0.90
P_2O_5	0.10	0.07	0.08	0.09	0.06	0.07	0.09
H_2O-	0.06	0.13	0.09	0.10	0.09	0.06	0.07
LOI	0.05	0.17	0.00	0.08	0.61	0.44	0.25
TOTAL	99.71	99.66	99.67	99.57	99.79	99.36	99.92

APPENDIX 1
MAJOR ELEMENT ANALYSES
(MICROGABBRONORITE)

SAMPLE NO.	K-18	K-22	K-30AG	K-30AT	KWR-30A(2)	KWR-38A(1)	KWR-38A(2)
SiO_2	50.25	49.55	49.87	49.99	49.08	50.30	47.88
TiO_2	0.49	0.63	0.32	0.31	0.49	0.49	0.47
Al_2O_3	16.57	16.29	16.83	16.70	15.51	16.54	15.15
Fe_2O_3	1.99	2.13	1.82	1.80	1.99	1.99	1.97
FeO	10.73	9.64	9.56	9.45	9.64	9.08	10.51
MnO	0.21	0.22	0.25	0.25	0.21	0.20	0.22
MgO	8.38	7.55	8.85	8.57	9.77	8.37	9.35
CaO	10.78	10.78	10.51	10.53	11.40	10.89	12.07
Na_2O	1.62	1.78	0.95	0.99	1.44	1.97	1.44
K_2O	0.13	0.39	0.36	0.37	0.38	0.19	0.21
P_2O_5	0.09	0.18	0.12	0.12	0.11	0.11	0.03
H_2O-	0.08	0.04	0.25	0.19	0.13	0.04	0.06
LOI	0.00	0.00	0.00	0.00	0.00	0.00	0.00
TOTAL	101.32	99.18	99.69	99.28	100.15	100.17	100.36

SAMPLE NO.	K-50	K-108A	KWR-108A	K-108B	K-109	KWR-109	KWR-113A
SiO_2	50.59	50.82	49.24	50.74	49.80	50.27	50.16
TiO_2	0.61	0.74	0.90	0.84	0.84	0.82	0.57
Al_2O_3	16.44	15.33	16.13	15.40	15.54	15.51	16.08
Fe_2O_3	2.11	2.24	2.40	2.34	2.34	2.32	2.07
FeO	9.36	9.40	10.05	9.38	9.58	10.68	8.50
MnO	0.20	0.20	0.21	0.19	0.20	0.22	0.21
MgO	7.70	8.28	7.96	7.17	7.49	6.32	8.05
CaO	10.48	10.56	11.53	10.74	10.83	10.63	10.68
Na_2O	2.21	2.26	1.59	2.33	2.43	2.28	1.88
K_2O	0.24	0.20	0.17	0.21	0.21	0.35	0.27
P_2O_5	0.18	0.16	0.20	0.18	0.19	0.23	0.13
H_2O-	0.07	0.09	0.01	0.09	0.01	0.05	0.10
LOI	0.00	0.00	0.00	0.00	0.00	0.00	0.00
TOTAL	100.19	100.28	100.39	99.61	99.46	99.68	99.70

APPENDIX 1
MAJOR ELEMENT ANALYSES
(MICROGABBRONORITE)

SAMPLE NO.	KWR-113Q	K-149A	K-159	KWR-160	K-160A	KWR-178AC	KWR-178A
SiO_2	51.08	52.61	48.98	50.09	51.19	50.48	50.42
TiO_2	0.65	0.23	0.80	0.72	0.60	0.64	0.64
Al_2O_3	15.02	16.97	16.81	16.06	15.92	16.53	16.58
Fe_2O_3	2.15	1.73	2.30	2.22	2.10	2.14	2.14
FeO	9.56	6.67	10.74	9.51	8.83	9.48	9.30
MnO	0.20	0.18	0.22	0.21	0.19	0.19	0.20
MgO	8.24	7.67	6.25	7.78	8.02	7.66	7.57
CaO	10.67	11.25	10.92	11.12	10.84	9.80	9.93
Na_2O	2.11	2.20	1.95	2.01	2.24	1.99	2.06
K_2O	0.17	0.38	0.38	0.28	0.29	0.46	0.46
P_2O_5	0.15	0.04	0.24	0.16	0.12	0.19	0.19
H_2O	0.07	0.07	0.07	0.08	0.02	0.16	0.11
LOI	0.00	0.00	0.00	0.00	0.00	0.00	0.00
TOTAL	100.07	100.00	99.66	100.24	100.36	99.72	99.60

SAMPLE NO.	KWR-194	KWR-194BC	KWR-194BH	KWR-195	KWR-207	KWR-248 (2)	KWR-255(1A)
SiO_2	51.37	50.37	50.17	50.26	50.08	50.45	51.51
TiO_2	0.47	0.26	0.25	0.45	0.75	0.28	0.52
Al_2O_3	15.31	17.13	17.13	16.19	16.57	16.29	14.04
Fe_2O_3	1.97	1.97	1.75	1.96	2.25	1.78	2.02
FeO	8.12	6.20	6.28	9.28	10.26	7.24	7.86
MnO	0.20	0.16	0.16	0.20	0.22	0.16	0.17
MgO	8.30	10.74	10.72	7.68	6.64	8.89	9.95
CaO	11.67	10.74	9.73	11.08	10.62	12.15	9.93
Na_2O	2.17	1.80	1.57	1.93	2.29	1.94	1.87
K_2O	0.22	0.15	0.15	0.22	0.25	0.24	0.52
P_2O_5	0.12	0.07	0.07	0.12	0.20	0.04	0.12
H_2O	0.10	0.16	0.17	0.11	0.12	0.03	0.06
LOI	0.00	0.09	0.12	0.00	0.00	0.07	0.18
TOTAL	100.02	100.20	98.27	99.48	100.25	99.56	98.75

APPENDIX 1
MAJOR ELEMENT ANALYSES

	(MICROGABBRONORITE)				(OLIVINE-PYROXENITE)	
SAMPLE NO.	KWR-255 (1B)	KWR-255 (2)	KWR-264 AC	KWR-264 AH	DI-75	DI-76
SiO_2	51.68	51.05	50.50	50.32	54.04	53.64
TiO_2	0.53	0.44	0.42	0.44	0.22	0.30
Al_2O_3	14.04	14.64	15.01	14.97	6.57	8.11
Fe_2O_3	2.03	1.94	1.92	1.94	1.72	1.80
FeO	8.03	8.15	7.71	7.73	7.39	8.07
MnO	0.17	0.18	0.17	0.17	0.16	0.18
MgO	10.39	10.03	10.21	10.25	23.01	20.69
CaO	9.90	10.87	11.23	11.20	3.99	4.54
Na_2O	1.89	1.82	1.58	1.54	1.48	1.55
K_2O	0.53	0.53	0.61	0.60	0.39	0.80
P_2O_5	0.13	0.11	0.06	0.06	0.03	0.06
H_2O-	0.12	0.08	0.16	0.13	0.03	0.06
LOI	0.11	0.00	0.35	0.42	0.00	0.00
	99.55	99.84	99.93	99.77	99.03	99.80

METADOLERITES

SAMPLE NO.	DI-62	DI-63	DI-63A	DI-64	DI-65	DI-66	DI-67
SiO_2	51.15	49.16	49.67	51.26	51.07	50.72	50.50
TiO_2	0.65	1.12	1.10	0.62	1.01	0.64	1.23
Al_2O_3	13.83	14.08	14.23	14.32	13.29	14.00	15.36
Fe_2O_3	2.15	2.62	2.60	2.12	2.51	2.14	2.73
FeO	8.70	9.86	9.37	8.46	10.31	8.60	8.60
MnO	0.19	0.19	0.21	0.19	0.23	0.18	0.17
MgO	7.53	8.14	7.47	7.62	7.71	7.92	6.85
CaO	8.53	10.45	10.52	9.94	9.51	10.41	10.11
Na_2O	1.52	1.64	2.14	2.11	1.92	2.23	1.86
K_2O	0.35	0.61	0.18	0.36	0.71	0.62	0.67
P_2O_5	0.09	0.17	0.15	0.08	0.09	0.08	0.19
H_2O-	0.24	0.22	0.22	0.15	0.13	0.16	0.10
LOI	3.48	1.55	1.57	2.13	1.53	2.47	1.84
TOTAL	98.41	99.81	99.43	99.36	100.02	100.17	100.21

APPENDIX 1
MAJOR ELEMENT ANALYSES
(META QUARTZ-DOLERITES)

SAMPLE NO.	DI-2G	DI-2T	DI-3G	DI-3T	DI-4	DI-7A
SiO_2	54.14	54.76	54.49	54.58	55.89	54.84
TiO_2	0.50	0.48	0.44	0.45	0.54	0.46
Al_2O_3	15.86	16.02	15.93	15.71	15.78	16.20
Fe_2O_3	2.00	1.98	1.94	1.95	2.04	1.96
FeO	6.71	6.55	6.82	6.67	6.81	6.42
MnO	0.15	0.15	0.18	0.18	0.15	0.14
MgO	7.15	7.22	6.21	6.16	5.87	6.84
CaO	8.22	8.27	8.47	8.41	8.05	8.52
Na_2O	1.91	1.79	1.82	1.82	1.70	1.53
K_2O	1.06	1.05	1.34	1.34	1.42	1.12
P_2O_5	0.11	0.10	0.12	0.11	0.12	0.10
H_2O-	0.17	0.14	0.22	0.15	0.12	0.08
LOI	2.06	1.92	2.36	2.33	1.92	1.60
	100.04	100.43	100.34	99.86	100.41	99.81

SAMPLE NO.	DI-9	DI-12	DI-15	DI-16	DI-17	DI-18
SiO_2	54.71	56.57	55.94	55.05	54.10	54.53
TiO_2	0.47	0.46	0.47	0.58	0.56	0.48
Al_2O_3	15.83	16.09	15.25	15.36	15.74	15.27
Fe_2O_3	1.97	1.96	1.97	2.08	2.06	1.98
FeO	6.57	6.53	7.17	6.88	7.14	7.64
MnO	0.15	0.13	0.15	0.19	0.19	0.18
MgO	6.57	5.51	6.20	6.83	6.44	6.54
CaO	8.47	7.24	7.63	8.14	8.41	8.88
Na_2O	1.79	1.99	1.80	1.93	1.75	1.20
K_2O	1.05	1.95	1.67	1.20	1.27	1.27
P_2O_5	0.10	0.13	0.12	0.13	0.13	0.11
H_2O-	0.07	0.08	0.07	0.07	0.09	0.00
LOI	2.15	2.13	2.02	1.81	1.87	1.98
	99.90	100.77	100.46	100.25	99.75	100.06

APPENDIX 1
MAJOR ELEMENT ANALYSES
(META QUARTZ-DOLERITES)

SAMPLE NO.	DI-20	DI-21	DI-26	DI-27	DI-32	DI-33
SiO_2	55.86	54.61	55.34	54.74	55.16	54.43
TiO_2	0.43	0.39	0.43	0.40	0.44	0.45
Al_2O_3	14.02	15.59	13.51	14.40	15.71	15.51
Fe_2O_3	1.93	1.89	1.93	1.91	1.94	1.95
FeO	7.27	6.69	7.22	7.09	6.87	7.68
MnO	0.17	0.15	0.16	0.18	0.16	0.17
MgO	7.24	7.34	8.22	7.83	6.64	6.31
CaO	7.72	7.93	7.20	7.72	7.56	8.70
Na_2O	1.33	1.53	1.81	1.71	1.31	1.27
K_2O	1.29	1.12	1.50	1.27	1.39	1.16
P_2O_5	0.11	0.01	0.11	0.10	0.11	0.10
H_2O-	0.07	0.00	0.02	0.18	0.13	0.16
LOI	2.25	2.43	2.42	1.64	2.32	1.86
	99.69	99.68	99.87	99.17	99.74	99.75

SAMPLE NO.	DI-35	DI-37	DI-38	DI-39	DI-41	DI-43
SiO_2	54.10	54.25	55.82	54.21	56.58	56.76
TiO_2	0.52	0.38	0.55	0.36	0.59	0.64
Al_2O_3	16.05	13.39	15.13	16.12	15.86	15.02
Fe_2O_3	2.02	1.88	2.05	1.87	2.09	2.14
FeO	7.05	6.75	7.40	6.76	7.93	7.77
MnO	0.16	0.14	0.17	0.16	0.15	0.16
MgO	6.98	5.71	7.52	7.90	5.79	5.96
CaO	8.41	8.91	7.72	9.17	7.76	7.90
Na_2O	1.15	1.67	1.71	1.79	1.73	1.82
K_2O	1.16	0.88	1.20	0.76	1.36	1.34
P_2O_5	0.11	0.09	0.11	0.08	0.13	0.15
H_2O-	0.15	0.15	0.09	0.09	0.03	0.07
LOI	1.90	1.39	1.23	0.91	1.08	0.25
	99.76	99.59	99.70	100.18	100.08	99.98

APPENDIX 1
MAJOR ELEMENT ANALYSES
(META QUARTZ-DOLERITES)

SAMPLE NO.	DI-20	DI-21	DI-26	DI-27	DI-32	DI-33
SiO_2	56.42	55.24	55.27	55.04	57.84	54.74
TiO_2	0.56	0.46	0.50	0.55	0.51	0.40
Al_2O_3	15.65	15.06	13.93	15.15	15.09	16.17
Fe_2O_3	2.06	1.96	2.00	2.05	2.01	1.90
FeO	6.80	7.26	7.02	7.07	5.45	6.86
MnO	0.15	0.13	0.20	0.16	0.16	0.16
MgO	5.29	5.94	8.52	6.90	6.49	7.66
CaO	7.79	8.22	6.91	8.22	6.49	8.77
Na_2O	1.52	1.30	1.59	1.68	2.25	1.83
K_2O	1.57	1.41	1.25	1.14	1.50	1.07
P_2O_5	0.12	0.12	0.11	0.12	0.09	0.09
H_2O-	0.00	0.34	0.30	0.17	0.18	0.15
LOI	2.41	2.40	2.25	1.84	2.03	0.39
	100.34	99.84	99.85	100.09	100.09	100.19

SAMPLE NO.	DI-57	DI-58	DI-60	DI-68	DI-69	DI-73
SiO_2	56.35	54.57	54.24	56.69	56.71	54.95
TiO_2	0.54	0.34	0.55	0.56	0.57	0.55
Al_2O_3	16.02	15.66	15.41	15.13	15.41	15.18
Fe_2O_3	2.04	1.84	2.05	2.06	2.07	2.05
FeO	6.83	6.64	6.83	7.07	7.42	7.65
MnO	0.15	0.15	0.17	0.16	0.17	0.19
MgO	7.05	8.79	7.65	5.69	6.02	6.49
CaO	7.13	8.28	7.89	8.31	7.53	7.99
Na_2O	1.60	1.53	1.40	1.82	1.56	1.85
K_2O	1.44	1.18	0.64	1.05	1.95	1.16
P_2O_5	0.12	0.08	0.06	0.13	0.14	0.12
H_2O-	0.10	0.12	0.25	0.07	1.12	1.14
LOI	0.61	0.64	1.70	0.78	1.14	1.79
	99.98	99.82	99.84	99.52	99.81	100.11

APPENDIX 1
MAJOR ELEMENT GEOCHEMISTRY
(MIDDELWATER LAYERED SILL – META QUARTZ DOLERITES)

SAMPLE NO.	KM–2	K–7A	K–7B	K–8B	KWR–11	KWR–21B	KG–23A
SiO_2	57.47	52.88	53.95	54.13	56.92	58.57	55.57
TiO_2	0.59	0.29	0.37	0.35	0.66	0.52	0.40
Al_2O_3	14.29	16.95	16.32	16.34	14.12	15.22	14.96
Fe_2O_3	2.09	1.79	1.87	1.85	1.16	2.02	1.90
FeO	7.03	5.38	5.64	5.66	7.04	6.43	6.37
MnO	0.17	0.13	0.13	0.13	0.16	0.09	0.15
MgO	4.69	9.41	8.36	7.85	4.24	4.08	7.32
CaO	6.98	9.18	8.01	8.01	7.27	6.62	8.21
Na_2O	2.14	1.63	1.73	1.52	2.69	1.46	2.26
K_2O	1.87	0.62	1.18	1.11	1.98	1.69	1.13
P_2O_5	0.13	0.08	0.08	0.07	0.15	0.12	0.09
H_2O-	0.13	0.11	0.01	0.16	0.18	0.01	0.04
LOI	1.23	1.30	1.84	1.81	0.99	2.34	1.08
TOTAL	98.81	99.75	99.49	98.99	98.56	99.17	99.48

SAMPLE NO.	K–27A	K–27B	KWR–28	K–28A(2)	KWR–38	KWR–46A	KWR–52
SiO_2	54.00	51 70	53.81	54.39	57.14	53.34	53.81
TiO_2	0.38	0.20	0.37	0.41	0.56	0.37	0.38
Al_2O_3	15.49	17.40	15.68	15.70	14.92	16.14	15.84
Fe_2O_3	1.88	1.70	1.87	1.91	2.06	1.84	1.88
FeO	5.55	4.04	5.60	5.85	6.43	5.26	6.71
MnO	0.15	0.12	0.15	0.14	0.14	0.13	0.17
MgO	7.44	9.29	7.10	6.55	4.75	7.11	7 26
CaO	10.12	12.82	10.72	10.21	7.69	10.57	8.30
Na_2O	2.01	1.63	1.89	1.88	2.44	1.88	1.49
K_2O	0.98	0.46	0.82	0.91	1.78	0.93	0.10
P_2O_5	0.08	0.06	0.09	0.09	0.14	0.08	0.10
H_2O-	0.13	0.11	0.10	0.14	0.00	0.13	0.04
LOI	0.00	0.00	0.00	0.00	0.00	0.00	0.00
TOTAL	99.92	100.06	99.32	99.79	99.40	99.40	99.04

APPENDIX 1

MAJOR ELEMENT GEOCHEMISTRY

(MIDDELWATER LAYERED SILL – META QUARTZ DOLERITES)

SAMPLE NO.	KWR-54	KWR-55	K-60	K-60B(1)	K-60B(2)	KG-61	KG-71
SiO_2	54.34	53.81	57.91	58.58	59.11	55.53	53.80
TiO_2	0.45	0.39	0.62	0.65	0.66	0.47	0.36
Al_2O_3	15.10	16.04	14.15	15.06	15.26	15.29	15.71
Fe_2O_3	1.95	1.89	2.12	2.15	2.17	1.97	1.86
FeO	7.61	7.24	6.68	5.42	5.45	7.37	6.07
MnO	0.21	0.20	0.16	0.15	0.15	0.27	0.15
MgO	5.75	6.54	4.71	5.10	5.04	6.49	8.69
CaO	7.96	8.29	7.81	7.72	7.77	8.05	8.68
Na_2O	2.15	2.04	2.17	2.60	2.60	2.05	1.76
K_2O	1.45	1.30	1.39	0.61	0.61	1.41	0.90
P_2O_5	0.11	0.09	0.13	0.13	0.15	0.11	0.08
H_2O-	0.09	0.04	0.00	0.19	0.23	0.11	0.00
LOI	1.65	1.45	1.25	1.25	0.21	0.80	1.60
TOTAL	98.82	99.32	99.10	99.61	100.41	99.92	99.72

SAMPLE NO.	KWR-72B	KWR-118	KWR-118A	K-130	K-130A	KWR-152A
SiO_2	57.91	54.54	55.26	53.71	53.16	55.46
TiO_2	0.60	0.40	0.42	0.35	0.29	0.43
Al_2O_3	14.29	15.67	15.64	15.29	17.16	15.45
Fe_2O_3	2.10	1.90	1.92	1.85	1.79	1.93
FeO	6.87	7.20	7.49	5.47	5.48	7.27
MnO	0.16	0.17	0.17	0.15	0.14	0.19
MgO	4.73	7.09	6.38	7.38	8.89	5.95
CaO	7.83	8.20	8.28	10.97	8.92	8.29
Na_2O	2.39	1.81	1.96	1.79	1.76	2.09
K_2O	1.45	1.21	1.21	0.89	1.01	1.21
P_2O_5	0.13	0.10	0.10	0.08	0.06	0.11
H_2O-	0.18	0.00	0.21	0.12	0.07	0.05
LOI	1.08	1.65	0.77	1.64	1.09	0.51
TOTAL	99.72	98.94	99.81	99.69	99.82	98.94

APPENDIX 1
MAJOR ELEMENT ANALYSES
(QUARTZ-GABBRONORITE)

SAMPLE NO.	KBWR-9A	KBWR-9B	KBWR-18A	K-29(C)	K-29(H)	K-35(C)
SiO_2	57.27	54.19	54.51	54.89	54.33	55.46
TiO_2	0.55	0.40	0.37	0.44	0.44	0.80
Al_2O_3	15.25	15.96	15.14	15.56	15.60	14.66
Fe_2O_3	2.05	1.90	1.87	1.94	1.94	2.30
FeO	7.30	7.04	5.99	7.27	7.23	8.38
MnO	0.15	0.18	0.14	0.18	0.18	0.18
MgO	5.81	7.56	9.33	6.50	6.26	4.40
CaO	6.94	8.27	8.27	8.07	8.12	7.97
Na_2O	1.94	1.83	2.17	1.82	1.79	2.85
K_2O	1.31	0.91	0.75	1.31	1.32	1.30
P_2O_5	0.14	0.09	0.08	0.10	0.10	0.23
H_2O-	0.02	0.20	0.11	0.25	0.18	0.19
LOI	1.09	0.77	0.62	1.30	1.27	0.51
TOTAL	98.82	98.94	99.35	99.65	98.76	99.23

SAMPLE NO.	K-35(H)	KWR-222C	KWR-222H	KWR-225A	KWR225B	KWR-227
SiO_2	55.07	53.96	53.93	56.66	56.16	55.12
TiO_2	0.80	0.27	0.27	0.40	0.40	0.39
Al_2O_3	14.64	16.53	16.68	15.22	15.10	14.38
Fe_2O_3	2.30	1.77	1.77	1.90	1.90	1.89
FeO	8.40	5.90	5.88	7.24	7.09	6.98
MnO	0.18	0.14	0.14	0.11	0.12	0.15
MgO	4.36	8.68	8.91	5.46	5.66	9.03
CaO	8.00	8.95	8.99	7.79	7.77	8.24
Na_2O	2.83	1.91	1.96	2.15	2.05	1.99
K_2O	1.31	0.66	0.65	1.23	1.18	0.77
P_2O_5	0.23	0.06	0.07	0.10	0.10	0.10
H_2O-	0.28	0.15	0.22	0.02	0.14	0.02
LOI	0.51	0.26	0.22	1.16	1.96	0.23
TOTAL	98.91	99.24	99.69	99.44	98.63	99.39

APPENDIX 1
MAJOR ELEMENT ANALYSES
(QUARTZ-GABBRONORITE)

SAMPLE NO.	KWR-243A	KWR-243 B(1)	KWR-243 B(2)	KWR-246C	KWR-246H	K-247B
SiO_2	54.81	54.30	54.33	56.30	55.80	55.55
TiO_2	0.52	0.47	0.49	1.47	1.47	1.17
Al_2O_3	14.97	15.44	15.31	14.48	14.56	15.18
Fe_2O_3	2.02	1.97	1.99	2.97	2.97	2.67
FeO	8.56	7.72	7.85	7.56	7.53	7.06
MnO	0.18	0.18	0.18	0.15	0.15	0.15
MgO	5.55	6.22	6.35	4.02	3.91	4.56
CaO	8.67	8.30	8.17	5.69	5.69	6.85
Na_2O	1.81	1.85	1.78	4.49	4.51	4.41
K_2O	1.08	1.30	1.35	1.65	1.65	1.47
P_2O_5	0.13	0.11	0.12	0.37	0.35	0.28
H_2O-	0.20	0.26	0.29	0.12	0.19	0.10
LOI	0.46	0.61	0.51	0.00	0.04	0.00
TOTAL	98.96	98.73	98.72	99.44	98.82	99.45

SAMPLE NO.	KWR-249C	KWR-249H	KWR-257C	KWR-257H	KWR-258
SiO_2	54.85	55.75	53.03	52.70	54.55
TiO_2	0.38	0.39	0.43	0.43	0.50
Al_2O_3	14.37	14.42	16.25	16.25	15.19
Fe_2O_3	1.88	1.89	1.93	1.93	2.00
FeO	6.43	6.35	7.45	7.40	8.07
MnO	0.15	0.14	0.16	0.16	0.18
MgO	7.71	7.81	7.21	7.21	6.23
CaO	8.26	8.46	9.00	8.96	8.58
Na_2O	2.06	2.19	2.01	1.94	1.95
K_2O	1.05	1.06	0.97	0.93	1.39
P_2O_5	0.09	0.08	0.10	0.10	0.12
H_2O-	0.23	0.36	0.09	0.22	0.03
LOI	1.24	0.93	0.69	0.68	0.98
TOTAL	98.70	99.83	99.32	98.91	99.77

APPENDIX 1
MAJOR ELEMENT ANALYSES
(QUARTZOFELDSPATHIC ROCKS)

SAMPLE NO.	K-1	K-11A	K-39A	K-154A	KWR-72	KM-3	K-8C
SiO_2	59.51	70.53	63.35	64.17	72.65	66.02	66.28
TiO_2	0.66	0.44	0.72	0.86	0.36	0.54	0.85
Al_2O_3	14.16	12.38	13.24	12.61	12.03	13.08	2.39
Fe_2O_3	2.16	1.94	2.22	2.36	1.86	2.04	2.35
FeO	7.31	2.29	5.89	5.93	1.76	1.82	6.06
MnO	0.22	0.07	0.21	0.18	0.09	0.06	0.11
MgO	3.84	1.72	2.83	1.79	1.29	3.25	1.13
CaO	8.17	3.65	6.40	5.05	3.29	8.32	3.66
Na_2O	0.64	2.01	2.39	2.80	1.90	3.16	2.91
K_2O	1.62	3.33	1.24	2.84	3.33	1.42	2.72
P_2O_5	0.16	0.12	0.19	0.21	0.11	0.14	0.30
H_2O-	0.17	0.00	0.12	0.22	0.12	0.03	0.12
LOI	0.40	1.38	0.15	0.91	1.00	0.49	0.95
TOTAL	99.02	99.86	98.95	99.93	99.79	100.37	99.83

SAMPLE NO.	KWR-8G	KWR-8T	KWR-9	K-(32)	K-60A	K-72A
SiO_2	73.62	74.00	75.71	59.10	66.06	64.06
TiO_2	0.32	0.31	0.26	1.07	0.58	0.65
Al_2O_3	11.43	11.59	10.92	13.03	13.16	13.51
Fe_2O_3	1.82	1.81	1.76	2.57	2.08	2.15
FeO	1.25	1.11	0.84	9.29	4.30	5.90
MnO	0.05	0.05	0.04	0.20	0.13	0.15
MgO	1.80	1.62	1.63	2.43	2.23	2.82
CaO	2.76	2.81	2.30	5.28	4.56	5.04
Na_2O	1.72	1.80	1.55	2.86	2.14	2.07
K_2O	3.48	3.42	3.76	2.98	2.91	1.61
P_2O_5	0.09	0.08	0.09	0.30	0.14	0.13
H_2O-	0.29	0.12	0.10	0.17	0.03	0.02
LOI	0.87	0.79	0.80	0.68	1.36	1.50
TOTAL	99.50	99.51	99.76	99.69	99.68	99.61

APPENDIX 1
MAJOR ELEMENT ANALYSES
(LAMINATED HORNFELS)

SAMPLE NO.	ZI-IH	ZI-2H	DI-7E	DI-46H	DI-49BH	DI-59A	DI-75H
SiO_2	69.36	69.35	63.75	65.11	69.10	69.21	59.38
TiO_2	0.62	0.75	0.80	0.80	0.61	0.78	0.88
Al_2O_3	15.10	14.22	16.54	15.58	13.89	13.15	18.37
Fe_2O_3	2.12	2.25	2.30	2.30	2.11	2.28	2.38
FeO	1.80	3.50	4.23	4.20	3.16	3.55	5.66
MnO	0.04	0.06	0.10	0.06	0.04	0.10	0.13
MgO	2.10	2.43	2.99	4.00	3.78	2.37	3.80
CaO	0.47	0.48	0.71	0.66	0.69	1.23	0.65
Na_2O	1.68	1.31	1.11	1.48	1.57	4.22	1.30
K_2O	5.38	4.78	4.49	4.31	4.05	2.61	4.56
P_2O_5	0.25	0.25	0.32	0.22	0.19	0.23	0.25
H_2O-	0.05	0.03	0.04	0.03	0.04	0.04	0.09
LOI	1.13	1.14	1.89	1.34	0.77	0.08	1.22
TOTAL	100.10	100.55	98.27	100.09	100.00	99.85	98.67

(MASSIVE HORNFELS)

SAMPLE NO.	DI-10	DI-10A	DI-10B	DI-11	DI-13
SiO_2	62.70	60.63	60.35	59.48	63.14
TiO_2	0.73	0.69	0.69	0.53	0.73
Al_2O_3	15.64	15.65	15.56	16.07	15.95
Fe_2O_3	2.24	2.19	1.18	2.03	2.23
FeO	5.15	5.75	6.28	5.58	5.20
MnO	0.08	0.05	0.17	0.11	0.07
MgO	3.63	4.06	4.16	4.28	3.80
CaO	2.74	4.62	5.15	6.11	2.47
Na_2O	1.96	1.69	1.39	1.36	1.41
K_2O	2.52	2.73	1.92	2.44	2.69
P_2O_5	0.11	0.14	0.13	0.16	0.12
H_2O-	0.11	0.12	0.10	0.08	0.00
LOI	2.28	1.97	1.12	1.96	1.95
TOTAL	99.89	100.29	99.20	100.19	99.76

APPENDIX 1
MAJOR ELEMENT ANALYSES
(MASSIVE HORNFELS)

SAMPLE NO.	K-17A	DI-14	DI-44	DI-49	DI-49A
SiO_2	63.48	63.51	63.35	61.62	64.26
TiO_2	0.73	0.73	0.73	0.73	0.76
Al_2O_3	15.71	16.00	15.74	15.55	15.78
Fe_2O_3	2.23	2.23	2.23	2.23	2.26
FeO	3.93	5.05	5.03	5.36	5.31
MnO	0.06	0.15	0.09	0.08	0.13
MgO	3.26	3.55	3.89	3.86	3.65
CaO	2.86	2.46	2.74	3.15	2.48
Na_2O	2.03	1.54	1.78	2.16	1.83
K_2O	2.71	2.72	2.48	3.00	2.82
P_2O_5	0.12	0.13	0.13	0.13	0.12
H_2O-	0.09	0.07	0.13	0.22	0.17
LOI	1.76	1.72	1.38	1.81	0.33
TOTAL	98.97	99.86	99.70	99.90	99.90

SAMPLE NO.	DI-51	DI-52	DI-54	DI-59D	DI-75A
SiO_2	64.32	63.85	68.70	65.48	65.13
TiO_2	0.76	0.76	0.69	0.74	0.65
Al_2O_3	15.54	16.11	13.98	15.91	15.81
Fe_2O_3	2.26	2.26	2.19	2.24	2.15
FeO	5.22	5.22	4.00	5.16	5.35
MnO	0.12	0.11	0.10	0.12	0.12
MgO	3.81	3.87	3.20	3.51	3.89
CaO	2.82	2.62	1.99	1.61	0.97
Na_2O	2.20	1.85	1.89	1.90	1.33
K_2O	2.69	2.81	2.37	2.77	3.67
P_2O_5	0.13	0.12	0.13	0.10	0.15
H_2O-	0.10	0.07	0.09	0.10	0.12
LOI	0.30	0.67	0.28	0.35	0.63
TOTAL	100.27	100.32	99.61	99.99	99.97

APPENDIX 1
MAJOR ELEMENT ANALYSES
(BASEMENT GRANITES – DATA FROM HUNTER (1974))

SAMPLE NO.	HGN-1	HGN-2	HGN-3	HGN-4	HGN-5	HGN-6
SiO_2	71.32	73.17	70.70	69.06	73.09	78.31
TiO_2	0.32	0.25	0.35	0.63	0.25	0.14
Al_2O_3	14.43	13.68	14.68	14.10	13.52	11.23
Fe_2O_3	0.59	0.85	1.05	1.88	0.83	0.92
FeO	1.73	1.68	1.18	2.23	1.48	0.83
MnO	0.08	0.10	0.04	0.25	0.04	0.06
MgO	0.57	0.29	0.89	0.94	0.59	0.30
CaO	1.33	1.03	1.92	1.99	1.59	0.57
Na_2O	3.92	2.88	4.69	3.14	3.35	2.54
K_2O	4.59	5.54	3.53	4.86	5.17	4.84
P_2O_5	0.31	0.08	0.14	0.20	0.08	0.01
H_2O-	0.06	0.06	0.12	0.07	0.08	0.06
LOI	0.61	0.64	0.69	1.06	0.45	0.38
TOTAL	99.86	100.25	99.98	100.41	100.52	100.19

APPENDIX 2
TRACE ELEMENT ANALYSES
(QUENCH-TEXTURED MICROPYROXENITES)

SAMPLE	CR	NI	CU	ZN	RB	SR	Y	ZR
DI-5	1191	334	46	71	33	156	11	58
DI-6	891	230	54	76	39	192	15	76
DI-7A	1283	367	47	75	32	147	12	72
DI-7B	1266	359	52	74	30	148	10	66
DI-8C	1105	309	49	70	31	162	11	75
DI-8H	1121	301	46	72	30	158	13	79
DI-19	981	248	52	74	36	193	15	76
DI-22	1531	448	48	67	36	144	10	49
DI-23	927	232	58	110	49	189	17	88
DI-24	1296	364	39	69	41	135	11	57
DI-25	1065	285	56	72	38	174	15	76
DI-28	1032	288	61	78	27	156	13	70
DI-29	978	259	55	73	52	165	15	79
DI-30	1034	288	55	72	38	190	14	70
DI-31	940	258	37	81	57	151	13	72
DI-34	1180	327	48	92	28	136	13	67
DI-36	1059	291	55	73	35	169	13	74
DI-42C	1003	278	54	86	34	153	15	70
DI-45	1212	325	28	75	39	128	13	68
DI-53	832	214	54	79	40	161	16	89
DI-56	1011	277	54	71	27	180	14	70
DI-57A	1210	326	53	73	37	168	14	71
DI-59B	1081	298	53	70	31	169	14	73
DI-59C	1231	343	52	71	27	156	14	69
DI-61	1127	319	29	115	18	117	7	64
DI-70	1391	411	42	78	38	175	10	61
DI-74	1064	290	55	71	30	183	14	68
DI-77	1014	269	55	65	42	124	14	57

APPENDIX 2
TRACE ELEMENT ANALYSES
(MICROGABBRONORITE)

SAMPLE	CR	NI	CU	ZN	RB	SR	Y	ZR
K-18	187	82	8	88	0	311	16	18
K-22	223	99	255	101	9	349	19	32
K-108A	282	131	92	97	3	323	22	91
K-108B	236	108	117	101	0	324	26	102
K-109	243	108	101	104	2	344	25	97
K-149A	258	117	10	71	8	382	12	25
K-159	189	82	84	119	6	364	25	38
K-160A	245	119	94	84	5	313	20	31
KWR-108A	259	116	69	110	3	332	26	103
KWR-109A	119	49	18	118	6	334	32	68
KWR-113A	252	112	50	77	5	306	20	78
KWR-113Q	246	115	88	97	0	309	19	85
KWR-160	239	107	76	97	6	325	21	38
KWR-194	248	109	137	82	0	303	20	45
KWR-195	172	76	37	102	0	320	21	23
KWR-207	94	33	4	122	0	345	29	33
KWR-38A(1)	182	86	63	94	0	309	19	22
KWR-38A(2)	270	130	3	89	0	308	14	10
KWR-50	194	87	45	109	3	374	21	30
KWR178AC	237	104	50	106	8	329	20	194
KWR178AH	240	108	50	113	6	330	21	89
KWR248(2)	268	129	94	60	3	329	10	14
KWR255(2)	345	204	123	75	8	348	15	28
KWR264AC	316	182	125	62	15	311	15	18
KWR264AH	331	180	123	64	14	310	15	74
KWR-30A(2)	303	154	19	100	7	272	19	27
K30A-G	255	111	182	112	11	353	19	46
K30A-T	243	109	181	109	12	357	20	34
KWR255(1A)	295	222	114	80	14	323	17	72
KWR255(1B)	320	224	108	78	16	322	18	36

APPENDIX 2
TRACE ELEMENT ANALYSES
(META QUARTZ–DOLERITES)

SAMPLE	NI	CU	ZN	RB	SR	Y	ZR
DI–2G	142	47	86	36	198	17	87
DI–2T	139	44	84	37	201	18	90
DI–3G	128	76	100	52	230	19	92
DI–3T	122	71	104	50	228	18	97
DI–4	105	59	82	62	215	20	109
DI–7A	127	46	79	46	198	17	93
DI–12	84	15	68	76	249	20	128
DI–15	92	73	54	66	235	19	114
DI–16	138	32	104	52	212	19	103
DI–17	121	74	104	49	222	19	96
DI–18	106	74	113	46	210	18	91
DI–20	133	45	84	52	193	18	103
DI–21	132	48	70	45	231	14	80
DI–26	165	58	82	75	197	17	99
DI–27	159	54	107	55	231	15	83
DI–32	113	70	76	80	229	16	99
DI–33	93	38	80	55	228	18	90
DI–35	138	68	84	44	184	19	97
Di–37	119	53	82	30	245	14	78
DI–38	175	84	97	47	173	19	101
DI–39	165	55	78	31	177	13	69
DI–41	80	42	86	57	210	22	108
DI–43	84	19	86	54	214	20	106
DI–46	118	36	74	67	190	20	117
DI–47	94	55	51	56	270	18	112
DI–48	216	16	83	56	180	18	102
DI–49B	141	69	80	47	214	19	96
DI–50	105	43	60	66	202	20	120
DI–55	163	108	68	42	233	15	83
DI–57	95	32	80	63	218	20	104
DI–58	156	51	62	48	238	14	71
DI–60	119	74	76	22	115	25	64
DI–68	84	187	72	45	191	22	109
DI–69	69	44	103	80	303	21	125
DI–73	139	67	76	54	182	19	106
DI–9	147	48	86	40	205	17	90

APPENDIX 2
TRACE ELEMENT ANALYSES
(QUARTZ-GABBRONORITE)

SAMPLE	NI	CU	ZN	RB	SR	Y	ZR
K-29(C)	97	64	73	48	257	17	90
K-29(H)	94	62	75	47	260	16	115
K 35 C	62	33	121	28	312	30	170
K 35 H	60	34	124	29	322	31	18
K-247B	48	179	85	39	474	18	107
KBWR-18A	209	82	60	27	273	14	62
KBWR-9A	91	29	78	60	225	21	123
KBWR-9B	155	99	76	31	266	16	81
KWR-222H	208	84	63	22	267	10	26
KWR-225A	75	80	42	45	423	18	93
KWR-225B	77	74	41	43	418	16	86
KWR-227	205	86	63	24	259	14	67
KWR-243A	64	68	97	38	261	21	96
KWR-246C	48	341	98	37	457	20	130
KWR-246H	49	337	100	8	434	20	75
KWR-249C	151	91	63	35	289	15	70
KWR-257H	111	55	62	35	262	17	48
KWR-258	82	72	107	42	258	19	88
KWR-222C	196	76	57	21	269	12	49
KWR243B(1)	101	68	76	44	267	17	197
KWR243B(2)	99	66	76	47	272	16	30
KWR-249H	159	98	71	38	291	15	21
KWR-257C	119	55	64	35	262	18	74

(MASSIVE HORNFELS)

SAMPLE	NI	CU	ZN	RB	SR	Y	ZR
DI-10	52	27	31	133	144	27	172
DI-10A	55	35	24	126	141	27	160
DI-10B	36	11	34	90	141	23	154
DI-11	49	17	47	98	148	21	141
DI-13	72	16	30	141	143	28	171
DI-14	30	18	96	135	123	28	180
DI-44	70	19	29	125	126	27	171
DI-49	37	10	18	152	145	26	168
DI-49A	59	18	75	132	133	28	179
DI-51	34	15	64	126	132	27	178
DI-52	60	19	75	131	150	28	174
DI-54	60	24	51	93	145	29	254
DI-59D	33	68	125	135	24	175	8
DI-75A	42	11	38	130	119	26	163
K-17A	36	9	33	145	186	28	177

APPENDIX 2
TRACE ELEMENT ANALYSES
(MIDDELWATER LAYERED SILL META QUARTZ-DOLERITES)

SAMPLE	NI	CU	ZN	RB	SR	Y	ZR
K-130	126	98	61	30	246	15	67
K-130A	184	106	56	36	265	10	52
K-27A	143	110	62	33	258	14	74
K-27B	181	164	39	13	254	10	30
K-28A(2)	137	107	74	33	259	18	84
K-60	51	20	78	47	260	21	124
K-60B(1)	102	17	44	17	317	24	136
K-60B(2)	99	15	45	17	311	23	132
K-7A	192	97	53	20	254	10	52
K-7B	174	38	63	44	239	13	78
K-8B	160	43	64	38	243	15	80
KG-23A	144	94	68	40	260	17	81
KG-61	81	59	104	50	255	19	97
KG-71	158	44	71	31	243	14	68
KM-2	73	86	74	86	265	24	128
KWR-11	66	41	96	68	254	26	146
KWR-118	117	77	101	49	246	15	85
KWR-118A	92	81	75	45	243	17	92
KWR-152A	74	63	76	38	342	17	96
KWR-21B	50	29	45	100	222	21	157
KWR-28	144	104	68	27	253	15	76
KWR-38	77	77	75	66	251	23	127
KWR-46A	141	89	56	30	260	14	65
KWR-52	131	69	82	43	233	14	78
KWR-54	75	22	65	72	238	17	98
KWR-55	106	89	85	71	226	17	85
KWR-72B	56	78	86	47	246	21	127

(QUARTZOFELDSPATHIC ROCKS)

SAMPLE	NI	CU	ZN	RB	SR	Y	ZR
K-(1)	21	12	37	91	307	27	182
K-(32)	24	70	140	88	349	34	241
K-11A	16	14	34	108	202	24	188
K-154A	11	23	73	64	231	34	208
K-39A	25	47	107	30	301	24	146
K-60A	25	0	56	102	219	25	179
K-72A	27	3	52	93	269	35	160
K-8C	14	6	48	53	244	41	283
KM-3	45	2	19	23	319	33	173
KWR-72	17	5	31	101	216	20	180
KWR-8G	24	3	29	112	207	23	90
KWR-9	23	4	21	135	201	21	195

APPENDIX 2
TRACE ELEMENT ANALYSES
(OLIVINE-PYROXENITES)

SAMPLE	CR	NI	CU	ZN	RB	SR	Y	ZR
DI-75	3029	828	32	64	15	79	8	31
DI-76	2221	578	55	71	26	84	13	65

TRACE ELEMENT ANALYSES
(METADOLERITES)

SAMPLE	CR	NI	CU	ZN	RB	SR	Y	ZR
DI-62	285	134	32	97	9	56	30	80
DI-63	358	208	153	72	22	110	34	92
DI-63A	276	139	255	103	9	97	31	93
DI-64	265	139	70	85	11	83	26	70
DI-65	213	97	181	115	34	143	27	68
DI-66	296	139	65	88	13	99	26	69
DI-67	221	102	173	121	29	141	39	80

APPENDIX 2
TRACE ELEMENT ANALYSES
(BASEMENT GRANITES)

SAMPLE	RB	SR	ZR
HGN-1	226	122	–
HGN-2	380	59	130
HGN-3	109	488	120
HGN-4	–	–	–
HGN-5	295	132	161
HGN-6	–	–	–

APPENDIX 3
CIPW NORMS
(QUENCH TEXTURED MICROPYROXENITES)

	SAMPLE NO.						
	DI-5	DI-6	DI-7BC	DI-7BH	DI-8C	DI-8H	DI-19
Q	4.16	8.47	2.92	2.79	5.50	5.55	7.37
Or	5.58	5.91	4.49	4.43	4.85	4.67	5.14
Ab	14.13	12.27	14.89	18.28	14.21	15.14	13.96
An	18.26	24.65	18.26	16.17	21.04	20.09	24.49
Di	8.69	7.93	9.96	11.44	8.97	9.78	9.89
Hy	45.25	36.41	45.51	42.86	41.57	40.54	35.20
Mt	2.62	2.74	2.64	2.64	2.67	2.67	2.71
Il	0.59	0.74	0.61	0.61	0.65	0.65	0.70
Ap	0.19	0.24	0.17	0.17	0.21	0.19	0.21

	SAMPLE NO.						
	DI-22	DI-23	DI-24	DI-25	DI-28	DI-29	DI-30
Q	2.65	5.76	3.82	6.35	6.45	7.50	6.09
Or	4.85	7.74	5.79	6.21	4.61	7.33	6.15
Ab	13.37	14.89	12.35	13.62	12.78	11.00	14.21
An	17.31	25.45	16.34	22.39	23.45	24.61	22.24
Di	8.65	7.25	7.96	10.01	10.46	7.42	9.11
Hy	49.48	34.88	49.80	37.56	37.61	38.05	38.73
Mt	2.58	2.86	2.62	2.71	2.71	2.75	2.68
Il	0.53	0.89	0.59	0.70	0.70	0.76	0.66
Ap	0.14	0.24	0.14	0.21	0.21	0.21	0.19

APPENDIX 3
CIPW NORMS
(QUENCH TEXTURED MICROPYROXENITES)

				SAMPLE NO.			
	DI-31	DI-34	DI-36	DI-42C	DI-45	DI-53	DI-56
Q	7.01	5.55	6.62	8.83	5.08	2.70	4.27
Or	5.85	4.55	5.85	4.79	5.67	5.97	4.91
Ab	12.61	13.37	13.45	9.31	14.81	25.97	17.26
An	22.75	22.94	22.36	23.42	17.96	15.06	21.03
Di	6.79	7.91	9.48	4.42	7.97	15.91	10.52
Hy	41.16	41.59	37.55	44.58	44.94	30.38	38.37
Mt	2.71	2.75	2.71	2.81	2.70	2.80	2.70
Il	0.70	0.76	0.70	0.84	0.68	0.82	0.68
Ap	0.19	0.19	0.21	0.24	0.17	0.21	0.19

				SAMPLE NO.			
	DI-57A	DI-59B	DI-59C	DI-61	DI-70	DI-74	DI-77
Q	4.33	5.45	4.07	4.06	0.56	8.99	5.79
Or	5.08	4.79	4.49	3.90	5.67	4.91	5.32
Ab	16.50	13.54	18.87	16.75	15.74	9.31	12.44
An	20.61	21.34	18.15	19.32	14.63	24.84	21.47
Di	8.98	10.49	11.58	11.07	8.96	7.11	9.59
Hy	40.31	40.50	39.05	40.93	50.87	40.66	41.75
Mt	2.81	2.70	2.65	2.67	2.62	2.70	2.68
Il	0.84	0.68	0.63	0.65	0.59	0.68	0.66
Ap	0.24	0.17	0.19	0.21	0.14	0.17	0.21

APPENDIX 3
CIPW NORMS
(MICROGABBRONORITES)

	K-18	K-22	KWR-30A(2)	KWR38A(1)	KWR38A(2)	KWR-50	K-108A
				SAMPLE NO.			
Q	0.27	0.57	—	—	—	0.23	0.14
Or	0.77	2.31	2.25	1.12	1.24	1.42	1.18
Ab	13.31	15.06	12.18	16.67	12.18	18.70	19.12
An	37.59	35.34	34.79	35.76	37.01	34.26	31.13
Di	12.63	13.94	17.21	14.35	18.62	13.62	16.58
Hy	32.33	27.25	24.30	27.58	16.59	27.34	27.11
Ol	—	—	5.33	0.61	10.90	—	—
Mt	2.89	3.09	2.89	2.89	2.86	3.06	3.25
Il	0.93	1.20	0.93	0.93	0.89	1.16	1.41
Ap	0.21	0.42	0.26	0.26	0.07	0.42	0.38

	KWR-108A	K-108B	K-109	KWR-109A	KWR-113A	KWR-113Q	K-149A
				SAMPLE NO.			
Q	0.54	1.27	—	0.85	2.37	1.09	2.39
Or	1.00	1.24	1.24	2.07	1.60	1.00	2.25
Ab	13.45	19.71	20.56	19.29	15.91	17.85	18.61
An	36.38	30.97	30.88	31.08	34.70	31.04	35.34
Di	16.02	17.40	17.74	16.75	14.28	17.17	16.46
Hy	27.33	23.60	20.97	24.19	26.46	27.22	21.91
Ol	—	—	2.65	—	—	—	—
Mt	3.48	3.39	3.39	3.36	3.00	3.12	2.51
Il	1.71	1.60	1.60	1.56	1.08	1.23	0.44
Ap	0.47	0.42	0.45	0.54	0.31	0.35	0.09

APPENDIX 3
CIPW NORMS
(MICROGABBRONORITES)

	SAMPLE NO.						
	K-159	KWR-160	K-160A	KWR-194	KWR-194C	KWR-194BH	KWR-195
Q	0.03	−	0.33	0.56	−	1.17	0.66
Or	2.25	1.65	1.71	1.30	0.89	0.89	1.30
Ab	16.50	17.01	18.95	18.36	15.23	13.28	16.33
An	36.02	34.00	32.53	31.44	38.33	39.39	34.92
Di	13.80	16.54	16.73	20.96	11.77	6.89	15.86
Hy	25.64	25.93	25.63	23.37	29.22	33.47	26.45
Ol	−	0.14	−	−	1.54	−	−
Mt	3.33	3.22	3.04	2.86	2.55	2.54	2.83
Il	1.52	1.37	1.14	0.89	0.49	0.47	0.85
Ap	0.57	0.38	0.28	0.28	0.17	0.17	0.28

	SAMPLE NO.				
	KWR-207	KWR-248(2)	KWR-255(2)	KWR-264AC	KWR-264AH
Q	0.08	−	−	−	−
Or	1.48	1.42	3.13	3.61	3.55
Ab	19.38	16.41	15.40	13.45	13.11
An	34.25	35.09	30.24	32.24	32.24
Di	14.20	20.25	18.66	18.91	18.71
Hy	25.70	20.96	27.34	26.20	26.60
Ol	−	2.22	1.16	1.80	1.67
Mt	3.26	2.58	2.81	2.78	2.81
Il	1.42	0.53	0.84	0.80	0.84
Ap	0.47	0.09	0.26	0.14	0.14

APPENDIX 3
CIPW NORMS
(METADOLERITES)

	DI-62	DI-63	DI-63A	DI-64	DI-65	DI-66
			SAMPLE NO.			
Q	9.52	1.29	1.94	3.62	3.04	0.75
Or	2.13	3.66	1.06	2.19	4.26	3.78
Ab	13.37	14.13	18.44	18.28	16.50	19.38
An	31.09	29.78	29.22	29.22	25.99	27.07
Di	5.87	17.92	18.78	16.94	17.59	20.79
Hy	30.78	26.63	23.69	24.65	26.81	23.83
Mt	3.16	3.83	3.80	3.09	3.67	3.13
Il	1.29	2.16	2.13	1.20	1.96	1.25
Ap	0.21	0.40	0.35	0.19	0.21	0.19

(QUARTZOFELDSPATHIC ROCKS)

	K-(1)	K-11A	K-39A	K-154A	KWR-72	KM-3
			SAMPLE NO.			
Q	22.79	35.37	24.44	21.77	39.63	23.72
Or	9.63	19.98	7.33	16.96	19.92	8.45
Ab	5.41	17.26	20.31	23.94	16.24	26.91
An	31.17	15.11	21.80	13.61	14.64	17.39
Di	7.16	2.03	7.39	8.82	0.96	18.59
Hy	19.25	7.05	13.95	10.69	5.52	2.04
Mt	1.86	1.87	1.84	1.86	1.86	1.86
Il	1.25	0.85	1.37	1.65	0.68	1.03
Ap	0.38	0.28	0.45	0.50	0.26	0.33

	K-8C	KWR-8G	KWR-8T	KWR-9	K-(32)	K-60A	K-72A
				SAMPLE NO.			
Q	26.45	42.27	42.52	45.22	11.67	28.54	28.17
Or	16.25	20.80	20.39	22.40	17.79	17.44	9.63
Ab	24.87	14.72	15.40	13.20	24.37	18.36	17.77
An	12.85	13.25	13.57	10.92	14.04	17.98	23.20
Di	3.06	–	–	–	8.93	3.33	1.13
Hy	12.02	4.94	4.22	5.04	18.43	9.56	15.00
Mt	1.86	2.64	2.62	1.86	1.86	3.03	3.13
Il	1.63	0.61	0.59	0.49	2.05	1.12	1.25
Ap	0.71	0.21	0.19	0.21	0.71	0.33	0.31

APPENDIX 4

MINERAL ANALYSES

(ORTHOPYROXENES FROM THE RUSTENBURG LAYERED SUITE)

SAMPLE NO.	K-261A	K-261A	K-261A	K13-200	K13-200	K13-200
SiO_2	53.84	52.78	53.45	53.00	51.98	54.63
Al_2O_3	1.55	1.59	1.04	1.40	1.35	1.05
TiO_2	0.26	0.22	0.27	0.27	0.31	0.36
MgO	27.16	25.40	26.58	30.74	30.75	29.43
FeO	15.09	16.11	14.94	11.95	11.58	12.34
MnO	0.40	0.45	0.28	0.36	0.31	0.18
Cr_2O_3	0.28	0.17	0.77	0.77	0.65	0.45
NiO	0.28	0.22	0.31	0.29	0.44	0.23
CaO	2.06	2.11	2.63	1.01	1.50	0.66
TOTAL	100.92	99.05	100.27	99.79	99.87	99.33

STRUCTURAL FORMULAE - ATOMS PER 6 OXYGEN ATOMS

Si	1.93	1.94	1.94	1.90	1.88	1.96
Al	0.07	0.07	0.04	0.06	0.06	0.04
Ti	0.01	0.01	0.01	0.01	0.01	0.01
Mg	1.45	1.39	1.44	1.64	1.66	1.57
Fe	0.45	0.50	0.45	0.35	0.35	0.37
Mn	0.01	0.01	0.01	0.01	0.01	0.01
Cr	0.01	—	0.02	0.02	0.02	0.01
Ni	0.01	0.01	0.01	0.01	0.01	0.01
Ca	0.08	0.08	0.10	0.04	0.06	0.03
TOTAL	4.02	4.01	4.02	4.04	4.06	4.01

$\dfrac{Mg^{2+}}{(Mg^{2+} + Fe^{2+})}$	.763	.735	.762	.824	.826	.809

APPENDIX 4

MINERAL ANALYSES

(ORTHOPYROXENES FROM THE RUSTENBURG LAYERED SUITE)

SAMPLE NO.	K13-150	K13-150	K13-150	K13-125	K13-125	K13-125
SiO_2	52.75	55.11	53.52	54.22	54.08	55.63
Al_2O_3	1.25	1.24	1.26	1.18	1.16	1.27
TiO_2	0.31	0.30	0.33	0.27	0.28	0.32
MgO	30.18	28.48	30.33	30.56	29.67	28.96
FeO	12.06	12.81	12.51	12.09	12.02	11.68
MnO	0.29	0.33	0.31	0.30	0.24	0.28
Cr_2O_3	0.61	0.57	0.37	0.41	0.46	0.63
NiO	0.35	0.33	0.35	0.30	0.46	0.37
CaO	0.83	0.84	0.90	0.98	0.77	0.75
TOTAL	98.63	100.01	99.88	100.31	99.26	99.89

STRUCTURAL FORMULAE - ATOMS PER 6 OXYGEN ATOMS

Si	1.91	1.97	1.92	1.93	1.94	1.97
Al	0.05	0.05	0.05	0.05	0.05	0.05
Ti	0.01	0.01	0.01	0.01	0.01	0.01
Mg	1.63	1.51	1.62	1.62	1.59	1.53
Fe	0.37	0.38	0.37	0.36	0.36	0.35
Mn	0.01	0.01	0.01	0.01	0.01	0.01
Cr	0.02	0.02	0.01	0.01	0.01	0.02
Ni	0.01	0.01	0.01	0.01	0.01	0.01
Ca	0.03	0.03	0.03	0.04	0.03	0.03
TOTAL	4.04	3.99	4.03	4.04	4.01	3.98

$\dfrac{Mg^{2+}}{(Mg^{2+} + Fe^{2+})}$	.815	.799	.814	.818	.815	.814

APPENDIX 4

MINERAL ANALYSES

(ORTHOPYROXENES FROM THE RUSTENBURG LAYERED SUITE)

SAMPLE NO.	K13-50	K13-50	K13-50	K13-16	K13-16	K13-16
SiO_2	54.79	54.44	54.91	53.52	53.26	53.35
Al_2O_3	1.25	1.38	1.16	1.16	0.96	1.10
TiO_2	0.31	0.24	0.32	0.33	0.39	0.39
MgO	28.04	28.54	28.30	25.72	26.56	24.76
FeO	11.88	10.88	10.68	15.58	15.91	16.31
MnO	0.38	0.37	0.33	0.39	0.44	0.51
Cr_2O_3	0.80	0.74	0.76	0.46	0.40	0.41
NiO	0.25	0.26	0.28	0.29	0.25	0.31
CaO	1.94	2.21	2.49	0.93	1.11	1.61
TOTAL	99.64	99.06	99.23	98.38	99.28	98.75

STRUCTURAL FORMULAE - ATOMS PER 6 OXYGEN ATOMS

Si	1.96	1.95	1.96	1.97	1.95	1.97
Al	0.05	0.06	0.05	0.05	0.04	0.05
Ti	0.01	0.01	0.01	0.01	0.01	0.01
Mg	1.50	1.53	1.51	1.41	1.45	1.36
Fe	0.36	0.33	0.32	0.48	0.49	0.50
Mn	0.01	0.01	0.01	0.01	0.01	0.02
Cr	0.02	0.02	0.02	0.01	0.01	0.01
Ni	0.01	0.01	0.01	0.01	0.01	0.01
Ca	0.07	0.09	0.10	0.04	0.04	0.06
TOTAL	3.99	4.01	3.99	3.99	4.01	3.99

$\dfrac{Mg^{2+}}{(Mg^{2+} + Fe^{2+})}$	.806	.823	.825	.746	.747	.731

APPENDIX 4

MINERAL ANALYSES

(ORTHOPYROXENES FROM THE RUSTENBURG LAYERED SUITE)

SAMPLE NO.	K14-75	K14-75	K14-75	K14-25	K14-25	K14-25	K11-275	K11-275	K11-275
SiO_2	54.40	53.46	53.92	53.32	54.33	53.45	53.77	53.39	52.60
Al_2O_3	0.93	0.84	0.81	1.08	1.29	1.04	1.18	1.29	1.33
TiO_2	0.31	0.37	0.36	0.47	0.39	0.27	0.23	0.25	0.24
MgO	25.74	23.56	26.17	28.04	27.09	26.58	26.27	27.60	26.64
FeO	16.09	14.20	16.57	15.06	13.83	14.94	15.13	13.49	14.82
MnO	0.46	0.43	0.43	0.44	0.43	0.28	0.29	0.26	0.09
Cr_2O_3	0.36	0.37	0.25	0.64	0.82	0.76	0.27	0.36	0.20
NiO	0.39	0.31	0.25	0.25	0.25	0.31	0.21	0.24	0.22
CaO	1.29	5.54	1.22	1.20	0.98	2.63	2.07	2.29	1.91
TOTAL	99.99	99.08	99.98	100.50	99.41	100.26	99.42	99.17	98.05

STRUCTURAL FORMULAE - ATOMS PER 6 OXYGEN ATOMS

Si	1.97	1.97	1.96	1.92	1.96	1.94	1.96	1.94	1.94
Al	0.04	0.04	0.03	0.05	0.05	0.04	0.05	0.06	0.06
Ti	0.01	0.01	0.01	0.01	0.01	0.01	0.01	0.01	0.01
Mg	1.39	1.29	1.42	1.51	1.46	1.44	1.43	1.49	1.46
Fe	0.49	0.44	0.50	0.45	0.42	0.45	0.46	0.41	0.46
Mn	0.01	0.01	0.01	0.01	0.01	0.01	0.01	0.01	0.00
Cr	0.01	0.01	0.01	0.02	0.02	0.02	0.01	0.01	0.01
Ni	0.01	0.01	0.01	0.01	0.01	0.01	0.01	0.01	0.01
Ca	0.05	0.22	0.05	0.05	0.04	0.10	0.08	0.09	0.08
TOTAL	3.98	4.00	4.00	4.03	3.98	4.02	4.02	4.03	4.03

$\frac{Mg^{2+}}{(Mg^{2+}+Fe^{2+})}$	.739	.746	.740	.770	.776	.762	.757	.784	.760

APPENDIX 4
MINERAL ANALYSES
(ORTHOPYROXENES FROM THE RUSTENBURG LAYERED SUITE)

SAMPLE NO.	K11-225	K11-225	K11-225	K11-175	K11-175	K11-175
SiO_2	53.82	53.88	54.46	54.29	54.40	55.38
Al_2O_3	1.24	1.33	1.33	1.16	1.17	1.18
TiO_2	0.34	0.39	0.29	0.37	0.37	0.32
MgO	26.66	27.72	25.47	28.25	27.72	27.46
FeO	14.67	13.90	13.98	13.33	13.29	12.54
MnO	0.25	0.37	0.31	0.49	0.49	0.28
Cr_2O_3	0.48	0.72	0.55	0.52	0.52	0.45
NiO	0.30	0.32	0.28	0.28	0.29	0.38
CaO	2.14	1.09	1.97	1.03	1.17	1.44
TOTAL	99.90	99.72	98.64	99.72	99.42	99.43

STRUCTURAL FORMULAE – ATOMS PER 6 OXYGEN ATOMS

Si	1.95	1.94	1.98	1.95	1.96	1.98
Al	0.05	0.06	0.06	0.05	0.05	0.05
Ti	0.01	0.01	0.01	0.01	0.01	0.01
Mg	1.44	1.49	1.38	1.51	1.49	1.47
Fe	0.44	1.42	0.43	0.40	0.40	0.38
Mn	0.01	0.01	0.01	0.01	0.02	0.01
Cr	0.01	0.02	0.02	0.01	0.01	0.01
Ni	0.01	0.01	0.01	0.01	0.01	0.01
Ca	0.08	0.04	0.08	0.04	0.05	0.06
TOTAL	4.00	4.00	3.98	3.99	4.00	3.98

$\frac{Mg^{2+}}{(Mg^{2+} + Fe^{2+})}$	.766	.780	.762	.791	.788	.795

APPENDIX 4

MINERAL ANALYSES

(ORTHOPYROXENES FROM THE RUSTENBURG LAYERED SUITE)

SAMPLE NO.	K11-125	K11-125	K11-125	K11-75	K11-75	K11-75
SiO_2	54.48	54.16	53.80	53.48	54.06	54.10
Al_2O_3	1.21	1.13	0.95	1.15	1.22	1.23
TiO_2	0.33	0.32	0.48	0.30	0.40	0.39
MgO	29.72	28.47	28.01	28.94	28.70	28.91
FeO	12.49	11.95	12.52	12.54	12.71	12.28
MnO	0.34	0.35	0.40	0.31	0.27	0.27
Cr_2O_3	0.62	0.44	0.35	0.60	0.47	0.47
NiO	0.26	0.29	0.30	0.25	0.28	0.28
CaO	1.14	1.99	1.58	0.88	1.05	1.55
TOTAL	100.59	99.10	98.39	98.45	99.16	99.48

STRUCTURAL FORMULAE - ATOMS PER 6 OXYGEN ATOMS

Si	1.94	1.95	1.96	1.94	1.95	1.94
Al	0.05	0.05	0.04	0.05	0.05	0.05
Ti	0.01	0.01	0.01	0.01	0.01	0.01
Mg	1.57	1.53	1.52	1.57	1.53	1.55
Fe	0.37	0.36	0.38	0.38	0.38	0.37
Mn	0.01	0.01	0.01	0.01	0.01	0.01
Cr	0.02	0.01	0.01	0.02	0.01	0.01
Ni	0.01	0.01	0.01	0.01	0.01	0.01
Ca	0.04	0.08	0.06	0.03	0.04	0.06
TOTAL	4.02	4.01	4.00	4.02	3.99	4.01

$\dfrac{Mg^{2+}}{(Mg^{2+} + Fe^{2+})}$	.809	.810	.800	.805	.800	.807

APPENDIX 4

MINERAL ANALYSES

(ORTHOPYROXENES FROM THE RUSTENBURG LAYERED SUITE)

SAMPLE NO.	K5-450	K5-450	K5-450	K9-25	K9-25	K9-25
SiO_2	54.77	53.81	54.71	53.36	53.73	54.42
Al_2O_3	1.26	1.30	1.33	0.88	0.86	0.94
TiO_2	0.42	0.25	0.36	0.36	0.37	0.31
MgO	28.52	27.35	27.07	23.47	25.16	25.77
FeO	12.67	12.76	11.19	14.16	17.49	16.11
MnO	0.37	0.26	0.49	0.43	0.41	0.53
Cr_2O_3	0.44	0.36	0.74	0.36	0.32	0.39
NiO	0.23	0.23	0.29	0.30	0.39	0.41
CaO	1.14	2.30	3.70	5.52	1.35	1.28
TOTAL	99.82	98.62	99.88	98.84	100.08	100.16

STRUCTURAL FORMULAE - ATOMS PER 6 OXYGEN ATOMS

Si	1.96	1.95	1.96	1.97	1.96	1.97
Al	0.05	0.06	0.06	0.04	0.04	0.04
Ti	0.01	0.01	0.01	0.01	0.01	0.01
Mg	1.52	1.48	1.44	1.29	1.37	1.39
Fe	0.38	0.39	0.33	0.44	0.53	0.49
Mn	0.01	0.01	0.01	0.01	0.01	0.02
Cr	0.01	0.01	0.02	0.01	0.01	0.01
Ni	0.01	0.01	0.01	0.01	0.01	0.01
Ca	0.04	0.09	0.14	0.22	0.05	0.05
TOTAL	3.99	4.01	3.98	4.00	3.99	3.99

$\dfrac{Mg^{2+}}{(Mg^{2+} + Fe^{2+})}$	.800	.791	.814	.745	.721	.739

APPENDIX 4
MINERAL ANALYSES
(ORTHOPYROXENES FROM THE RUSTENBURG LAYERED SUITE)

SAMPLE NO.	K5-225	K5-225	K5-225	K5-150	K5-150	K5-150
SiO_2	54.30	54.49	53.29	53.95	54.29	53.33
Al_2O_3	1.25	0.95	0.96	0.79	0.92	1.04
TiO_2	0.25	0.40	0.42	0.41	0.36	0.34
MgO	26.80	26.41	26.69	26.17	25.22	25.94
FeO	14.71	14.65	15.52	16.58	17.15	16.65
MnO	0.28	0.50	0.44	0.49	0.51	0.50
Cr_2O_3	0.37	0.27	0.28	0.25	0.22	0.29
NiO	0.30	0.32	0.25	0.27	0.28	0.30
CaO	1.65	1.07	1.33	1.28	1.22	1.36
TOTAL	99.91	99.06	99.18	100.19	100.17	99.75

STRUCTURAL FORMULAE - ATOMS PER 6 OXYGEN ATOMS

Si	1.96	1.98	1.95	1.96	1.97	1.95
Al	0.05	0.04	0.04	0.03	0.04	0.04
Ti	0.01	0.01	0.01	0.01	0.01	0.01
Mg	1.44	1.43	1.45	1.42	1.37	1.41
Fe	0.44	0.45	0.47	0.50	0.52	0.51
Mn	0.01	0.02	0.01	0.01	0.02	0.02
Cr	0.01	0.01	0.01	0.01	0.01	0.01
Ni	0.01	0.01	0.01	0.01	0.01	0.01
Ca	0.06	0.04	0.05	0.05	0.05	0.05
TOTAL	3.99	3.99	4.00	4.00	4.00	4.01

$\dfrac{Mg^{2+}}{(Mg^{2+} + Fe^{2+})}$	.766	.761	.755	.740	.725	.734

APPENDIX 4
MINERAL ANALYSES
(ORTHOPYROXENES FROM THE RUSTENBURG LAYERED SUITE)

SAMPLE NO.	K5-100	K5-100	K5-100	K1-150	K1-150	K1-150
SiO_2	53.05	53.13	52.74	54.21	53.66	53.52
Al_2O_3	0.85	1.65	1.66	1.09	0.95	0.95
TiO_2	0.37	0.37	0.37	0.29	0.42	0.40
MgO	25.95	24.97	25.26	24.85	25.04	24.59
FeO	17.38	16.48	16.65	16.45	16.69	16.81
MnO	0.31	0.48	0.49	0.27	0.59	0.55
Cr_2O_3	0.29	0.39	0.40	0.29	0.26	0.21
NiO	0.29	0.24	0.23	0.27	0.34	0.27
CaO	0.99	2.73	2.76	2.26	1.38	1.61
TOTAL	99.48	100.44	100.56	99.98	99.33	98.91

STRUCTURAL FORMULAE - ATOMS PER 6 OXYGEN ATOMS

Si	1.95	1.93	1.92	1.97	1.97	1.97
Al	0.04	0.07	0.07	0.05	0.04	0.04
Ti	0.01	0.01	0.01	0.01	0.01	0.01
Mg	1.42	1.35	1.37	1.35	1.37	1.35
Fe	0.53	0.50	0.51	0.50	0.51	0.52
Mn	0.01	0.01	0.01	0.01	0.02	0.02
Cr	0.01	0.01	0.01	0.01	0.01	0.01
Ni	0.01	0.01	0.01	0.01	0.01	0.01
Ca	0.04	0.11	0.11	0.09	0.05	0.06
TOTAL	4.02	4.00	4.02	4.00	3.99	3.99

$\dfrac{Mg^{2+}}{(Mg^{2+} + Fe^{2+})}$	.728	.730	.729	.730	.729	.722

APPENDIX 4
MINERAL ANALYSES
(ORTHOPYROXENES FROM THE RUSTENBURG LAYERED SUITE)

SAMPLE NO.	K5-50	K5-50	K5-50	K1-100	K1-100	K1-100
SiO_2	54.58	54.33	53.43	52.19	53.73	53.26
Al_2O_3	1.22	1.05	0.98	1.41	1.18	1.03
TiO_2	0.37	0.40	0.39	0.20	0.21	0.38
MgO	25.15	25.11	26.07	24.75	26.05	25.65
FeO	16.97	16.75	16.79	17.44	16.55	17.45
MnO	0.51	0.44	0.60	0.48	0.37	0.09
Cr_2O_3	0.34	0.30	0.27	0.35	0.30	0.30
NiO	0.25	0.27	0.25	0.27	0.28	0.20
CaO	1.10	1.29	1.01	1.86	1.31	1.46
TOTAL	100.49	99.94	99.79	98.95	99.98	99.82

STRUCTURAL FORMULAE - ATOMS PER 6 OXYGEN ATOMS

Si	1.97	1.98	1.95	1.93	1.95	1.95
Al	0.05	0.04	0.04	0.06	0.05	0.04
Ti	0.01	0.01	0.01	0.01	0.01	0.01
Mg	1.36	1.36	1.42	1.37	1.41	1.40
Fe	0.51	0.51	0.51	0.54	0.50	0.53
Mn	0.02	0.01	0.02	0.02	0.01	0.00
Cr	0.01	0.01	0.01	0.01	0.01	0.01
Ni	0.01	0.01	0.01	0.01	0.01	0.01
Ca	0.04	0.05	0.04	0.07	0.05	0.06
TOTAL	3.98	3.98	4.01	4.02	4.00	4.01

$\frac{Mg^{2+}}{(Mg^{2+} + Fe^{2+})}$ | .727 | .727 | .736 | .717 | .738 | .725 |

APPENDIX 4

MINERAL ANALYSES

(PLAGIOCLASES FROM THE RUSTENBURG LAYERED SUITE)

SAMPLE NO.	K13-200	K13-200	K13-200	K13-200	K13-125	K13-125
SiO_2	49.85	48.38	49.05	49.51	47.78	48.36
Al_2O_3	31.63	32.85	33.09	31.40	32.83	32.48
TiO_2	0.02	0.02	0.03	0.03	0.00	0.03
MgO	0.02	0.00	0.00	0.00	0.00	0.00
FeO	0.29	0.27	0.36	0.29	0.34	0.51
MnO	0.02	0.00	0.00	0.02	0.00	0.00
CaO	14.78	15.39	15.33	14.93	15.07	14.58
Na_2O	2.96	2.58	2.71	2.63	2.45	2.92
K_2O	0.17	0.07	0.09	0.12	0.09	0.12
TOTAL	99.74	99.56	100.63	98.93	98.56	99.00

STRUCTURAL FORMULAE - ATOMS PER 32 OXYGEN ATOMS

Si	9.13	8.90	8.91	9.13	8.87	8.94
Al	6.83	7.12	7.09	6.83	7.18	7.08
Ti	0.00	0.00	0.00	0.00	0.00	0.00
Mg	0.01	0.00	0.00	0.00	0.00	0.00
Fe	0.05	0.04	0.06	0.05	0.05	0.08
Mn	0.00	0.00	0.00	0.00	0.00	0.00
Ca	2.90	3.03	2.98	2.95	3.00	2.89
Na	1.05	0.92	0.96	0.94	0.88	1.05
K	0.04	0.02	0.02	0.03	0.02	0.03
TOTAL	20.00	20.03	20.02	19.93	20.00	20.07

An*	.745	.778	.768	.769	.783	.745

*Ignores K and is calculated as:

$$\frac{Ca \times 278.2}{(Ca \times 278.2) + (Na \times 262.23)}$$

APPENDIX 4

MINERAL ANALYSES

(PLAGIOCLASES FROM THE RUSTENBURG LAYERED SUITE)

SAMPLE NO.	K13-125	K13-125	K13-50	K13-50	K13-50	K13-50
SiO_2	49.90	48.19	48.63	48.74	48.18	49.00
Al_2O_3	31.65	32.54	30.71	31.47	31.09	31.58
TiO_2	0.03	0.03	0.14	0.00	0.14	0.11
MgO	0.00	0.01	0.10	0.00	0.09	0.09
FeO	0.29	0.57	0.32	0.32	0.29	0.27
MnO	0.02	0.00	0.13	0.00	0.13	0.12
CaO	15.05	15.16	15.61	15.63	15.83	15.57
Na_2O	2.65	2.62	2.72	2.70	2.25	2.72
K_2O	0.12	0.10	0.23	0.23	0.20	0.22
TOTAL	99.71	99.22	98.59	99.09	98.20	99.68

STRUCTURAL FORMULAE - ATOMS PER 32 OXYGEN ATOMS

Si	9.13	8.90	9.04	9.02	8.98	9.00
Al	6.83	7.08	6.73	6.86	6.83	6.83
Ti	0.00	0.00	0.02	0.00	0.02	0.01
Mg	0.00	0.00	0.03	0.00	0.03	0.03
Fe	0.05	0.09	0.05	0.05	0.05	0.04
Mn	0.00	0.00	0.02	0.00	0.02	0.02
Ca	2.95	3.00	3.11	3.10	3.16	3.06
Na	0.94	0.94	0.98	0.97	0.81	0.97
K	0.03	0.02	0.05	0.05	0.05	0.05
TOTAL	19.93	20.03	20.03	20.05	19.95	20.01
An	.769	.772	.771	.772	.805	.770

APPENDIX 4
MINERAL ANALYSES
(PLAGIOCLASES FROM THE RUSTENBURG LAYERED SUITE)

SAMPLE NO.	K14-75	K14-75	K14-75	K14-75	K14-25	K14-25
SiO_2	47.99	47.57	46.81	47.34	48.45	47.48
Al_2O_3	31.72	31.21	31.27	31.26	32.03	31.69
TiO_2	0.13	0.13	0.14	0.14	0.14	0.15
MgO	0.11	0.11	0.08	0.08	0.11	0.11
FeO	0.20	0.20	0.25	0.25	0.22	0.21
MnO	0.08	0.16	0.12	0.12	0.12	0.15
CaO	17.79	17.38	17.62	17.62	15.81	15.70
Na_2O	2.04	1.95	1.97	1.97	2.79	2.70
K_2O	0.09	0.09	0.13	0.12	0.31	0.26
TOTAL	100.15	98.80	98.39	98.90	99.98	98.45

STRUCTURAL FORMULAE - ATOMS PER 32 OXYGEN ATOMS

Si	8.82	8.85	8.78	8.82	8.89	8.86
Al	6.87	6.84	6.91	6.86	6.93	6.97
Ti	0.01	0.02	0.02	0.02	0.02	0.02
Mg	0.03	0.03	0.02	0.02	0.03	0.03
Fe	0.03	0.05	0.04	0.04	0.03	0.03
Mn	0.01	0.02	0.02	0.02	0.02	0.02
Ca	3.50	3.46	3.54	3.52	3.11	3.14
Na	0.73	0.70	0.72	0.71	0.99	0.98
K	0.02	0.02	0.03	0.03	0.07	0.06
TOTAL	20.02	19.99	20.08	20.02	20.09	20.11

An	.836	.840	.839	.840	.769	.773

APPENDIX 4

MINERAL ANALYSES

(PLAGIOCLASES FROM THE RUSTENBURG LAYERED SUITE)

SAMPLE NO.	K14-25	K14-25	K11-225	K11-225	K11-225	K11-225
SiO_2	48.16	48.38	48.92	48.99	49.26	48.85
Al_2O_3	32.48	32.58	32.14	32.20	32.87	32.13
TiO_2	0.13	0.13	0.12	0.12	0.04	0.12
MgO	0.08	0.08	0.11	0.11	0.00	0.12
FeO	0.26	0.26	0.27	0.27	0.26	0.40
MnO	0.11	0.11	0.12	0.12	0.00	0.12
CaO	16.08	15.49	15.51	15.56	14.88	15.51
Na_2O	2.58	2.59	2.74	2.92	2.73	2.91
K_2O	0.30	0.30	0.17	0.13	0.08	0.13
TOTAL	100.18	99.92	100.10	100.42	100.12	100.29

STRUCTURAL FORMULAE – ATOMS PER 32 OXYGEN ATOMS

Si	8.82	8.87	8.94	8.93	8.98	8.92
Al	7.01	7.04	6.92	6.92	7.06	6.91
Ti	0.02	0.02	0.02	0.02	0.01	0.02
Mg	0.02	0.02	0.03	0.03	0.00	0.03
Fe	0.04	0.04	0.04	0.04	0.04	0.06
Mn	0.02	0.02	0.02	0.02	0.00	0.02
Ca	3.16	3.04	3.04	3.04	2.91	3.04
Na	0.92	0.92	0.97	1.03	0.97	1.03
K	0.07	0.07	0.04	0.03	0.02	0.03
TOTAL	20.08	20.04	20.02	20.06	19.99	20.06
An	.785	.778	.769	.758	.761	.758

APPENDIX 4

MINERAL ANALYSES

(PLAGIOCLASES FROM THE RUSTENBURG LAYERED SUITE)

SAMPLE NO.	K11-175	K11-175	K11-175	K11-175	K11-125	K11-125
SiO_2	48.19	48.21	49.45	49.42	48.67	48.51
Al_2O_3	32.00	31.98	32.17	32.18	32.29	32.73
TiO_2	0.14	0.13	0.16	0.16	0.14	0.03
MgO	0.09	0.09	0.11	0.11	0.11	0.00
FeO	0.38	0.38	0.29	0.29	0.46	0.36
MnO	0.16	0.15	0.13	0.13	0.08	0.00
CaO	15.76	15.38	14.34	14.66	15.24	15.16
Na_2O	2.65	2.65	3.02	3.03	2.24	2.68
K_2O	0.24	0.24	0.22	0.22	0.24	0.09
TOTAL	99.61	99.21	99.89	100.20	99.68	99.56

STRUCTURAL FORMULAE - ATOMS PER 32 OXYGEN ATOMS

Si	8.88	8.90	9.02	9.00	8.93	8.91
Al	6.95	6.96	6.92	6.91	6.98	7.09
Ti	0.02	0.02	0.02	0.02	0.02	0.00
Mg	0.02	0.02	0.03	0.03	0.03	0.00
Fe	0.06	0.06	0.04	0.04	0.07	0.06
Mn	0.02	0.02	0.02	0.02	0.01	0.00
Ca	3.11	3.04	2.80	2.86	3.00	2.98
Na	0.95	0.95	1.07	1.07	0.87	0.96
K	0.06	0.06	0.05	0.05	0.06	0.02
TOTAL	20.07	20.03	19.97	20.00	19.97	20.02

An	.776	.772	.735	.739	.785	.767

APPENDIX 4

MINERAL ANALYSES

(PLAGIOCLASES FROM THE RUSTENBURG LAYERED SUITE)

SAMPLE NO.	K11-75	K11-75	K11-75	K11-75	K5-450	K5-450
SiO_2	48.48	49.65	49.67	47.97	49.73	49.75
Al_2O_3	32.09	32.22	32.22	32.08	32.15	30.19
TiO_2	0.13	0.16	0.16	0.15	0.14	0.12
MgO	0.10	0.11	0.11	0.13	0.11	0.10
FeO	0.34	0.46	0.46	0.38	0.18	0.26
MnO	0.06	0.18	0.18	0.18	0.11	0.10
CaO	15.52	13.87	13.88	14.73	15.01	15.16
Na_2O	2.47	2.91	2.91	2.65	3.02	2.17
K_2O	0.24	0.22	0.22	0.21	0.18	0.17
TOTAL	99.43	99.78	99.81	98.48	100.63	98.56

STRUCTURAL FORMULAE - ATOMS PER 32 OXYGEN ATOMS

Si	8.92	9.06	9.07	8.90	9.02	9.21
Al	6.96	6.93	6.94	7.02	6.87	6.59
Ti	0.02	0.02	0.02	0.02	0.02	0.02
Mg	0.03	0.03	0.03	0.03	0.03	0.03
Fe	0.05	0.07	0.07	0.06	0.03	0.04
Mn	0.01	0.03	0.03	0.03	0.02	0.02
Ca	3.06	2.71	2.72	2.93	2.92	3.01
Na	0.88	1.03	1.03	0.95	1.06	0.97
K	0.06	0.05	0.05	0.05	0.04	0.04
TOTAL	19.99	19.93	19.96	19.99	20.01	19.93
An	.787	.736	.737	.740	.745	.767

APPENDIX 4

MINERAL ANALYSES

(PLAGIOCLASES FROM THE RUSTENBURG LAYERED SUITE)

SAMPLE NO.	K5-450	K5-450	K5-425	K5-425	K5-425	K5-425
SiO_2	50.04	48.89	49.22	49.18	49.66	48.45
Al_2O_3	31.97	32.48	31.35	31.94	31.50	32.68
TiO_2	0.12	0.16	0.13	0.03	0.03	0.01
MgO	0.10	0.12	0.07	0.05	0.01	0.01
FeO	0.26	0.20	0.33	0.30	0.29	0.35
MnO	0.10	0.26	0.15	0.00	0.02	0.02
CaO	15.16	15.26	15.36	15.71	14.97	15.34
Na_2O	2.71	2.48	2.41	2.40	2.63	2.48
K_2O	0.17	0.27	0.22	0.11	0.12	0.27
TOTAL	100.63	100.12	99.24	99.72	99.23	99.61

STRUCTURAL FORMULAE — ATOMS PER 32 OXYGEN ATOMS

Si	9.07	8.92	9.06	9.02	9.13	8.91
Al	6.83	6.99	6.80	6.91	6.83	7.09
Ti	0.02	0.02	0.02	0.00	0.00	0.00
Mg	0.03	0.03	0.02	0.01	0.00	0.00
Fe	0.04	0.03	0.05	0.05	0.05	0.05
Mn	0.01	0.04	0.02	0.00	0.00	0.00
Ca	2.94	2.98	3.03	3.09	2.95	3.02
Na	0.95	0.88	0.86	0.85	0.94	0.89
K	0.04	0.06	0.05	0.03	0.03	0.06
TOTAL	19.93	19.95	19.91	19.96	19.93	20.02
An	.767	.782	.789	.794	.769	.783

APPENDIX 4
MINERAL ANALYSES
(PLAGIOCLASES FROM THE RUSTENBURG LAYERED SUITE)

SAMPLE NO.	K9-25	K9-25	K9-25	K5-225	K5-225	K5-225
SiO_2	50.77	48.38	50.34	50.78	51.04	50.44
Al_2O_3	31.01	32.22	31.72	31.64	30.82	31.78
TiO_2	0.11	0.04	0.14	0.01	0.14	0.01
MgO	0.11	0.02	0.09	0.01	0.12	0.00
FeO	0.25	0.41	0.17	0.35	0.42	0.38
MnO	0.12	0.00	0.18	0.00	0.13	0.01
CaO	13.90	14.40	13.80	14.15	13.91	13.89
Na_2O	3.38	3.25	3.15	3.29	3.33	3.34
K_2O	0.26	0.14	0.28	0.13	0.34	0.13
TOTAL	99.91	99.86	99.87	100.36	100.25	99.88

STRUCTURAL FORMULAE - ATOMS PER 32 OXYGEN ATOMS

Si	9.24	9.04	9.16	9.22	9.27	9.19
Al	6.66	6.96	6.80	6.77	6.60	6.83
Ti	0.02	0.01	0.02	0.00	0.02	0.00
Mg	0.03	0.00	0.02	0.00	0.03	0.00
Fe	0.04	0.06	0.03	0.05	0.06	0.06
Mn	0.02	0.00	0.03	0.00	0.02	0.00
Ca	2.71	2.83	2.69	2.75	2.71	2.71
Na	1.19	1.15	1.11	1.16	1.17	1.18
K	0.06	0.03	0.06	0.03	0.08	0.03
TOTAL	19.97	20.08	19.92	19.98	19.96	20.00
An	.707	.723	.720	.716	.711	.709

APPENDIX 4
MINERAL ANALYSES
(PLAGIOCLASES FROM THE RUSTENBURG LAYERED SUITE)

SAMPLE NO.	K5-225	K5-225	K5-150	K5-150	K5-150	K5-150
SiO_2	49.11	49.91	48.81	50.12	50.10	51.00
Al_2O_3	31.41	31.64	31.69	31.19	32.15	29.89
TiO_2	0.16	0.13	0.14	0.16	0.02	0.16
MgO	0.11	0.09	0.10	0.11	0.01	0.12
FeO	0.43	0.46	0.36	0.44	0.55	0.42
MnO	0.11	0.14	0.10	0.16	0.02	0.15
CaO	13.78	14.44	14.99	14.20	14.29	13.92
Na_2O	3.36	3.09	3.11	3.18	3.23	3.54
K_2O	0.35	0.32	0.29	0.36	0.11	0.43
TOTAL	98.82	100.22	99.59	99.92	100.48	99.63

STRUCTURAL FORMULAE - ATOMS PER 32 OXYGEN ATOMS

Si	9.07	9.09	8.97	9.15	9.11	9.34
Al	6.84	6.79	6.87	6.71	6.89	6.45
Ti	0.02	0.02	0.02	0.02	0.00	0.02
Mg	0.03	0.03	0.03	0.03	0.00	0.03
Fe	0.07	0.07	0.06	0.07	0.08	0.06
Mn	0.02	0.02	0.01	0.02	0.00	0.02
Ca	2.73	2.82	2.95	2.78	2.78	2.73
Na	1.20	1.09	1.11	1.13	1.14	1.26
K	0.08	0.08	0.07	0.08	0.03	0.10
TOTAL	20.06	20.01	20.09	19.99	20.03	20.01
An	.707	.733	.738	.723	.721	.697

APPENDIX 4

MINERAL ANALYSES

(PLAGIOCLASES FROM THE RUSTENBURG LAYERED SUITE)

SAMPLE NO.	K5-100	K5-100	K5-100	K5-100	K1-150	K1-150
SiO_2	49.31	48.29	49.51	50.43	49.66	50.45
Al_2O_3	31.65	31.96	32.00	30.82	31.61	31.56
TiO_2	0.15	0.12	0.02	0.13	0.14	0.01
MgO	0.12	0.11	0.01	0.10	0.11	0.00
FeO	0.37	0.40	0.31	0.38	0.51	0.30
MnO	0.00	0.12	0.02	0.05	0.25	0.02
CaO	14.53	15.27	15.12	14.53	14.36	14.06
Na_2O	2.92	2.65	2.91	3.14	3.31	3.25
K_2O	0.25	0.31	0.12	0.26	0.38	0.10
TOTAL	99.30	99.23	100.02	99.84	100.33	99.75

STRUCTURAL FORMULAE - ATOMS PER 32 OXYGEN ATOMS

Si	9.03	8.92	9.05	9.21	9.05	9.21
Al	6.83	6.96	6.90	6.63	6.80	6.79
Ti	0.02	0.02	0.00	0.02	0.02	0.00
Mg	0.03	0.03	0.00	0.03	0.03	0.00
Fe	0.06	0.06	0.05	0.06	0.08	0.05
Mn	0.00	0.02	0.00	0.01	0.04	0.00
Ca	2.85	3.02	2.96	2.84	2.80	2.75
Na	1.04	0.95	1.03	1.11	1.17	1.15
K	0.06	0.07	0.03	0.06	0.09	0.02
TOTAL	19.92	20.05	20.02	19.97	20.08	19.97

An	.744	.771	.753	.731	.717	.717

APPENDIX 4

MINERAL ANALYSES

(PLAGIOCLASES FROM THE RUSTENBURG LAYERED SUITE)

SAMPLE NO.	K1-150	K1-150	K5-50	K5-50	K5-50	K5-50
SiO_2	50.86	49.24	50.00	49.34	49.55	49.95
Al_2O_3	30.28	31.43	32.24	31.43	32.01	31.70
TiO_2	0.14	0.13	0.02	0.15	0.12	0.11
MgO	0.12	0.12	0.02	0.08	0.12	0.11
FeO	0.25	0.39	0.28	0.37	0.43	0.36
MnO	0.21	0.13	0.01	0.09	0.19	0.21
CaO	13.74	15.03	14.27	13.90	14.73	14.55
Na_2O	3.19	2.80	2.99	3.36	3.07	2.85
K_2O	0.35	0.18	0.12	0.37	0.29	0.37
TOTAL	99.14	99.45	99.95	99.09	100.51	100.21

STRUCTURAL FORMULAE – ATOMS PER 32 OXYGEN ATOMS

Si	9.33	9.05	9.11	9.09	9.02	9.10
Al	6.55	6.81	6.93	6.82	6.87	6.80
Ti	0.02	0.02	0.00	0.02	0.02	0.02
Mg	0.03	0.03	0.00	0.03	0.03	0.03
Fe	0.04	0.06	0.04	0.06	0.06	0.05
Mn	0.03	0.02	0.00	0.02	0.03	0.03
Ca	2.70	2.96	2.79	2.74	2.84	2.84
Na	1.14	1.00	1.06	1.20	1.07	1.01
K	0.08	0.04	0.03	0.09	0.07	0.09
TOTAL	19.92	19.99	19.96	20.07	20.01	19.97
An	.715	.758	.736	.708	.738	.749

APPENDIX 4

MINERAL ANALYSES

(PLAGIOCLASES FROM THE RUSTENBURG LAYERED SUITE)

SAMPLE NO.	K1-100	K1-100	K1-100	K1-50	K1-50	K1-50
SiO_2	49.69	50.50	49.58	49.46	50.29	49.47
Al_2O_3	31.57	31.52	32.14	32.23	31.67	31.52
TiO_2	0.12	0.10	0.05	0.10	0.10	0.10
MgO	0.11	0.12	0.09	0.14	0.09	0.09
FeO	0.49	0.51	0.36	0.30	0.39	0.47
MnO	0.17	0.11	0.03	0.09	0.12	0.12
CaO	14.41	14.10	15.12	14.73	13.92	14.39
Na_2O	3.35	3.29	2.99	3.06	3.36	3.35
K_2O	0.32	0.13	0.12	0.07	0.12	0.12
TOTAL	100.23	100.37	100.48	100.18	100.06	99.63

STRUCTURAL FORMULAE - ATOMS PER 32 OXYGEN ATOMS

Si	9.09	9.18	9.03	9.02	9.17	9.09
Al	6.74	6.69	6.83	6.86	6.74	6.75
Ti	0.02	0.01	0.01	0.01	0.01	0.01
Mg	0.03	0.03	0.02	0.04	0.02	0.02
Fe	0.07	0.08	0.06	0.05	0.06	0.07
Mn	0.03	0.02	0.00	0.01	0.02	0.02
Ca	2.82	2.75	2.95	2.88	2.72	2.83
Na	1.19	1.16	1.06	1.08	1.19	1.19
K	0.07	0.03	0.03	0.02	0.03	0.03
TOTAL	20.06	19.95	19.99	19.97	19.94	20.01
An	.715	.716	.747	.739	.708	.716

APPENDIX 4
MINERAL ANALYSES
(ORTHOPYROXENES FROM THE MICROPYROXENITES)

SAMPLE NO.	DI-36	DI-36	DI-36	DI-56	DI-56	DI-56
SiO_2	53.61	54.70	54.88	55.15	55.91	54.81
Al_2O_3	1.70	1.45	1.44	1.14	1.25	1.40
TiO_2	0.23	0.20	0.20	0.21	0.22	0.20
MgO	31.61	32.86	33.17	30.60	30.63	29.73
FeO	9.16	8.48	7.84	9.33	9.79	10.70
MnO	0.20	0.23	0.25	0.32	0.29	0.38
Cr_2O_3	0.62	0.83	0.81	0.68	0.80	0.72
NiO	0.30	0.41	0.33	0.32	0.34	0.25
CaO	1.30	1.06	1.08	1.12	1.06	1.13
TOTAL	98.73	100.22	100.00	98.87	100.29	99.32

STRUCTURAL FORMULAE - ATOMS PER 6 OXYGEN ATOMS

Si	1.92	1.92	1.92	1.96	1.96	1.95
Al	0.07	0.06	0.06	0.05	0.05	0.06
Ti	0.01	0.01	0.01	0.01	0.01	0.01
Mg	1.68	1.72	1.73	1.62	1.60	1.58
Fe	0.27	0.25	0.23	0.28	0.29	0.32
Mn	0.01	0.01	0.01	0.01	0.01	0.01
Cr	0.02	0.02	0.02	0.02	0.02	0.02
Ni	0.01	0.01	0.01	0.01	0.01	0.01
Ca	0.05	0.04	0.04	0.04	0.04	0.04
TOTAL	4.04	4.04	4.03	4.00	3.99	4.00

$\dfrac{Mg^{2+}}{(Mg^{2+} + Fe^{2+})}$	.862	.873	.883	.853	.847	.832

APPENDIX 4

MINERAL ANALYSES
(ORTHOPYROXENES FROM THE MICROPYROXENITES AND
OLIVINES FROM THE OLIVINE-BEARING PYROXENITES)

	ORTHOPYROXENES			OLIVINES		
SAMPLE NO.	DI-74	DI-74	DI-74	DI-75	DI-75	DI-76
SiO_2	54.98	54.84	55.00	37.84	38.16	38.96
Al_2O_3	1.53	1.53	1.35	0.16	0.16	0.27
TiO_2	0.30	0.30	0.21	0.19	0.19	0.21
MgO	32.04	31.10	29.83	40.58	40.16	39.41
FeO	8.26	8.26	9.99	19.03	19.35	18.81
MnO	0.33	0.33	0.36	0.41	0.32	0.15
Cr_2O_3	0.30	0.30	0.77	0.18	0.25	0.22
NiO	0.30	0.30	0.29	0.51	0.63	0.63
CaO	1.65	1.65	1.07	0.11	0.10	0.88
TOTAL	99.69	98.61	98.87	99.01	99.32	99.54

STRUCTURAL FORMULAE

	ON THE BASIS OF 6 OXYGENS			ON THE BASIS OF 4 OXYGENS		
Si	1.93	1.95	1.96	0.98	0.99	1.00
Al	0.06	0.06	0.06	0.01	0.00	0.01
Ti	0.01	0.01	0.01	0.00	0.00	0.00
Mg	1.68	1.65	1.59	1.57	1.55	1.51
Fe	0.24	0.25	0.30	0.41	0.42	0.41
Mn	0.01	0.01	0.01	0.01	0.01	0.00
Cr	0.01	0.01	0.02	0.00	0.01	0.00
Ni	0.01	0.01	0.01	0.01	0.01	0.01
Ca	0.06	0.06	0.04	0.00	0.00	0.02
TOTAL	4.01	4.01	4.00	2.99	2.99	2.96

$\dfrac{Mg^{2+}}{(Mg^{2+} + Fe^{2+})}$	.875	.868	.841	.793	.787	.786

APPENDIX 4
MINERAL ANALYSES
(CLINOPYROXENES FROM THE MICROPYROXENITES)

SAMPLE NO.		DI-56	DI-56	DI-56	DI-74	DI-74	DI-74
SiO_2		51.53	51.79	51.77	51.27	51.57	51.34
Al_2O_3		1.64	1.65	2.07	1.81	1.64	2.01
TiO_2		0.37	0.39	0.44	0.47	0.43	0.36
MgO		15.83	15.86	17.40	16.29	16.50	16.32
FeO		11.05	11.11	9.90	10.34	10.36	10.43
MnO		0.46	0.38	0.42	0.39	0.32	0.30
Cr_2O_3		0.36	0.43	0.67	0.37	0.32	0.47
NiO		0.28	0.23	0.23	0.22	0.21	0.25
CaO		17.43	16.65	16.89	17.30	17.28	17.29
Na_2O		0.20	0.20	0.26	0.27	0.14	0.18
TOTAL		99.15	98.69	100.05	98.73	98.77	98.95

STRUCTURAL FORMULAE - ATOMS PER 6 OXYGEN ATOMS

Si		1.94	1.95	1.92	1.93	1.94	1.93
Al		0.07	0.07	0.09	0.08	0.07	0.09
Ti		0.01	0.01	0.01	0.01	0.01	0.01
Mg		0.89	0.89	0.96	0.92	0.93	0.91
Fe		0.35	0.35	0.31	0.33	0.33	0.33
Mn		0.01	0.01	0.01	0.01	0.01	0.01
Cr		0.01	0.01	0.02	0.01	0.01	0.01
Ni		0.01	0.01	0.01	0.01	0.01	0.01
Ca		0.70	0.67	0.67	0.70	0.70	0.70
Na		0.01	0.01	0.02	0.02	0.01	0.01
TOTAL		4.00	3.98	4.02	4.02	4.02	4.01
Mol. %	Wol	36.08	35.08	34.54	35.90	35.71	36.08
	En	45.88	46.60	49.48	47.18	47.45	46.91
	Fs	18.04	18.32	15.98	16.92	16.84	17.01

APPENDIX 5

RB-SR ISOTOPE ANALYSES

SAMPLE NO.	RB	SR	$^{87}RB/^{86}SR$	$^{87}SR/^{86}SR$	2 S.E.M.
MICROPYROXENITES					
DI-7B	33.33	152.3	0.6342	0.725013 ±	0.000009
DI-36	31.56	157.0	0.5824	0.721283 ±	0.000011
DI-53	28.02	127.8	0.6353	0.723195 ±	0.000010
DI-59C	25.13	134.1	0.5428	0.718461 ±	0.000012
DI-74	29.76	154.5	0.5579	0.719185 ±	0.000016
MICROGABBRONORITES					
K-18	1.806	301.5	0.0173	0.708885 ±	0.000010
K-50	8.997	336.2	0.0774	0.708929 ±	0.000011
K-108A	3.797	308.8	0.0356	0.707318 ±	0.000012
KWR-109	3.218	316.8	0.0294	0.707131 ±	0.000010
KWR-178A	18.99	341.3	0.1611	0.712157 ±	0.000011
KWR-194	3.558	293.0	0.0351	0.708663 ±	0.000013
KWR-195	3.962	293.0	0.0391	0.708046 ±	0.000012

INITIAL $^{87}SR/^{86}SR$ RATIOS[1]

SAMPLE NO.	$^{87}SR/^{86}SR$		1 σ
MICROPYROXENITES			
DI-7B	0.70628	±	0.00017
DI-36	0.70408	±	0.00016
DI-53	0.70443	±	0.00017
DI-59C	0.70243	±	0.00015
DI-74	0.70271	±	0.00015
MICROGABBRONORITES			
K-18	0.70837	±	0.00007
K-50	0.70664	±	0.00007
K-108A	0.70627	±	0.00007
KWR-109	0.70626	±	0.00007
KWR-178A	0.70740	±	0.00008
KWR-194	0.70763	±	0.00007
KWR-195	0.70669	±	0.00007

[1] All initial $^{87}Sr/^{86}Sr$ ratios were calculated using the GEODATE software package (Eglington and Harmer 1989), utilising a decay constant of 1.42 x 10^{-11} yr^{-1} and assuming an age of 2050 Ma for the Bushveld Complex. Details of analytical techniques are described in Harmer and Sharpe (1985).